# *Evaluation of Loss Factor Estimation Techniques For Free Hanging Flat Panels Excited Mechanically*

**By,**

**Himanshu Amol Dande**

Submitted to the graduate degree program in Aerospace Engineering and the Graduate faculty of the University of Kansas in partial fulfillment of the requirements for the degree of Doctor of Philosophy

_____

Chairperson: Dr. Mark Ewing

_____

Dr. Richard Hale

_____

Dr. Saeed Farokhi

_____

Dr. Ray Taghavi

_____

Dr. Adolfo Matamoros

The Ph.D. Committee for Himanshu Amol Dande

certifies this is the approved version of the following dissertation:

# *Evaluation of Loss Factor Estimation Techniques For Free Hanging Flat Panels Excited Mechanically*

_____

Chairperson: Dr. Mark Ewing

_____

Dr. Richard Hale

_____

Dr. Saeed Farokhi

_____

Dr. Ray Taghavi

_____

Dr. Adolfo Matamoros

**Date Approved: 24th January 2013**

# Abstract

To establish the "best" technique to estimate a damping loss factor for mechanically-excited panels, three loss factor estimation techniques—PIM, IRDM, and RDT—are compared. In experimental and computational analyses, panels with two damping levels and three sizes were tested. The loss factor estimates from each of the three techniques are then evaluated in four distinct frequency bands centered at one-third octave frequencies of 500 Hz, 1000 Hz, 2000 Hz and 4000 Hz (for computational analysis only).

Unlike IRDM and RDT, the quality of PIM-based loss factor estimates have presented a strong correlation between the region of response measurement and its distance from the excitation location. PIM-based loss factors were *significantly* underestimated when responses are measured inside the direct field. PIM-based loss factors are relatively accurate only if the measurements are made from wide-spread response locations.

For a lightly damped panel, loss factor estimates using PIM, IRDM and RDT with direct averaging agree within reasonable accuracy. For intermediately to highly damped panels, IRDM and RDT with direct averaging *under-predicted* the loss factor; RDT with an autocorrelation function averaging approach slightly *over-predicted* the loss factor. Both RDT approaches might be used to set a bound on panel loss factor. Even when significantly fewer response locations are considered, it is evident that loss factor estimates from RDT are as reliable as IRDM and more reliable than PIM especially for highly damped panels.

For the analysis of freely hanging plates, excitation "close to an edge", especially for PIM, is not recommended. When analyzing the panel loss factor, arbitrary or central excitation is acceptable.

# Acknowledgements

First and foremost, I would like to thank Dr. Mark S. Ewing, my advisor, for providing me with an opportunity to conduct the research herein. During the course of the research he provided the required tools and technical knowledge for successful completion of this research project. The training and motivation I received, in and out of the structural acoustics lab at KUAE, under his mentorship, have inspired me to opt for research in the field of structural dynamics/ acoustics in my career. Thank you for being a great tutor, mentor and for having faith in me.

I would like to thank Dr. Richard Hale for being on my committee. His courses, which typically went beyond theory and often landed in experimental and computational domain, enhanced my understanding of manufacturing processes and materials used in aerospace engineering.

I would like to thank Dr. Saeed Farokhi for motivation he provided all these years. The conversations on our way back from classes were some of the most enlightening moments of my day. Thank you for serving on my committee.

I would also like to thank Dr. Adolfo Matamoros for being on my committee. The courses I have taken came in very handy during the research and provided me insight into techniques of experimental analyses.

I am thankful to Dr. Ray Taghavi for being on my committee and reviewing my dissertation. I would like to acknowledge Dr. Mark Moeller, Judy Gallman, Mary Drouin and Albert Allen, of Spirit AeroSystems, for proving me the necessary hardware, tools and technical assistance. I would like to thank Dr. Wanbo Liu for helping with the computational plate model and always being there to teach something new or resolve some technical issues.

I am thankful to Amy Borton, and department staff, for helping me in all the official matters and for providing a cheerful company. I am thankful to Wes Ellison for helping us with lab related hardware and software installation works.

I would like to thank all the students I studied with or taught. Teaching students was never a one–sided affair, as I have learned and improved a lot from my GTA experience.

I am thankful for all the love and encouragement I received from my relatives. I am especially thankful to my uncles, Dr. Pinak Dande, who sponsored my initial part of education, and Ravi Boratkar, who provided the necessary motivation to continue my education after bachelor degree. I am also grateful to my best friend Ravishankar who made me realize my true potential and ambitions.

I feel fortunate to have Anand as a friend and roommate. He stood by me during my best and worst days. Like Anand, his mother, Jayshree Joshi, and his wife, Kanchan, provided the all the required support whenever I needed it. I would like to express my love and appreciation to my Lawrence friends: Santosh, Urvashi, Nikunj, Mitali, Rohita, Sweta, Sudarshan, Sudhir, Prashi and Amool. I cannot thank them enough for what they have done for me.The time I spent in Learned 2122, with Julien, Vivek, Saatvika, Sarah, Alec, Samantha, David and Geoff, will remain the as one of the most memorable one. Thank you guys for being such a nice company. Without you guys this journey could not have been pleasant.

Finally, I would like to express my gratitude to my parents. Their encouragement, sacrifices, love and constant support is the primary reason for all that I am today. I dedicate this work to my parents.

# Table of Contents

# List of Figures

# List of Tables

# List of Symbols

| | |
|---|---|
| $1DOF$ | Single or One Degree Of Freedom |
| $A(\omega)$ | Fourier transform of the acceleration of a measurement point |
| $b$ | Beam width |
| $C$ | Vector of damping coefficients |
| $c$ | Damping coefficient |
| $c_l$ | Wave speed in material |
| $c_c$ | Critical damping coefficient |
| $c_g$ | Group velocity in the plate |
| $c_\phi$ | Phase velocity |
| $CLD$ | Constrained Layer Damping |
| $DAQ$ | Data AcQuisition |
| $DC$ | decay Curve |
| $D_X$ | Randomdec signature |
| $DR$ | Decay Rate |
| $dB$ | Decibels |
| $EI$ | Composite panel's flexural rigidity |
| $E_D$ | Dissipated energy |
| $E_i$ | Young's modulus of the $i^{th}$ plate |
| $E_d$ | Young's modulus of the damping layer |

| | |
|---|---|
| $E_s$ | Young's modulus of the base plate/ structure |
| $E_{K.E.}$ | Kinetic energy |
| $E_{K.E.}(\omega_c)$ or $\varepsilon^k(\omega_c)$ | Kinetic energy for the narrow band with central frequency $\omega_c$ |
| $E_{P.E.}$ | Potential energy |
| $E_{S.E.}$ | Strain Energy |
| $E_{Tot}$ | Total mechanical energy |
| $E$ | Young's modulus of elasticity |
| $E_D$ | Dissipated energy |
| $E_{Tot}$ | Total mechanical energy |
| $F$ | Vector of forcing functions |
| $F^*(\omega)$ | Complex conjugate of the Fourier transform of the input force |
| *FEA* | Finite Element Analysis |
| *FFFF* | All edge free boundary conditions (Free-Free-Free-Free) |
| *FFT* | Fast Fourier Transformation |
| *FIR* | Finite–duration Impulse Response |
| *FLD* | Free Layer Damping |
| *FRF* | Frequency Response Function |
| $F(\omega)$ | Force in frequency domain |
| $F(t)$ | Normalized force in time domain |
| *Fs* | Sampling frequency (Hz) |
| $f(t)$ | Forcing function |

| | |
|---|---|
| $f$ | Frequency of interest (Hz) |
| $f_c$ | Band's central frequency (Hz) |
| $f_1$ and $f_2$ | Half power frequencies |
| $f_n$ | Natural frequency (Hz) |
| $\Delta f$ | Frequency resolution (Hz) |
| $G_{2r}$ or $G_2$ | Real part of the shear modulus of the damping material |
| $H$ | Hilbert transformation |
| $\Delta H$ | Change in amplitude of the exponential decay curve in $\Delta t$ seconds |
| *HPBM* | Half Power Bandwidth Method |
| $h(t)$ | Impulse response function, time domain |
| $h_i$ or $H_i$ | Thickness of the i$^{th}$ plate |
| $h_{21}$ | Distance between the central axes of base layer and damping layer |
| $h_{31}$ | Distance between the mid-planes of the top and bottom plates |
| $H(\omega)$ | Frequency response function, frequency domain |
| *IFFT* | Inverse Fast Fourier Transformation |
| *IIR* | Infinite–duration Impulse Response |
| *IR* | Impulse Response |
| *IRDM* | Impulse Response Decay Method |
| $\mathrm{Im}(K)$ | Imaginary part of extensional stiffness $K$ |
| $\mathrm{Re}(K)$ | Real part of extensional stiffness $K$ |
| $K$ | Stiffness matrix |
| *KUAE* | The University of Kansas, Department of Aerospace Engineering |

| | |
|---|---|
| $k$ | Stiffness of the spring |
| $k_B$ | Bending wave number of the composite |
| $L$ | Length of the beam |
| $LF$ | Loss Factor |
| $m$ | Mass |
| $m_i$ | Distributed mass |
| $M$ | Mass of the substructure under analysis |
| $M''$ | Mass per unit area of the composite |
| $MDOF$ | Multiple Degree Of Freedom |
| $N$ | Number of measurement locations |
| $N_C$ | Length of sample in terms of cycles |
| $P$ | Perimeter of the panel |
| $PARAM, G$ | MSC/NASTRAN's input parameter card—the overall structural damping coefficient |
| $P_D$ | Dissipated power |
| $P_{IN}(\omega_c)$ | Input power measured for the narrow band with central frequency $\omega_c$ |
| $P_{IN}$ | Input power |
| $PIM$ | Power Input Method |
| $p$ | Wave number |
| $Q$ | Quality factor |
| $R_x(\tau)$ | Autocorrelation function |
| $R_D$ | Radius of direct field |

| | |
|---|---|
| $RDM$ | Reverberation Decay Method |
| $RDT$ | Random Decrement Technique |
| $RDT_{AA}$ | Random Decrement Technique with Averaging Autocorrelation functions approach |
| $RDT_{DA}$ | Random Decrement Technique with Direct Averaging approach |
| $RKU$ | Ross-Kerwin-Ungar methodology to estimate beam's loss factor |
| $TR$ | Reverberation time |
| $t$ | Time (seconds) |
| $t_2$ and $t_1$ | Corresponds to values of time 't' on linear time scale |
| $\Delta t = t_2 - t_1$ | Time period for $DR$ estimation |
| $x$ | Displacement of a system |
| $x_0$ | Amplitude of trigger condition or initial displacement |
| $\dot{x}$ | Velocity of a system |
| $\dot{x}_0$ | Slope of triggering condition or initial velocity |
| $\ddot{x}$ | Acceleration of a system |
| $X$ | Vector of displacement |
| $X(\omega)$ | Fourier transformation of response |
| $\dot{X}$ | Vector of velocity |
| $\ddot{X}$ | Vector of acceleration |
| $\dot{X}(\omega)$ | Complex velocity response—in frequency domain |

| | |
|---|---|
| $\dot{X}^*(\omega)$ | Complex conjugate of velocity response—in frequency domain |
| $\ddot{X}(\omega)$ | Complex acceleration response—in frequency domain |
| $\ddot{X}^*(\omega)$ | Complex conjugate of acceleration response—in frequency domain |
| $Y_{if}(\omega)$ | Mobility between the driving point *f* and point *i* |
| $Y_{ff}(\omega)$ | Driving point mobility |
| $x$ | Displacement of a system |
| $\dot{x}$ | Velocity of a system |
| $\ddot{x}$ | Acceleration of a system |
| $x_0$ | Amplitude of trigger condition or initial displacement |
| $\dot{x}_0$ | Slope of triggering condition or initial velocity |
| *VEM* | ViscoElastic Material |
| $\langle v^2 \rangle$ | Total mean square velocity |
| $\langle v_D^2 \rangle$ | Direct field velocity |
| $\langle v_R^2 \rangle$ | Reverberant field velocity |

**Greek**

| | |
|---|---|
| $\delta(t)$ | Unit impulse function |
| $\phi$ | Phase angle (radians) |
| $\eta$ | Loss factor |

| | |
|---|---|
| $\eta_{12}$ & $\eta_{21}$ | Coupling loss factor |
| $\eta_{est}$ | Initial "guess" of the loss factor |
| $\eta_B^{LF}$ | Loss factor for constrained layer damping treatment for bending motion at low frequency |
| $\eta_B^{HF}$ | Loss factor for constrained layer damping treatment for bending motion at high frequency |
| $\eta_B^{constr.}$ | Loss factor for constrained layer damping treatment for bending motion |
| $\eta_i$ | Loss factor of the $i^{th}$ plate |
| $\eta_L^{free}$ | Loss factor for free layer damping treatment for longitudinal motion |
| $\eta_B^{free}$ | Loss factor for free layer damping treatment for bending motion |
| $\kappa_i$ | Radius of gyration for $i^{th}$ layer |
| $\rho$ | Mass density |
| $\rho_s$ | Surface mass density |
| $\zeta$ | Damping ratio |
| $\xi_n$ | $n^{th}$ Eigen value |
| $\omega$ | Radial frequency (radians/sec) |
| $\omega_n$ | Natural frequency (radians/sec) |
| $\omega_d$ | Damped natural frequency (radians/sec) |
| $\omega_c$ | Narrow band's central frequency (radians/sec) |
| $\omega_1$ & $\omega_2$ | Start and end frequencies of bandwidth of analysis (radians/sec) |

| | |
|---|---|
| $\tau$ | Dummy time variable (seconds) |
| $\omega_n$ | Radial natural frequency (radians/second) |
| $\omega_d$ | Radial damped natural frequency (radians/second) |
| $\phi$ | Phase angle (radians) |

# 1 Introduction

This chapter introduces some of the basic concepts and terms associated with the identification of vibration characteristics of a system, in particular the damping loss factor. This chapter also includes a brief discussion of contemporary experimental loss factor estimation techniques, their applications and limitations.

Vibration, in its general sense, is a periodic motion about an equilibrium position due to a disturbing force. Undesired vibrations can cause premature fatigue and unpleasant noise. These undesired vibrations can be suppressed using a variety of damping treatments. One commonly used measure of damping in structures is the damping loss factor. There are many processes for estimating the damping loss factor. To experimentally estimate the damping loss factor, structures are typically subjected to mechanical excitation and the structure's response to the disturbing force is measured. For a mechanical excitation, the damping estimation is dependent on the location of excitation and location of response measurement, which suggests processes which involve considering (and, possibly averaging) multiple response measurements and multiple excitation locations.

Most of the contemporary damping estimation techniques are restricted to low damping levels. Hence, the challenge here lies in being able to accurately estimate the higher damping.

## 1.1 Damping

The vibrations induced in a structure due to a finite-duration excitation eventually "damp-out". This ability of a structure to dissipate vibrational energy is associated with an important characteristic of the system, known as damping which can be quantified as the

damping ratio ($\zeta$) or loss factor ($\eta$). When subjected to persistent excitation, a structure has the highest amplitude of vibratory response at its natural frequency, which primarily depends on the structure's mass and stiffness; the effect of damping in general is less important (except at very low frequencies). The overall response level of a structure is inversely proportional to its damping [1]. Thus, the level of damping is an important design variable in number of fields of study, such as noise reduction, earthquake resistant structures, instrument safety, and defining flutter boundaries for airfoils. Therefore, accurate estimation of damping, usually experimentally, is an integral and critical part of all types of dynamic analysis.

For an inadequately damped structure, damping can be added explicitly, either actively or passively. Active damping, generally in a narrow frequency band, is enforced by the use of actuators. On the other hand, passive damping increases damping by application of layer(s) of energy-dissipating materials. Passive damping treatments are simple to apply, cost effective and rather well established. Constrained Layer Damping (CLD) is one of the most commonly used passive damping treatments. In CLD, a base structure is coated with a thin layer of a Visco-Elastic Material (VEM) which is then covered by a constraining layer (cover sheet). Under dynamic loading, this layer of damping material undergoes shear, as represented in Figure 1.1, and dissipates energy [2]. In general, the stiffness and loss factor properties of materials used in CLD treatments are temperature dependent and ideally, the structures should be tested at their respective service temperatures. The process of estimating the loss factor remains unchanged with respect to ambient temperature conditions. Theoretical estimation of damping for a panel with a CLD treatment is discussed in Chapter 2.

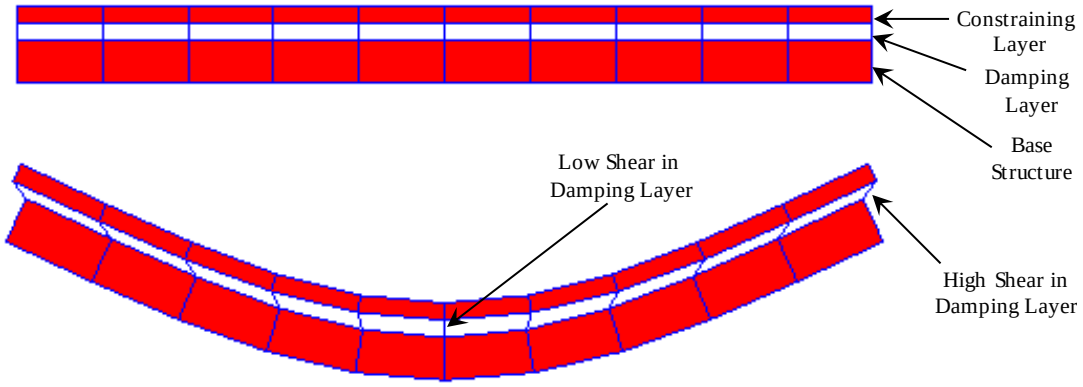


**Figure 1.1: Schematic of constrained layer damping treatment. Reprinted with permission from Liu [2].**

### 1.1.1 Damping Loss Factor – Single Degree of Freedom System

The equation of motion for a single Degree Of Freedom (1DOF) system, acted upon by force, is given by

$$m\ddot{x}(t) + c\dot{x}(t) + k\,x(t) = f(t) \tag{1.1}$$

where,

$f(t)$ is the externally applied force as a function of time

$m$ is the mass of the system

$c$ is the damping coefficient of the system

$k$ is the stiffness of the system

$x(t)$ is the displacement of the system

$\dot{x}(t)$ is the velocity of the system

$\ddot{x}(t)$ is the acceleration of the system.

The damping quantities of a SDOF system are typically assessed based on the non-dimensional ***damping ratio***:

$$\zeta = \frac{c}{c_c} = \frac{c}{2\sqrt{k \cdot m}} \tag{1.2}$$

where,

$c_c$ is the critical damping level. For damping levels above critical damping the system will not oscillate.

The ***damping loss factor*** is defined as the ratio of the energy dissipated by the structural system to the total energy of the system, per cycle of vibration. That is:

$$\eta \equiv \frac{E_D}{2\pi \cdot E_{Tot}} \tag{1.3}$$

where,

$\eta$ is the loss factor

$E_D$ is the dissipated energy

$E_{Tot}$ is the total mechanical energy.

The relation between the damping ratio and loss factor, for a 1DOF system, can be shown to be:

$$\eta = 2 \cdot \zeta = \frac{1}{Q} \tag{1.4}$$

where,

$Q$ is the ***quality factor***.

However, the loss factor can also be represented in terms of ratios of energies, decay rate and half power bandwidth frequencies. A few of these relations are discussed in the following section.

## 1.2 Experimental Loss Factor Estimation

A real structure can have multiple natural frequencies in a frequency band of interest. For each mode of vibration a unique loss factor exists, i.e. damping in real structures is frequency dependent. Unlike other system properties, such as mass and stiffness, estimation of loss factor is rarely straightforward and it is often evaluated experimentally. Most of the experimental techniques for loss factor estimation rely on the assumption of a linear system with viscous damping [3]. On one hand, underestimation of loss factor may result in an unacceptable design requiring additional damping thereby increasing weight; on the other hand, overestimation of loss factor may lead to failure before the predicted life and/or discomfort because of unwanted and/or under–suppressed vibrations [4].

The equation of motion for a Multiple Degree Of Freedom (MDOF) system is:

$$[M]\left\{\ddot{X}\right\}+[C]\left\{\dot{X}\right\}+[K]\{X\}=\{F\} \tag{1.5}$$

where,

$[M]$ is the mass matrix, for a linear system

$[C]$ is the damping matrix

$[K]$ is the stiffness matrix

$\{F\}$ is the vector of externally applied force

$\{X\}$ is the vector of displacement

$\left\{\dot{X}\right\}$ is the vector of velocity

$\left\{\ddot{X}\right\}$ is the vector of acceleration.

A linear MDOF system can be decoupled, via the "model transformation", to identify 1DOF system characteristics for each mode of vibration. With such an approach, an frequency-dependent loss factor can be estimated at each of the system's natural frequencies.

### 1.2.1 Loss Factor Estimation Techniques

The techniques discussed in the following section can be used to compute the total loss factor of a structure. It should be emphasized that each technique has its limitations and requirements, hence no one technique is applicable to all situations. It has been empirically realized by many researchers that ***experimentally determined loss factors typically vary between alternative processes by up to 20% or more*** [1].

In general, these loss factor estimation techniques can be classified as time domain or frequency domain. For further simplification, in this report, the experimental loss factor estimation techniques are broadly segregated as decay-rate-based or power-measurement-based.

#### 1.2.1.1 Decay Rate Based Loss Factor Estimation Techniques

The time required for a structure's impulse response to damp out is dependent on the structure's loss factor. The decaying (i.e. transient) response of the structure can be generated by either an impulsive or an interrupted steady-state excitation. The following three techniques can be implemented to estimate loss factor from the decay rate:

1. Reverberation Decay Method (RDM).
2. Random Decrement Technique (RDT)
3. Impulse Response Decay Method (IRDM)

For these techniques the procedures to evaluate the loss factor, from the decay rate of an impulse response or free decay, are similar. Loss factor, for a 1DOF system, can be mathematically expressed in terms of decay rate as [1, 2 and 5]:

$$\eta = \frac{DR}{27.3 \cdot f_n} \tag{1.6}$$

where,

$DR$ is the decay rate (dB/sec)

$f_n$ is the natural frequency or central frequency of a band (Hz).

Figure 1.2 represents the process of determining decay rate from the slope of the decay curve. Equation (1.6) is then used to estimate the loss factor. The derivation and analysis procedures to extract decay rate from free decay, the impulse response, or the autocorrelation function are explained in Section 2.2. These three decay rate-based techniques are briefly discussed in the following section.

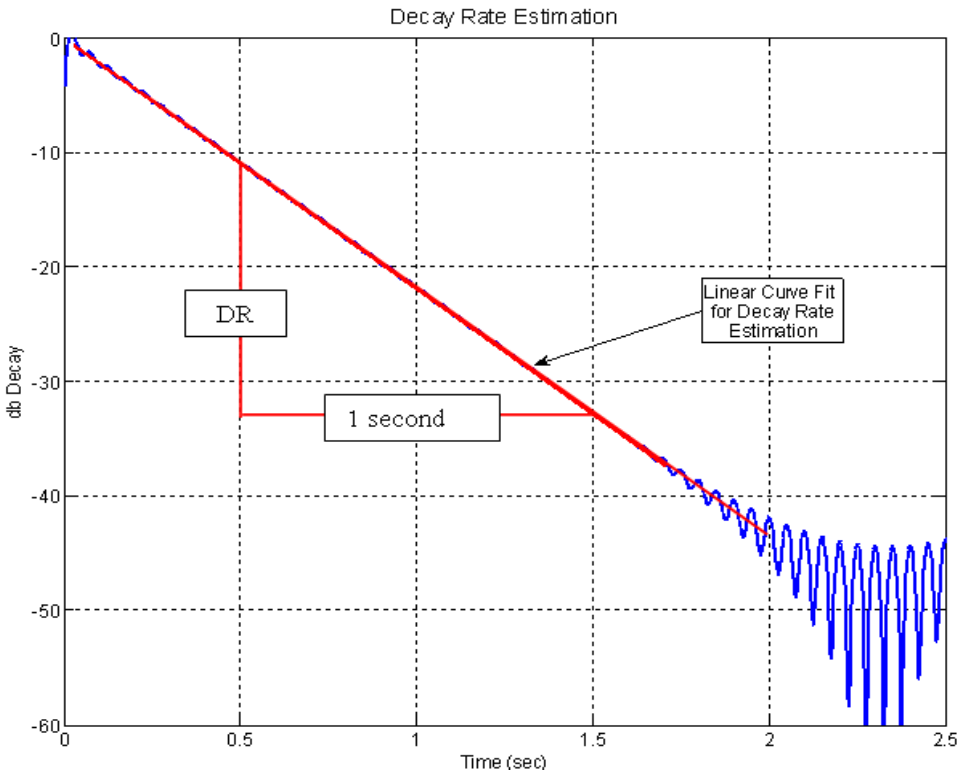


**Figure 1.2: Decay curve (in dB) of a 1DOF system**

#### 1.2.1.1.1 Reverberation Decay Method (RDM)

Loss factor estimation from the RDM is based on the calculation of the decay rate of free vibrations after the steady state excitation is suddenly interrupted. The structure is allowed to reach a steady state before interrupting the force. When the vibration energy reaches steady state, the energy density at any point is comprised of two components: one from the direct field (forced vibration) and the other from the reverberant field (free vibration). When the excitation source is "switched-off", the steady state energy density starts to decay [6]. The decay rate, and eventually the loss factor, is measured from the decaying response. This technique is only applicable for first few natural frequencies of the structure. As such, it is appropriate for seismic structures, but not for plate like structures.

#### 1.2.1.1.2 Random Decrement Technique (RDT)

RDT is solely based on measurement of a structure's response to a steady state random excitation. In this very unique technique, the estimation of free decay (or the autocorrelation function) is based on an ensemble of recorded samples triggered from identical initial conditions. By setting up triggers, i.e. when peaks in response are within certain response levels, these triggered response samples are extracted. The average of these triggered samples, referred to as "randomdec signature", is the positive part of the autocorrelation function [7]. The decay characteristics of the autocorrelation function and free decay are identical and are directly used to estimate damping. ***Note that RDT only requires the response of a system, not the input to it.***

#### 1.2.1.1.3 Impulse Response Decay Method (IRDM)

As the name suggests, loss factor estimation using IRDM is based on the determination of the decay rate of narrow band impulse responses. The time domain impulse response functions are computed by taking the inverse Fourier transform of a narrow-band Frequency Response Function (FRF). The force-to-acceleration (or -velocity) FRFs can be generated either using an impulsive force, as with an impulse hammer, or using a steady state excitation, using a mechanical shaker. ***Note that IRDM requires knowledge of the force and the structure's response to that force, that is, both input and response.***

### 1.2.1.2 Power Based Loss Factor Estimation Techniques

Loss factor can also be estimated from the measurement of power. Two of the common methodologies are:

1. Power Input Method (PIM)–based on power balance
2. Half Power Bandwidth Method (HPBM)–based on determination of the half power points (3 dB below the maximum response level of the FRF).

These two techniques are briefly introduced in the following section. PIM is further discussed in Chapter 2. ***As with IRDM, power-based estimation techniques require both input and response.***

#### 1.2.1.2.1 Power Input Method (PIM)

Principles involved with PIM are based on the very definition of the loss factor, and hence there is no theoretical limitation to this technique. The loss factor ($\eta$), using PIM, is defined in terms of dissipated power (or $P_D$) and total energy through the following relations:

$$\eta = \frac{P_D}{\omega \cdot E_{Tot}} = \frac{E_D}{2 \cdot \pi \cdot E_{Tot}} \tag{1.7}$$

where,

$\omega$ is the frequency in radians/sec

$E_{Tot}$ is the total mechanical energy

$E_D$ is the dissipated energy.

If a structure is excited to a steady state condition, the input power (or $P_{IN}$) equals the dissipated power (or $P_D$), therefore:

$$\eta = \frac{P_{IN}}{2\pi \cdot f_c \cdot E_{Tot}} \tag{1.8}$$

where,

$f_c$ is the band's central frequency (Hz).

Since the PIM is based on steady state response measurements, i.e. after the transients have died out, a continuous source of power, or excitation, is required for the process. Frequency domain filtering is typically implemented to estimate loss factors in narrow frequency bands, thereby establishing the frequency-dependency of the loss factor. The accuracy of loss factor estimates along with a number of required measurement points has been a topic of discussion in many papers. By exercising appropriate care taken during experimentation, PIM has been used for all frequency ranges and damping levels [2, 8].

#### 1.2.1.2.2 Half-Power Bandwidth Method (HPBM)

The HPBM is a frequency domain technique, in which the loss factor is estimated from the FRF. The performance of this technique is optimum only for isolated modes for which the half power points can be reliably calculated. In practice this is often the case only

for the fundamental (lower) natural frequencies of a structure or structural element. The half power points are 3dB below the maximum magnitude of an isolated mode's FRF. The schematic of HPBM is presented in Figure 1.3. The loss factor can be measured from the observed natural frequency and the half power frequencies using the following equation:

$$2 \cdot \zeta = \eta = \frac{f_2 - f_1}{f_n} \tag{1.9}$$

where,

$f_1$ and $f_2$ are the half power frequencies (Hz or rad/sec)

$f_n$ is the natural frequency (Hz or rad/sec).

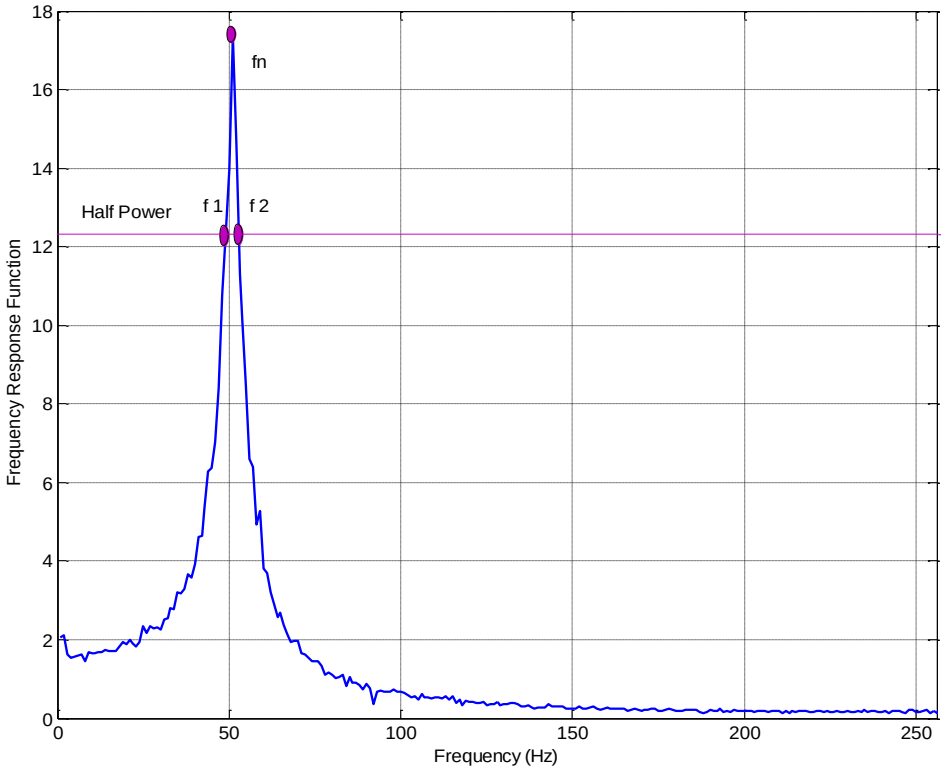


**Figure 1.3: Schematic of Half-Power Bandwidth Method**

The FRF is defined as:

$$H(\omega) = \frac{X(\omega)}{F(\omega)} \tag{1.10}$$

where,

$H(\omega)$ is the Frequency Response Function (FRF)

$X(\omega)$ is the Fourier transformation of response

$F(\omega)$ is the Fourier transformation of force.

The HPBM is relatively simple and relies only on the measurement of FRF, which can be obtained as an output from most commercially-available data acquisition systems. Experimental measurements, in general, do not yield a smooth and noise-free frequency response function. In order to obtain a "smooth" FRF, the response signal needs to be averaged to generate a stable FRF estimate. For accurate estimation of loss factor, especially for lightly damped structures, the frequency resolution of the measured FRF should be high enough to capture the peak in the FRF and the half power frequencies. To reduce experimental error, the value of loss factor should be averaged over multiple excitation and response points on the structure.

If a structure is symmetric or close to being symmetric, there is a high probability of multiple peaks existing in a small frequency range, and separation of these "close modes" might not be simple. Two close modes will result in a beating phenomenon, which is recognizable in the time domain record. This technique is not recommended when it is difficult to separate the modes.

## 1.3 Bias Error in PIM-Based Estimations: Size of the Direct Field

Consider a continuous system, such as a flat panel, excited by a steady state point excitation. The input energy flows radially outward, in the form of waves, from the point of excitation towards the system's boundaries. The interaction of incident waves, from the excitation location, and reflected waves from the panel boundaries, eventually creates a "reverberant" field except near the excitation point and, possibly, at the boundaries. The region near the excitation point is called the "direct" field. For a finite, damped panel, the kinetic energy attenuates from its maximum value—close to the excitation location—to a near uniform value in the reverberant field.

The distance to the "boundary" of the direct field from the excitation point is called the "radius of the direct field" by Lyon and DeJong [1]. They defined this distance, $R_D$, as the distance from the source at which the kinetic energy measured in the direct field and in the reverberant field are equal. The radius of the direct field is given by:

$$R_D = \frac{\omega \eta M}{2\pi \rho_s c_g} \tag{1.11}$$

where,

$\rho_s$ is the surface density and

$c_g$ is the group velocity in the plate (which is proportional to the square root of the frequency).

In the following Figure 1.4 the experimentally measured squared velocity field—i.e. total energy per unit mass—of a damped panel is presented. The approximate loss factor for this panel is 0.10 and the panel is analyzed at 1000 Hz. The circle indicates the theoretically estimated radius of the direct field.

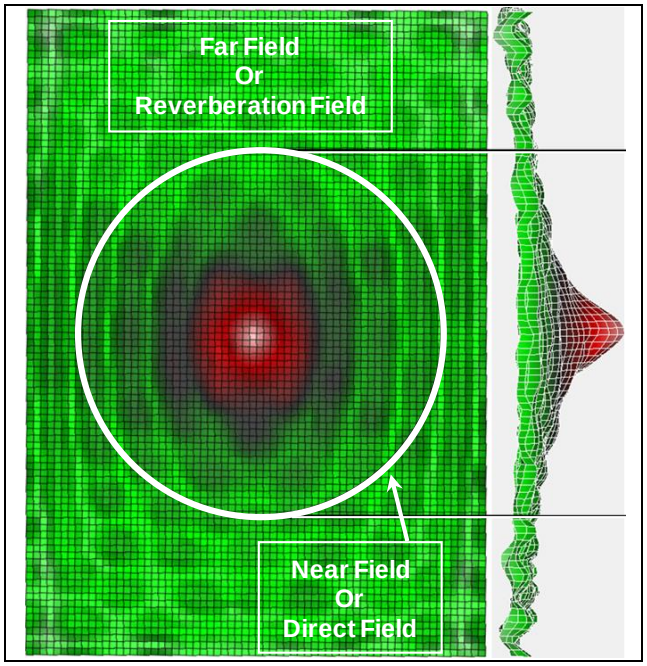


**Figure 1.4: Velocity-squared fields from measurements on a damped plate. Theoretical radii of direct field estimated from Equation (1.11) are indicated.**

From the side view of plate, it is evident that the squared velocity has reached, a nearly, uniform value in the reverberant field. The squared velocity has relatively higher values in the direct field.

The theory associated with loss factor estimation, using PIM, assumes that the kinetic energy is measured from the reverberant field. From Equation (1.11) it is evident that the radius of the direct field is directly proportional to the loss factor. In the case of an undamped plate, the direct field is so small that almost all randomly positioned sensors would be inside the reverberant field [9]. For panels with very high loss factor, these radial waves emerging from excitation point will damp out before they reach panel boundaries. In this case the reverberant field is never established and only a direct field exists.

For loss factor less than 0.3, the total energy is within 5% of twice the kinetic energy. Therefore, from Equations (1.7) and (1.8), the loss factor is inversely proportional to the

kinetic energy. The kinetic energy measured from the direct field is higher than that in the reverberant field; hence the loss factor measured from the direct field will be underestimated.

In the analysis of a highly damped panel, for which the direct field is large, the loss factor estimated from an array of randomly positioned sensors will have a higher probability of underestimating the loss factor.

## 1.4 Other Issues Associated With Loss Factor Estimation Techniques

As no single approach to estimate loss factor is applicable to all situations, it is important to understand the requirements and limitations of each method. Most of the techniques fail to accurately estimate high loss factors, particularly when insufficient or limited information is available [10].

The positioning of sensors and excitation locations plays a critical role when taking measurements from multiple locations response locations—and, possibly an input location—on the structure. Considering modal response, node lines on a "regular", for instance, a rectangular structure, are regions with very low response levels for many modes. Therefore it is important to neither excite a structure along a "popular" mode line—such as central axes of a plate—nor measure response from a point on such a node line. To efficiently simulate a continuous system and remove spatial effect in measurements, it is suggested to record and analyze long sets of response time history from multiple locations, preferably randomly chosen, on the test specimen.

For analysis involving multiple input-output locations on the structure, slope fitting can be another tricky and sensitive issue. If a large number of slope fits are to be executed by an operator, human error is inevitable and the results may not be reproducible. Hence, it is recommended to use an automated slope fitting algorithm. All the slope fits on the decay curves should be at least visually inspected to avoid possibility of a bias error.

For the experimental evaluation with the PIM, it is assumed that the mass is distributed (i.e. lumped) at the measurement locations. For accurate measurements of loss factor from these frequency-domain techniques a noise-free FRF is required. Thus, to achieve stable FRFs, averaging of frequency-domain data is required. Loss factor estimation techniques and associated processing parameters are discussed in Chapter 2 and 3.

## 1.5 Scope of Work

The foremost purpose of this research is to attain a better understanding of experimental loss factor estimation techniques and the parameters associated with them. For a structure excited by persistent mechanical excitation, the following three techniques are evaluated:

1. Impulse Response Decay Method
2. Random Decrement Technique
3. Power Input Method.

The positioning of sensors for response measurement plays a critical role in loss factor estimation. Hence, loss factor is estimated from a cluster of sensors with common spatial characteristics, for example: (a) a group of measurements along the free edge or (b) a group of measurements that are, say, between 6 to 8 inches from the excitation location or (c) all the measurements from the direct field.

Further, the excitation location is equally critical as the measurement location. Hence, the plate is excited at multiple locations primarily categorized as: center, corner and/or edge, and a few arbitrarily chosen.

In the experimental and computational analyses, two plates with different damping treatments are tested for the effect of selecting multiple excitation locations, measurement locations, choice of narrow-band central frequency and plate size.

In the experimental and computational analyses of plates, the loss factor estimates from the RDT, IRDM and PIM are compared. Methods and results published herein and other papers published by University of Kansas, Department of Aerospace Engineering, (KUAE) authors on loss factor estimation techniques will give structural dynamists a better insight into the effect of the process variables associated with experimental loss factor estimation. Further, it is expected that the recommendations and observations from this research will serve as a guide for choosing the "best fit technique" for a specific experimental scenario.

# 2 Loss Factor Estimation Techniques

In this chapter the experimental and analytical methods for estimating the total loss factor are presented. For a subsystem, the overall level of response is inversely proportional to its loss factor. In the case of an under-damped subsystem(s), the structure's energy dissipative qualities can be enhanced by applying damping treatment(s), a few of which are discussed in this chapter.

## 2.1 Damping Treatments

Typical aerospace materials have very low inherent damping. Polymers, such as Visco-Elastic Materials (VEM), have a significantly high loss factor as compared to metals. To increase the damping of a structure, a layer of damping material is bonded to the base structure to dissipate energy, thereby decreasing the response. This method of adding damping is more effective in constraining the bending motion than in-plane (or extensional) motion.

Deformation of polymeric materials causes significant, irreversible loss of energy, in the form of heat. For steady-state excitation this energy loss can be interpreted in terms of the dissipated power. The loss factor characteristics of these polymeric materials are frequency- and temperature-dependent [1, 2 and 11]. Free layer and CLD treatments are two of the most commonly used and cost-effective methods to add damping, and these are discussed in following sections.

### 2.1.1 Free Layer Damping Treatment

The Free (or unconstrained) Layer Damping (FLD) treatment involves bonding the layer of damping material to the base structure. The outer surface of damping layer remains unconstrained. This configuration is represented in Figure 2.1 (top).

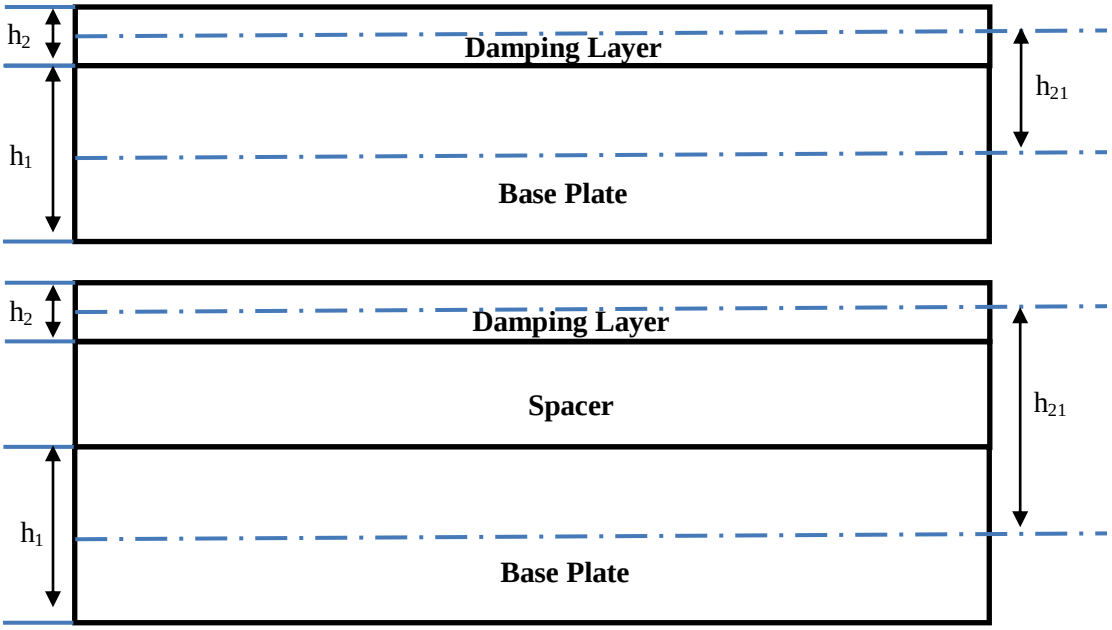


**Figure 2.1: Typical configurations for free layer damping treatments: without spacer(top) and with spacer (bottom).**

Loss factor can be shown to be the ratio of the internal restoring forces in a solid due to ***displacement*** to those due to ***velocity***. Therefore, the effective extensional stiffness, $K$ , for a solid is [1]:

$$K = E(1+i\eta)\cdot h \tag{2.1}$$

where,

$E$ is the Young's modulus and

$h$ is the thickness of the panel.

From Equation (2.1), loss factor for FLD is defined as:

$$\eta = \frac{\mathrm{Im}(K)}{\mathrm{Re}(K)} \tag{2.2}$$

where,

$\mathrm{Im}(K)$ is the imaginary part of extensional stiffness $K$

$\mathrm{Re}(K)$ is the real part of extensional stiffness $K$.

For longitudinal motion, the strains induced in the base plate and damping layer are same. Therefore, the extensional stiffness of composite is equal to:

$$K = K_1 + K_2 \tag{2.3}$$

$$\Rightarrow K = E_1(1+i\eta_1)\cdot h_1 + E_2(1+i\eta_2)\cdot h_2 .$$

where,

$\eta_i$ is the loss factor of the i$^{th}$ plate

$E_i$ is the Young's modulus of the i$^{th}$ plate

$h_i$ is the thickness of the i$^{th}$ plate.

Based on Equation (2.2) and (2.3) the effective damping loss factor is:

$$\eta_L^{free} = \frac{\eta_1 \cdot K_{1r} + \eta_2 \cdot K_{2r}}{K_{1r} + K_{2r}} \tag{2.4}$$

where,

$K_{ir} = E_i \cdot h_i$,

subscript "$L$"is for longitudinal motion, and

superscript "$free$" is for the free layer damping treatment.

Typically, the base plate is metallic and the free layer is of polymeric material. The free layer has significantly lower extensional stiffness, i.e. $K_{2R} << K_{1R}$; therefore, the approximate loss factor is:

$$\eta_L^{free} = \eta_1 + \frac{\eta_2 \cdot K_{2r}}{K_{1r}}. \tag{2.5}$$

In an alternate configuration, to increase the second moment of area (or bending stiffness), a spacer is used to further offset the damping layer. Spacer materials such as honeycomb—which have lower values of density, stiffness, and damping—are are used to enhance strain characteristics in layered damping materials.

Ross *et al*. [12] have shown that for $K_{2R} << K_{1R}$ effective damping loss factor is:

$$\eta_B^{free} = \eta_1 + \frac{\eta_2 \cdot K_{2r}\left[\kappa_2^2 + \dfrac{h_{21}^2}{\left(1 + K_{1r}/K_{2r}\right)^2}\right]}{K_{1r}\left[\kappa_1^2 + \dfrac{h_{21}^2}{\left(1 + K_{1r}/K_{2r}\right)^2}\right]} \approx \eta_1 + \frac{\eta_2 \cdot K_{2r}\left(\kappa_2^2 + h_{21}^2\right)}{K_{1r} \cdot \kappa_1^2} \tag{2.6}$$

where,

$\kappa_i = \dfrac{h_i}{2\sqrt{3}}$ is radius of gyration for the i[th] layer,

$h_{21}$ is the distance between the central axes of base layer and damping layer, and subscript "$B$" is for the bending motion.

### 2.1.2 Constrained Layer Damping (CLD) Treatment

In a typical CLD treatment, a layer of visco-elastic damping material is sandwiched between the base structure and a cover plate. The cover plate constrains the response of the composite. In comparison to the base and cover plate, the VEMs used as the damping layer have considerably higher shear modulus and lower Young's modulus. The shear deformation

of the VEM layer, due to the bending of the composite beam, leads to energy dissipation in the form of heat. Stand-offs can also be added to improve the performance of the CLD treatment. A conventional configuration of a CLD treatment is presented in Figure 2.2.

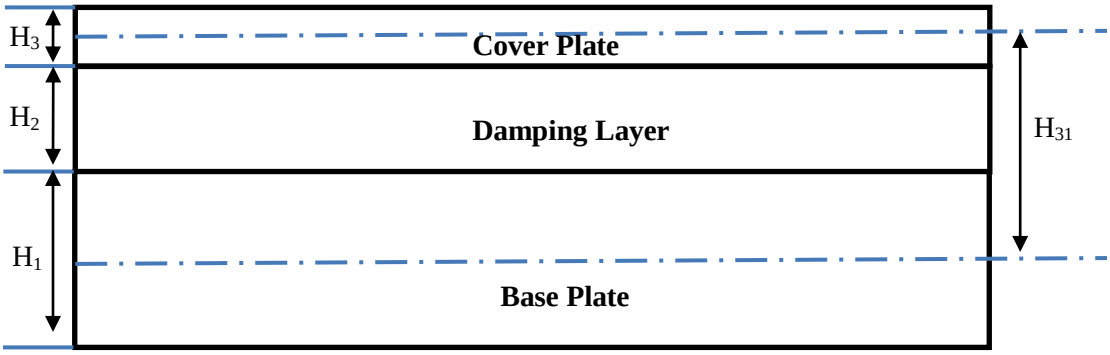


**Figure 2.2: Typical configurations for constrained layer damping treatments.**

The Young's modulus of the damping layer is considered to be insignificant in comparison to that of the base plate or cover plate, i.e. $E_1, E_3 >> E_2$. Ross *et al.*[12] established a theoretical approach to estimate a beam's loss factor based on the material properties. This approach is commonly referred to as RKU analysis. If the structural loss factor of the damping layer is considerably higher than the inherent damping of cover and base plates, i.e. $\eta_1, \eta_3 << \eta_2$, then total flexural rigidity of the composite plate (or beam) is given by [12 and 13]:

$$\begin{aligned} EI = {} & E_1 \cdot \frac{H_1^3}{12} + E_2 \cdot \frac{H_2^3}{12} + E_3 \cdot \frac{H_3^3}{12} - E_2 \cdot \frac{H_2^2}{12}\left(\frac{H_{31} - D}{1+g}\right) \\ & + E_1 H_1 D^2 + E_2 H_2 \left(H_{21} - D\right)^2 + E_3 H_3 \left(H_{31} - D\right)^2 \\ & - \left[\frac{E_2 H_2}{2}\left(H_{21} - D\right) + E_3 H_3 \left(H_{31} - D\right)\right]\left(\frac{H_{31} - D}{1+g}\right) \end{aligned} \tag{2.7}$$

where,

$EI$ is the flexural rigidity,

$E_i$ is the Young's modulus of elasticity of the i$^{th}$ layer,

$H_i$ is the thickness of the i[th] layer,

$\xi_n$ is the n[th] Eigen value, $\xi_n = n\pi$.

$D$ is the distance from the neutral axis of the three layers system to that of the original beam, $H_1$, and it is defined as:

$$D = \frac{E_2 H_2 \left(H_{21} - H_{31}/2\right) + g\left(E_2 H_2 H_{21} + E_3 H_3 + H_{31}\right)}{E_1 H_1 + E_2 H_2/2 + g\left(E_1 H_1 + E_2 H_2 + E_3 H_3\right)} \tag{2.8}$$

where,

$H_{31} = \frac{H_1 + H_3}{2} + H_2$,

$H_{21} = \frac{H_1 + H_2}{2}$,

$g = \frac{G_2}{E_3 H_3 H_2 p^2}$,

$G_2$ is the shear modulus of the damping layer (or second layer),

$p$ is the wave number, $p = \xi_n / L$,

$L$ is the length of the beam,

The natural frequency of the simply supported beam, $\omega_n$, is defined in terms of beam's flexural rigidity, length, mass density ( $\rho$ ), width ( $b$ ) and thickness as:

$$\omega_n = \frac{\xi_n^2}{L^2}\sqrt{\frac{EI}{\rho H b}} \tag{2.9}$$

Finally, the beam's loss factor is estimated from the ratio of imaginary and real parts of the beam's bending rigidity. To estimate damping from Equation (2.7), the material properties are expressed as complex quantities, that is:

$$g \to g(1+i\eta_2),\ E_1 \to E_1(1+i\eta_1),\ E_2 \to E_2(1+i\eta_2), \text{ and } E_3 \to E_3(1+i\eta_3).$$

### 2.1.3 Particle Damping

For particle damping, top and bottom plate sheets in a composite panel are separated by enclosed cavities (typically honeycomb) filled with fine particles. When the structure is excited mechanically, particle-particle and particle-wall interactions cause energy dissipation in the form of friction and/or heat [2]. Referring back to Equation (1.7), higher energy dissipation is indicative of higher loss factor. Liu [2] has reported "The mechanism of particle damping is still not fully understood. It has been found to be closely related to many factors, including particle size, particle density, particle shape, particle surface friction, vibrational direction, packing ratio, vibration amplitude, etc."

## 2.2 Loss Factor Estimation Techniques

The damping loss factor ($\eta$), whether quantified for a structural element or an entire structure, is known to have frequency dependence. This frequency dependence is partly due to frequency dependent material properties of the constituent materials, and partly due to the distribution of strain energy as a function of frequency.

Assigning a single damping loss factor for a structure requires specifying some sort of process to account for the spatially-variable response (mobility or accelerance) upon which the damping loss factor is based. Analytically, an integrated response can be used for the prediction of a frequency- and spatially-dependent loss factor. Experimentally, of course, only a finite number of points are available, which suggests averaging the response from multiple points. Ewing *et al.* [14] have shown that loss factors estimated from responses measured from a small, but sufficiently large, number of randomly-selected points converge

to a common value. It is also known that response is significantly affected by the excitation point as well [9 and 15]. Hence, multiple "randomly-dispersed" excitation points are often considered during experimental trade studies.

Panel damping loss factors can be estimated using a number of techniques requiring the measurement of response and/or excitation. These techniques are established for a range of mathematical models, including both continuous and discretized formulations. Most of the contemporary damping estimation techniques, such as the Impulse Response Decay Method (IRDM), Power Input Method (PIM), and modal curve fitting, are based on the relation between input excitation and measured response. These techniques, typically, are restricted to lower damping levels; hence, the challenge here lies in being able to accurately estimate higher damping loss factors. The Random Decrement Technique (RDT) solely depends on the measured random response caused due to the steady state random excitation. For panels with high loss factor, RDT has outperformed IRDM [11 and 16]. This observation became the driving motivation for a systematic analysis of parameters associated with the conventional loss factor estimation processes. The research methodology for computational and experimental analysis is included in Chapter 3. The performance of these three techniques is presented in Chapter 4 and is discussed in Chapter 5. The theoretical basis of these loss factor estimation methods are explained in the following sections.

### 2.2.1 Impulse Response Decay Method (IRDM)

The equation of motion for a 1DOF system, as shown in Figure 2.3, is:

$$\ddot{x} + 2 \cdot \zeta \cdot \omega_n \cdot \dot{x} + \omega_n^2 \cdot x = f(t) \tag{2.10}$$

where,

$f(t) = \frac{\overline{f}(t)}{m}$ is the mass normalized force

$\omega_n = \sqrt{\frac{k}{m}}$ is the natural frequency of the system

$c_c = 2\sqrt{k \cdot m}$ is the critical damping coefficient

$\zeta = \frac{c}{c_c}$ is the damping ratio

$m$ is the mass

$k$ is the stiffness of the spring.

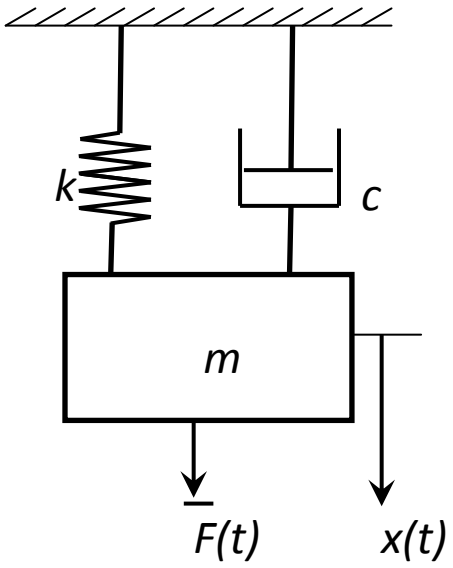


**Figure 2.3: Representative 1DOF system**

The transient forcing function "$f(t)$" can be expressed in terms of its Fourier transformation "$F(\omega)$" as:

$$f(t) = \frac{1}{2\pi} \int_{\omega=-\infty}^{\infty} F(\omega) \cdot e^{i \cdot \omega \cdot t} \cdot d\omega . \qquad (2.11)$$

The response of system to an arbitrary force $f(t)$ is [17 and 18]:

$$x(t) = \int_0^t f(\tau) \cdot h(t-\tau) \cdot d\tau \tag{2.12}$$

where,

$\tau = t_2 - t_1$ is a dummy (or secondary) time variable, and

$h(t)$ is the impulse response.

If $X(\omega)$ is the Fourier transformation of the response function $x(t)$, we can express $x(t)$ in terms of $X(\omega)$ as:

$$x(t) = \frac{1}{2\pi} \int_{-\infty}^{\infty} X(\omega) \cdot e^{i \cdot \omega \cdot t} \cdot d\omega \,. \tag{2.13}$$

The complex frequency response function, $H(\omega)$, is defined as:

$$H(\omega) = \frac{X(\omega)}{F(\omega)}. \tag{2.14}$$

Therefore, response of system can be expressed as:

$$x(t) = \frac{1}{2\pi} \int_{-\infty}^{\infty} H(\omega) \cdot F(\omega) \cdot e^{i \cdot \omega \cdot t} \cdot d\omega \,. \tag{2.15}$$

If the system is excited by an unit impulse, i.e. $f(t) = \delta(t)$, then the (unit) impulse function is:

$$h(t) = \frac{1}{2\pi} \int_{-\infty}^{\infty} H(\omega) \cdot e^{i \cdot \omega \cdot t} \cdot d\omega \tag{2.16}$$

and alternately:

$$H(\omega) = \int_{-\infty}^{\infty} h(t) \cdot e^{-i \cdot \omega \cdot t} \cdot d\omega \tag{2.17}$$

The basic philosophy of IRDM, for loss factor estimation, is embedded in the evaluation of the structure's narrow-band impulse response. Multiple complex FRFs are computed using a "turn-key" DAQ system, and are averaged (in the frequency domain) to provide a sufficiently "converged" estimate. Frequency domain filtering, as shown in Figure 2.4, is implemented to extract band-limited FRFs. The filtered band-limited FRF when inverted, in the Fourier sense, yields a narrow-band impulse response. Using Equation (2.18), the loss factor is estimated from the impulse response's decay rate ($DR$) and the center frequency of the narrow frequency band ($f_c$). The procedure to determine the loss factor from the decay rate, as explained in the Section 2.2.3, is:

$$\eta = \frac{DR}{27.3 \cdot f_c} \tag{2.18}$$

The applied excitation can be either steady-state, by using a mechanical shaker, or transient by using an impulse hammer. The bandwidth of an impulse excitation is sensitive to the type of hammer tip used. A hard tip hammer is used to excite a wider range of frequencies while the soft tip hammer can only excite lower frequency modes. When a hard tip hammer is used on a lightly damped structure, it is very difficult to achieve a single "hit" because the structure's motion reverses before the hammer is retracted causing double (or multiple) hits, which are undesirable. If the excitation point is located on a node line, the loss factors will be over-estimated for that mode of vibration [8 and 19]. With some engineering judgment and precaution taken during experimentation, these errors can be overcome.

The ease of using a roving hammer often overshadows the benefits of using a stationary electro-mechanical shaker. However, the time span, in which the impulsive force has a non-zero magnitude, is very short. For this reason, when exciting a structure using an impulse hammer, the sampling frequency should be high enough to reliably represent the hammer hit. One rule of thumb is to characterize the impulsive force with about 10 measurements in the time domain. When time domain hammer-based response is filtered, and the group delay is taken into consideration, the length of measured response should be long enough to completely capture the decay characteristics of the impulse response. Failing to follow this may result in inaccurate loss factor estimation.

An electro-mechanical shaker is typically mounted on a stand. Unlike the response and excitation due to an impulse hammer, long time histories can be recorded if a mechanical shaker is used.

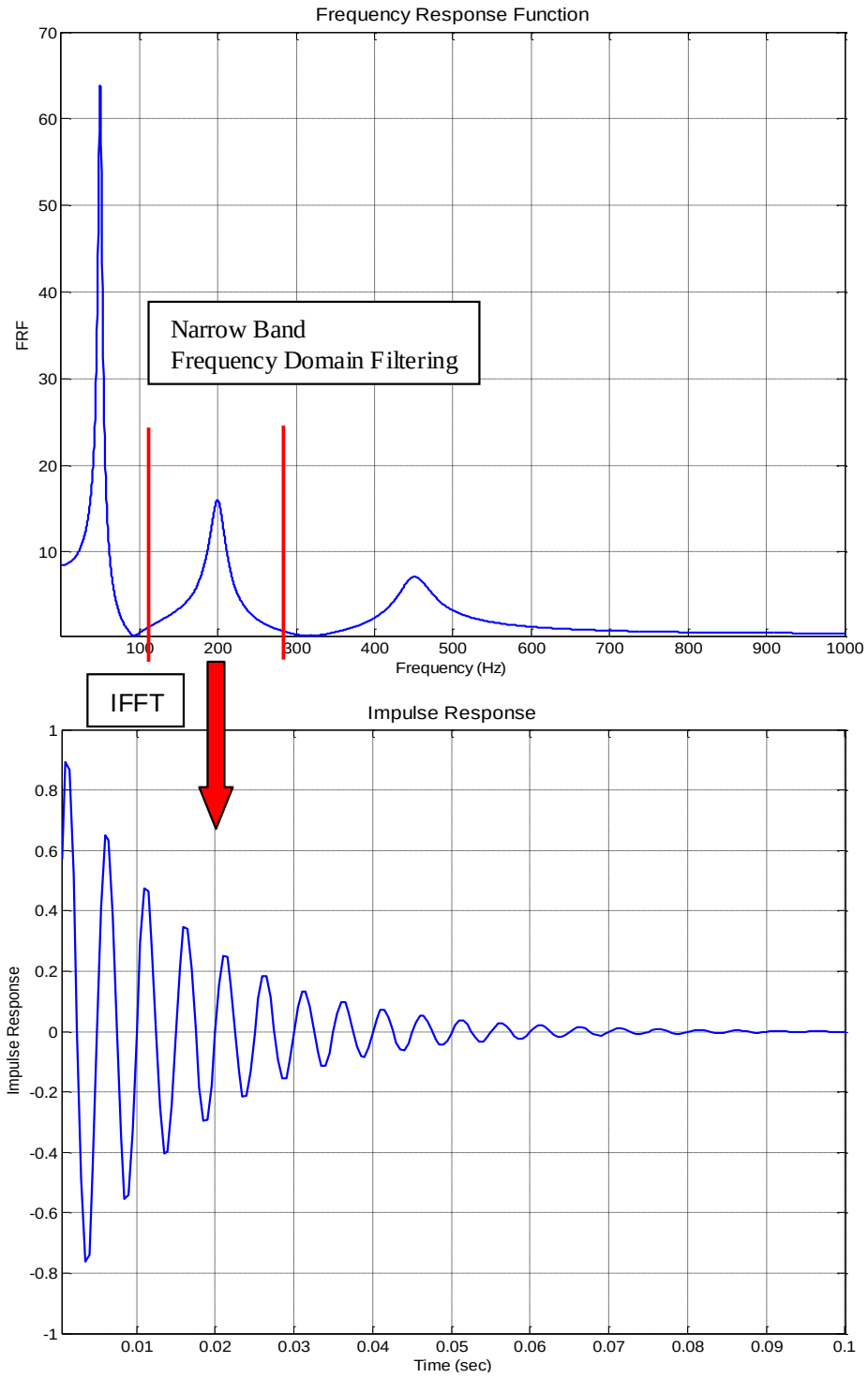


**Figure 2.4: Schematic of Impulse Response Decay Method**

### 2.2.2 Random Decrement Technique (RDT)

The Random Decrement Technique (RDT) was developed by Henry Cole[5] in the late 1960's. Driven by the motive of "on-line failure detection" by monitoring the damping of a structure (excited by white noise), Cole intuitively came up with a process of averaging the time samples with the same initial conditions (or "trigger conditions") to obtain the free decay. In one such trigger setting, as shown in Figure 2.5, the local peak in the measured response inside the trigger band is called a "trigger". The trigger sets up the initial condition for the free decay.

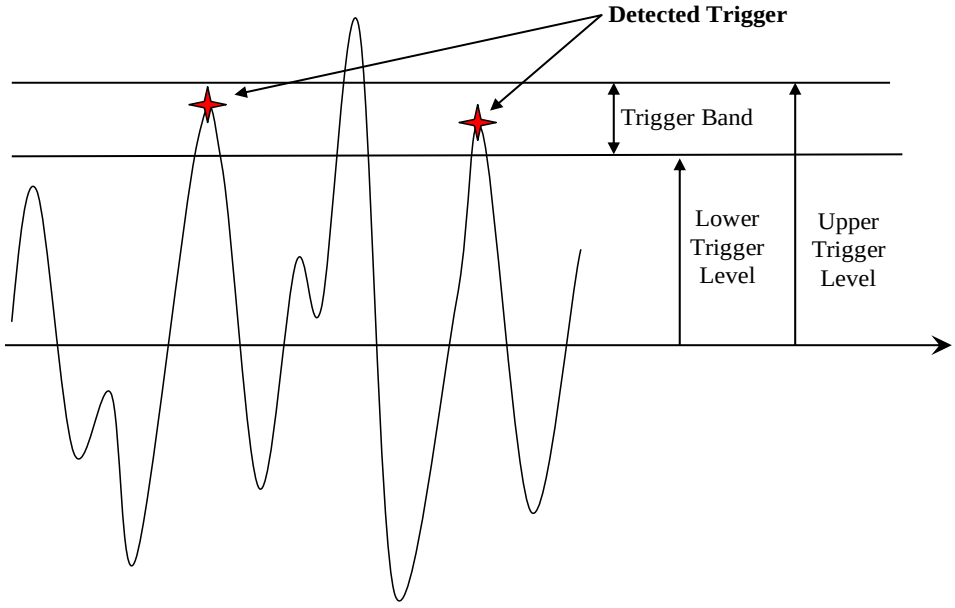


**Figure 2.5: Schematic of a triggering event**

Response of a system to Gaussian white noise excitation is theoretically equal to the time domain convolution of force and impulse response function.

$$x(t) = \int_0^t f(\tau) \cdot h(t-\tau) \cdot d\tau \tag{2.12}$$

The RDT processes starts with a set of response time histories with identical initial conditions. When these time-domain records are averaged, the random component of

response averages out to zero and only the free decay (or, "randomdec signature") survives. This procedure of extracting the free decay, from only the random response, is carried out entirely in the time domain (Refer to Figure 2.8). The choice of the "trigger" or initial conditions, length of samples, filter settings and averaging schemes are discussed in greater details in Reference [11].

RDT, unlike IRDM, PIM, half-power bandwidth and modal curve–fitting techniques, is based solely on the system's response to random excitation. As such, one's expectations for loss factor estimation using RDT might be somewhat low. In fact, Ewing *et al*. [14] have shown that, for panels with very high damping loss factors ($\approx 0.1$), RDT out-performs IRDM.

For such highly damped structure, there can be a significant portion of the structure which is not experiencing "reverberant field" conditions, especially in higher frequency bands. That is, localized disturbances "die-out" before they can reflect off the panel boundaries. Therefore, the usual input-output relationships of forced vibration are not in force. Specifically, the response is higher than what would be expected in a reverberant field where the energy is uniformly distributed. Instead, kinetic energy is flowing away from the excitation point and is attenuating due to damping of plate. Thus, the energy level in the "near field" (close to the excitation location) is higher than elsewhere, resulting in a higher response level than the "far field". Since the level of response is inversely proportional to damping, the loss factor predicted inside the near field, by forced vibration theory, is underestimated.

The advantage of RDT stems from the fact that it does not depend on an input–output relationship. Instead, the temporal decay rate of response at a point on a structure is equal to the decay rate of that point's response autocorrelation function. For RDT, it simply does not matter if a response is measured inside the near field or not. Loss factor estimation processes

based on kinetic energy measurements, like PIM, are presumably best implemented by not including response measurements in the near field.

For the studies presented herein, the impulse response function is convolved with a random force to generate an arbitrarily-long random response signal. This signal is then "processed" to extract the randomdec signature. The random response is first sampled for a particular set of trigger settings and then the ensemble of these samples yield the randomdec signature. In this context, the trigger setting refers to attainment of response in a pre-selected ***amplitude band*** with ***zero slope***. RDT's theoretical basis is presented in the following sections.

#### 2.2.2.1 Theoretical Background

The randomdec signature ($D_{x0}$) for a signal, $x(t)$, with initial conditions $\dot{x}(0) = 0$ and $x(0) = 0$, is proportional to the autocorrelation function, $R_x(\tau)$, of the system and their relation can be expressed through the following equation [20]:

$$D_{x0}(\tau) = x_0 R_x(\tau) / R_x(0) \tag{2.19}$$

where,

$x_0$ is the initial displacement, or trigger's amplitude level

$\dot{x}_0$ is the initial velocity, or trigger's slope; if peaks in the response are selected as trigger then, $\dot{x}_0 = 0$

$\tau = t_2 - t_1$ is a dummy (or secondary) time variable

$t_2$ and $t_1$ corresponds to values of time 't' on a linear time scale.

For a single degree of freedom system excited with Gaussian, zero-mean, white noise, the randomdec signature is equivalent to the autocorrelation function, as given in Equation (2.20), below [20]:

$$D_{x0}(\tau) \equiv E[x(t_2) \mid x(t_1) = x_0 and \dot{x}(t_1) = \dot{x}_0] \tag{2.20}$$

The autocorrelation function can be normalized to be represented in the following form [21]:

$$R_x(\tau) = Ce^{-\zeta\omega_n\tau}\cos(\omega_d\tau) \tag{2.21}$$

where,

$C = x_0 / R_x(0)$

$\omega_n$ is the natural frequency

$\omega_d$ is the damped natural frequency

$\zeta$ is the damping ratio

$x(t)$ is the measured response.

Comparing Equations (2.19) and (2.21), it is concluded that the randomdec signature is equivalent to free decay for a 1DOF system excited with Gaussian, zero-mean, white noise [21].

Figure 2.6 represents a response record satisfying a trigger event (top figure), the resulting autocorrelation function and the magnitude of the Hilbert transformation—to generate the equivalent of an exponentially decaying envelope—of the positive portion of the autocorrelation function (bottom figure). Later, Vandiver[20] proved that the averaged response is a free decay only when the excitation is Gaussian, zero-mean, white noise.

To get an arbitrarily long history of random response, the impulse response function is convolved with random force. The Gaussian white noise—a zero mean true random—force has a constant power spectral density but random phase. Figure 2.7 illustrates the frequency domain characteristics of a simulated band-limited random force. In this figure, the power spectral density of force is constant in the frequency range of 10 Hz to 200 Hz. The random response generated from this force will also be random and in a narrow–band of 10 Hz to 200 Hz.

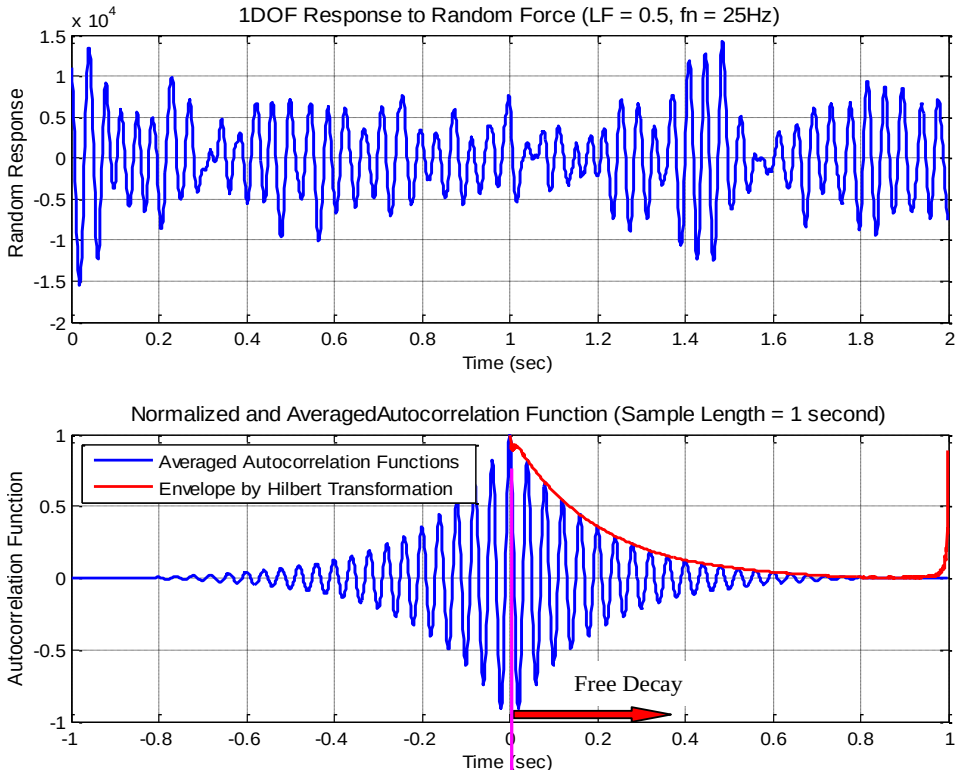


**Figure 2.6: Schematic of process of loss factor estimation using autocorrelation functions**

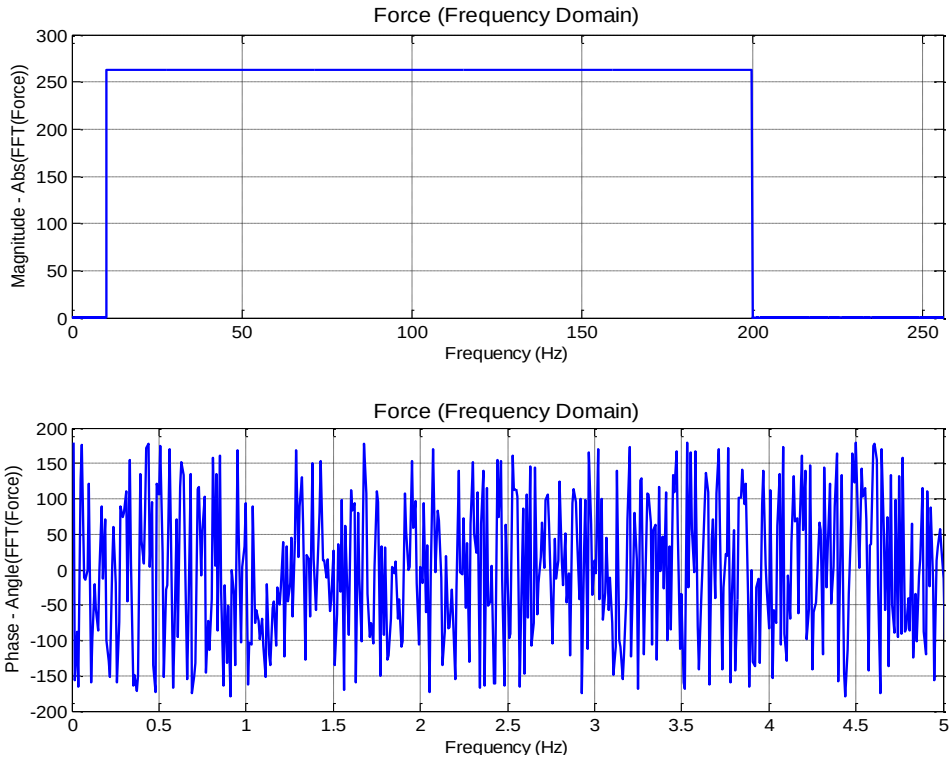


**Figure 2.7: Gaussian white noise – Frequency Domain**

In Figure 2.8, the first three subplots illustrate the triggered samples from a response filtered in a narrow frequency band. The final subplot is an average of 1000 such triggered samples. Although, some "beating" is observed, the averaged response clearly decays. The beating indicates there are two or more strong resonances within the narrow frequency band.

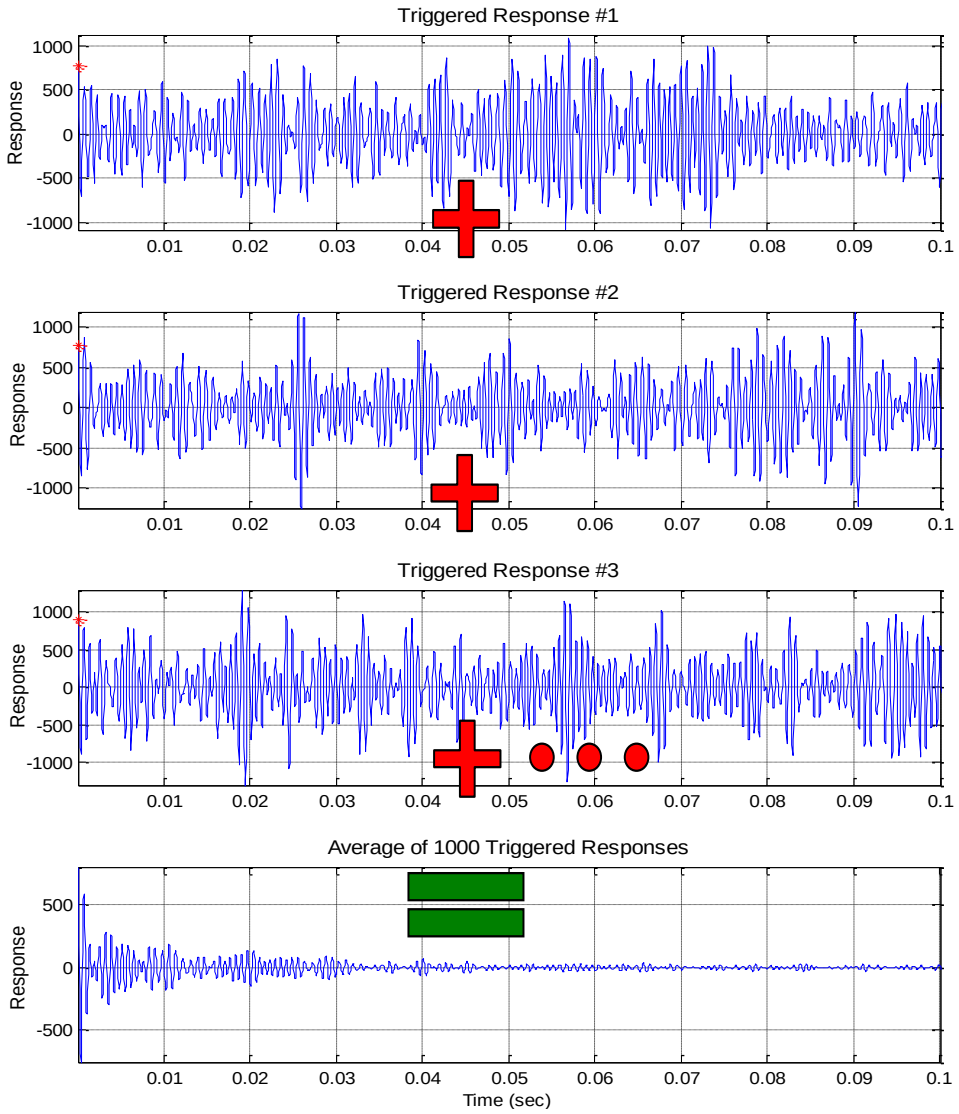


**Figure 2.8: Schematic of the Random Decrement Technique**

As RDT is not very popular among structural dynamists, the literature pertaining to the same is very limited with respect to other known techniques, such as IRDM and PIM. Mathematical explanations of RDT have already been published, but the limitations and optimum variable settings for experimental analysis are still a matter for study. Theoretically, RDT can be used for any damping levels. For a lightly damped system longer time histories,

as compared to highly damped panels, are required. Due to practical limitations, on data storage and analysis, RDT is not recommended for lightly damped systems [11].

### 2.2.3 Theory Associated With Decay Rate Based Loss Factor Estimation

The impulse response function for a 1DOF system is mathematically described as [17, 18 and 22]:

$$h(t) = \frac{e^{-\zeta \cdot \omega_n \cdot t}}{m \cdot \omega_d} \sin(\omega_d \cdot t) \tag{2.22}$$

where,

$h(t)$ is the impulse response function

$m$ is the mass of the system

$\omega_n$ is the natural frequency (rad/sec)

$\omega_d$ is the damped natural frequency (rad/sec); $\omega_d = \omega_n \sqrt{1-\zeta^2}$

$\zeta$ is the damping ratio.

The exponential decay, $e^{-\zeta \cdot \omega_n \cdot t}$, for a 1DOF system subjected to non-zero initial displacement and zero velocity, is identical to the exponential decay of the impulse response function. The Hilbert transformation of the free decay or impulse response can be used to determine the exponential decay of the free decay or impulse response. Using Equation (2.23), the loss factor can be estimated from the decay rate of the exponentially decaying envelope of the impulse response or free decay [1 and 19].

$$\eta = \frac{DR}{27.3 \cdot f_n} \tag{2.23}$$

where,

$f_n$ is the 1DOF system's natural frequency.

When dealing with a MDOF system, $f_n$ is replaced by $f_c$ – the band's central frequency.

Equation (2.23) is derived below. The decay rate is defined as:

$$DR = \frac{\Delta H}{\Delta t}$$

where,

$\Delta t = t_2 - t_1$ is the time period in for $DR$ estimation

$\Delta H$ is the change in amplitude of the exponential decay curve in $\Delta t$ seconds

$t_1$ and $t_2$ are instances of time between which the decay rate is to be estimated

$H$ is measured in decibels, that is:

$$H_1 = 20 \cdot \log_{10}(e^{-\zeta \cdot \omega_n \cdot t_1})$$

$$H_2 = 20 \cdot \log_{10}(e^{-\zeta \cdot \omega_n \cdot t_2})$$

$$\Rightarrow \Delta H = H_2 - H_1 = -\zeta \cdot \omega_n \cdot t_2 \cdot 20 \cdot \log_{10} e - (-\zeta \cdot \omega_n \cdot t_1 \cdot 20 \cdot \log_{10} e)$$

$\omega_n = 2\pi \cdot f_n$ is the cyclic frequency (radians/ seconds)

$$\Rightarrow \zeta = \frac{\Delta H}{\Delta t \cdot 2\pi \cdot f_n \cdot 20 \cdot \log_{10} e} \quad \text{and} \quad 20 \cdot 2\pi \cdot \log_{10} e = 54.5757$$

Equation (1.4) $\Rightarrow 2\zeta = \eta = \frac{DR}{27.3 \cdot f_n}$

It is evident from equation (2.23) that the decay rate is proportional to the loss factor and is inversely proportional to system's natural frequency.

The magnitude of Hilbert transformation of the impulse response is nearly equal to the exponential decay of the impulse response, as shown in Figure 2.9, that is:

$$e^{-\omega_n \cdot \zeta \cdot t} \approx \left| H(h(t)) \right| \tag{2.24}$$

where,

$H()$ is the Hilbert transformation of a function

$h(t)$ is the impulse response function.

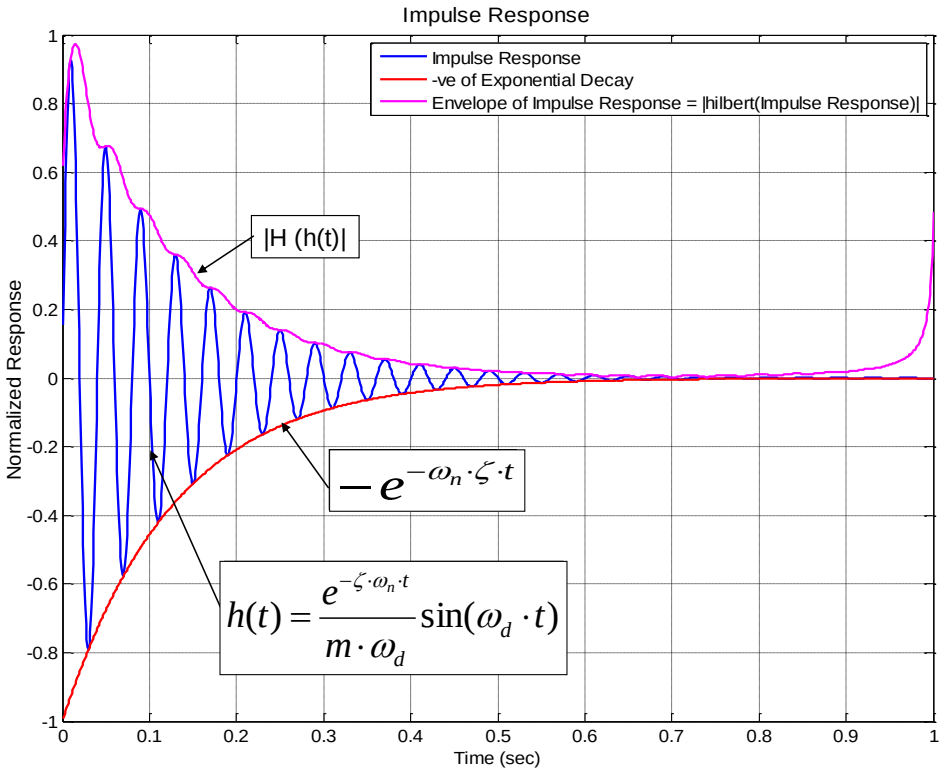


**Figure 2.9: Impulse response and exponential decay of 1DOF system**

In his book titled "Theory and Application of Statistical Energy Analysis", Lyon [1] suggests that the decay rate can be easily determined when the response signal is plotted as the log-rms amplitude versus time. The decay rate obtained by the log-rms amplitude is equivalent to the decay rate estimated from the exponential decay (measured in decibels-dB) versus time. In either approach, the decay rate (dB/sec) of an exponentially decaying envelope is measured. For a single mode and constant loss factor, the decay curve (in dB) is

linear with the slope of this curve being equal to the decay rate. (Refer to Figure 2.10). The decay curve (or $DC$), of an impulse response, can be calculated by the following equation.

$$DC = 20 \cdot \log_{10} | H(h(t)) | \tag{2.25}$$

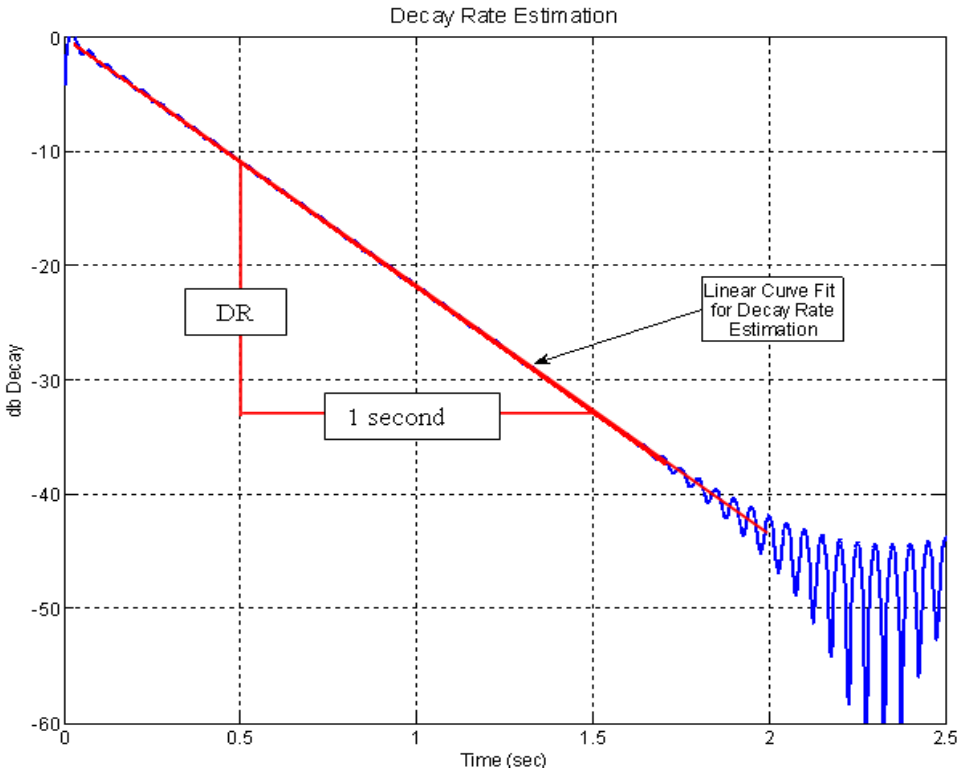


**Figure 2.10: dB decay curve of 1DOF system**

### 2.2.3.1 Slope-Fitting

The decay curves from experimental or computational analyses are rarely linear like the decay "slope" in Figure 2.10. Therefore, to estimate decay rate, a least squares linear curve fit can be implemented. The curve fitting can involve either a user or be automated. Automated slope fitting is recommended especially when a very large number of decay curves are to be evaluated.

The proposed automated slope fitting algorithm identifies the local peaks in the dB decay curves and then fits a least squares linear curve through them. The slope of the least

squares linear curve fit is the decay rate. If less than two peaks are detected, which can occur at high damping levels, manual slope fitting is chosen over the automated slope fitting approach to avoid bias.

The initial slope of the decay curve is proportional to the total loss factor of the system, hence the curve fit algorithm is applied to determine the initial decay rate [1]. Figure 2.11 presents the schematic of automated slope fitting on the decay curve. The markers '*' are the local peaks in the decay curve and the straight line is the linear slope fit through the indicated local peaks. MATLAB's least squares linear curve fitting function is implemented in this automated slope fitting approach.

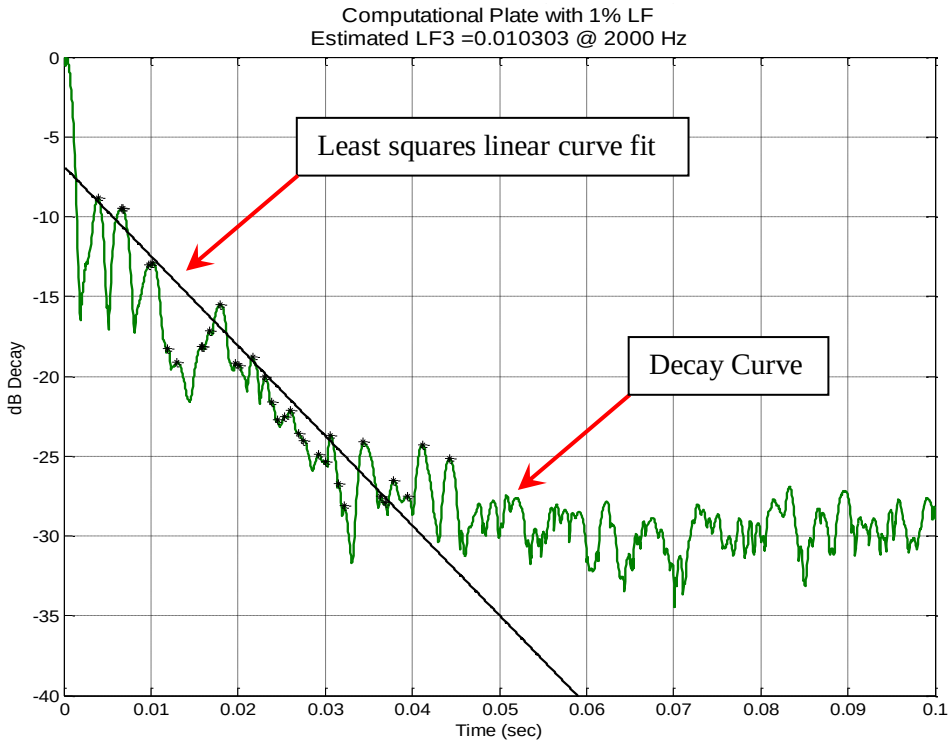


**Figure 2.11: Slope fit and loss factor estimation**

Manual slope fitting may turn out to be a better option for a small number of decay curves, but when a large number of curves are to be fitted, human error in fitting a curve is inevitable and the results are difficult to reproduce. On the other hand, automated slope fitting

is faster and efficient, but its performance must be studied extensively before general use. It is suggested that the slope fitting should be automated with some supervision or control over the process. In the analysis presented, all the slope fits from which the loss factors are estimated are visually inspected. For decay curves on which the slope fitting does not seem to work accurately, the manual slope fitting approach is used.

### 2.2.4 Power Input Method (PIM)

The Power Input Method (PIM) is based on an energy balance between input power and measured total energy. The loss factor, using PIM, is defined in terms of dissipated power and total energy through the following relations [1, 2 and 8]:

$$\eta = \frac{P_D}{\omega \cdot E_{Tot}} = \frac{E_D}{2 \cdot \pi \cdot E_{Tot}} \tag{2.26}$$

where,

$\eta$ is the loss factor

$\omega$ is the frequency in radians/sec

$P_D$ is the dissipated power

$E_D$ is the dissipated energy

$E_{Tot}$ is the total mechanical energy.

Once the excitation and response levels have reached steady state the power dissipated by the structure is equal to the input power and the modified Equation (2.26), for PIM based loss factor estimation, is:

$$\eta = \frac{P_{IN}}{2\pi \cdot f_c \cdot E_{Tot}} \tag{2.27}$$

where,

$P_{IN}$ is the input power and $P_D = P_{IN}$ after steady-state is attained,

$f_c$ is the band's central frequency (Hz).

The total energy is essentially the sum of kinetic energy and potential energy. That is:

$$E_{Tot} = E_{P.E.} + E_{K.E.} \tag{2.28}$$

where,

$E_{P.E.}$ is the potential energy

$E_{K.E.}$ is the kinetic energy.

Often, it is complicated to measure the potential energy, hence the kinetic energy is measured, instead. For $\eta < 0.3$, the kinetic energy within 5% of the potential energy, and thus the total energy is approximately twice the kinetic [1 and 2]:

$$E_{P.E.} \approx E_{K.E.} \tag{2.29}$$

$$(2.28) \Rightarrow E_{Tot} = 2 \cdot E_{K.E.} \tag{2.30}$$

Loss factor as a function of a narrow band central frequency, $f_c$, is:

$$\eta(f_c) = \frac{P_{IN}(f_c)}{2\pi \cdot f_c \cdot E_{Tot}(f_c)} \tag{2.31}$$

Experimentally, either velocity or acceleration can be measured. To measure accelerations, accelerometers are used and to measure velocity, a Polytec scanning laser vibrometer is used. Mathematically, input power and kinetic energy (or half of the total energy) is defined in equations (2.32) through (2.34) [23 and 24].

$$P_{IN}(\omega_c) = \frac{1}{\pi} \int_{\omega_1}^{\omega_2} \mathrm{Re}\left\{ F(\omega) \cdot \dot{X}^*(\omega) \right\} \cdot d\omega \tag{2.32}$$

$$P_{IN}(\omega_c) = \frac{1}{\pi} \int_{\omega_1}^{w_2} \mathrm{Im}\left\{ F(\omega) \cdot \ddot{X}^*(\omega) \right\} \cdot d\omega \tag{2.33}$$

$$E_{K.E.}(\omega_c) = \frac{M}{2\pi}\int_{\omega_1}^{\omega_2}\left|\dot{X}(\omega)\right|^2 \cdot d\omega \tag{2.34}$$

$$E_{K.E.}(\omega_c) = \frac{M}{2\pi}\int_{\omega_1}^{\omega_2}\left|\frac{\ddot{X}(\omega)}{\omega}\right|^2 \cdot d\omega \tag{2.35}$$

where,

$\omega_c$ is the narrow band's central frequency

$\omega_1$ & $\omega_2$ are the start and end frequencies of bandwidth of analysis

$P_{IN}(\omega_c)$ is the input power measured for the narrow band with central frequency $\omega_c$

$E_{K.E.}(\omega_c)$ is the measured kinetic energy for the narrow band with central frequency $\omega_c$

$\dot{X}(\omega)$ is the complex velocity response—in the frequency domain

$\dot{X}^*(\omega)$ is the complex conjugate of velocity response—in the frequency domain

$F(\omega)$ is the force—in the frequency domain

$\ddot{X}(\omega)$ is the complex acceleration response—in the frequency domain

$\ddot{X}^*(\omega)$ is the complex conjugate of acceleration response—in the frequency domain

$M$ is the mass of the structure.

Alternatively, loss factor in terms of mobility is defined as [2 and 8]:

$$\eta(\omega) = \frac{\mathrm{Re}\left(Y_{ff}(\omega)\right)}{\sum_{i=1}^{N} m_i \cdot \omega \cdot \left|Y_{if}(\omega)\right|^2} \tag{2.36}$$

where,

$Y_{if}(\omega)$ is the mobility between the driving point *f* and point *i*,

$Y_{ff}(\omega)$ is the driving point mobility

$m_i$ is the distributed mass = $\frac{M}{N}$, and

$N$ refers to the number of measurement locations.

Most of the conventional modal analysis instruments and software are capable of accurately measuring all of the terms presented in Equation (2.36).

Note that the total energy does not include in-plane vibrations. For a linear model, the in-plane and out-of-plane motions are not coupled. Therefore, when the applied force is normal to surface, the in-plane motion and energy stored in in-plane motion can be ignored.

Also note that the total energy dissipated includes losses due to radiation to the air. But, for engineering structures vibrating in air, the magnitude of radiation loss factors rarely exceeds 0.001 [37]. The radiation loss factor is significantly smaller as compared to the structural damping loss factor of panels with CLD treatment. Therefore, energy dissipation due to sound radiation is not considered.

When modeling the structure using Finite Element Analysis (FEA) tools, such as MSC/NASTRAN, strain energy is readily available and is an appropriate measure of potential energy in an elastic system. Therefore, the total energy can be estimated as in Equation (2.37). Eventually, the loss factor is estimated using Equation (2.38) which is modified form of Equation (2.36).

$$E_{Tot} = E_{S.E.} + E_{K.E.} \tag{2.37}$$

$$\eta(\omega) = \frac{\frac{1}{2} \cdot |F(\omega)|^2 \cdot \mathrm{Re}(Y_{ff}(\omega))}{\omega \cdot (E_{S.E.} + E_{K.E.})} \tag{2.38}$$

As strain is the first derivative of displacement, an effort should be made to use a mesh with sufficient fineness to ensure convergence of strain to avoid numerical error(s). In

order to simulate modal response of the structure, the finite element model should have a *sufficient* number of degrees of freedom, possibly by using *higher* order elements. In an experiment, it is difficult to accurately measure the strain energy. To maintain consistency in experimental and computational analyses, loss factor estimated from PIM is measured only from the kinetic energy.

#### 2.2.4.1 Application of PIM in Statistical Energy Analysis (SEA)

When dealing with complex and/or connected structures a significant variation in modal parameter estimations are observed. Thus, the value of estimated loss factor also falls in a broader range. In cases like these, the system characteristics are statistically determined, thereby accepting a certain degree of randomness. The statistical measurement of energy and power balance to estimate structure's damping loss factors (or coupling loss factors in case of connected subsystems) form the founding principles of Statistical Energy Analysis (SEA). In recent years, SEA has established itself, as an important tool, in the field of vibro-acoustic research.

Using the power and energy relations, Manning and Lee [25] analyzed beam and plate interactions, while Mercer *et al*.[26] have tested weakly coupled oscillators. Theory associated with transient SEA has been discussed and presented by Pinnigton and Lednik [26]. Ewing and Dande [28] and Ewing *et al*. [29 and 30] have analyzed these systems for transient excitation. The coupling loss factors and damping loss factors, for two connected panels, are determined using the following energy and power balance equations [23 and 24]:

$$\begin{bmatrix} \eta_1 & \eta_{21} \\ \eta_{12} & \eta_2 \end{bmatrix} = \frac{1}{2 \cdot D \cdot \omega_c} \begin{bmatrix} E^{in}{}_{1,I} \cdot \varepsilon^k{}_{2,II} - E^{in}{}_{2,II} \cdot \varepsilon^k{}_{2,I} & E^{in}{}_{1,I} \cdot \varepsilon^k{}_{1,II} \\ E^{in}{}_{2,II} \cdot \varepsilon^k{}_{2,I} & E^{in}{}_{2,II} \cdot \varepsilon^k{}_{1,I} - E^{in}{}_{1,I} \cdot \varepsilon^k{}_{1,II} \end{bmatrix} \tag{2.39}$$

where,

$D = \varepsilon^{k}{}_{1,I} \cdot \varepsilon^{k}{}_{2,II} - \varepsilon^{k}{}_{2,I} \cdot \varepsilon^{k}{}_{1,II}$

$\eta_{12}$ and $\eta_{21}$ are the coupling loss factors

$\eta_1$ and $\eta_2$ are loss factors of the individual plates

$E_i^{\,in}(\omega_c)$ is the input energy at a point within a bandwidth $\Delta\omega$ centered on $\omega_c$:

$$E_i^{\,in}(\omega_c) = \frac{1}{\pi} \int_{\omega_c - \Delta\omega/2}^{\omega_c + \Delta\omega/2} \mathrm{Im}\{F^*(\omega) A(\omega)/\omega\} d\omega \tag{2.40}$$

$\varepsilon^k(\omega_c)$ is the kinetic energy at a point integrated over a narrow frequency range:

$$\varepsilon_i^{\,k}(\omega_c) = \frac{M}{2 \cdot \pi} \int_{\omega_c - \Delta\omega/2}^{\omega_c + \Delta\omega/2} |A(\omega)|^2 / \omega^2 \, d\omega \tag{2.41}$$

$A(\omega)$ is the Fourier transform of the acceleration of a measurement point

$F^*(\omega)$ is the complex conjugate of the Fourier transform of the input force

$M$ is the mass of the plate.

Regarding the subscripts:

I and II correspond to the plate on which the response is measured

1 and 2 correspond to the plate on which the force or excitation is applied.

The coupled panels, tested by KUAE researchers, are shown in the following Figure 2.12. In the left figure two plates are connected along a point and in the right figure the plates are connected along a line.

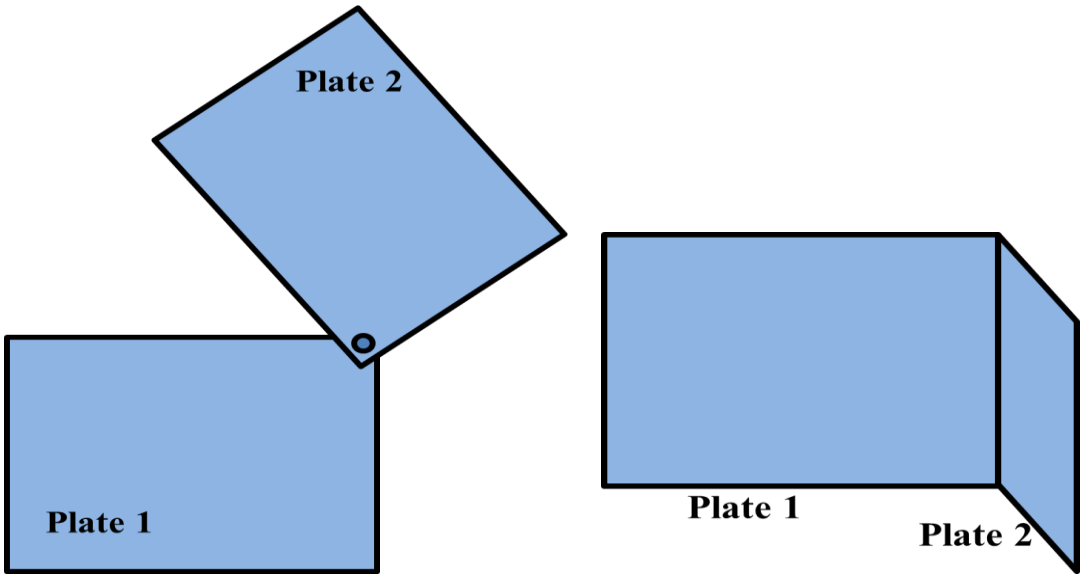


**Figure 2.12: Schematic representation of two connected panels analyzed using SEA**

## 2.3 Radius of the Direct Field

Consider a flat panel on which an oscillatory point force is applied. The energy from this excitation flows radially outward towards the panel boundaries. Wave reflections, from the boundaries, along with the incident wave set up a 'reverberant field'[1 and 31]. In this reverberant field the measured kinetic energy is nearly uniform. If the panel is highly damped and/or the panel size is very large, then these radial waves will "die-out" before they reflect off the boundaries—thereby never setting up a reverberant field. The direct field is defined as the region near the excitation location where the kinetic energy has not yet converged to the near-uniform value of the reverberant field.

Kinetic energy is directly proportional to the squared velocity. In the direct field the mean square velocity is given by Equation (2.42) and in the reverberant field the mean square velocity is given by Equation (2.43). Because the velocity components, direct and indirect,

are incoherent the total mean square velocity is the summation of $\left\langle v_D^2 \right\rangle$ and $\left\langle v_R^2 \right\rangle$, as presented in Equation (2.44).

$$\left\langle v_D^2 \right\rangle = \frac{P_{IN}}{2\pi \cdot \rho_s \cdot c_g \cdot r} e^{\frac{-\omega \cdot \eta \cdot r}{c_g}} \tag{2.42}$$

$$\left\langle v_R^2 \right\rangle = \frac{P_{IN}}{\omega \cdot \eta \cdot M} e^{\frac{-\omega \cdot \eta \cdot (d/2)}{c_g}} \tag{2.43}$$

$$\left\langle v^2 \right\rangle = \left\langle v_D^2 \right\rangle + \left\langle v_R^2 \right\rangle \tag{2.44}$$

At large distances from the excitation location the reverberation field will dominate, and close to the excitation location the direct field will dominate. At the boundary between the direct and reverberant field, these fields contribute equally. The distance of this boundary, from the excitation location is "the radius of the direct field i.e. $R_D$ " and it is mathematically expressed as [1]:

$$R_D = \frac{\omega \eta M}{2\pi \rho_s c_g} \tag{2.45}$$

where,

$\rho_s$ is the surface density = $\frac{M}{A_p}$ (Kg/m$^2$ or lbm/in.$^2$)

$M$ is the mass of the plate (Kg or lbm)

$A_p$ is the area of the plate (m$^2$ or in.$^2$), and

$c_g$ is the group velocity (m/sec or in./sec).

The group velocity is twice the phase velocity $c_\phi$ and phase velocity is expressed as:

$$c_\phi = \sqrt{\omega \cdot \kappa \cdot c_l} \tag{2.46}$$

where,

$\kappa$ is the radius of gyration, $\kappa = \frac{h}{2\sqrt{3}}$,

$h$ is the thickness of the plate,

$c_l$ is the wave speed in material $\cong$ 17000 ft/sec $\cong$ 204000 in./sec $\cong$ 5181 m/sec for steel or aluminum.

Therefore the group velocity is:

$$(2.46) \Rightarrow \; c_g = 2 \cdot \sqrt{2\pi \cdot f \cdot \frac{h}{2\sqrt{3}} \cdot c_l}$$

A further simplified equation the size of the direct field is:

$$R_D = \frac{2\pi \cdot f \cdot \eta \cdot M}{2\pi \cdot \frac{M}{A_p} \cdot 2 \cdot \sqrt{2\pi \cdot f \cdot \frac{h}{2\sqrt{3}} \cdot c_l}} = \frac{A_p \cdot \eta}{2.694} \cdot \sqrt{\frac{f}{h \cdot c_l}} \qquad (2.47)$$

A good estimate of an upper bound on the characteristic dimension of the reverberant field is the mean free path,"$d$". This mean free path is the distance traversed between reflections. Mathematically, mean free path for a regular polyhedron is given by [1]:

$$d = \frac{\pi \cdot A_p}{P} \qquad (2.48)$$

where,

$P$ is the perimeter of the plate.

### 2.3.1 Effect of the Size of the Direct Field on PIM-Based Loss Factor Estimation

Note that the radius of the direct field is directly proportional to the loss factor and the square root of frequency. The effect of damping on the size of the direct field is represented in Figure 2.13 through experimentally-derived velocity-squared fields for two plates: the left being a highly damped ($\eta \approx 0.10$) plate and the right one is a bare plate with a very low damping level [9, 15 and 32]. The experimental activities are discussed in more detail in Chapter 3. Figure 2.13 includes circles with the radius of the direct field predicted by Equation (2.45). Viewing the side view of the surface of the velocity squared field of the damped plate, there appears to be a rather uniform amplitude—indicative of reverberant field—outside the radius of the direct field for an infinite plate.

Both plates were mechanically excited at the center using a mechanical shaker. A persistent narrow-band point force was applied using a conventional stinger-shaker assembly. The spatial variation of kinetic energy is established on the basis of the velocity-squared field. To record the velocity, a scanning laser vibrometer was used.

The key assumption for input-output based experimental loss factor estimation techniques is that the measurements are recorded from the reverberant field. In the case of an undamped plate, the direct field is so small that almost all randomly positioned response measurements would be in the reverberant field. As the radius of the direct field is proportional to the level of damping, for a highly damped plate the direct field can be large enough to cover the entire plate. That is, for a highly damped plate the kinetic energy measurements are more likely to be recorded in the direct field—where kinetic energy has not yet attenuated to a uniform level.

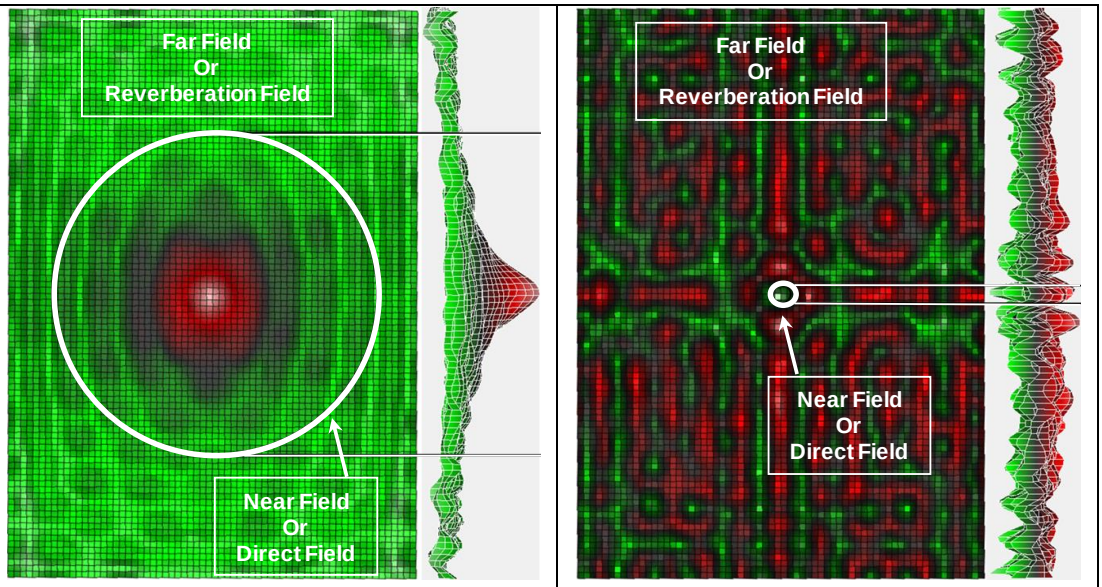


Damped plate analyzed at one third octave central frequency of 1000 Hz. $R_D$=13.5 in. (0.3416 m)

Undamped plate analyzed at one third octave central frequency of 1000 Hz. $R_D$=0.75 in. (0.0192 m)

**Figure 2.13: Velocity-squared fields from measurements on two plates: damped (upper) and undamped (lower). Theoretical radii of direct field estimated from Equation (2.45) are indicated.**

The kinetic energy measured inside the direct field is higher than that in the reverberant field. Therefore, for a highly damped and small plate, loss factor estimation based on randomly positioned sensors–which have a higher probability of being inside the direct field–will underestimate damping. For such highly-damped structures, there can be a significant portion of the structure which is not experiencing reverberant field conditions, especially in higher frequency bands. That is, localized disturbances "die-out" before they can reflect off boundaries. Therefore, the usual input-output relationships of vibration are not in force.

Panels with three different sizes, i.e. different mean free paths, are analyzed in the computational and experimental analyses. In this research the correlation of loss factor with respect to distance from excitation location is evaluated. Special attention is given to the role of $R_D$ and $d$ in the distance-based loss factor estimation study.

# 3 Research Methodology

The qualitative analysis of loss factor estimation techniques was performed on panels with two damping levels and three sizes. A CLD treatment is applied to the plates to achieve the desired damping levels. For these panels the dimensions and damping level are tabulated in Table 3.1 and 3.2.

The estimated loss factors of the panels analyzed experimentally are in the range, 0.05 to 0.13. The value of loss factor assigned to the computationally modeled plates, of the similar size as that of the physical plates, is either 0.01 or 0.10. The conclusions drawn from the computational models are directly adapted in the experimental studies.

The performance of loss factor estimation techniques—IRDM, PIM, and RDT—is evaluated by comparing the loss factor estimated from multiple response measurement locations on the panel. At each of these measurement locations, the loss factor is determined by processing the velocity based FRFs (or mobility). Frequency domain filtering is implemented to extract the band–limited FRF. A detailed discussion of the process, test, and analysis parameters is included in the following sections.

## 3.1 Panel Parameters

To evaluate the effect of mean free path on the loss factor estimation process, panels with three sizes are analyzed. The three panel sizes are labeled: “Small”, “Medium” and “Large”. The Medium panel is half the size of the Large panel and the Small panel is approximately half the size of the Medium panel.

The size of the direct field is proportional to loss factor; therefore, panels with two damping levels are analyzed. That is, the performance of loss factor estimation techniques is

evaluated for six different panels. These panel properties are presented in the following sections.

### 3.1.1 Panel Damping Loss Factor Range

Most of the experimental loss factor estimation techniques rely on the assumption that the dissipation of energy is due to viscous damping. Typically, for a structure with CLD treatment, the loss factor will range between 0.01 and 0.2 [1]. The empirical damping loss factor range for thin steel and aluminum plates is represented in Figure 3.1 (adapted from Figure 9.4 of Reference [1]). The plates analyzed experimentally and computationally have estimated loss factors in the similar range.

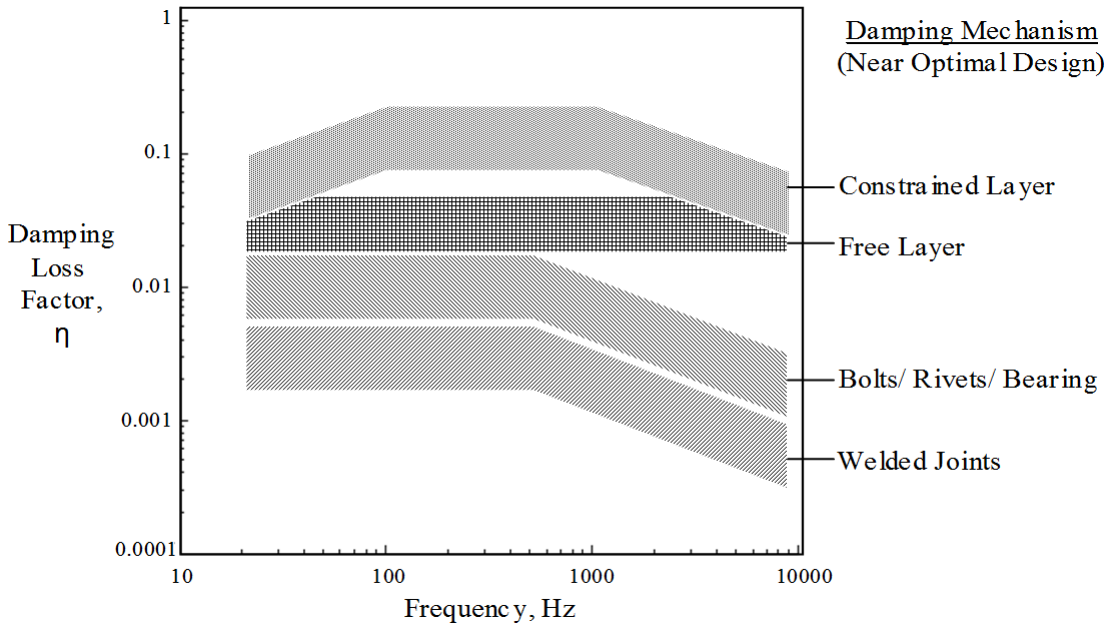


**Figure 3.1: Empirical damping loss factors for steel and aluminum thin plates and shells.**

### 3.1.2 Panel Sizes

The size of the direct field of an infinite plate is dependent on the frequency of analysis and the loss factor of the panel, while mean free path is dependent on the panel size. For the largest panels tested, the panel size is greater than the direct field. For the Small and

Medium plates, the size of the direct field in certain frequency bands is larger than the panel size. The significance of $R_D$ and $d$ in the distance based loss factor estimation processes is established by testing panels of different sizes and damping levels.

The summary of panel dimensions is presented in Figure 3.2, Table 3.1 and 3.2.

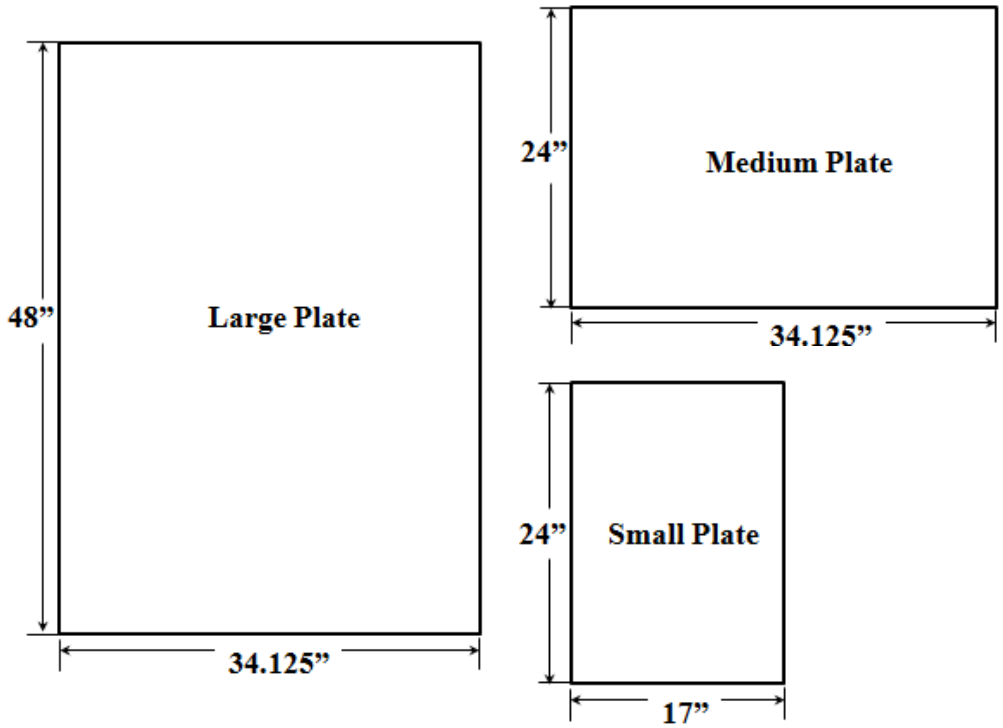


**Figure 3.2: Pictorial summary of panel dimensions**

For the experimental analysis, the panels were designed using the RKU [12] beam theory approach and the estimated loss factors were used as a guide to spanning the range of loss factor from “intermediate” to “highly” damped. Using RKU beam theory, the estimations of the Large *highly* damped panel loss factor range is from 0.090 to 0.127 (500 Hz to 2000 Hz) and the Large *intermediately* damped panel loss factor range is from 0.048 to 0.077. Thus, the highly damped plates were designated tentatively as plates with 10% loss factor and the intermediately damped plates were designated as plates with a 6% loss factor. It is assumed that the smaller panels will retain the same loss factor as the Large panels. In the

results section, Figure 4.50, the RKU-based loss factor estimates for each frequency band and panel size are presented.

In the computational studies, panels were modeled as thin plates using MSC/ PATRAN, and the mobility functions were retrieved using the MSC/NASTRAN's "Direct Frequency Analysis". The mobility for a specific response location is extracted from the MSC/NASTRAN output (.f06 files). For the computational plate model, aluminum 2024-T3 sheet properties [33] are assigned to the model. The generated shell-type QUAD elements are square with an edge length of 0.25 inches and shell thickness of 0.10 inches.

The total loss factor is assigned to the structure via a parameter "Overall Structural Damping Coefficient". Loss factor is defined as the ratio of real and imaginary components of stiffness. Thus, if structural damping coefficient is <u>not</u> applied through the virtual MATi "material card", then the overall structural damping coefficient is equivalent of the loss factor. The mathematical relation between the stiffness and structural damping coefficients is presented in Equation (3.1) [34 and 35]:

$$[K_{Total}] = [K](1 + iG) \tag{3.1}$$

where,

$[K]$ is the stiffness matrix

$G$ is the overall structural damping coefficient (MSC/NASTRAN's input "parameter card", PARAM,G); which in this case is equivalent to structure's total loss factor ($\eta$).

**Table 3.1: Dimensions of panels tested experimentally**

| | **Intermediate Damped Plates** | **Highly Damped Plates** |
|---|---|---|
| **Thicknesses** | | |
| Base Plate (in.)<br>Material ➔ Al 2024-T3 | 0.125 | 0.080 |
| VEM Layer (in.)<br>Material ➔3M F9469PC | 0.005 | 0.005 |
| Cover Plate (in.)<br>Material ➔ Al 2024-T3 | 0.016 | 0.016 |
| Total (in.) | 0.146 | 0.101 |
| **Panel Sizes** | | |
| Area #1 (in.$^2$) | 34.125 x 48 | 34.125 x 48 |
| Area #2 (in.$^2$) | 34.125 x 24 | 34.125 x 24 |
| Area #3 (in.$^2$) | 17 x 24 | 17 x 24 |
| **Estimated loss factor , $\eta_{RKU}$ , based on beam bending theory presented by Ross *et al.*[12 and 13] (For the largest panel - 48" x 34.125" )** | | |
| $\eta_{RKU}$ | 0.048 to 0.077 | 0.090 to 0.127 |

**Table 3.2: Dimensions of panels used to evaluate computational loss factor estimation process**

| | **Lightly Damped Plates** | **Highly Damped Plates** |
|---|---|---|
| **Thicknesses** | | |
| Total (in.) | 0.10 | 0.10 |
| **Simulated loss factor , $\eta$ , (or Structural damping coefficient)** | | |
| $\eta$ | 0.01 | 0.10 |
| **Panel Size** | | |
| Area #1 (in.$^2$) | 34 x 48 | 34 x 48 |
| Area #2 (in.$^2$) | 34 x 24 | 34 x 24 |
| Area #3 (in.$^2$) | 17 x 24 | 17 x 24 |

## 3.2 Test Parameters

To assess the effect of selecting excitation and measurement location(s), on the quality of estimated loss factor, the panels were excited at multiple locations and response was measured from equally spaced grid points. These grid points in the FEM-based analysis correspond to the "nodes" of elements from which the mobility is measured. In the experimental analysis, the scanning laser vibrometer is programmed to measure velocity at equally spaced grid points.

The test panels were excited at four locations and simulated panels were excited at six locations including the same four used in the experiment. For the computational analysis all edge free, i.e. Free-Free-Free-Free or FFFF, boundary conditions are simulated. To create a FFFF condition in the experimental analysis, the panels were hung from two thin steel wires.

Persistent random excitation is applied by the use of a mechanical shaker. A force gage is used to measure the applied force. To avoid moment loading, the mechanical excitation from the shaker is transferred to the plate through a thin and flexible stinger. The force gage is positioned between the stinger and the panel. The panels were excited from the base plate side and the response was measured from the cover plate side.

The sampling frequency for the experimentation and computational analyses are close to 20 kHz. In the research presented herein the highest frequency of analysis is 4000 Hz for which the recommended Nyquist, or cutoff, sampling frequency is 8000 Hz. Thus the sampling frequency of 20 kHz is high enough to accurately analyze the system's response in the frequency bands up to 4 kHz.

The force gage-stinger-shaker assembly is presented in the following Figure 3.3 (Left). The test set-up to hang the panels is shown in Figure 3.3 (Right). The shaker is placed

on the back side of the panel and vibrometer is facing the surface of panel shown. The data flow for the experimental analysis is presented in Figure 3.4.

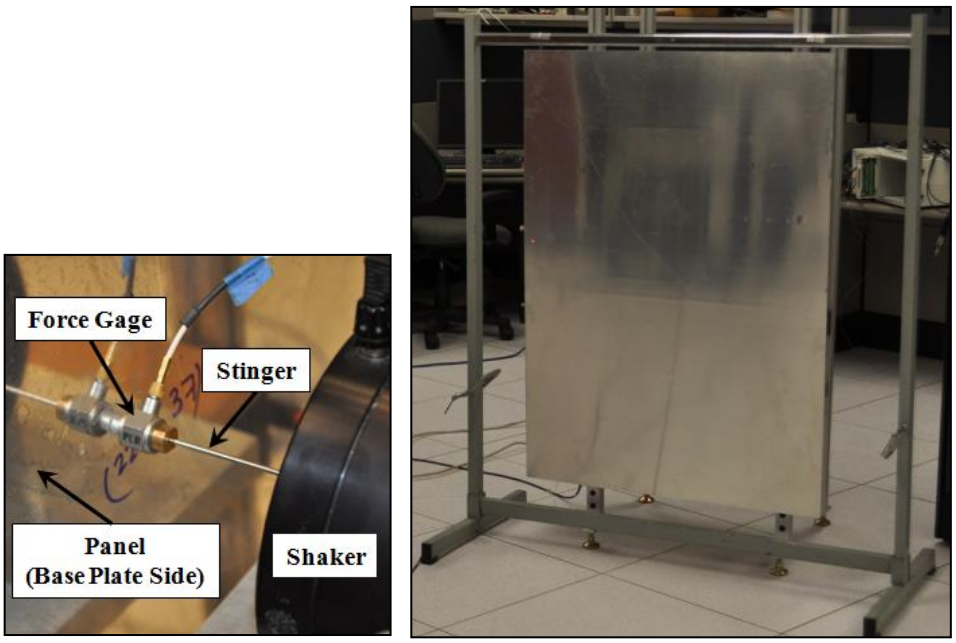


**Figure 3.3: Shaker-Stinger-Force Gage assembly (left) and test setup to hang the panels (right).**

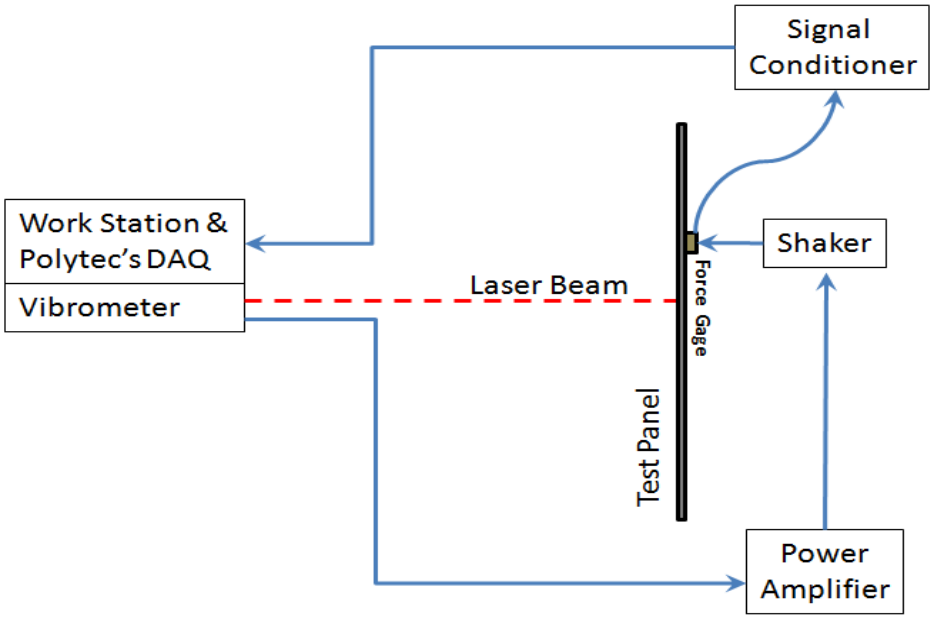


**Figure 3.4: Data flow for the experimental analyses.**

### 3.2.1 Choice of the Excitation Locations

To analyze a continuous system, theoretically, an infinite number of measurements should be recorded for an infinite number of excitation locations. Due to practical limitations on data analysis, loss factor is estimated from a limited number of excitation and measurement locations.

In a conventional experimental setup to estimate loss factor, the structure is excited mechanically using either a mechanical shaker or an impulse hammer. In the research presented herein, persistent white random force (i.e. with constant spectral density) is used to excite the panel. The bandwidth of the applied random force is 350 Hz to 6400 Hz. Bandpass filters are also employed to restrict the force to the desired frequency range. For the computational model, four one-third octave frequency bands were considered:

1. 500 Hz: 445 to 561 Hz
2. 1000 Hz: 891 to 1123 Hz
3. 2000 Hz: 1782 to 2245 Hz
4. 4000 Hz: 3564 to 4490 Hz.

A pictorial summary of the selected excitation locations is presented in Figure 3.5. The excitation locations are broadly classified as:

1. Central
2. Corner & Edge
3. Arbitrary.

In all the studies performed herein, the Excitation #1 and Excitation #2 correspond to central and corner excitation respectively. In the computational analyses, Excitation #3 is the location for edge excitation. The corner or edge excitations are less than (or equal to) an inch away from the panel edge. The rest of the excitation locations are arbitrarily chosen.

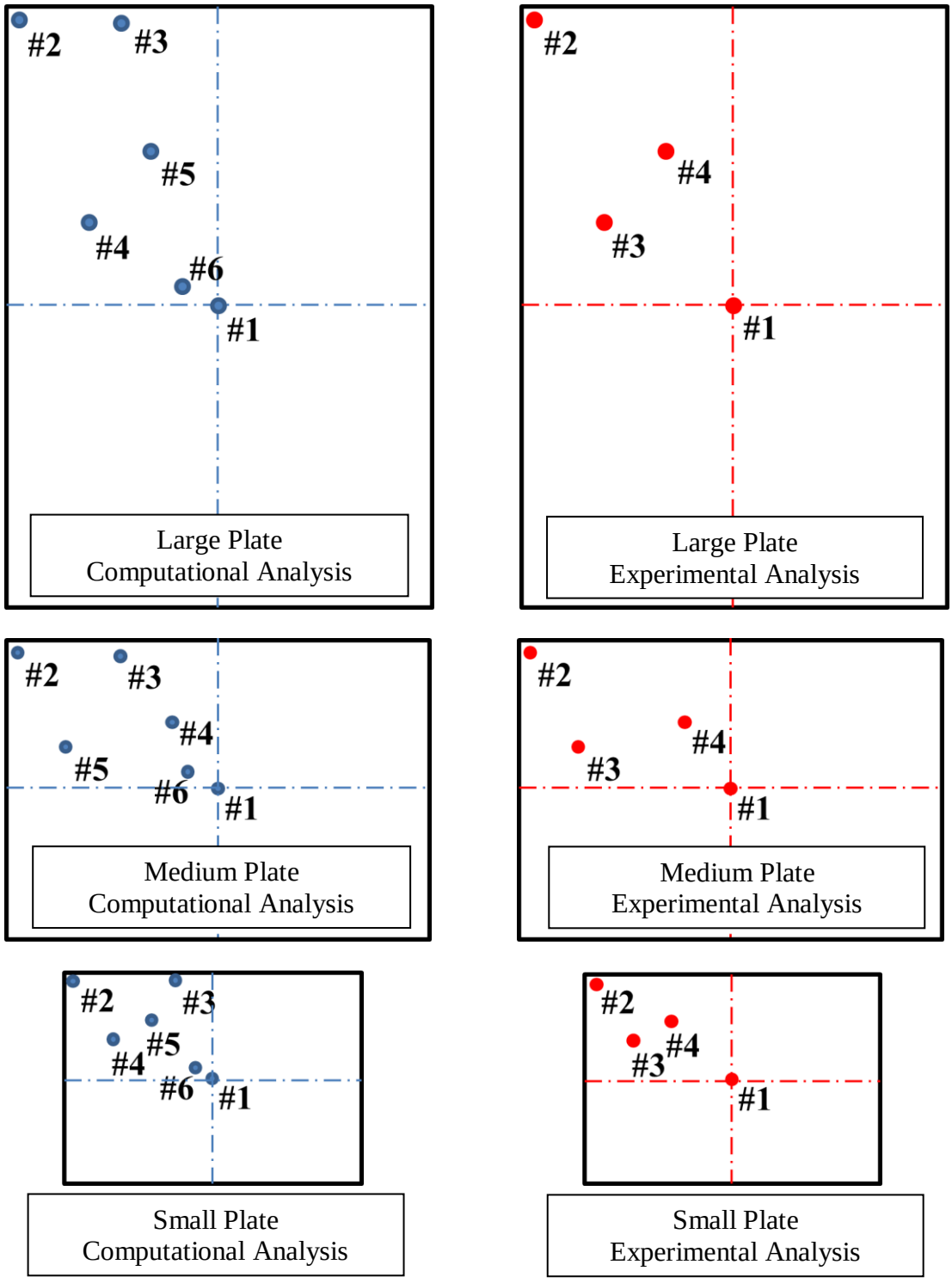


**Figure 3.5: Selected excitation locations for: computational plate model and panels tested experimentally.**

For an all-edge-free panel, the corner and edge are considered to be the most flexible points on the panel for mechanical excitation. Considering all the panel sizes, the distance of edge or corner excitation from panel boundary is always less than one-tenth of panel's minor dimension.

For any mode of vibration, a system has theoretically zero response levels along "node lines". This leads one to consider the effect of excitation or response measurement on a "popular" node line.

### 3.2.2 Choice of the Response Measurement Regions

A similar qualitative study is performed for the evaluation of response measurement locations. The level of response is higher close to the free edge, causing an underestimation of damping. To document and quantify this underestimation, measurements close to the panel boundaries, within one inch of the panel edge, are analyzed. Mean free path, i.e. the distance between wave reflections, is associated with the panel geometric attributes. Loss factors are also estimated from the response locations inside an annular sector—with the excitation location as center—at a distance approximately equal to the mean free path.

The kinetic energy measured inside the direct field is higher than in the reverberation field. To establish the dependence of the loss factor estimation to the distance from the excitation location, the loss factors are averaged: inside the direct field, outside the direct field and in annular sectors. These response measurement regions are presented in Figure 3.6 as shaded portions of the panel.

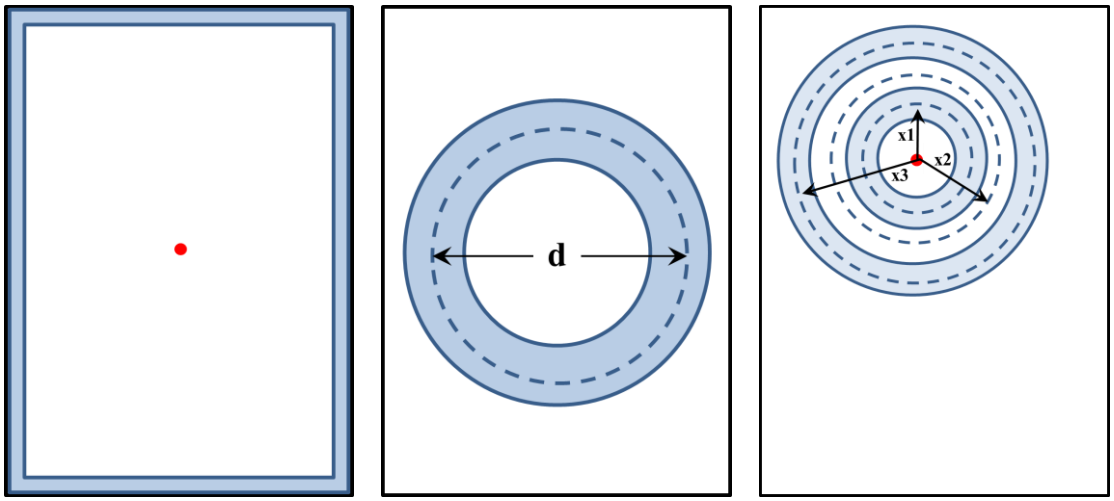


(a) Boundary – close to free edge

(b) Mean Free Path

(c) Multiple annular sectors

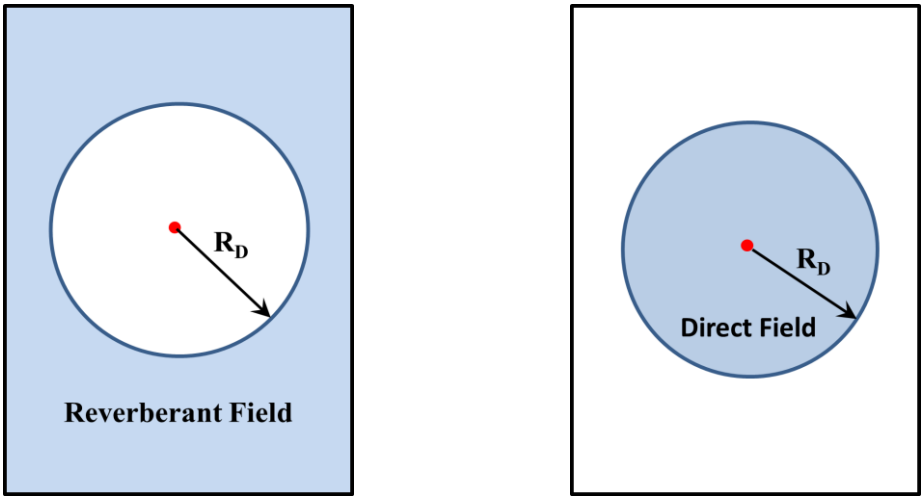


(d) Inside the reverberant field

(e) Inside the direct field

**Figure 3.6: Selection of response measurement regions**

#### 3.2.2.1 Spatial Resolution for Computational Model

To achieve computational efficiency, the required mesh size for elements—i.e. node spacing—needs to be established. This objective is attained by: (a) observing the smallest feature size in the highest frequency band of interest, and (b) checking for the convergence of finite element model for selected natural frequencies of the system.

A normal mode analysis in the 4000 Hz one-third octave band of the largest panel indicates that the smallest feature is ~1.8 inches. This dimension of the smallest feature is determined from the highest number of node lines (26) along the edge with a length of 48 inches. To accurately observe such a feature, i.e. a half sine wave of displacement, the element edge length should be no less than half the feature size, or ~ 0.9 inches. If the spacing between the nodes is higher than 0.9 inches then spatial aliasing will occur and the computed data cannot be used for a modal analysis at 4000 Hz.

Based on the feature size requirements, a convergence study was performed for square QUAD elements with edge length: 1 in., 0.5 in., 0.25 in. and 0.125 in. It is not uncommon to represent mode shapes as the "m x n mode", where "m" is the number of node lines along the x-axis and "n" is the number of node lines along the y-axis. For each of the four frequency bands of analysis, one mode shape, closest to band's central frequency, is chosen to observe the convergence of the finite element model. These results are tabulated in Table 3.3 and Figure 3.7 .

Based on this study of element sizes, it is observed that the computational models converge within 4% for a mesh size smaller than 0.5 inches. Thus, for computational analysis, element edge length of 0.25 inches—which has converged to values within 0.75% w.r.t. to the mesh size of 0.125 inches—is chosen. With an element edge length of 0.25 inches, 96 half sine waves on the longer edge and 68 half sine waves on the shorter edge, can

be accurately observed. To conclude, the edge length of 0.25 inches has enough spatial resolution to observe the smallest possible feature size in the frequency bands of interest and is thus chosen in the simulated panel studies.

**Table 3.3: Evaluation of mesh size for convergence**

| | **Band's Central Frequency** | | | |
|---|---|---|---|---|
| | **500 Hz** | **1000 Hz** | **2000 Hz** | **4000 Hz** |
| Expected Mode → (Normal Mode Analysis) | 4 x 10 | 9 x 10 | 16 x 3 | 13 x 26 |
| **Edge Length For FEM-based Analysis** ↓ | | | | |
| 0.10" | | | 1980.80 Hz | |
| 0.125" | 496.93 Hz | 1003.90 Hz | 1982.40 Hz | 3990.50 Hz |
| 0.20" | | | 1989.80 Hz | |
| 0.25" | 497.32 Hz | 1004.70 Hz | 1996.50 Hz | 3992.80 Hz |
| 0.50" | 498.71 Hz | 1008.20 Hz | 2057.70 Hz | 4009.00 Hz |
| 1.00" | 505.92 Hz | 1033.10 Hz | 2308.80 Hz | 4873.30 Hz |

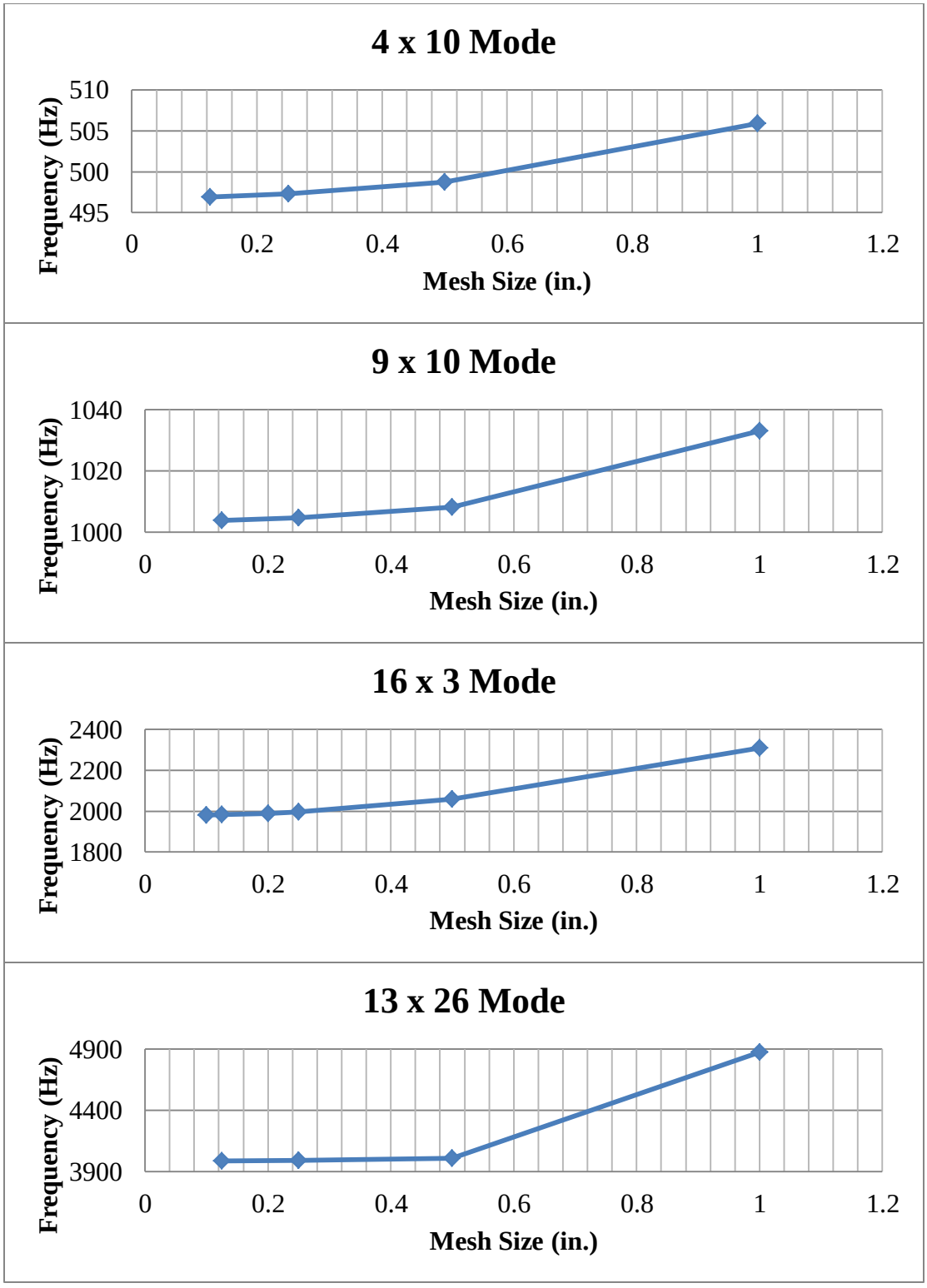


**Figure 3.7: Convergence study to determine the optimum mesh size.**

#### 3.2.2.2 Selected Grid Points as Response Measurement Locations

PIM based loss factor algorithms do not require any user inputs and thus, once the FRFs are processed, PIM procedures can be completely automated. On the contrary, decay rate based techniques, such as IRDM and RDT, require user inputs for slope fitting on decay curves. Each slope-fit, even with the automated slope-fit algorithms (discussed in Section 2.2.3.1), needs to be visually inspected.

For IRDM, at each of selected measurement location a loss factor is determined by slope fitting. Ewing *et al.*[14] have evaluated the effect of the number of measurement locations on the accuracy of loss factor estimated using IRDM and RDT. We have concluded that only a few number of response locations are sufficient for reliably estimating the loss factor.

If only FRFs are available from the tests performed, then the RDT procedures require convolution of random force and narrow-band impulse response function to generate an arbitrarily long random response. This convolution process and then the course of action to extract the randomdec signature are the most time consuming procedures in the RDT.

Considering computational efficiency, in terms of data analysis and storage, RDT based loss factor evaluations have been done for fewer response measurement locations than the IRDM and PIM studies. In the analysis presented herein, the least number of response locations (or grid points) analyzed to estimate IRDM and RDT-based loss factor are thirty five. Note that these many response locations are considerably higher than the number of accelerometers used in a typical experimental loss factor estimation setup.

In Table 3.4 and 3.5, a pictorial summary of selected response locations is presented. Also in these tables, the grid spacing and total the number of grid points analyzed are tabulated.

**Table 3.4: Selected grid point locations for the computational loss factor estimation processes.**

| PIM ($\eta$ =0.01 & $\eta$ =0.10) | IRDM ($\eta$ =0.01) | RDT ($\eta$ =0.01 & $\eta$ =0.10) & IRDM ($\eta$ =0.10) |
|---|---|---|
| 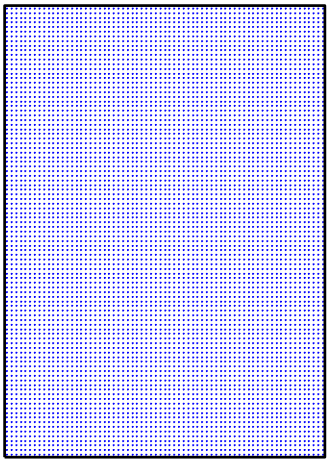 Grid Points Tested: 6693 dx = 0.5 in. & dy = 0.5 in. | 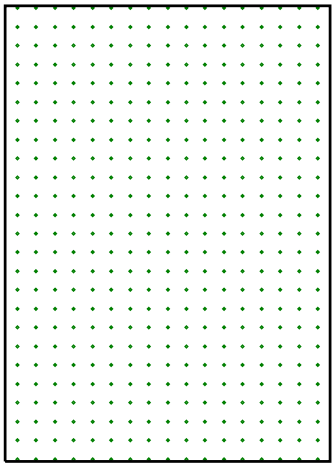 Grid Points Tested: 425 dx = 2.0 in. & dy = 2.0 in. | 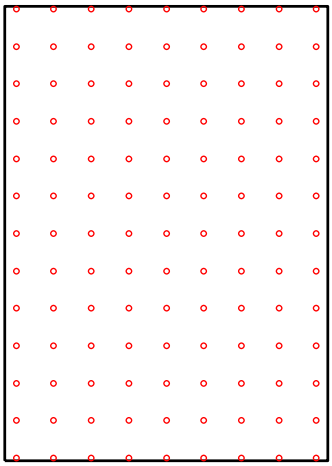 Grid Points Tested: 117 dx = 4.0 in. & dy = 4.0 in. |
| 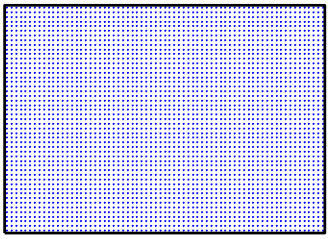 Grid Points Tested: 3381 dx = 0.5 in. & dy = 0.5 in. | 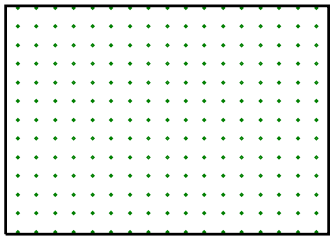 Grid Points Tested: 221 dx = 2.0 in. & dy = 2.0 in. | 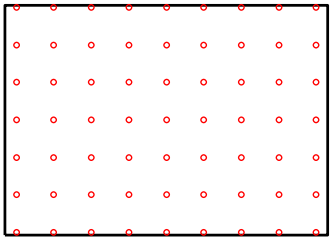 Grid Points Tested: 63 dx = 4.0 in. & dy = 4.0 in. |
| 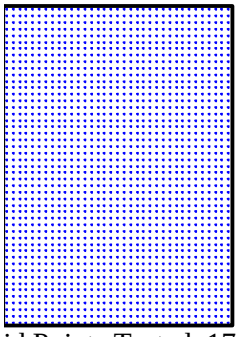 Grid Points Tested: 1715 dx = 0.5 in. & dy = 0.5 in. | 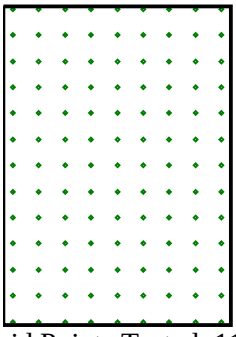 Grid Points Tested: 117 dx = 2.0 in. & dy = 2.0 in. | 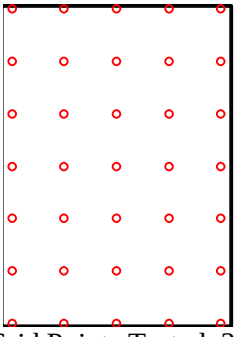 Grid Points Tested: 35 dx = 4.0 in. & dy = 4.0 in. |

**Table 3.5: Selected grid point locations for the experimental loss factor estimation processes**

| PIM | IRDM | RDT |
|---|---|---|
| 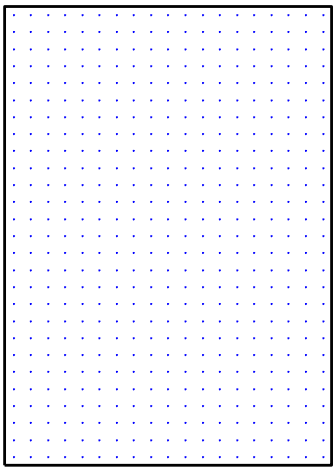 <br>Grid Points Tested: 513<br>dx = 1.8 in. & dy = 1.78 in. | 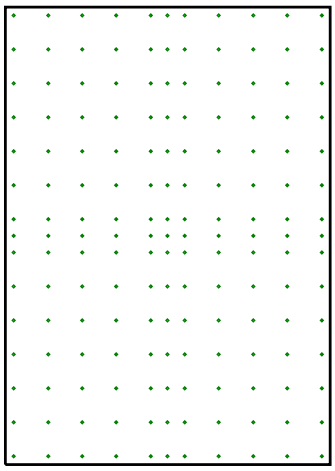 <br>Grid Points Tested: 165<br>dx = 3.6 in. & dy = 3.56 in. | 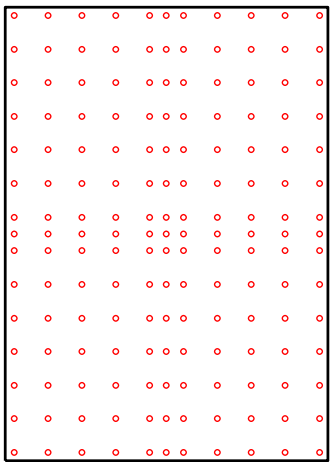 <br>Grid Points Tested: 165<br>dx = 3.6 in. & dy = 3.56 in. |
| 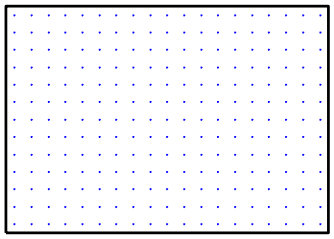 <br>Grid Points Tested: 247<br>dx = 1.80 in. & dy = 1.85 in. | 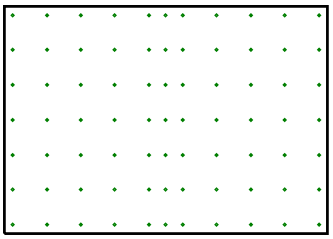 <br>Grid Points Tested: 77<br>dx = 3.6 in. & dy = 3.69 in. | 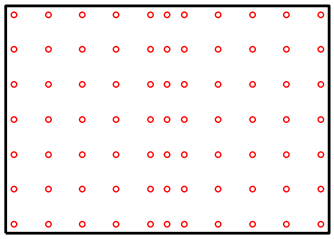 <br>Grid Points Tested: 77<br>dx = 3.6 in. & dy = 3.69 in. |
| 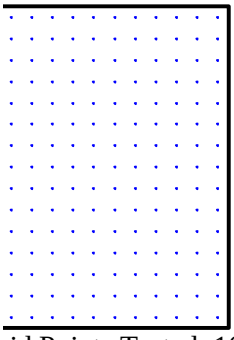 <br>Grid Points Tested: 165<br>dx = 1.60 in. & dy = 1.55 in. | 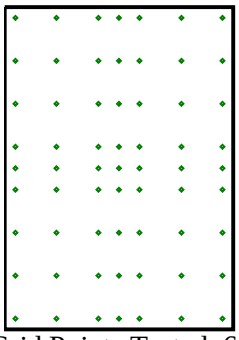 <br>Grid Points Tested: 63<br>dx = 3.6 in. & dy = 3.09 in. | 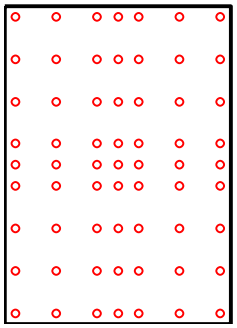 <br>Grid Points Tested: 63<br>dx = 3.6 in. & dy = 3.09 in. |

## 3.3 Analysis Parameters

In the following sections the significant parameters associated with loss factor estimation techniques, such as choice of frequency bands and grid spacing are discussed.

### 3.3.1 Frequency of Analysis for Loss Factor Analysis

Panel total loss factors are estimated in four one-third octave frequency bands with central frequencies of: 500 Hz, 1000 Hz, 2000 Hz and 4000 Hz. Filtering is essential to obtain narrow-band time histories. Only the FRFs are recorded from MSC/NASTRAN and experiments. Frequency domain filtering is employed to extract the band-limited or "chunked" FRFs. This approach, to extract point by point band-limited FRFs, is used to estimate loss factor using PIM. For loss factor estimation by IRDM, these chunked FRFs are inverted in the Fourier sense to estimate the impulse response. The narrow-band impulse responses are then convolved with a narrow-band random force to generate arbitrary length time histories of response. This long time history is processed to compute the randomdec signature.

The frequency resolution, $\Delta f$ , for the experimental analysis of panels is 1.25 Hz and the sampling frequency is 20480 Hz. For the simulated plate models, the frequency resolution is 1 Hz which corresponds to a sampling frequency of 20000 Hz.

#### 3.3.1.1 Frequency Domain Filtering (FDF)

Frequency domain filtering is required for the RDT since the random response is not generally available in the time domain. To operate in the time domain, one would need to excite a structure only in narrow frequency band, which is a reasonable alternative to the

process used here. As the process name suggests, the narrow–band response is calculated using filters in the frequency domain. The steps involved with FDF are:

1. The complete FRF (broad-band) are read from either .unv files from scanning laser vibrometer for experimental analysis or .f06 files for computational analysis.
2. The FRFs are filtered in the frequency domain by "zero–padding" the out–of–band FRF elements. By computing the inverse of this "chunked" FRF, in the Fourier sense, the narrow–band impulse response is estimated.
3. The convolution of this band–limited impulse response with a time domain band-limited random force yields a narrow–band random response.

### 3.3.2 Length of Sample

In an experimental analysis, the length of sample should be long enough to capture the decay characteristics of the free decay or impulse response or randomdec signature. The length of data to be recorded is often dictated by the reverberation time, that is the time required for the amplitude of the free decay to drop by 60 dB. To optimize the memory usage and reduce computation time, a target sample length needs to be established.

For a 1DOF system, the transient displacement response is given by:

$$x(t) = e^{-\zeta \cdot \omega_n \cdot t} \cdot \sin(\omega_d \cdot t + \phi), \tag{3.2}$$

transient velocity response is given by:

$$\dot{x}(t) = e^{-\zeta \cdot \omega_n \cdot t} \cdot \left(-\zeta \cdot \omega_n \cdot \sin(\omega_d \cdot t + \phi) + \omega_d \cdot \cos(\omega_d \cdot t + \phi)\right), \tag{3.3}$$

and transient acceleration response is given by the following relation:

$$\ddot{x}(t) = e^{-\zeta \cdot \omega_n \cdot t} \cdot \left\{(\zeta^2 \cdot {\omega_n}^2 - {\omega_d}^2) \cdot \sin(\omega_d \cdot t + \phi) - 2 \cdot \zeta \cdot \omega_n \cdot \omega_d \cdot \cos(\omega_d \cdot t + \phi)\right\}. \tag{3.4}$$

It can be noted that the exponential decay of displacement, velocity and acceleration, from Equations (3.2) through (3.4), are equal to $e^{-\zeta \cdot \omega_n \cdot t}$. The reverberation time ( or $TR$) is the time taken the decaying response to attenuate by 60 dB and is [1 and 36]:

$$TR \cong \frac{2.2}{f_c \cdot \eta_{est}} . \tag{3.5}$$

where,

$\eta_{est}$ is the initial "guess" of the loss factor.

For a constant damping level, the numbers of cycles for vibrations to damp–out will remain the same in all the frequency bands. For a particular level of damping, the length of sample in terms of number of cycles, can be established as a fixed parameter for the entire frequency range. Based on the reverberation time, the length of sample (or triggered sample) in terms of cycles to damp out is given by [11]:

$$N_C \cong \frac{2.2}{\eta_{est}} \tag{3.6}$$

where,

$N_C$ is the length of sample in terms of cycles, for narrow–band time history

Equation (3.5) indicates that the length of sample in terms of cycles is independent of the frequency and is only dependent on the loss factor.

Based on Equations (3.5) and (3.6) it can recognized that for a lightly damped structure the length of sample, i.e. of decaying response, will be longer than the length of sample for a highly damped structure. This is an important observation, especially for lower damping levels or central frequencies, for which very long time records need to be recorded and analyzed. Assuming "n" is the number of triggered samples required to extract the randomdec signature, and "$TR$" is reverberation time (in seconds), then length of total time

history for analysis should be at least equal to "$n \cdot TR$" (in seconds). Thus, due to practical limitations on analysis and DAQ software, RDT is not recommended for panels with very low damping levels (below 0.01) [11].

### 3.3.3 Estimating Loss Factors from FRFs

The procedures to estimate the loss factor from PIM, IRDM, and RDT are presented in Figures 3.8 through 3.10. The theory for these techniques have already been discussed in Chapter 2. Some of the RDT-specific parameters are discussed in Section 3.3.3.1.

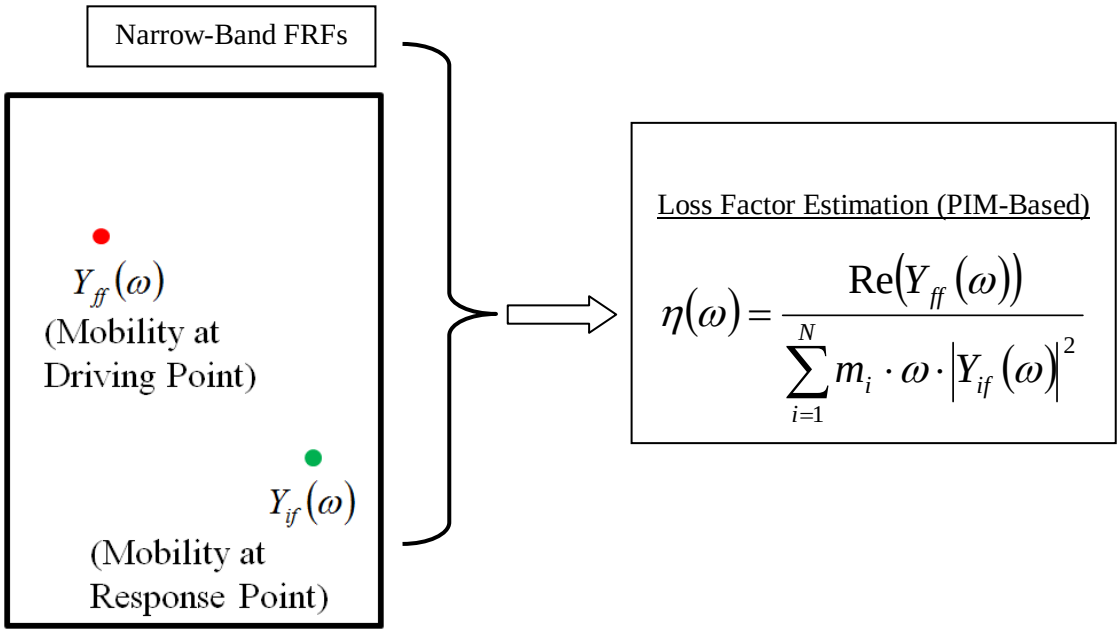


**Figure 3.8: Loss factor estimation methodology for PIM**

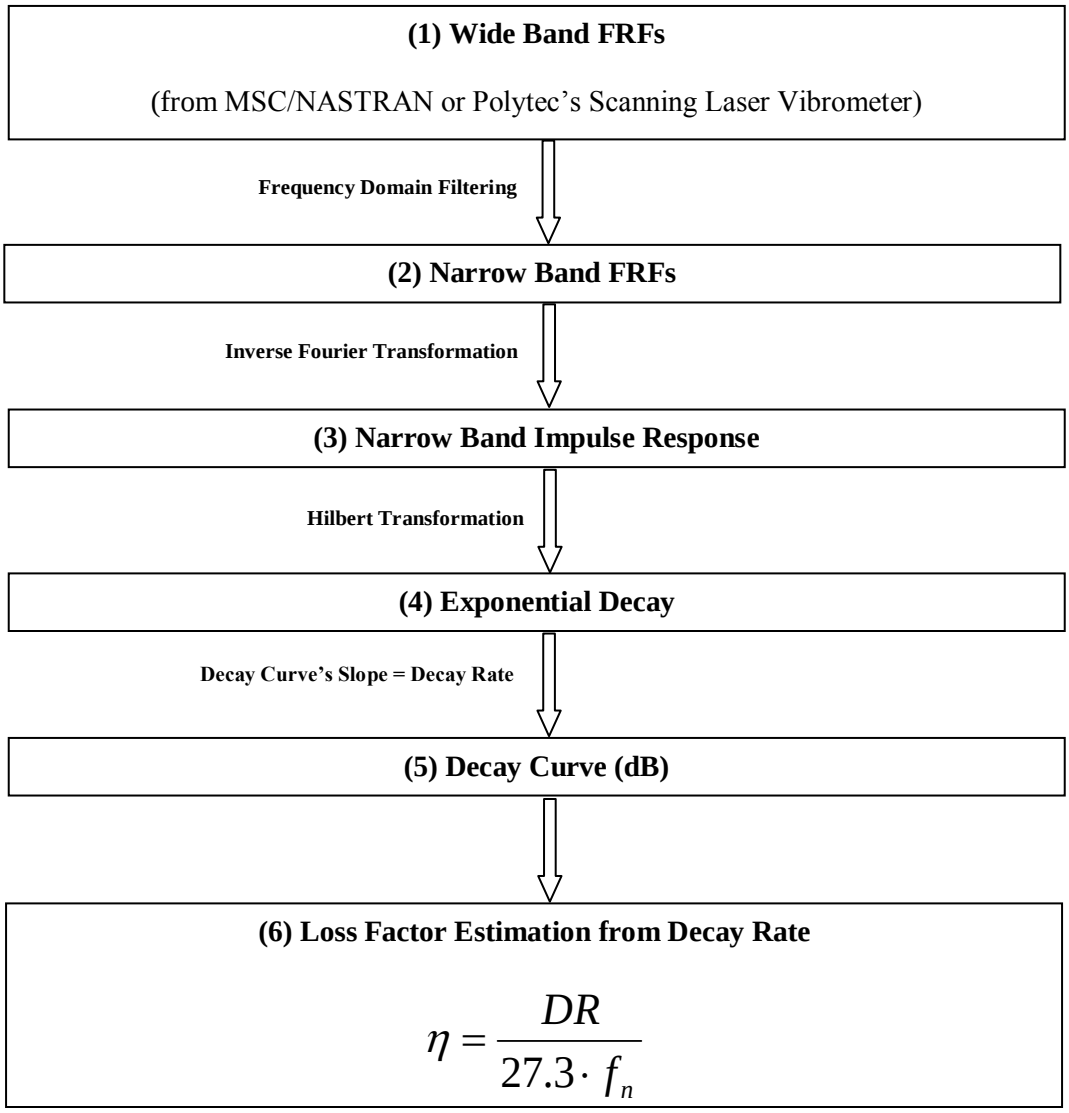


**Figure 3.9: Loss factor estimation methodology for IRDM**

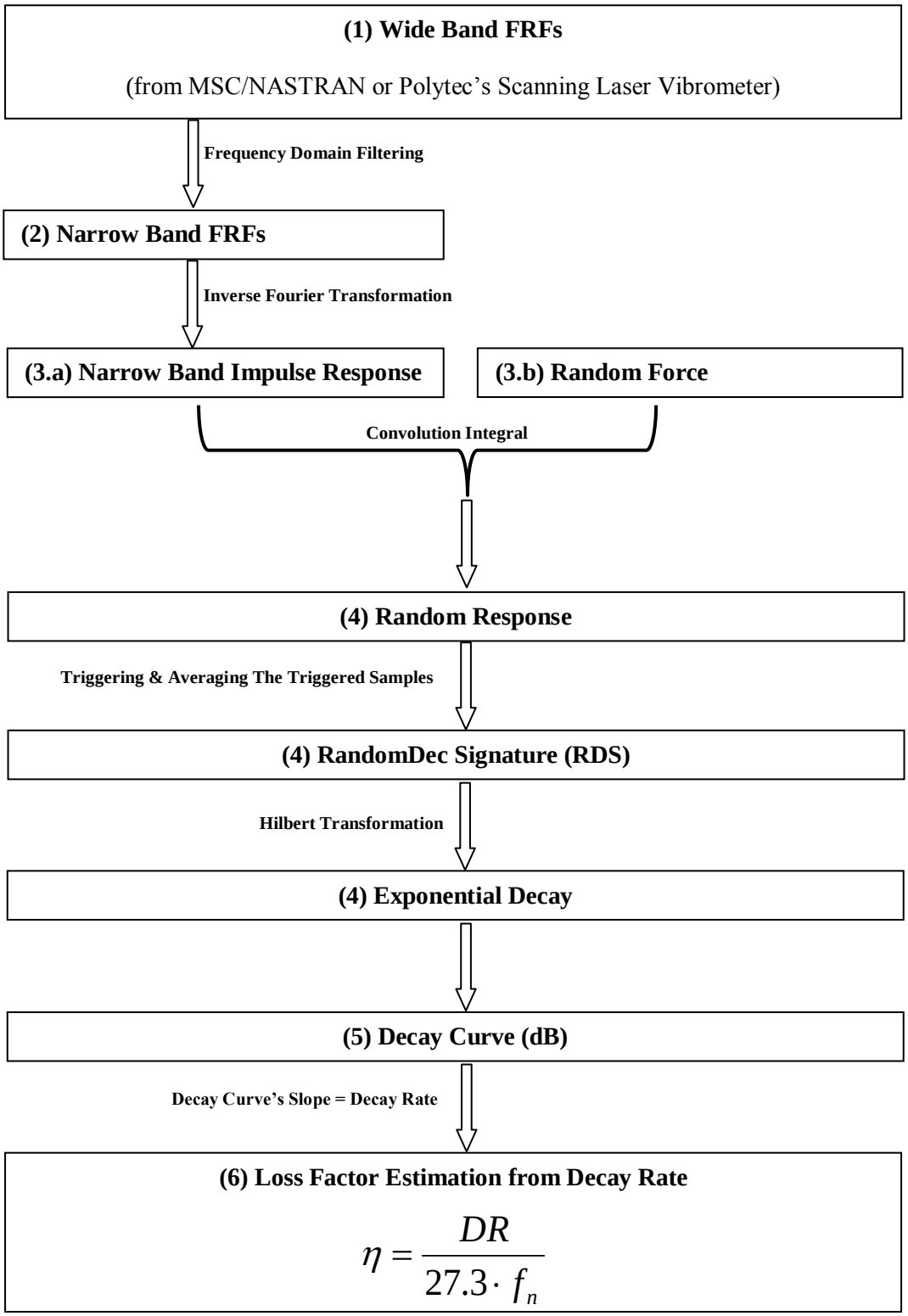


**Figure 3.10: Loss factor estimation methodology for RDT**

### 3.3.3.1 RDT Parameters

For the case of a single degree of freedom system excited with white noise (a stationary, Gaussian process), the randomdec signature is equivalent to the free decay [7] or autocorrelation function [20 and 21]. The fact that the decay of the autocorrelation function of random response is equivalent to the free decay of response offers an option to select one of two possible averaging schemes to extract the free decay rate. ***In the conventional RDT approach the triggered responses are directly averaged***; the alternate way is to average the autocorrelation functions of triggered response samples. In the alternate averaging scheme—averaging autocorrelation functions—the positive part of autocorrelation functions from the triggered responses are averaged.

**Number of Triggered Samples to Generate Randomdec Signature**

In the estimation of loss factor of plates, with simulated loss factor of 0.10 and experimentally tested panels, 500 triggered samples are averaged. For the lightly damped plate, with a simulated loss factor of 0.01, 200 triggered samples are averaged to estimate the randomdec signature, from which the decay rate is measured.

**Averaging Schemes – Estimating the dB Decay**

From each response location, one randomdec signature is processed. An average loss factor is calculated by averaging the decay curves from all the output locations. From the averaged decay curve, the decay rate is measured to estimate loss factor. This approach is consistent with the averaging scheme used in conventional IRDM loss factor estimation when the response is measured from multiple locations on a panel [14]. Even though RDT with direct averaging and averaging autocorrelation function approaches are considered equivalent the later approach tends to overestimate the loss factor. In Figure 3.11 the two approaches to estimate the decay curves (and decay rate) are compared. The decay rate from the

autocorrelation function averaging approach is higher as compared to the decay rate estimated using the direct averaging approach. Similar trends were also observed, and reported, in the previous study by Dande [11].

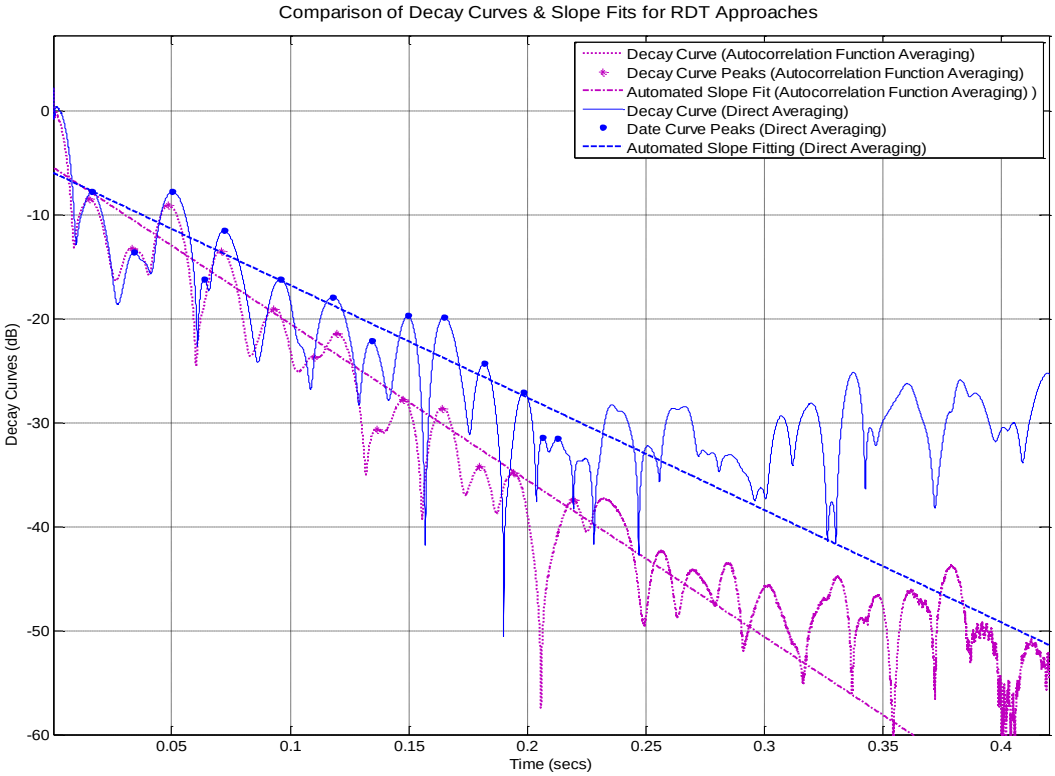


**Figure 3.11: A representative comparison of decay curves and slope fits for the two possible RDT approaches.**

RDT-based analysis of an 1DOF system to evaluate the effect of number of triggered samples on both RDT approaches is presented—as a case study—in the Appendix C.

# 4 Results

This chapter is aimed at the qualitative analysis of PIM, IRDM, and RDT as loss factor estimation techniques. Loss factors are evaluated in specific response regions such as: the direct field, the reverberant field, close to a boundary, and in equally-spaced annular sectors centered on the excitation location. In Section 4.2, the quality of estimated loss factors for the computational models with simulated loss factors of 0.01 and 0.10 are reported. Similarly, experimentally determined loss factors, for six damped plates, are presented in the Section 4.3. Finally, in Section 4.4 the loss factor estimates from experimental and RKU-beam theory are compared.

## 4.1 Distance–Based Loss Factor Estimates

To establish the relevance of the distance of a response region from the excitation location to loss factor estimation, the responses are measured in equally- spaced annular sectors. This methodology is schematically presented in Figure 4.1. The two circled loss factors on the distance based loss factor curve are determined from highlighted annular regions on the panel. The dot, in the center of these annular sectors, is the excitation location.

The choice of excitation location is also evaluated in this chapter. In the figures presented in sections to follow (i.e. Figures 4.2 through 4.49) a consistent set of markers have been used: the marker ‘○’ is used to indicate loss factors from central (or close to center) excitation location(s); the marker ‘×’ is used to indicate loss factors from edge (or corner) excitation location(s); and the marker ‘◇’ is used to indicate loss factors from arbitrarily-chosen excitation locations. In these figures the dashed line represents the radius of direct

field and the dotted line indicates the radius of region encompassed by the mean free path (or simply half the measure of mean free path).

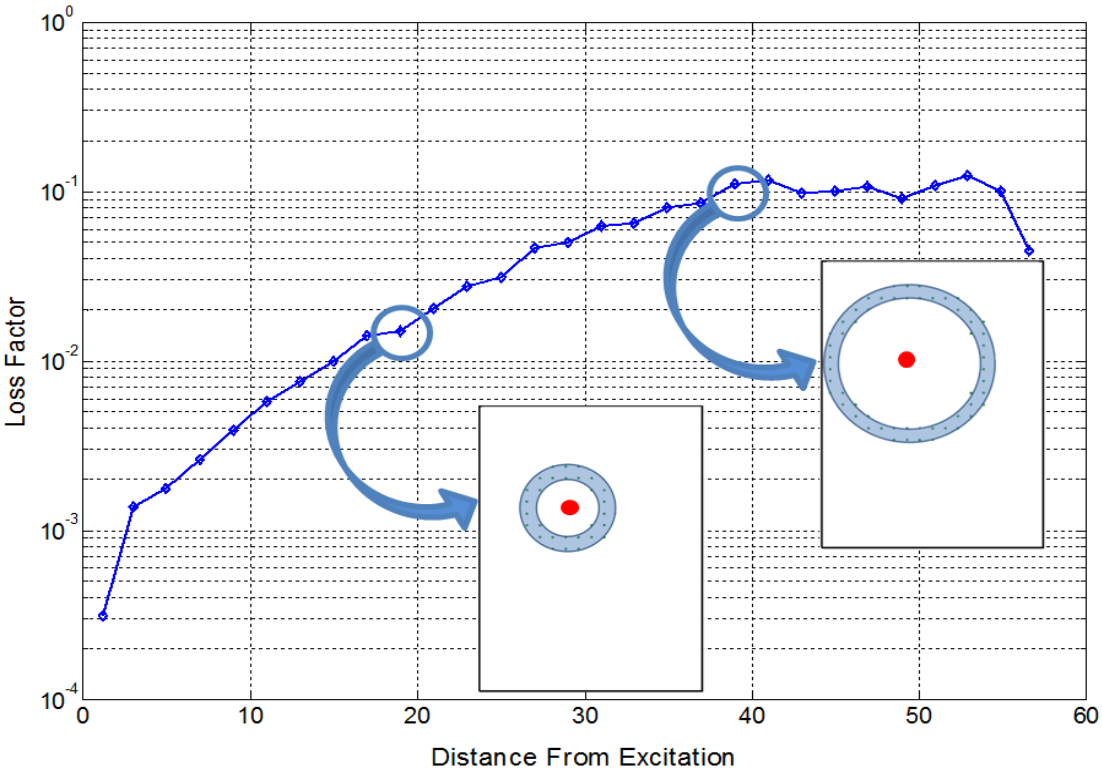


**Figure 4.1: Schematic representation of measuring loss factor in annular sectors (not to scale).**

## 4.2 Computational Plate Model

Plate models were simulated using MSC/PATRAN and were analyzed by using MSC/NASTRAN. For the simulation purposes, square "QUAD4 SHELL" elements with an edge length of 0.25 inches are used. Even though for these plate models the FRFs were available for nodes separated by 0.25 inches, due to limitations on data storage the FRFs were read, from .f06 files, for nodes spaced at every 0.50 inches. These panels were modeled for two damping loss factors: 0.01 and 0.10. Three panel sizes were chosen and panels were excited at six different locations as shown in Figure 3.5. That is, a total of six plates (two damping levels and three sizes) were evaluated for a choice of six excitation locations, in four

frequency bands. The three techniques—PIM, IRDM and RDT—were employed to estimate the loss factor for each case. In this computational study, Excitation #1 and #6 are central excitation locations, Excitation #2 and #3 are edge excitation locations and Excitation #4 and #5 are arbitrarily chosen excitation locations. In the following section the process-wise loss factor estimates are presented.

### 4.2.1 Power Input Method

For the computational plate models, the distance-based loss factors are presented in Figures 4.2 through 4.7. The estimated loss factors for central, edge, and corner excitations are plotted for each of the six panels (two damping levels and three panel sizes) in four frequency bands. In these figures, the theoretical radius of the direct field is indicated—using a dashed line—to give an estimate of the boundary between the direct and reverberant fields.

In most of the cases analyzed for PIM, it is observed that excitation close to an edge yields unreliable loss factor estimates and hence edge excitation is not recommended. Therefore, the averaged loss factor estimates are computed from the arbitrary and central excitation locations only and these estimates are tabulated in Tables 4.1 and 4.2.

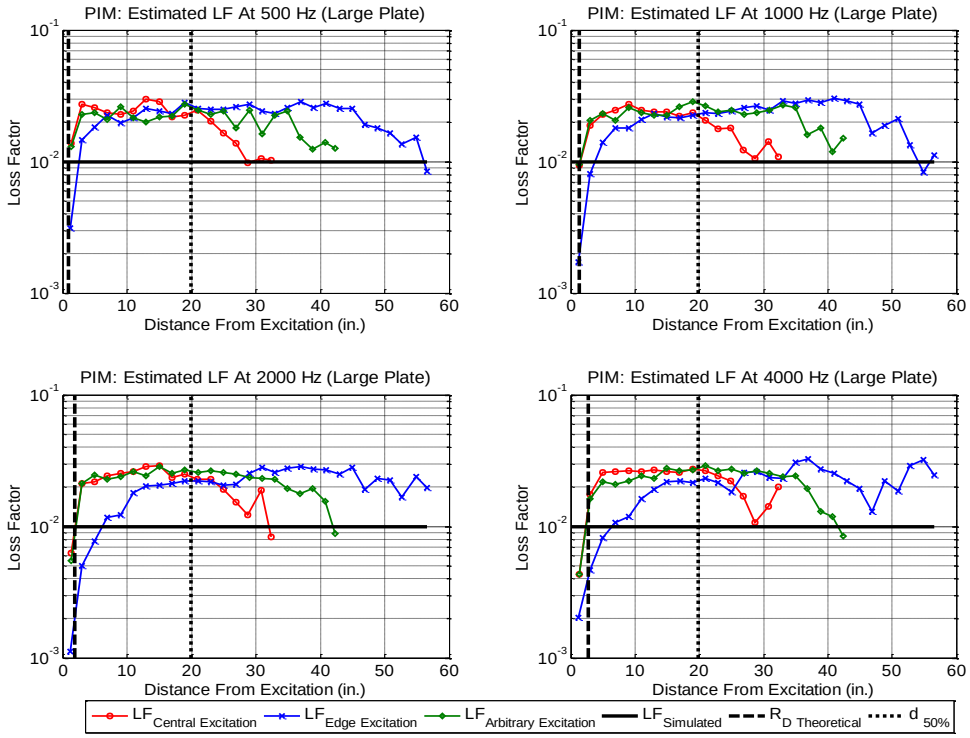


**Figure 4.2: PIM based estimated loss factor for Large plate (simulated loss factor of 0.01)**

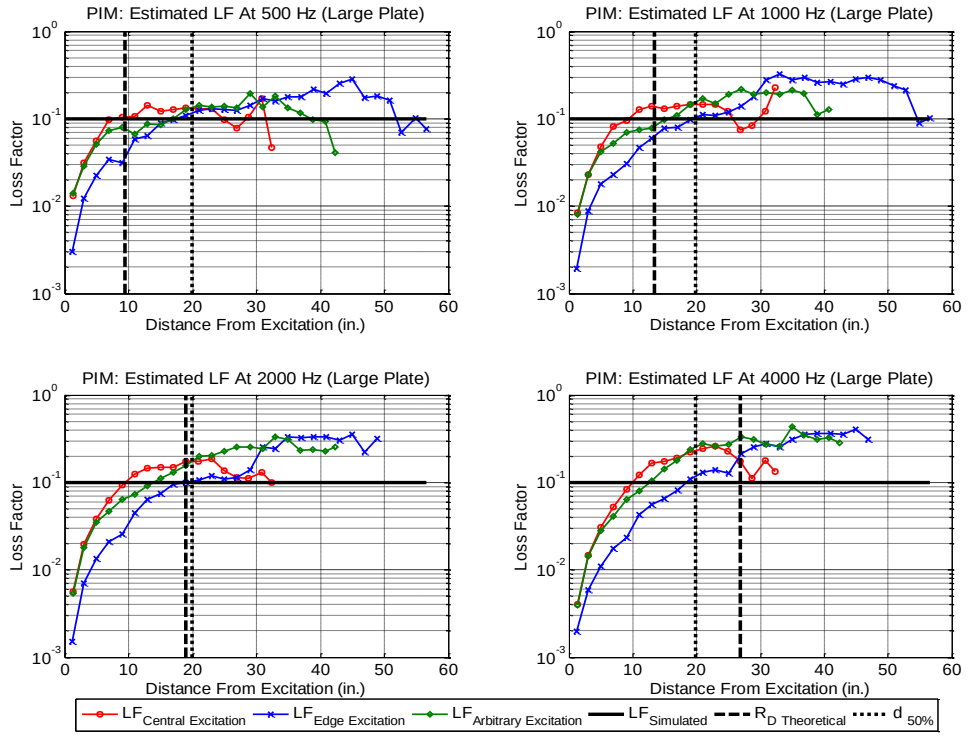


**Figure 4.3: PIM based estimated loss factor for Large plate (simulated loss factor of 0.10)**

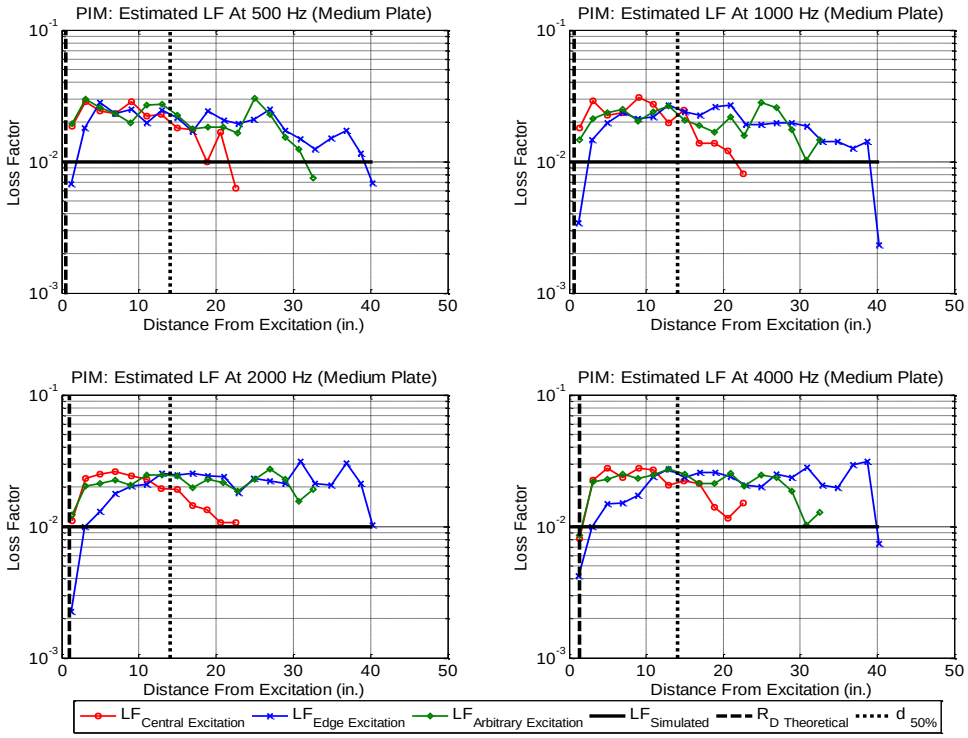


**Figure 4.4: PIM based estimated loss factor for Medium plate (simulated loss factor of 0.01)**

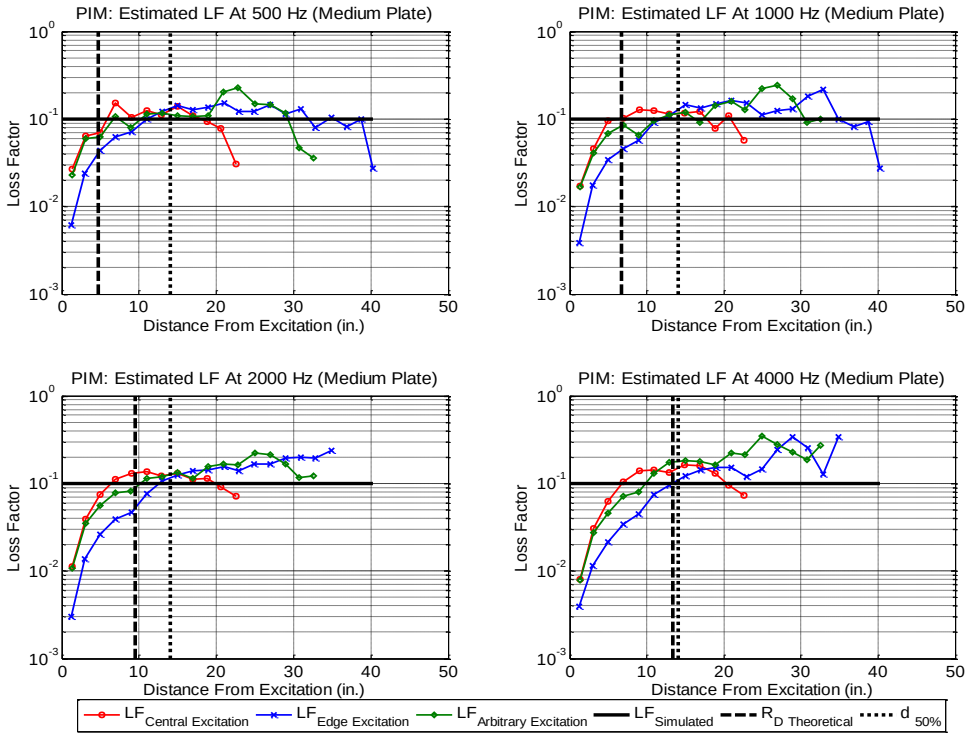


**Figure 4.5: PIM based estimated loss factor for Medium plate (simulated loss factor of 0.10)**

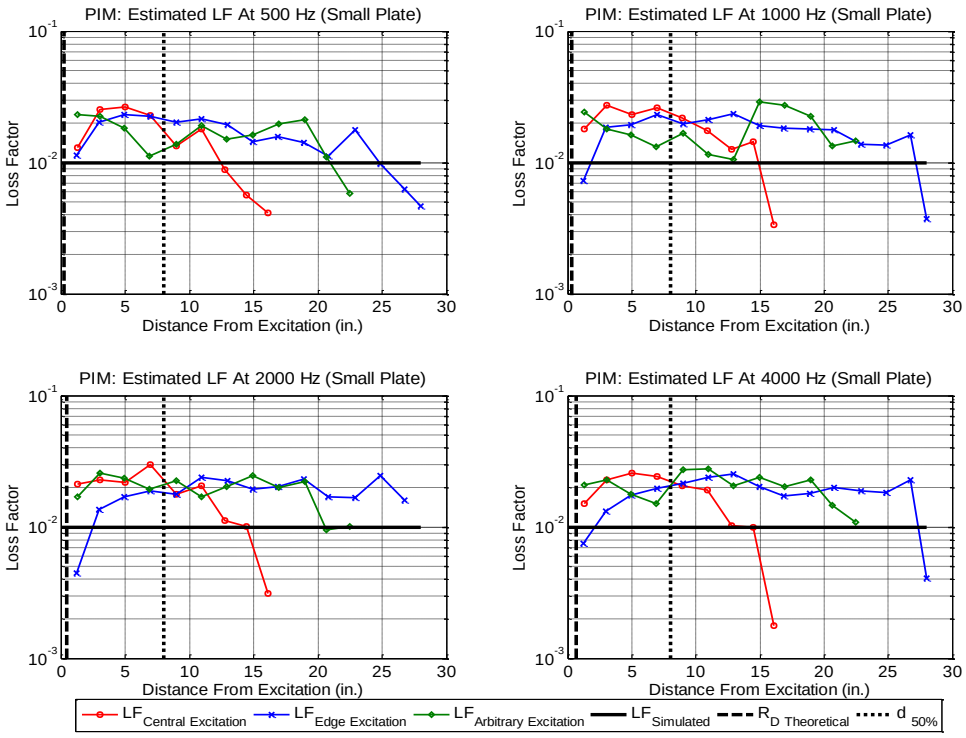


**Figure 4.6: PIM based estimated loss factor for Small plate (simulated loss factor of 0.01)**

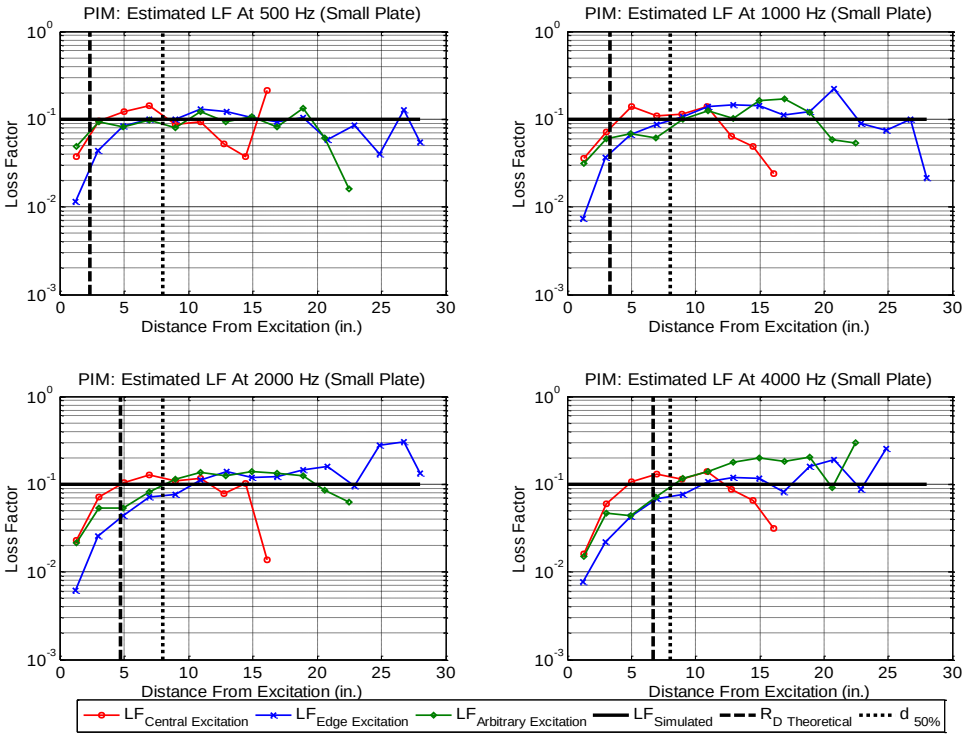


**Figure 4.7: PIM based estimated loss factor for Small plate (simulated loss factor of 0.10)**

**Table 4.1: PIM based estimated loss factor for panels with simulated loss factor of 0.01**

| | Frequency of Analysis | | | |
|---|---|---|---|---|
| **Measurement Regions** | **500 Hz** | **1000 Hz** | **2000 Hz** | **4000 Hz** |
| **PIM: Large Plate (Simulated Loss Factor = 0.01)** | | | | |
| **Close to Boundary** | 0.0045 | 0.0051 | 0.0057 | 0.0059 |
| **Inside the Direct Field** | 0.0097 | 0.0052 | 0.0036 | 0.0035 |
| **Inside the Reverberant Field** | 0.0094 | 0.0093 | 0.0092 | 0.0091 |
| **Close to Mean Free Path** | 0.0091 | 0.0093 | 0.0092 | 0.0093 |
| **Plate Average** | 0.0093 | 0.0093 | 0.0091 | 0.0089 |
| **PIM: Medium Plate (Simulated Loss Factor = 0.01)** | | | | |
| **Close to Boundary** | 0.0049 | 0.0052 | 0.0056 | 0.0058 |
| **Inside the Direct Field** | 0.0049 | 0.0095 | 0.0049 | 0.0036 |
| **Inside the Reverberant Field** | 0.0092 | 0.0091 | 0.0089 | 0.0087 |
| **Close to Mean Free Path** | 0.0085 | 0.0086 | 0.0088 | 0.0085 |
| **Plate Average** | 0.0092 | 0.0090 | 0.0089 | 0.0087 |
| **PIM: Small Plate (Simulated Loss Factor = 0.01)** | | | | |
| **Close to Boundary** | 0.0050 | 0.0053 | 0.0056 | 0.0057 |
| **Inside the Direct Field** | 0.0061 | 0.0047 | 0.0032 | 0.0049 |
| **Inside the Reverberant Field** | 0.0088 | 0.0088 | 0.0086 | 0.0084 |
| **Close to Mean Free Path** | 0.0080 | 0.0089 | 0.0081 | 0.0084 |
| **Plate Average** | 0.0088 | 0.0088 | 0.0086 | 0.0083 |

For the plates with simulated loss factor of 1% (lightly damped), the PIM-based panel's loss factor estimate for Large and Medium plates are all low and within 13% accuracy; and the loss factor estimates for Small plates are all low and within 16%. Of all the cases of lightly damped plates considered, the least accurate results are observed for the highest frequency of analysis i.e. at 4000 Hz. For these lightly damped panels, the size of the direct field is small as compared to the entire plate and hence the loss factors estimated from the reverberant field are essentially the same as the loss factor computed for the entire panel.

Inside the direct field and close to the panel's boundary (or within an inch from the panel edges) the estimated loss factors are generally severely underestimated.

**Table 4.2: PIM based estimated loss factor for panels with simulated loss factor of 0.10**

| | Frequency of Analysis | | | |
|---|---|---|---|---|
| **Measurement Regions** | **500 Hz** | **1000 Hz** | **2000 Hz** | **4000 Hz** |
| **PIM: Large Plate (Simulated Loss Factor = 0.10)** | | | | |
| **Close to Boundary** | 0.057 | 0.076 | 0.106 | 0.142 |
| **Inside the Direct Field** | 0.046 | 0.052 | 0.064 | 0.082 |
| **Inside the Reverberant Field** | 0.120 | 0.154 | 0.257 | 0.620 |
| **Close to Mean Free Path** | 0.145 | 0.179 | 0.264 | 0.456 |
| **Plate Average** | 0.095 | 0.095 | 0.094 | 0.094 |
| **PIM: Medium Plate (Simulated Loss Factor = 0.10)** | | | | |
| **Close to Boundary** | 0.056 | 0.067 | 0.086 | 0.108 |
| **Inside the Direct Field** | 0.043 | 0.045 | 0.052 | 0.064 |
| **Inside the Reverberant Field** | 0.105 | 0.116 | 0.146 | 0.224 |
| **Close to Mean Free Path** | 0.113 | 0.139 | 0.163 | 0.224 |
| **Plate Average** | 0.093 | 0.092 | 0.092 | 0.091 |
| **PIM: Small Plate (Simulated Loss Factor = 0.10)** | | | | |
| **Close to Boundary** | 0.053 | 0.059 | 0.074 | 0.082 |
| **Inside the Direct Field** | 0.047 | 0.041 | 0.045 | 0.048 |
| **Inside the Reverberant Field** | 0.093 | 0.099 | 0.110 | 0.144 |
| **Close to Mean Free Path** | 0.093 | 0.121 | 0.126 | 0.172 |
| **Plate Average** | 0.089 | 0.089 | 0.089 | 0.088 |

For the highly damped panel, the accuracies in the estimation of loss factor (the plate average), of the highly damped panel, are all low and within 6%, 9%, and 12% for Large, Medium and Small panels, respectively. For these computational plate models, the value of loss factors estimated from the panel boundaries are also underestimated except for Large and Medium panels analyzed in the higher frequency bands.

If the radius of the direct field is smaller than one-fourth of the mean free path the loss factors estimated from the reverberant field range from 07% low to 20% high; otherwise, the loss factors in the reverberant field are always overestimated. The loss factors measured from the response locations inside the direct field severely underestimate the loss factors.

From this computational analysis, it is concluded that the loss factors estimated from responses measured from either the direct field or close to panel's boundary are underestimated. In general, for the highly damped panel the loss factors estimated from the reverberant field are overestimated.

For PIM-based loss factor estimation processes, it matters where the panel is excited and where the response is measured. These choices are even more significant for smaller panels. It may seem "serendipitous" that the average loss factor is within 12% lower accuracy, but these loss factor estimates are accurate because the total energy is determined from hundreds of wide spread response measurements.

### 4.2.2 Impulse Response Decay Method

An automated slope-fitting algorithm to determine the decay rate from the decay curve has been developed. In the analysis presented herein, the loss factors for the lightly damped panels are accurately determined by using the automated slope-fitting algorithm. Panels with higher damping loss factor produce decay signatures with only a small number of oscillations before reaching the "out of band noise floor". This "noise floor" is similar to an actual noise floor in an experimental analysis. As a result, automated slope-fitting approach required supervision, especially, in the analysis of the highly damped panels and in some cases manual slope fitting as an "over-ride" is implemented (Refer to Appendix C). Eventually, all the loss factors for the panel with 10% loss factor were determined by using the conventional manual slope fitting approach. The choice of manual slope fitting may cause some level of human error in the estimation of decay rate (and loss factor). In Table 4.3, the number of response locations—from which the loss factors are estimated—are presented. For each of these response locations, loss factors in each frequency band are determined.

**Table 4.3: Number of response locations for IRDM based loss factor analysis**

| **Simulated $\eta$** | **Large Panel** | **Medium Panel** | **Small Panel** |
|---|---|---|---|
| **0.01**<br>**Slope Fitting – Entirely Automated** | 425 | 221 | 117 |
| **0.10**<br>**Slope Fitting – Manual** | 117 | 63 | 35 |

In Figures 4.8 to 4.13 the IRDM based loss factor estimates, in four frequency bands, are presented for three plate sizes and two damping levels. In Tables 4.4 and 4.5 the IRDM based loss factor estimates for the computational plates are summarized.

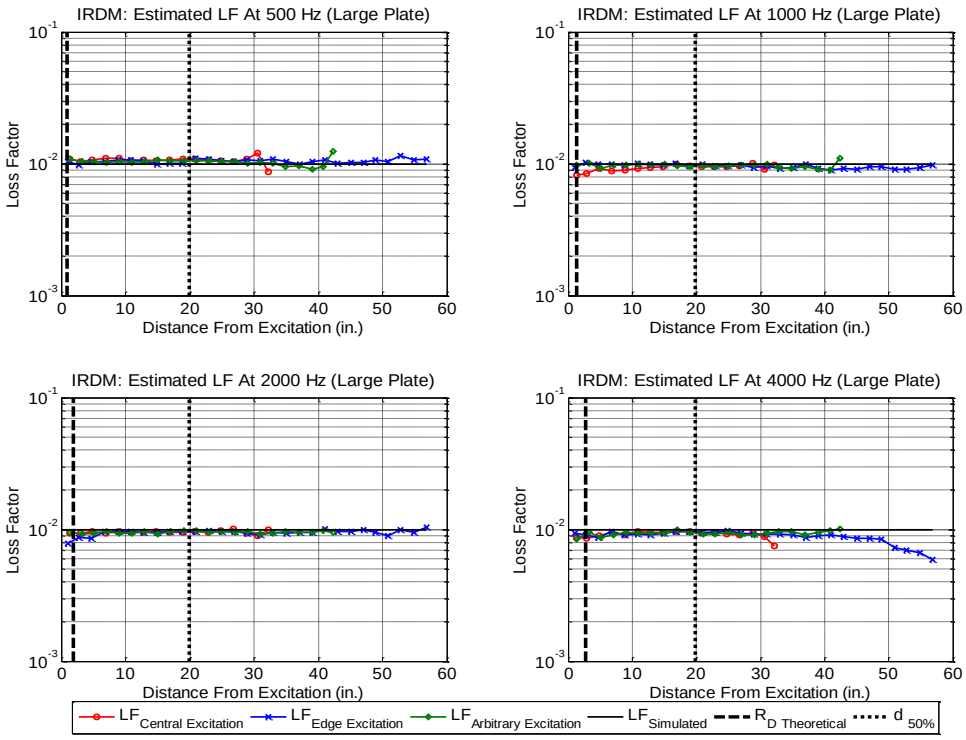


**Figure 4.8: IRDM based estimated loss factor for Large plate (simulated loss factor of 0.01)**

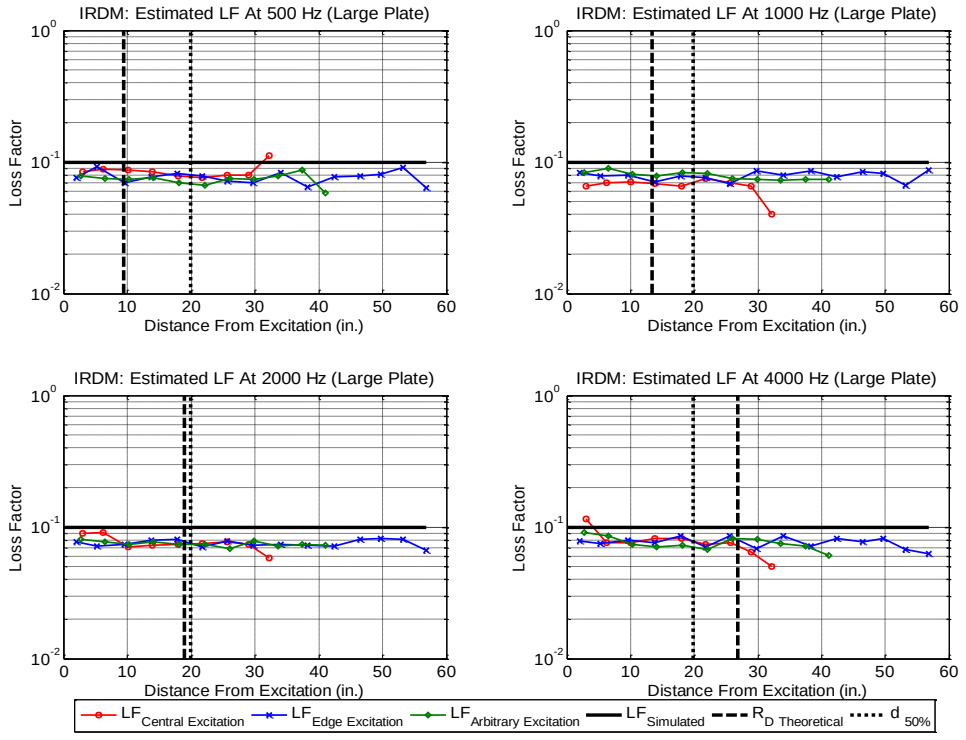


**Figure 4.9: IRDM based estimated loss factor for Large plate (simulated loss factor of 0.10)**

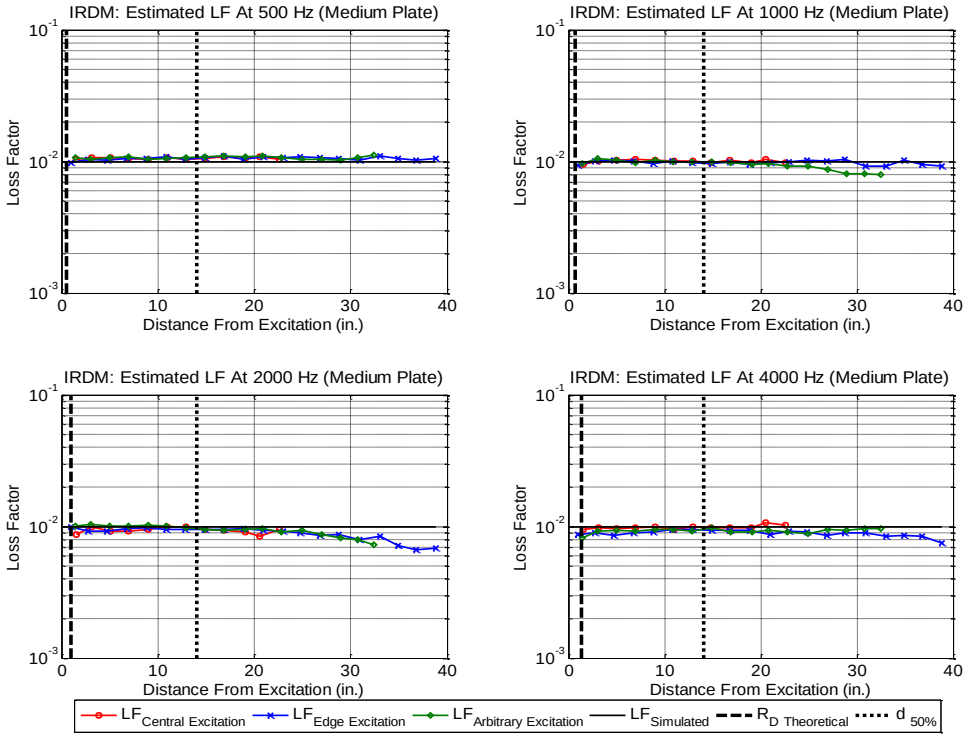


**Figure 4.10: IRDM based estimated loss factor for Medium plate (simulated loss factor of 0.01)**

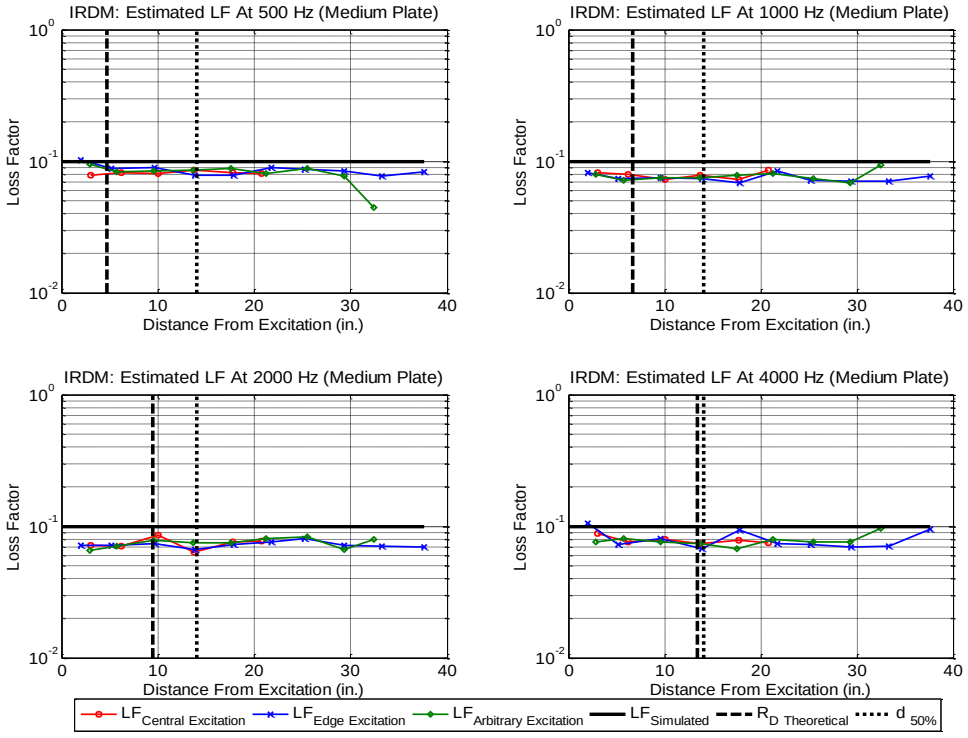


**Figure 4.11: IRDM based estimated loss factor for Medium plate (simulated loss factor of 0.10)**

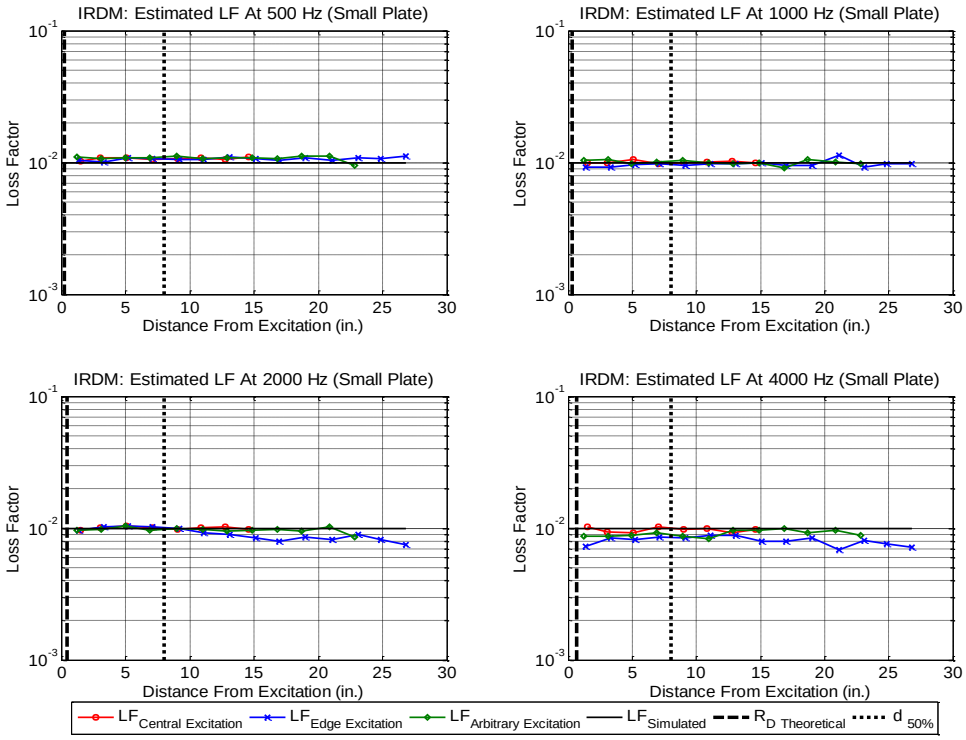


**Figure 4.12: IRDM based estimated loss factor for Small plate (simulated loss factor of 0.01)**

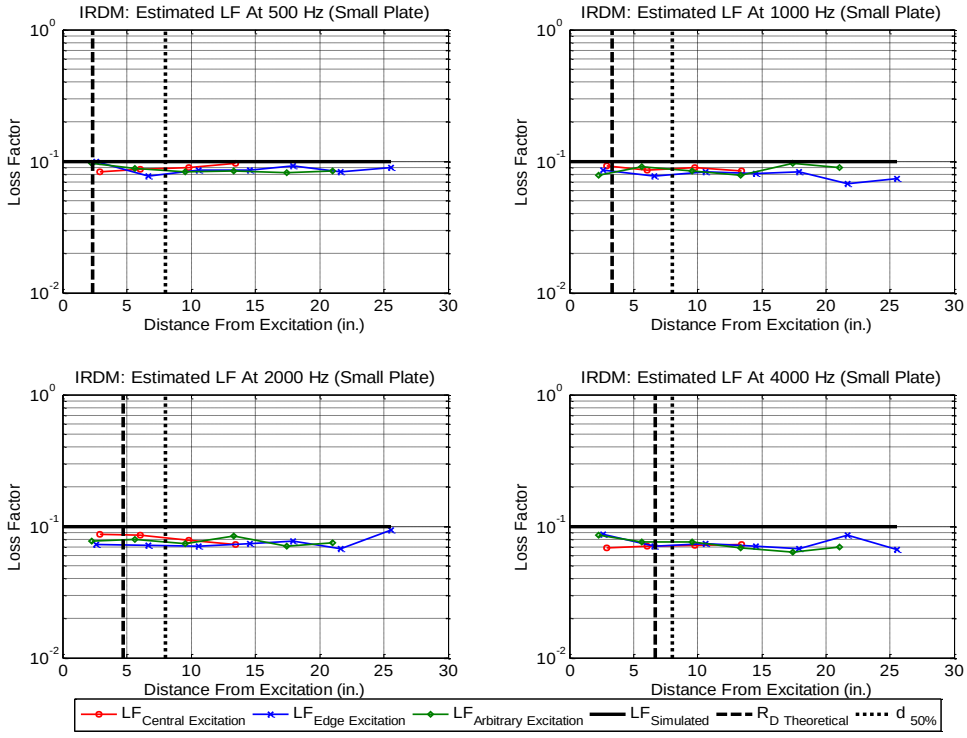


**Figure 4.13: IRDM based estimated loss factor for Small plate (simulated loss factor of 0.10)**

**Table 4.4: IRDM based estimated loss factor for panels with simulated loss factor of 0.01**

| | Frequency of Analysis | | | |
|---|---|---|---|---|
| **Measurement Regions** | **500 Hz** | **1000 Hz** | **2000 Hz** | **4000 Hz** |
| **IRDM: Large Plate (Simulated Loss Factor = 0.01)** | | | | |
| **Close to Boundary** | 0.0105 | 0.0098 | 0.0097 | 0.0094 |
| **Inside the Direct Field** | 0.0119 | 0.0089 | 0.0093 | 0.0083 |
| **Inside the Reverberant Field** | 0.0105 | 0.0096 | 0.0096 | 0.0094 |
| **Close to Mean Free Path** | 0.0104 | 0.0096 | 0.0096 | 0.0093 |
| **Plate Average** | 0.0105 | 0.0096 | 0.0096 | 0.0094 |
| **IRDM: Medium Plate (Simulated Loss Factor = 0.01)** | | | | |
| **Close to Boundary** | 0.0108 | 0.0099 | 0.0094 | 0.0095 |
| **Inside the Direct Field** | 0.0102 | 0.0087 | 0.0101 | 0.0087 |
| **Inside the Reverberant Field** | 0.0106 | 0.0099 | 0.0096 | 0.0096 |
| **Close to Mean Free Path** | 0.0107 | 0.0098 | 0.0094 | 0.0096 |
| **Plate Average** | 0.0106 | 0.0099 | 0.0096 | 0.0096 |
| **IRDM: Small Plate (Simulated Loss Factor = 0.01)** | | | | |
| **Close to Boundary** | 0.0107 | 0.0100 | 0.0100 | 0.0097 |
| **Inside the Direct Field** | 0.0102 | 0.0108 | 0.0090 | 0.0107 |
| **Inside the Reverberant Field** | 0.0108 | 0.0100 | 0.0099 | 0.0094 |
| **Close to Mean Free Path** | 0.0107 | 0.0100 | 0.0099 | 0.0095 |
| **Plate Average** | 0.0108 | 0.0100 | 0.0099 | 0.0094 |

It is observed that loss factor estimates, using IRDM, do not have a strong or consistent pattern of dependence on distance from the excitation location. For all the test cases considered for lightly damped computational plate model, the accuracy of panel estimated loss factor is typically low (except at low frequency) and within 8% of the target.

**Table 4.5: IRDM based estimated loss factor for panels with simulated loss factor of 0.10**

| | Frequency of Analysis | | | |
|---|---|---|---|---|
| **Measurement Regions** | **500 Hz** | **1000 Hz** | **2000 Hz** | **4000 Hz** |
| **IRDM: Large Plate (Simulated Loss Factor = 0.10)** | | | | |
| **Close to Boundary** | 0.077 | 0.074 | 0.077 | 0.076 |
| **Inside the Direct Field** | 0.081 | 0.078 | 0.077 | 0.076 |
| **Inside the Reverberant Field** | 0.077 | 0.074 | 0.073 | 0.074 |
| **Close to Mean Free Path** | 0.076 | 0.075 | 0.074 | 0.074 |
| **Plate Average** | 0.079 | 0.076 | 0.078 | 0.078 |
| **IRDM: Medium Plate (Simulated Loss Factor = 0.10)** | | | | |
| **Close to Boundary** | 0.087 | 0.078 | 0.074 | 0.076 |
| **Inside the Direct Field** | 0.083 | 0.082 | 0.074 | 0.077 |
| **Inside the Reverberant Field** | 0.084 | 0.075 | 0.074 | 0.074 |
| **Close to Mean Free Path** | 0.088 | 0.075 | 0.073 | 0.075 |
| **Plate Average** | 0.086 | 0.078 | 0.076 | 0.078 |
| **IRDM: Small Plate (Simulated Loss Factor = 0.10)** | | | | |
| **Close to Boundary** | 0.088 | 0.087 | 0.079 | 0.068 |
| **Inside the Direct Field** | 0.096 | 0.080 | 0.080 | 0.072 |
| **Inside the Reverberant Field** | 0.086 | 0.086 | 0.080 | 0.071 |
| **Close to Mean Free Path** | 0.089 | 0.084 | 0.079 | 0.069 |
| **Plate Average** | 0.088 | 0.088 | 0.079 | 0.072 |

For the highly damped computational plate models (simulated loss factor of 0.10) the predicted loss factors are all underestimated. The worst underestimations for these panels are: 24% for Large sized panel, 24% for Medium sized panel and 29% for Small panel. These results are consistent with previous studies by KUAE authors [11 and 14].

### 4.2.3 Random Decrement Technique

To extract the randomdec signature at a response location a random force of arbitrary length is convolved with an impulse response function and this is the most computationally time consuming step in the RDT-based analysis. Therefore, compared to IRDM, relatively fewer response points were used for RDT for the highly damped plate. The distance based loss factor is estimated averaging the decay curves from all response locations in a region of interest (e.g., an annular sector) to compute the decay curve from which the loss factor is estimated. In Table 4.6, the number of response locations for RDT-based analysis are presented. For loss factor of 0.01, the number of response locations chosen are one-fourth of the number of number of response locations used in IRDM.

**Table 4.6: Number of response locations for RDT based loss factor analysis**

| **Simulated $\eta$** | **Large Panel** | **Medium Panel** | **Small Panel** |
|---|---|---|---|
| **0.01 (Slope Fitting – Manual)** | 117 | 63 | 35 |
| **0.10 (Slope Fitting – Manual)** | 117 | 63 | 35 |

In the RDT loss factor estimation processes, all the decay rates are determined by using a manual slope-fitting approach. Like IRDM, no strong correlation between distance of response location from the excitation location and loss factor is observed. Randomdec signature could be extracted by either averaging the autocorrelation functions of triggered samples ("Averaging Autocorrelation Functions") or directly averaging the triggered samples ("Direct Averaging" ). In Figures 4.14 to 4.25, RDT based loss factor estimates for these two processes are presented and these are summarized in Tables 4.7 and 4.8.

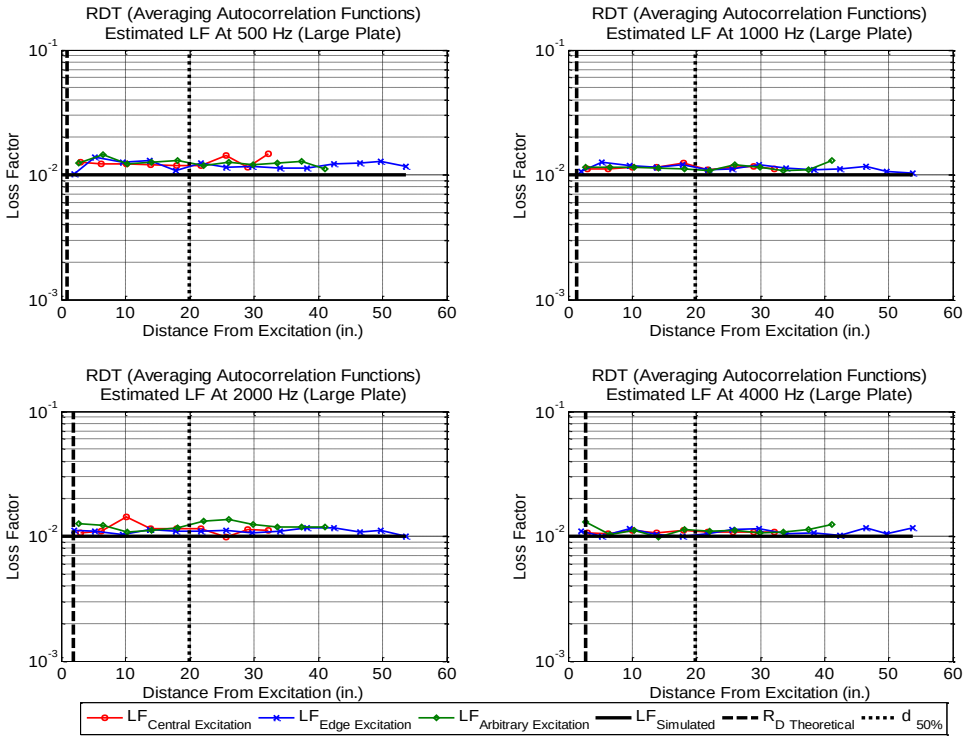


**Figure 4.14: RDT (averaging autocorrelation functions) based estimated loss factor for Large plate (simulated loss factor of 0.01)**

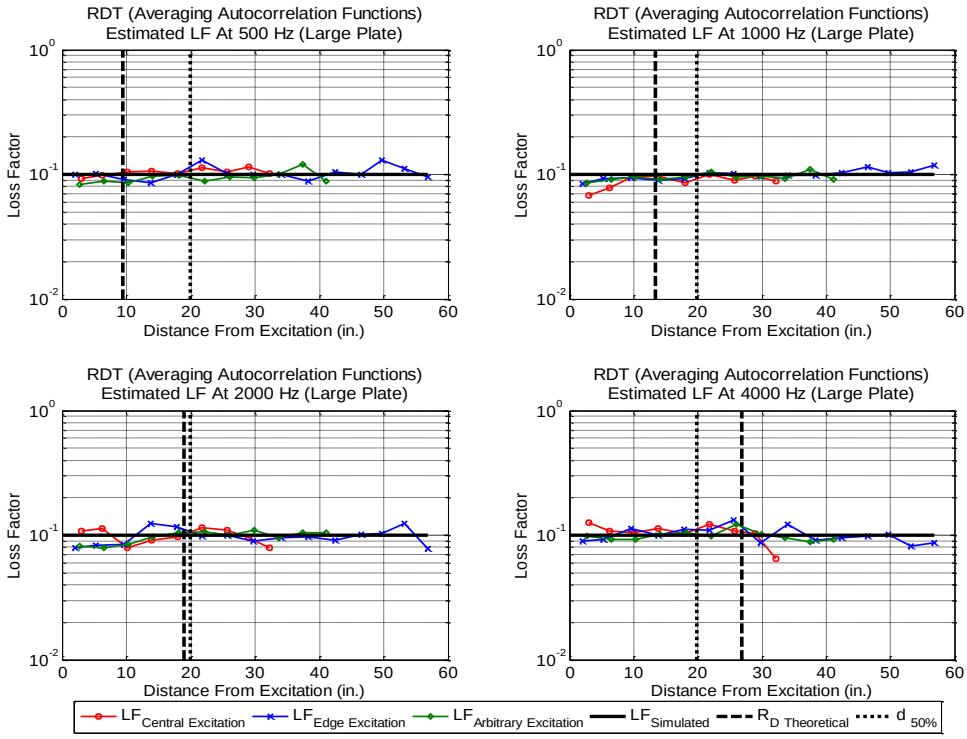


**Figure 4.15: RDT (averaging autocorrelation functions) based estimated loss factor for Large plate (simulated loss factor of 0.10)**

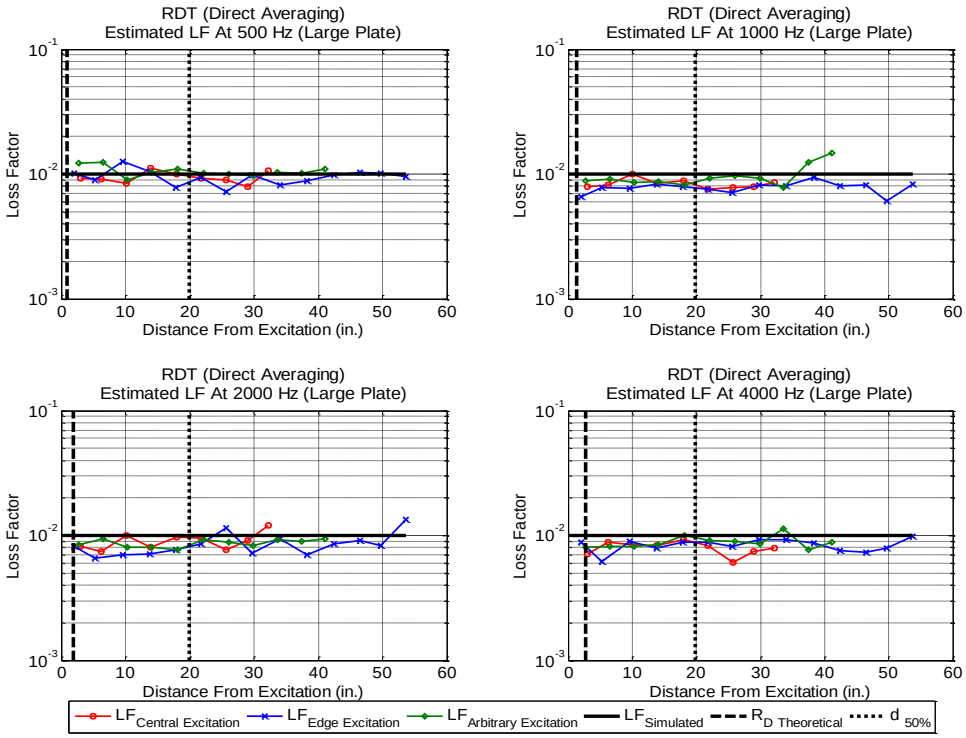


**Figure 4.16: RDT (directly averaging the triggered samples) based estimated loss factor for Large plate (simulated loss factor of 0.01)**

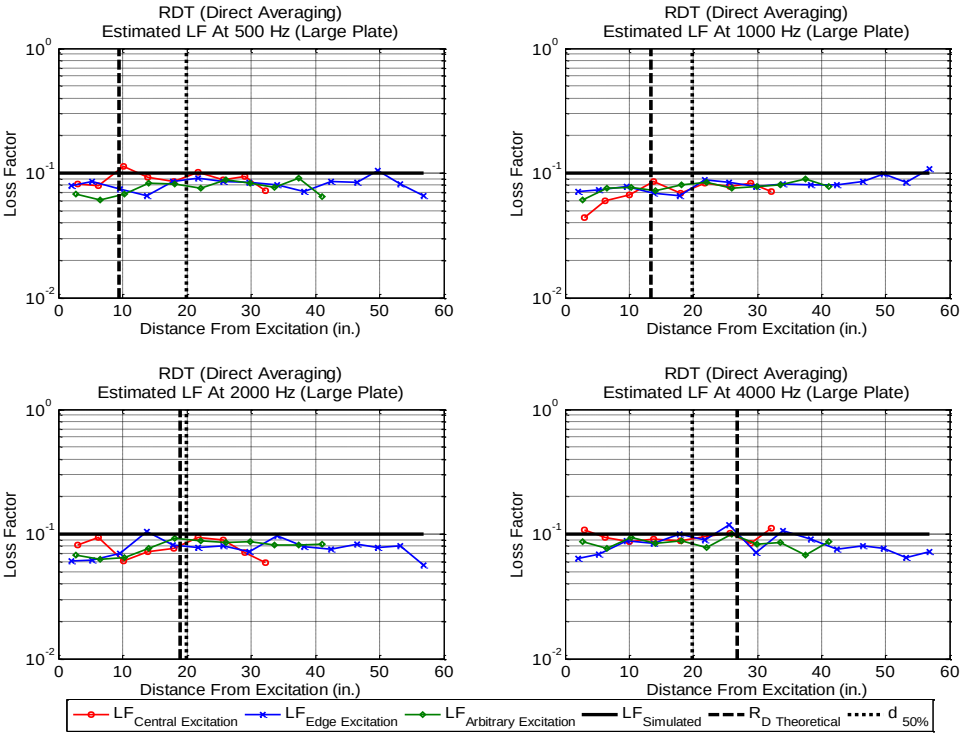


**Figure 4.17: RDT (directly averaging the triggered samples) based estimated loss factor for Large plate (simulated loss factor of 0.10)**

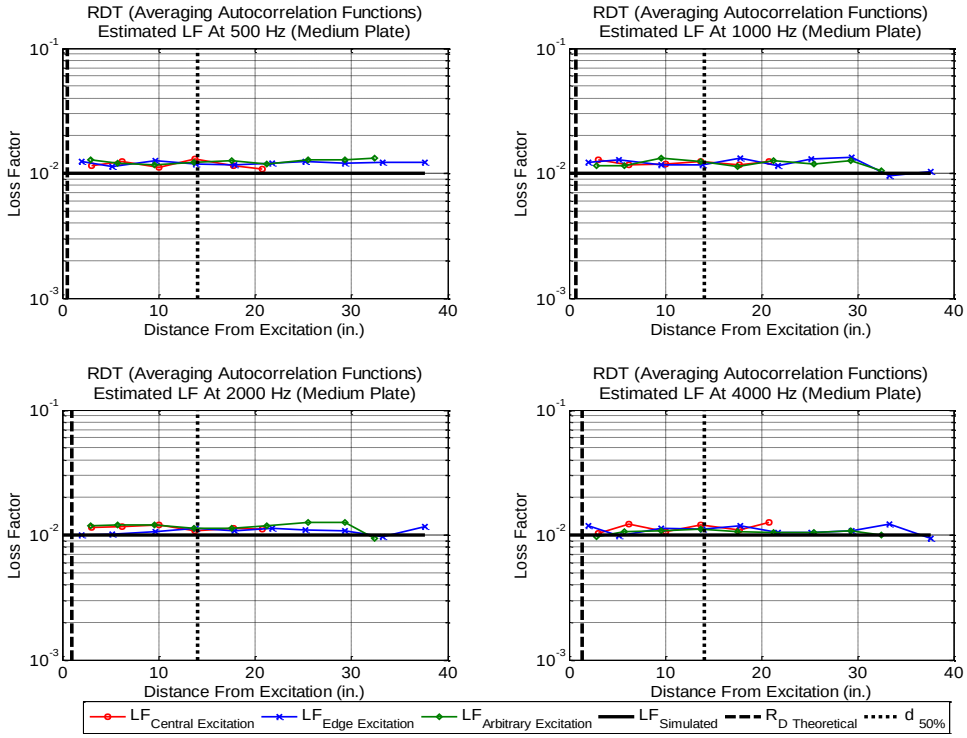


**Figure 4.18: RDT (averaging autocorrelation functions) based estimated loss factor for Medium plate (simulated loss factor of 0.01)**

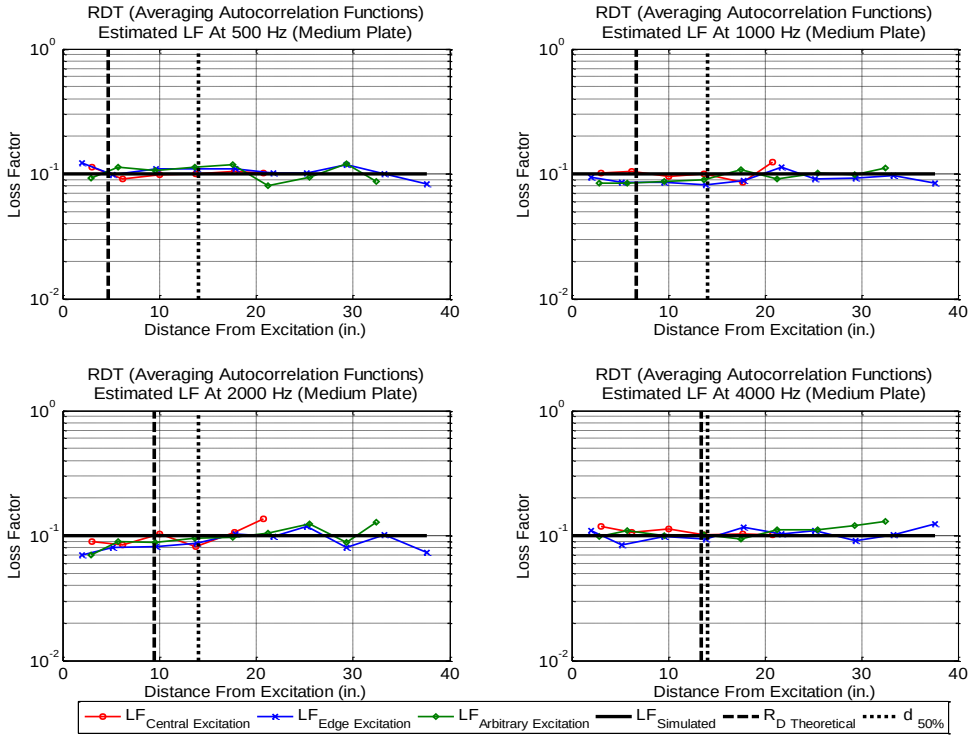


**Figure 4.19: RDT (averaging autocorrelation functions) based estimated loss factor for Medium plate (simulated loss factor of 0.10)**

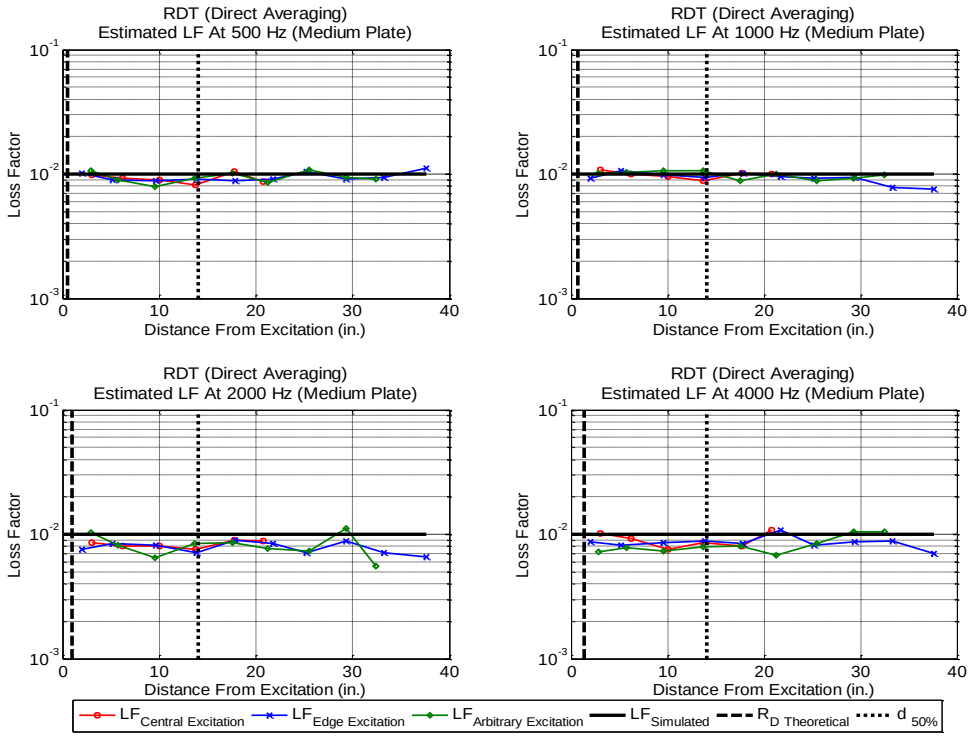


**Figure 4.20: RDT (directly averaging the triggered samples) based estimated loss factor for Medium plate (simulated loss factor of 0.01)**

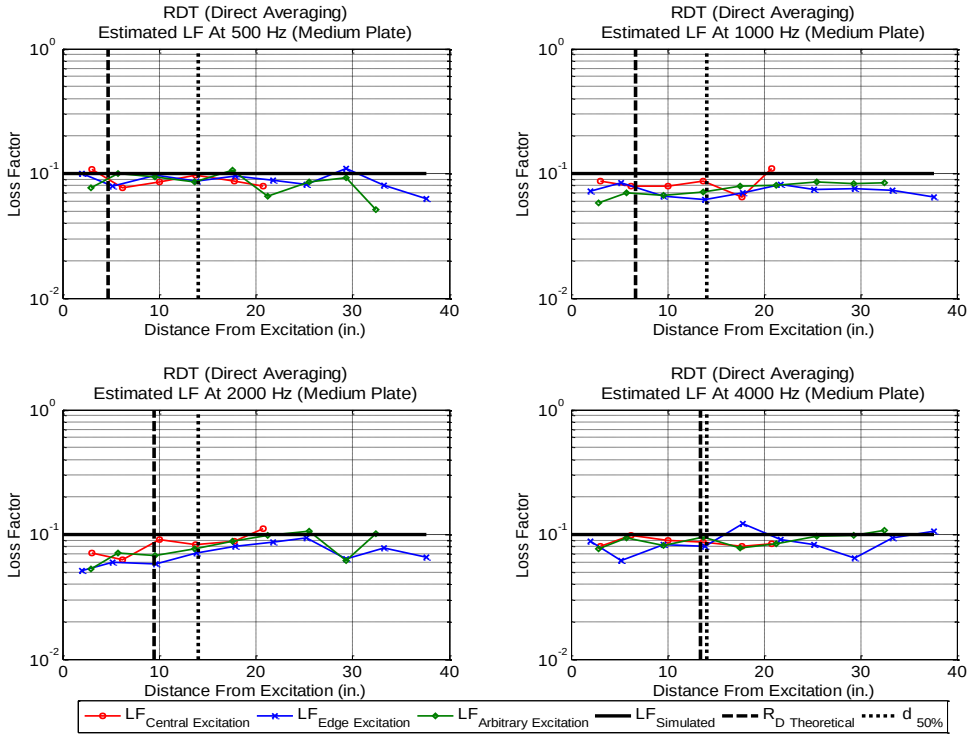


**Figure 4.21: RDT (directly averaging the triggered samples) based estimated loss factor for Medium plate (simulated loss factor of 0.10)**

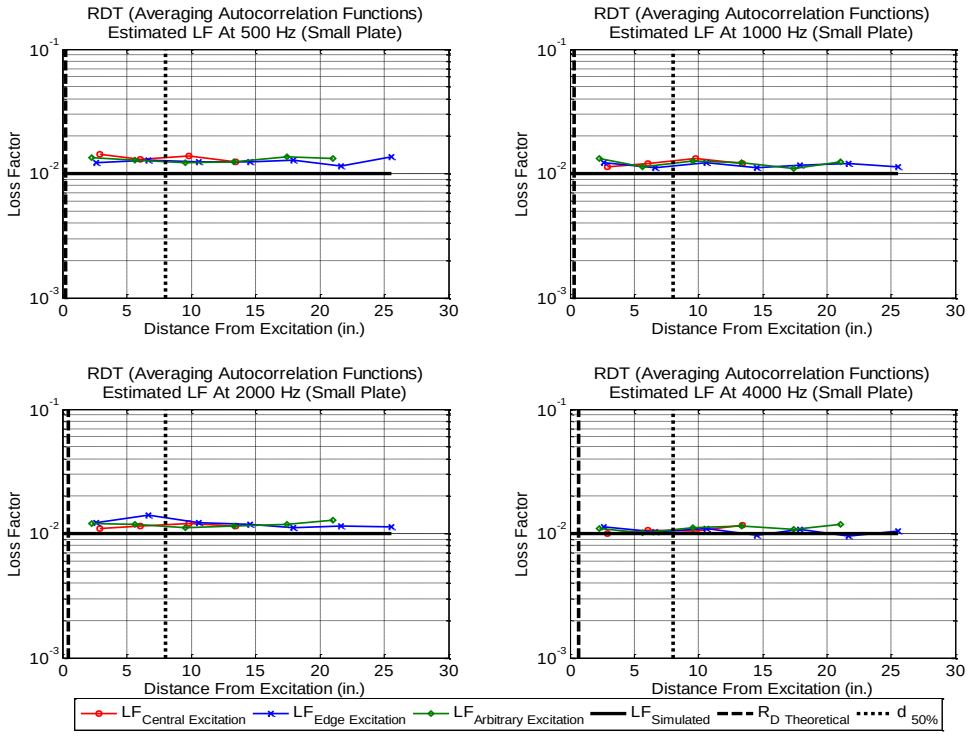


**Figure 4.22: RDT (averaging autocorrelation functions) based estimated loss factor for Small plate (simulated loss factor of 0.01)**

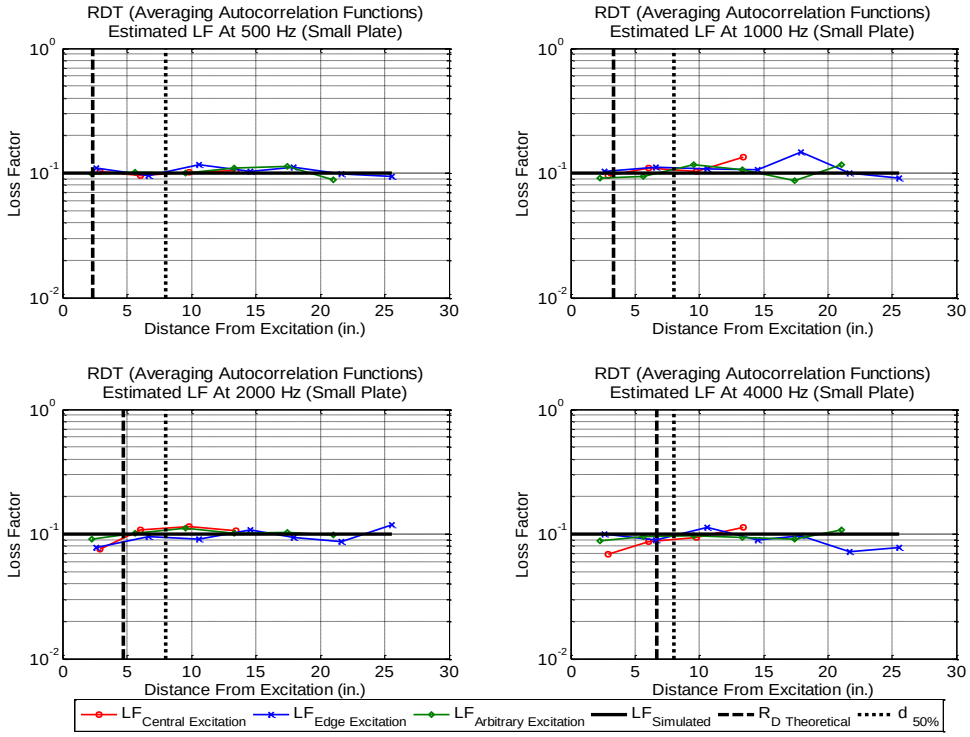


**Figure 4.23: RDT (averaging autocorrelation functions) based estimated loss factor for Small plate (simulated loss factor of 0.10)**

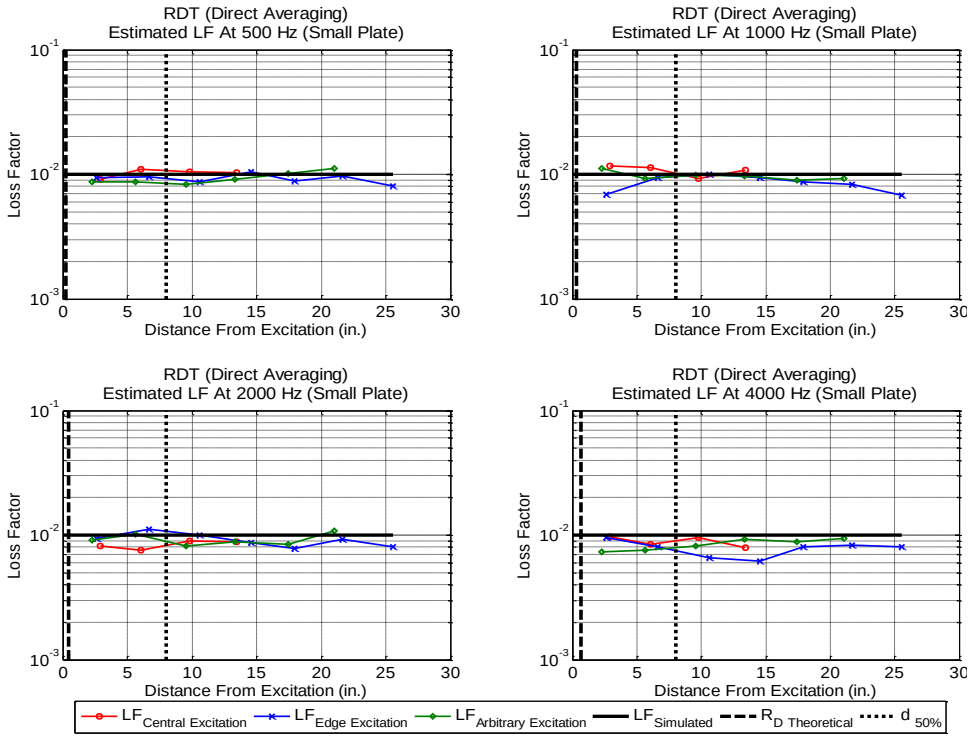


**Figure 4.24: RDT (directly averaging the triggered samples) based estimated loss factor for Small plate (simulated loss factor of 0.10)**

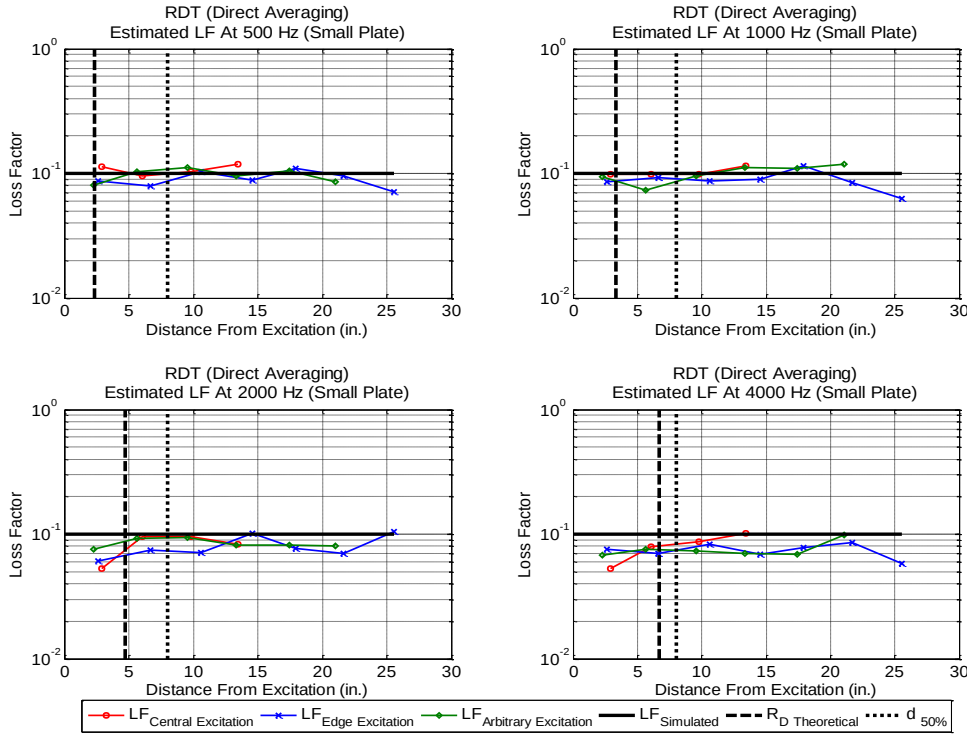


**Figure 4.25: RDT (directly averaging the triggered samples) based estimated loss factor for Small plate (simulated loss factor of 0.10)**

**Table 4.7: RDT based estimated loss factor for panels with simulated loss factor of 0.01**

| | Frequency of Analysis | | | |
|---|---|---|---|---|
| **Measurement Regions** | **500 Hz** | **1000 Hz** | **2000 Hz** | **4000 Hz** |
| **RDT: Large Plate (Simulated Loss Factor = 0.01)** | | | | |
| **Averaging the Autocorrelation Functions** | | | | |
| **Inside the Direct Field** | 0.0134 | 0.0106 | 0.0115 | 0.0104 |
| **Inside the Reverberant Field** | 0.0127 | 0.0113 | 0.0116 | 0.0108 |
| **Plate Average** | 0.0123 | 0.0113 | 0.0115 | 0.0109 |
| **Direct Averaging** | | | | |
| **Inside the Direct Field** | 0.0113 | 0.0093 | 0.0102 | 0.0084 |
| **Inside the Reverberant Field** | 0.0095 | 0.0090 | 0.0095 | 0.0081 |
| **Plate Average** | 0.0102 | 0.0088 | 0.0089 | 0.0088 |
| **RDT: Medium Plate (Simulated Loss Factor = 0.01)** | | | | |
| **Averaging the Autocorrelation Functions** | | | | |
| **Inside the Direct Field** | 0.0121 | 0.0123 | 0.0117 | 0.0108 |
| **Inside the Reverberant Field** | 0.0120 | 0.0120 | 0.0113 | 0.0105 |
| **Plate Average** | 0.0121 | 0.0122 | 0.0112 | 0.0110 |
| **Direct Averaging** | | | | |
| **Inside the Direct Field** | 0.0107 | 0.0102 | 0.0089 | 0.0080 |
| **Inside the Reverberant Field** | 0.0093 | 0.0099 | 0.0089 | 0.0083 |
| **Plate Average** | 0.0102 | 0.0106 | 0.0088 | 0.0092 |
| **RDT: Small Plate (Simulated Loss Factor = 0.01)** | | | | |
| **Averaging the Autocorrelation Functions** | | | | |
| **Inside the Direct Field** | 0.0138 | 0.0121 | 0.0115 | 0.0109 |
| **Inside the Reverberant Field** | 0.0130 | 0.0114 | 0.0112 | 0.0106 |
| **Plate Average** | 0.0127 | 0.0118 | 0.0118 | 0.0107 |
| **Direct Averaging** | | | | |
| **Inside the Direct Field** | 0.0088 | 0.0114 | 0.0089 | 0.0075 |
| **Inside the Reverberant Field** | 0.0102 | 0.0100 | 0.0084 | 0.0087 |
| **Plate Average** | 0.0101 | 0.0102 | 0.0093 | 0.0087 |

**Table 4.8: RDT based estimated loss factor for panels with simulated loss factor of 0.10**

| | Frequency of Analysis | | | |
|---|---|---|---|---|
| **Measurement Regions** | **500 Hz** | **1000 Hz** | **2000 Hz** | **4000 Hz** |
| **RDT: Large Plate (Simulated Loss Factor = 0.10)** | | | | |
| **Averaging the Autocorrelation Functions** | | | | |
| **Inside the Direct Field** | 0.096 | 0.090 | 0.094 | 0.104 |
| **Inside the Reverberant Field** | 0.102 | 0.093 | 0.105 | 0.100 |
| **Plate Average** | 0.105 | 0.099 | 0.103 | 0.110 |
| **Direct Averaging** | | | | |
| **Inside the Direct Field** | 0.083 | 0.076 | 0.084 | 0.087 |
| **Inside the Reverberant Field** | 0.088 | 0.078 | 0.089 | 0.084 |
| **Plate Average** | 0.089 | 0.080 | 0.084 | 0.093 |
| **RDT: Medium Plate (Simulated Loss Factor = 0.10)** | | | | |
| **Averaging the Autocorrelation Functions** | | | | |
| **Inside the Direct Field** | 0.100 | 0.099 | 0.086 | 0.102 |
| **Inside the Reverberant Field** | 0.108 | 0.096 | 0.096 | 0.100 |
| **Plate Average** | 0.115 | 0.104 | 0.103 | 0.115 |
| **Direct Averaging** | | | | |
| **Inside the Direct Field** | 0.096 | 0.088 | 0.089 | 0.084 |
| **Inside the Reverberant Field** | 0.091 | 0.083 | 0.092 | 0.088 |
| **Plate Average** | 0.098 | 0.086 | 0.086 | 0.096 |
| **RDT: Small Plate (Simulated Loss Factor = 0.10)** | | | | |
| **Averaging the Autocorrelation Functions** | | | | |
| **Inside the Direct Field** | 0.095 | 0.092 | 0.080 | 0.085 |
| **Inside the Reverberant Field** | 0.105 | 0.103 | 0.099 | 0.095 |
| **Plate Average** | 0.107 | 0.112 | 0.109 | 0.100 |
| **Direct Averaging** | | | | |
| **Inside the Direct Field** | 0.110 | 0.093 | 0.091 | 0.094 |
| **Inside the Reverberant Field** | 0.107 | 0.098 | 0.097 | 0.090 |
| **Plate Average** | 0.103 | 0.103 | 0.092 | 0.083 |

For the lightly damped panels, with simulated loss factor of 0.01, the direct averaging approach performed better than averaging autocorrelation functions. The loss factors predicted using the averaging autocorrelation function is always overestimated by 10% to 25%. For direct averaging, the estimated loss factors for the entire panel are mostly underestimated by up to 17% but sometimes over-predicted by up to 14%.

For highly damped plates (simulated loss factor of 0.10) the autocorrelation averaging approach performed better than the direct averaging approach. The direct averaging has shown an underestimation no worse than 25% and the occasional over-prediction of as much as 10% for the small plate, at low frequency. The averaging autocorrelation approach, overestimations up to 7% and underestimations up to 7% were noted. For the highly damped panels, the estimated loss factors from IRDM are comparable to RDT with direct averaging.

## 4.3 Experimental Analysis

In the experimental analysis of plates, two plates with CLD treatments were designed using RKU [12 and 13] beam theory for loss factors approximately equal to 0.06 (intermediate damping level) and 0.10 (high damping level). Plate thicknesses and dimensions are provided in Table 3.1. First, the large plates were tested, and then these plates were segmented into a half and a quarter of the initial plate size. Each plate is excited mechanically, using a mechanical shaker, at four excitation locations: center, corner and two arbitrarily chosen. That is, a total of six plates were analyzed experimentally, in three frequency bands, for four excitation locations. For PIM, IRDM, and RDT loss factors are estimated, from multiple response locations such as in annular sectors, inside the direct field, inside the reverberant field and over the entire panel.

In this experimental study, Excitation #1 is a central excitation location, Excitation #2 is a corner excitation location and Excitation #3 and #4 are arbitrarily chosen excitation locations as shown in Figure 3.5. In the following sections the technique-specific estimated loss factors are presented.

Unlike the computational analyses, the experimental analyses are often bound by hardware (such as shaker or sensor) limitations and noise during the experiment. Therefore, in experimental analysis it is not uncommon for outliers to exist. For these panels tested experimentally, loss factors close to 0.5 and above are not practically possible and hence are considered outliers. These type of outliers were removed to establish a better estimation of loss factor.

### 4.3.1 Selected Frequency Bands of Analysis

From the definition of loss factor, referring to Equation (2.36), the denominator term—based on a sum of squared mobility functions—is positive definite and the numerator term—the real part of the driving point mobility function—should be positive for a realistic loss factor estimate. In the tests performed by KUAE authors in the Spirit AeroSystems Structural Acoustics Lab, it has been observed that the real part of the driving point FRF is entirely negative in the 4000 Hz band. Thus, in the 4000 Hz band the determined loss factor is negative which is not practically possible for the type of panels tested. One possible explanation for negative driving point FRF could be shaker's limitations in these high frequency bands. Therefore, for the panels tested experimentally the loss factors could not be determined in the 4000 Hz band and hence the experimental study was limited to 500 Hz, 1000 Hz and 2000 Hz.

### 4.3.2 Power Input Method

In Figures 4.26 to 4.31, the experimentally determined loss factors, in annular sectors, for multiple excitation locations are presented. Loss factors in specific regions, such as the direct field, the reverberant field and the entire plate, are summarized in Tables 4.9 and 4.10. Unlike computational analysis, an exact estimate of panel's loss factor is not known; thus, the approximate loss factor, from RKU based beam analysis, is used to estimate the relevant size of the direct field.

Even for the experimentally tested panels, it is observed that the corner excitation is the least reliable one. Thus the loss factor estimates of the entire panels are based on central and arbitrary excitation locations.

In this experimental analysis of real plates using PIM, the loss factors are underestimated inside the direct field and are significantly overestimated inside the reverberant field. The results clearly indicate that the loss factors estimated from only a few response locations cannot reliably estimate the panel's loss factor. To accurately determine the total kinetic energy—and in turn the panel's loss factor—it is apparently required to measure the mobility from a large number of well-distributed response locations.

Estimated panel loss factor is determined from the ratio of input power per cycle to total energy. Loss factors are estimated for each of the response locations. When analyzing a specific measurement region, such as in an annular sector, the loss factors that were outside the two standard deviation bound, and with value more than 0.5, were not considered in the region's loss factor ensemble. The sample size of the sorted loss factors turned out to be always more than half the sample size of the unsorted loss factors. The panel's loss factor is by averaging the ensemble of these sorted loss factors.

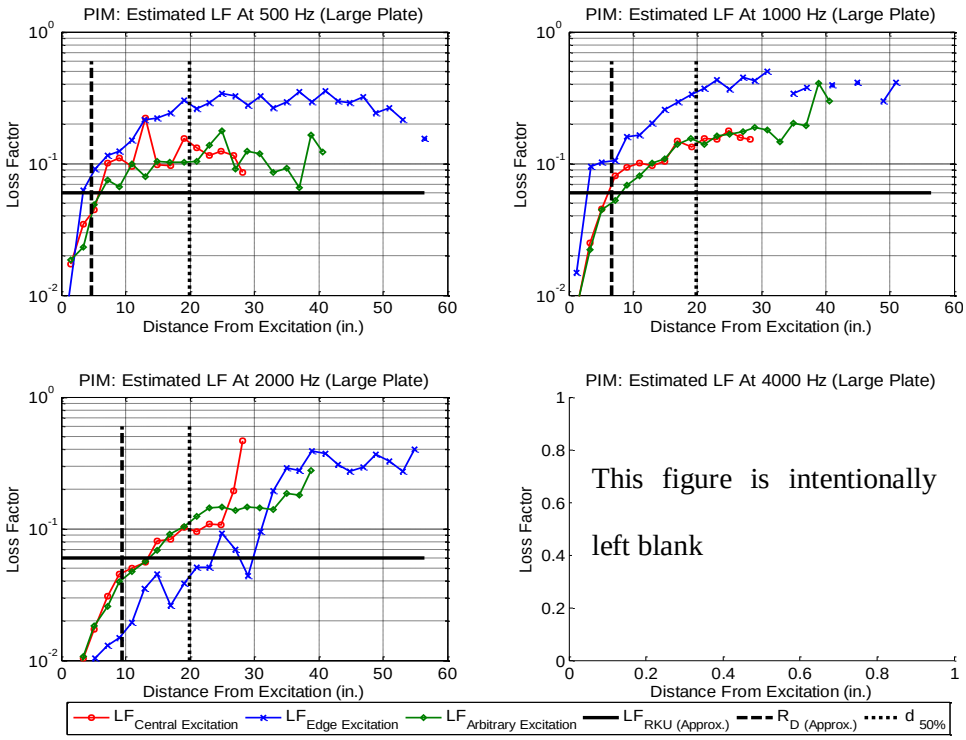


**Figure 4.26: PIM based estimated loss factor for Large plate (approximate loss factor of 0.06)**

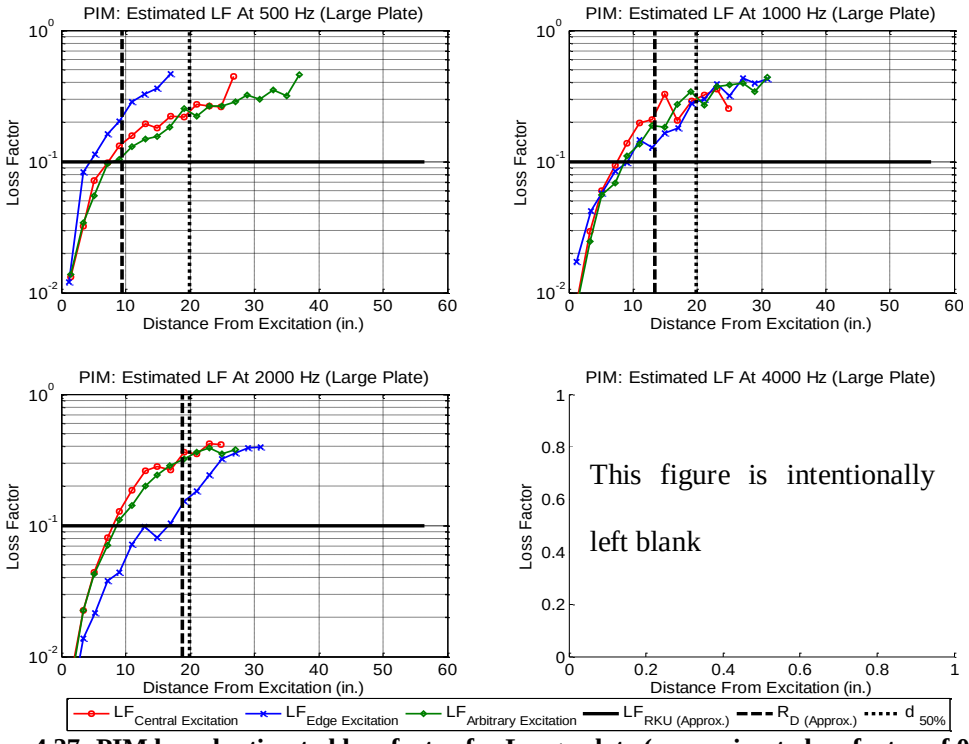


**Figure 4.27: PIM based estimated loss factor for Large plate (approximate loss factor of 0.10)**

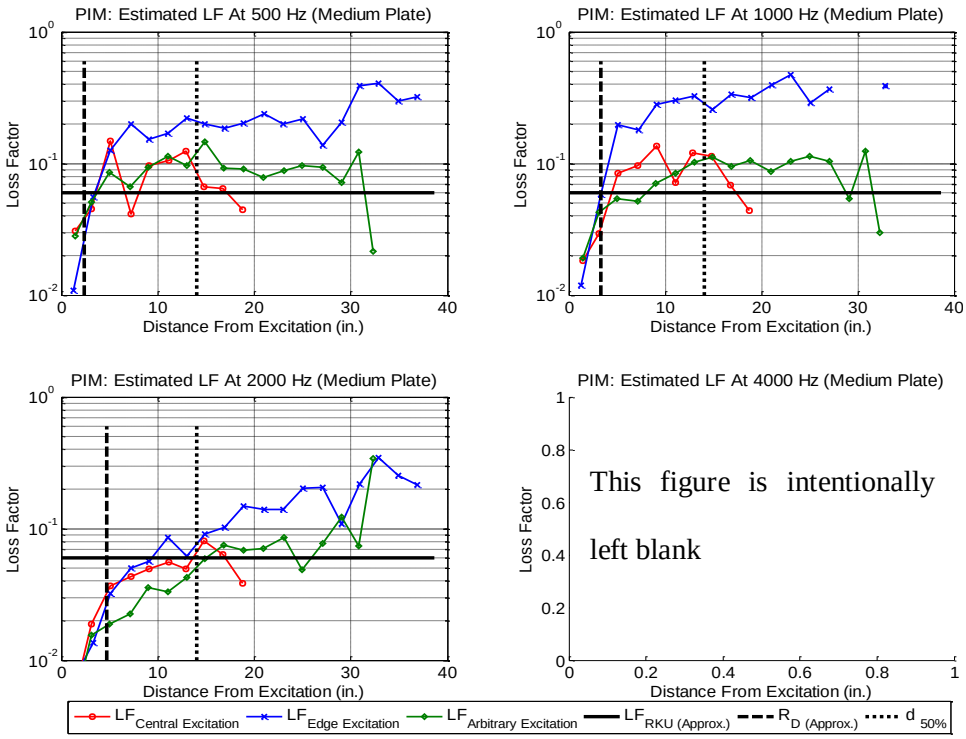


**Figure 4.28: PIM based estimated loss factor for Medium plate (approximate loss factor of 0.06)**

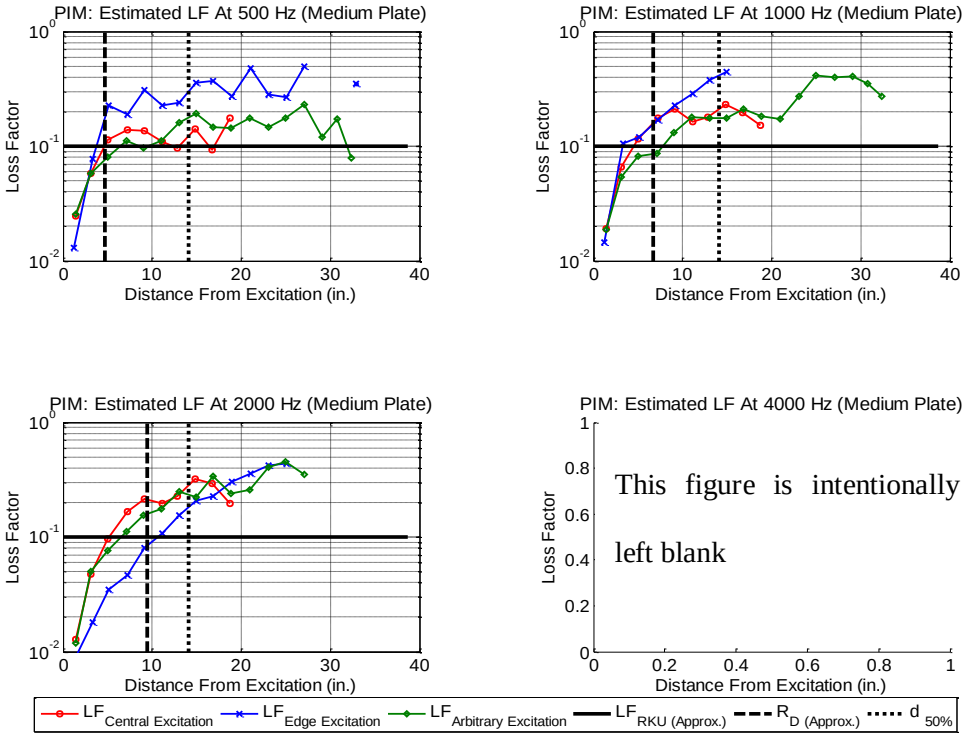


**Figure 4.29: PIM based estimated loss factor for Medium plate (approximate loss factor of 0.10)**

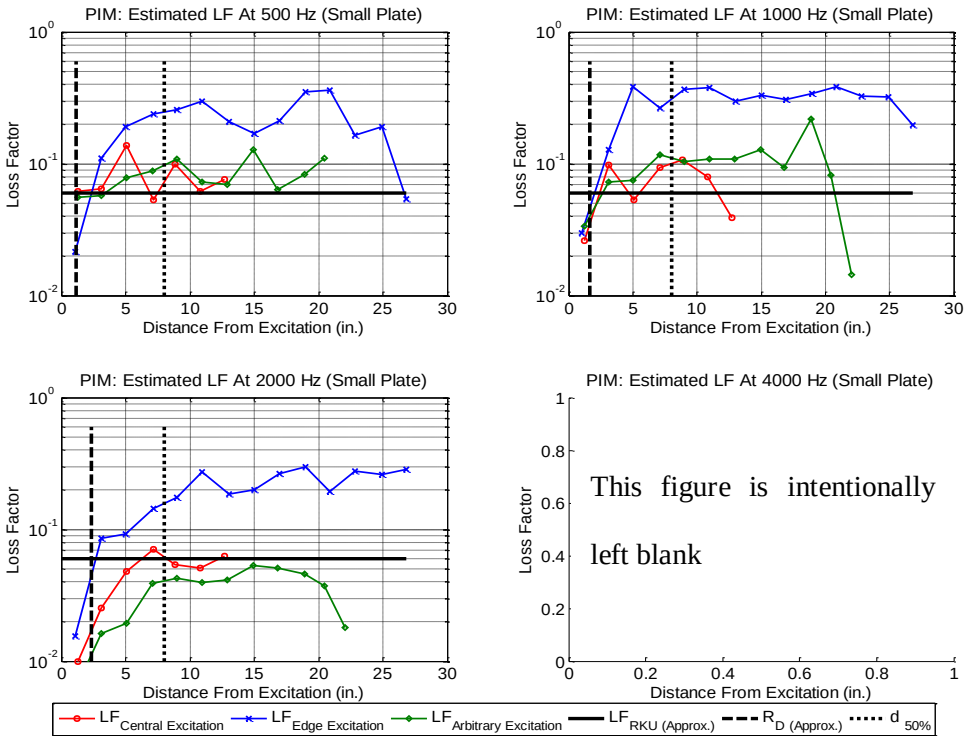


**Figure 4.30: PIM based estimated loss factor for Small plate (approximate loss factor of 0.06)**

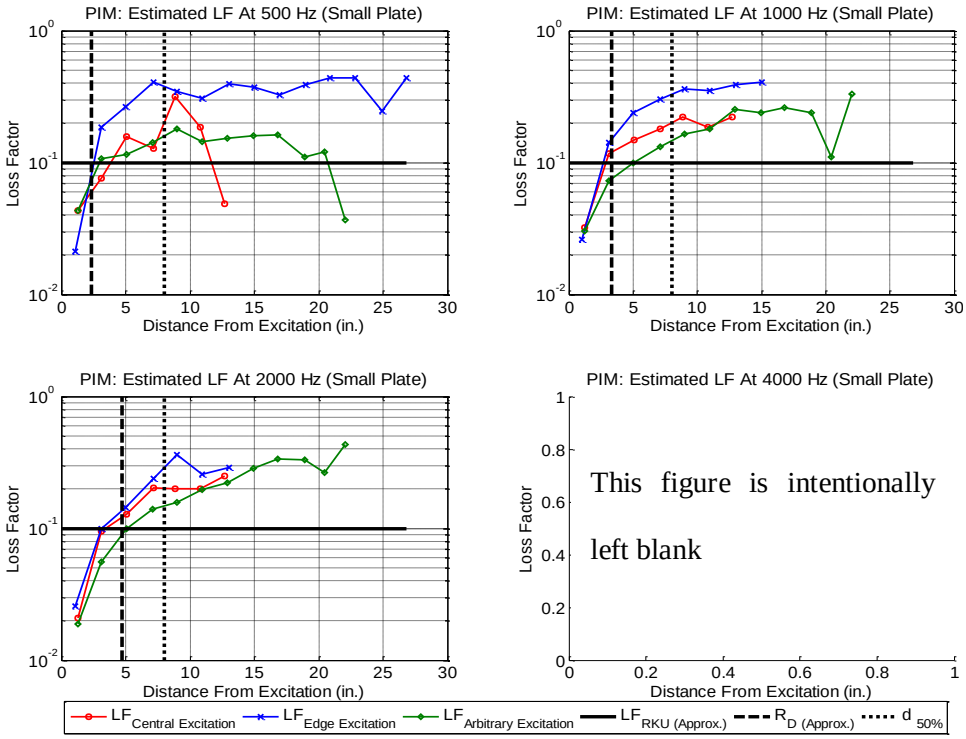


**Figure 4.31: PIM based estimated loss factor for Small plate (approximate loss factor of 0.10)**

**Table 4.9: PIM based estimated loss factor for panels with approximate loss factor of 0.06**

| | Frequency of Analysis | | | |
|---|---|---|---|---|
| **Measurement Regions** | **500 Hz** | **1000 Hz** | **2000 Hz** | **4000 Hz** |
| **PIM: Large Plate (Approximate Loss Factor = 0.06)** | | | | |
| **Inside the Direct Field** | 0.025 | 0.026 | 0.016 | -- |
| **Inside the Reverberant Field** | 0.097 | 0.115 | 0.083 | -- |
| **Close to Mean Free Path** | 0.106 | 0.161 | 0.128 | -- |
| **Plate Average** | 0.082 | 0.081 | 0.043 | -- |
| **PIM: Medium Plate (Approximate Loss Factor = 0.06)** | | | | |
| **Inside the Direct Field** | 0.029 | 0.023 | 0.011 | -- |
| **Inside the Reverberant Field** | 0.082 | 0.079 | 0.045 | -- |
| **Close to Mean Free Path** | 0.082 | 0.091 | 0.064 | -- |
| **Plate Average** | 0.078 | 0.071 | 0.035 | -- |
| **PIM: Small Plate (Approximate Loss Factor = 0.06)** | | | | |
| **Inside the Direct Field** | 0.041 | 0.031 | 0.010 | -- |
| **Inside the Reverberant Field** | 0.074 | 0.086 | 0.039 | -- |
| **Close to Mean Free Path** | 0.069 | 0.092 | 0.048 | -- |
| **Plate Average** | 0.074 | 0.079 | 0.033 | -- |

For the intermediately damped panels (target $\eta$=0.06) excited at the corner, loss factors are significantly overestimated. As a result, this data has been ignored. The loss factor estimates in the reverberant field and close to the mean free path, of the Large Medium and Small panels analyzed in the 500 and 1000 Hz bands, have significant overestimation. As observed from the analysis of simulated panels, the estimated loss factors of the three intermediately damped panels are underestimated inside the direct field.

The loss factor of the entire plate is determined from the response measured from a large number of points spread over the entire panel. For these three intermediately damped panels, loss factor estimated in the 2000 Hz band is also underestimated. In comparison to

500 and 1000 Hz, the size of the direct field for 2000 Hz band is relatively large and thus a majority of the plate may experience a direct field leading to an underestimation of the loss factor. Even after removing outliers, the quality of estimated loss factors in 500 and 1000 Hz frequency band is overestimated by 19% to 37%. The panel's loss factor, determined in the 2000 Hz band, has indicated an underestimation of the loss factor by 28% to 45%.

**Table 4.10: PIM based estimated loss factor for panels with approximate loss factor of 0.10**

| | **Frequency of Analysis** | | | |
|---|---|---|---|---|
| **Measurement Regions** | **500 Hz** | **1000 Hz** | **2000 Hz** | **4000 Hz** |
| **PIM: Large Plate (Approximate Loss Factor = 0.10)** | | | | |
| **Inside the Direct Field** | 0.053 | 0.063 | 0.066 | -- |
| **Inside the Reverberant Field** | 0.194 | 0.275 | 0.353 | -- |
| **Close to Mean Free Path** | 0.277 | 0.369 | 0.364 | -- |
| **Plate Average** | 0.115 | 0.089 | 0.058 | -- |
| **PIM: Medium Plate (Approximate Loss Factor = 0.10)** | | | | |
| **Inside the Direct Field** | 0.047 | 0.057 | 0.063 | -- |
| **Inside the Reverberant Field** | 0.118 | 0.166 | 0.227 | -- |
| **Close to Mean Free Path** | 0.145 | 0.191 | 0.274 | -- |
| **Plate Average** | 0.099 | 0.107 | 0.092 | -- |
| **PIM: Small Plate (Approximate Loss Factor = 0.10)** | | | | |
| **Inside the Direct Field** | 0.050 | 0.045 | 0.047 | -- |
| **Inside the Reverberant Field** | 0.134 | 0.157 | 0.169 | -- |
| **Close to Mean Free Path** | 0.137 | 0.214 | 0.219 | -- |
| **Plate Average** | 0.119 | 0.123 | 0.101 | -- |

For all the highly damped panels tested experimentally, the loss factors estimated from the direct field responses are underestimated and the loss factors estimated from the reverberant field and the region close to mean free path are overestimated. For these highly damped panels, the quality of estimated loss factor can be considered acceptable as the highest overestimation is about 23% and the lowest underestimation is 11% (except for the Large plate analyzed at 2000 Hz where the loss factor is underestimated by almost 42%).

The PIM-based loss factor estimates are considered to be reliable if: (a) responses from the entire plate are considered, (b) significant outliers are removed, and (c) the direct field is considerably smaller than panel's mean free path—as in the case of low frequency and low damping levels.

### 4.3.3 Impulse Response Decay Method

The velocity FRFs are recorded from the Polytec's scanning laser vibrometer. The process to generate the impulse response from the FRFs is the same for computational and experimental analyses.

In Figures 4.32 to 4.37, the experimentally determined loss factors using IRDM, as a function of distance from excitation locations are presented. IRDM-based panel loss factor estimates in specific regions, such as the direct field, the reverberant field and over the entire plate, are summarized in Tables 4.11 and 4.12.

The distance-based loss factor analysis of the Large panel indicates that for the annular region farthest from the excitation location the loss factors are lower than other annular sectors. For Medium and Small panels, the loss factors in these farthest annular sectors are not reliable. In the experimental analysis of IRDM, response measurements inside and outside the direct field yield similar loss factor estimates.

The loss factors in annular regions, direct field and reverberant field are averaged from the loss factor of corresponding measurement locations inside the region. In a specific frequency band, the panel's loss factor is determined by averaging the loss factors from all the response locations.

In the summary section, for the six panels tested, the loss factors are based on central and arbitrary excitation locations. For loss factor estimation using IRDM, the performance of edge (or corner) excitation is not as worse as in PIM but to have an equivalent comparison between PIM, IRDM, and RDT the edge excitation is not considered for final analysis of loss factor estimates from IRDM.

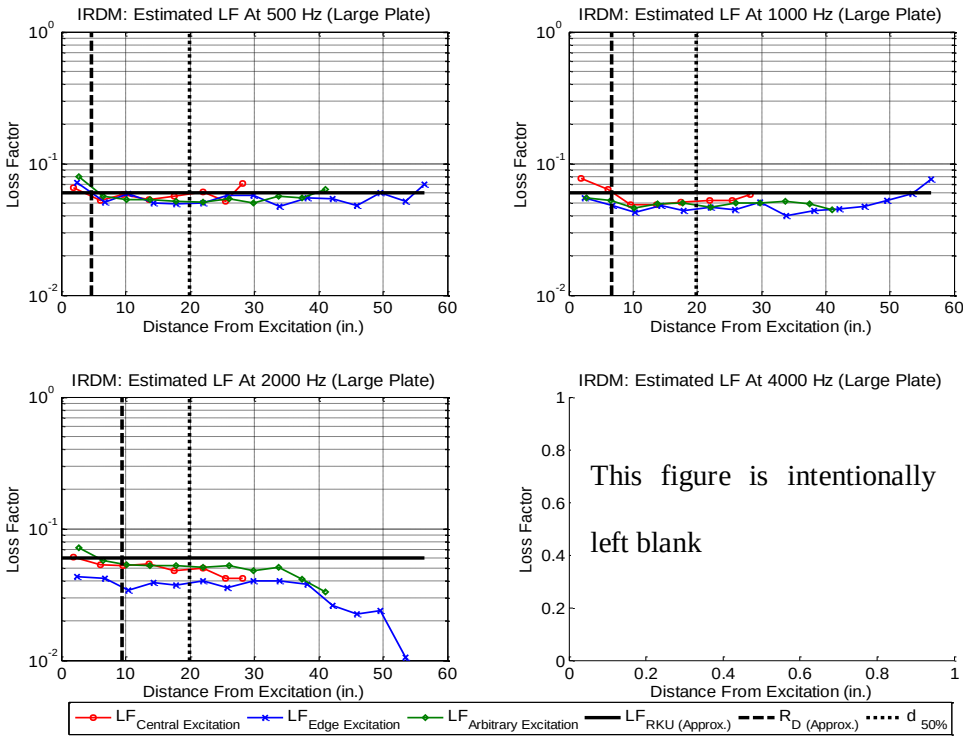


**Figure 4.32: IRDM based estimated loss factor for Large plate (approximate loss factor of 0.06)**

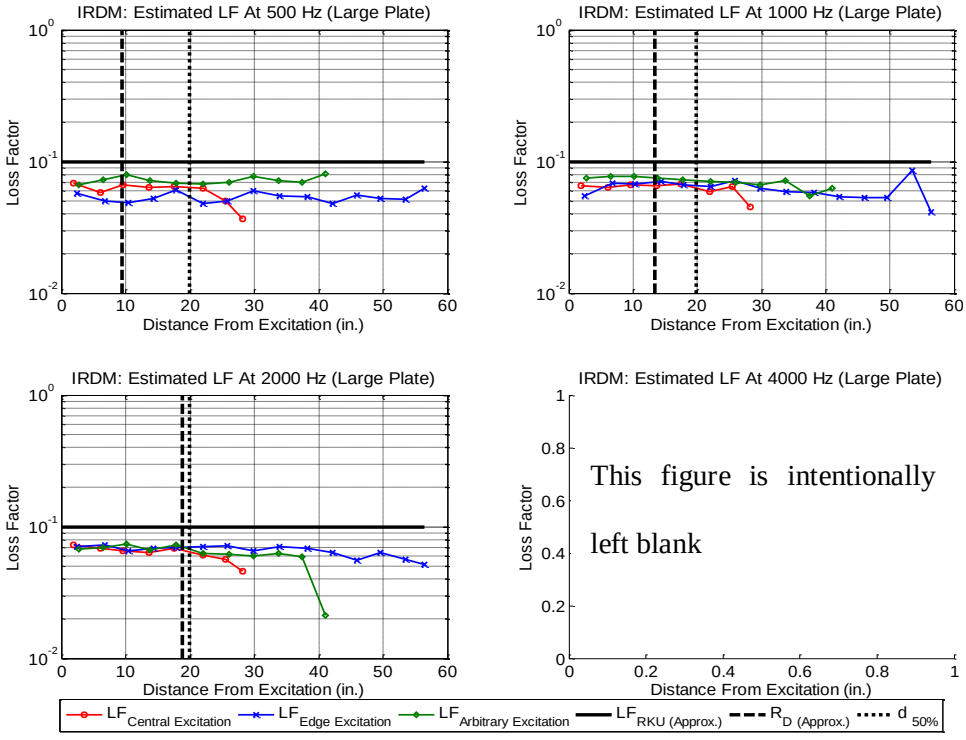


**Figure 4.33: IRDM based estimated loss factor for Large plate (approximate loss factor of 0.10)**

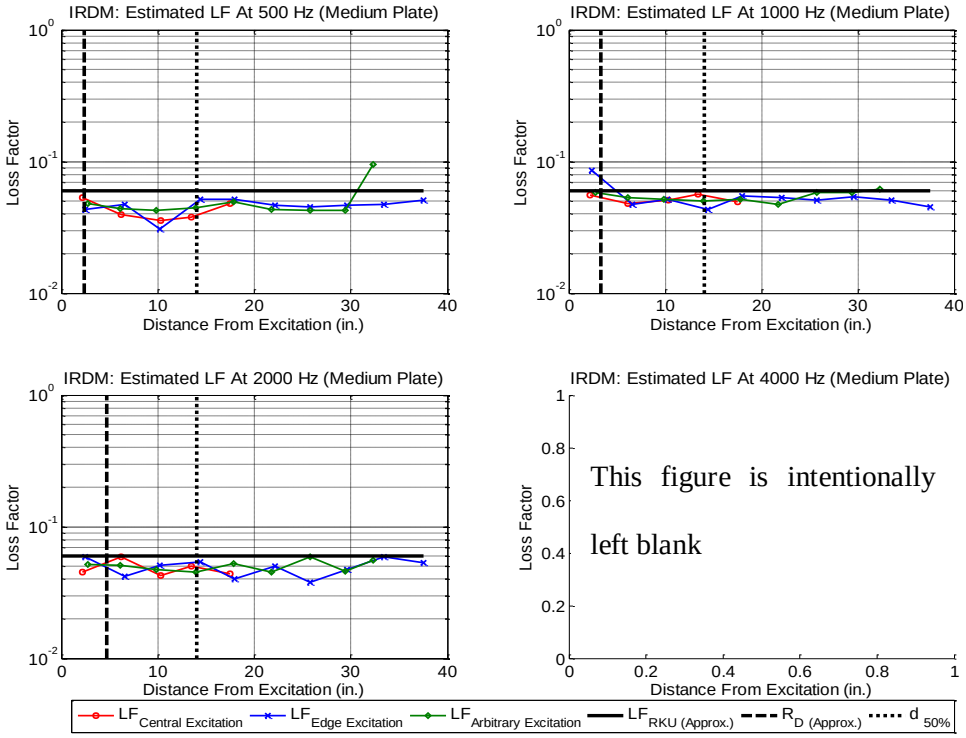


**Figure 4.34: IRDM based estimated loss factor for Medium plate (approx. loss factor of 0.06)**

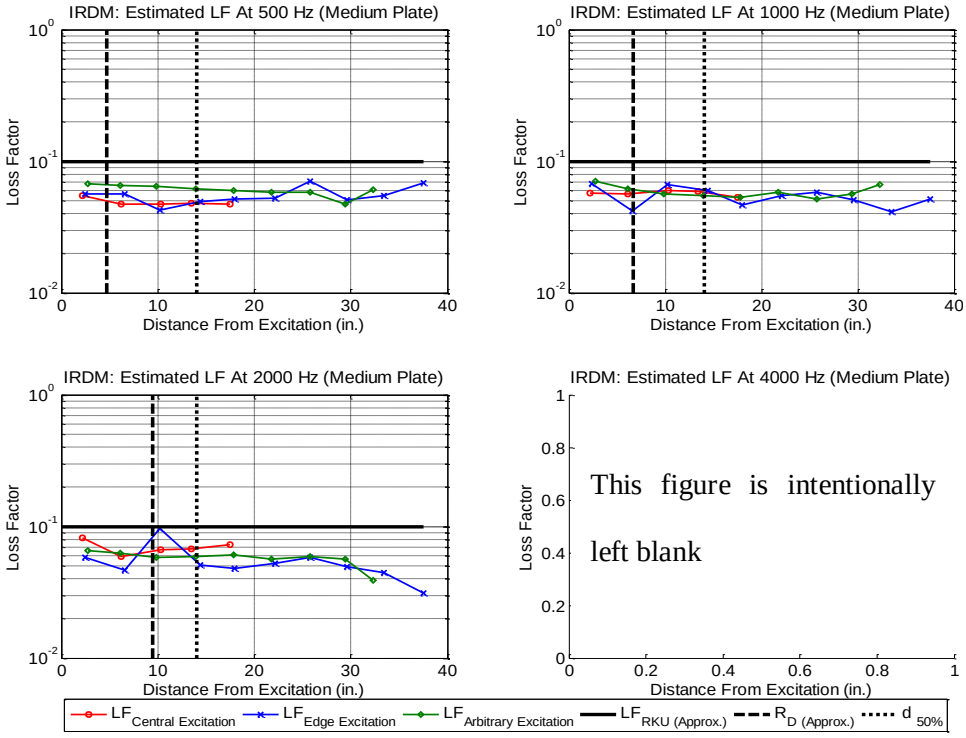


**Figure 4.35: IRDM based estimated loss factor for Medium plate (approx. loss factor of 0.10)**

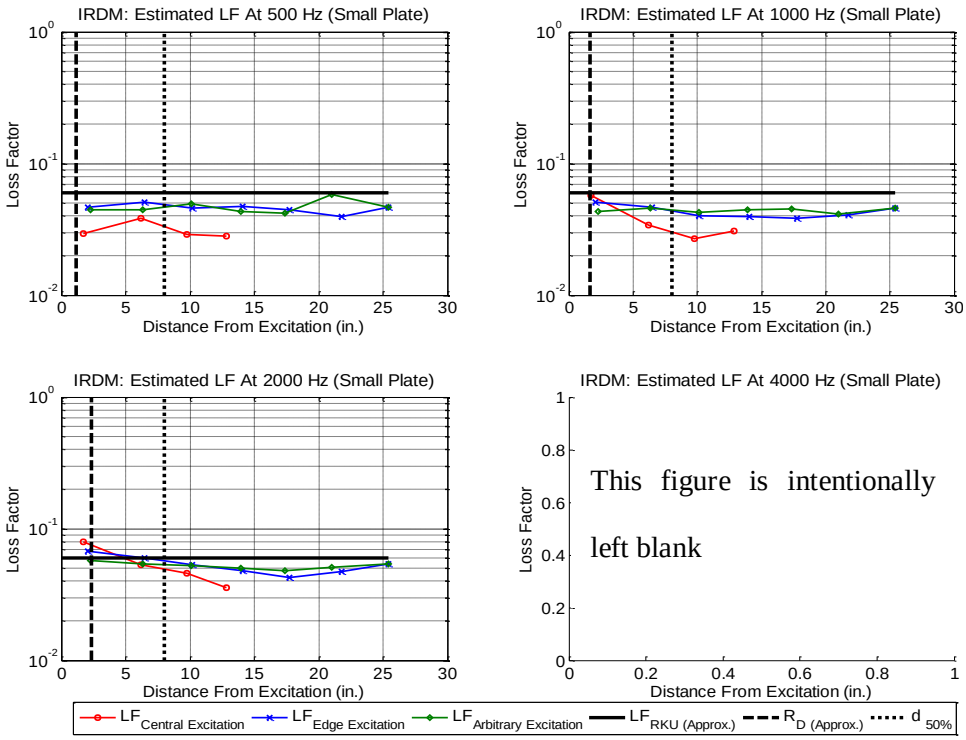


**Figure 4.36: IRDM based estimated loss factor for Small plate (approximate loss factor of 0.06)**

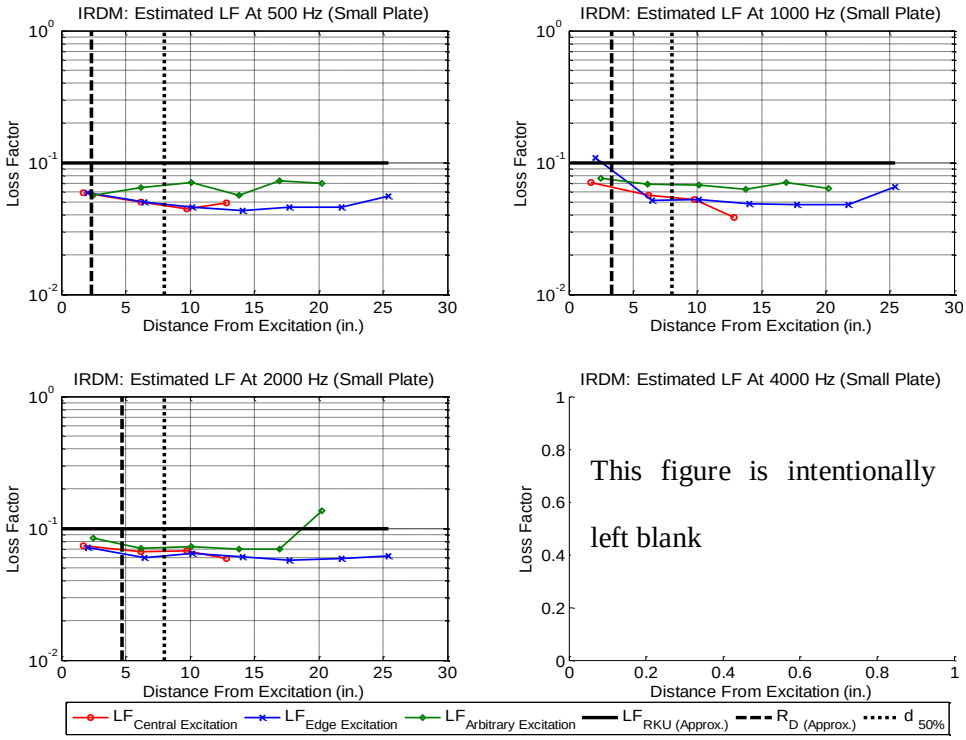


**Figure 4.37: IRDM based estimated loss factor for Small plate (approximate loss factor of 0.10)**

**Table 4.11: IRDM based estimated loss factor for panels with approximate loss factor of 0.06**

| | Frequency of Analysis | | | |
|---|---|---|---|---|
| **Measurement Regions** | **500 Hz** | **1000 Hz** | **2000 Hz** | **4000 Hz** |
| **IRDM: Large Plate (Approximate Loss Factor = 0.06)** | | | | |
| **Inside the Direct Field** | 0.074 | 0.058 | 0.057 | -- |
| **Inside the Reverberant Field** | 0.054 | 0.050 | 0.051 | -- |
| **Close to Mean Free Path** | 0.055 | 0.050 | 0.049 | -- |
| **Plate Average** | 0.055 | 0.051 | 0.052 | -- |
| **IRDM: Medium Plate (Approximate Loss Factor = 0.06)** | | | | |
| **Inside the Direct Field** | 0.047 | 0.060 | 0.053 | -- |
| **Inside the Reverberant Field** | 0.044 | 0.052 | 0.048 | -- |
| **Close to Mean Free Path** | 0.045 | 0.051 | 0.050 | -- |
| **Plate Average** | 0.044 | 0.052 | 0.049 | -- |
| **IRDM: Small Plate (Approximate Loss Factor = 0.06)** | | | | |
| **Inside the Direct Field** | 0.037 | 0.044 | 0.065 | -- |
| **Inside the Reverberant Field** | 0.040 | 0.042 | 0.049 | -- |
| **Close to Mean Free Path** | 0.039 | 0.042 | 0.046 | -- |
| **Plate Average** | 0.040 | 0.043 | 0.051 | -- |

From the computational studies, it is expected that loss factors would be underestimated for these highly damped panels. For the Large panel with intermediate damping levels, the IRDM-based loss factor estimation process predicted the loss factors no better than 8% but no worse than to 15% below the target values. The predicted loss factor for Medium and Small panels is underestimated, but no worse than 33%. The best estimates of loss factor for Medium and Small plate are underestimated by 13%.

For a single mode of vibration a panel reverberation time might be used as a guide to indicate the start and end point w.r.t. time scale for slope fitting. But in experimental analysis of highly damped panels, the out-of-band noise floor and measurement noise floors exist. In

cases like these, very few cycles of response measurement are available to fit a linear curve—which makes the slope fitting a challenging task.

**Table 4.12: IRDM based estimated loss factor for panels with approximate loss factor of 0.10**

| | Frequency of Analysis | | | |
|---|---|---|---|---|
| **Measurement Regions** | **500 Hz** | **1000 Hz** | **2000 Hz** | **4000 Hz** |
| **IRDM: Large Plate (Approximate Loss Factor = 0.10)** | | | | |
| **Inside the Direct Field** | 0.071 | 0.072 | 0.069 | -- |
| **Inside the Reverberant Field** | 0.068 | 0.068 | 0.061 | -- |
| **Close to Mean Free Path** | 0.066 | 0.065 | 0.061 | -- |
| **Plate Average** | 0.068 | 0.069 | 0.065 | -- |
| **IRDM: Medium Plate (Approximate Loss Factor = 0.10)** | | | | |
| **Inside the Direct Field** | 0.063 | 0.061 | 0.064 | -- |
| **Inside the Reverberant Field** | 0.057 | 0.057 | 0.062 | -- |
| **Close to Mean Free Path** | 0.055 | 0.055 | 0.065 | -- |
| **Plate Average** | 0.057 | 0.057 | 0.062 | -- |
| **IRDM: Small Plate (Approximate Loss Factor = 0.10)** | | | | |
| **Inside the Direct Field** | 0.062 | 0.071 | 0.074 | -- |
| **Inside the Reverberant Field** | 0.054 | 0.060 | 0.069 | -- |
| **Close to Mean Free Path** | 0.054 | 0.056 | 0.066 | -- |
| **Plate Average** | 0.055 | 0.061 | 0.070 | -- |

From the analysis of computational panel with simulated loss factor of 0.10 (and thickness 0.10 inches), it is expected that IRDM-based loss factors would be underestimated by 29% in the worst cases. For the Large panel with intermediate damping levels, IRDM-based loss factor estimation process predicted loss factor no worse than 35% below the target values. The predicted loss factor for Medium and Small panels is underestimated by 30% to 43%. Although somewhat better estimates are observed in the direct field region, no

significant correlation is observed between the distance of response region from the excitation location and the quality of loss factor estimated.

On the basis of our computational studies, underestimation in prediction of loss factor of highly damped system is expected. But the observed underestimation is greater than expected. It is quite apparent that the target loss factor, initially estimated to be 0.10, is closer to 0.085. Further discussion is included in Section 4.4.

### 4.3.4 Random Decrement Technique

The methodology to estimate the randomdec signature in the experimental analysis is the same as that used in computational analyses. The decay curves are averaged inside many annular sectors. Using manual slope fitting on this averaged decay curves the distance based loss factor are determined. Panel average loss factor is estimated by averaging the loss factors determined for central and arbitrary excitation locations.

In Figures 4.38 to 4.49, RDT-based loss factor estimates are compared for: two damping levels, three plate sizes, three excitation locations, and two averaging approaches of RDT. Similar to IRDM, and in accordance to computational studies, the estimated loss factor using RDT does not show a strong dependence on distance of response location from excitation location. The summarized RDT based loss factor estimates are tabulated in Table 4.13 and 4.14.

As observed in the computational studies, the direct averaging approach tends to underestimate the loss factor of a highly damped panel. However, considerably less variation in loss factor estimates—comparing the direct averaging and averaging autocorrelation functions—is observed for the intermediate damping level. In the RDT based loss factor analysis of highly damped panels the averaging autocorrelation functions of triggered samples has performed better than the direct averaging approach.

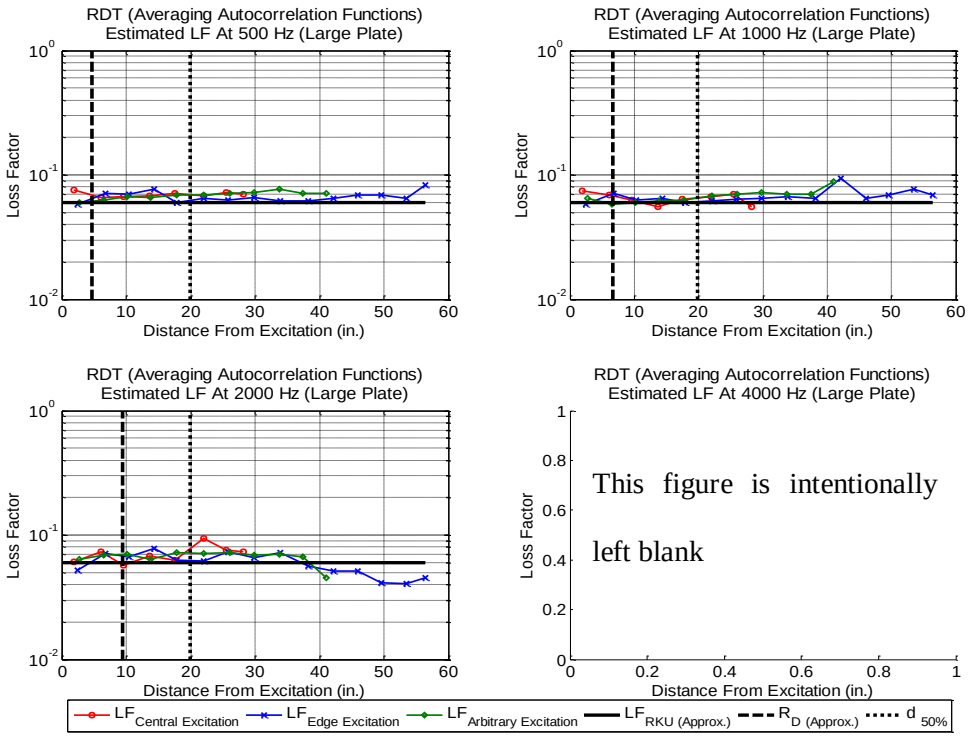


**Figure 4.38: RDT (averaging autocorrelation functions) based estimated loss factor for Large plate (approximate loss factor of 0.06)**

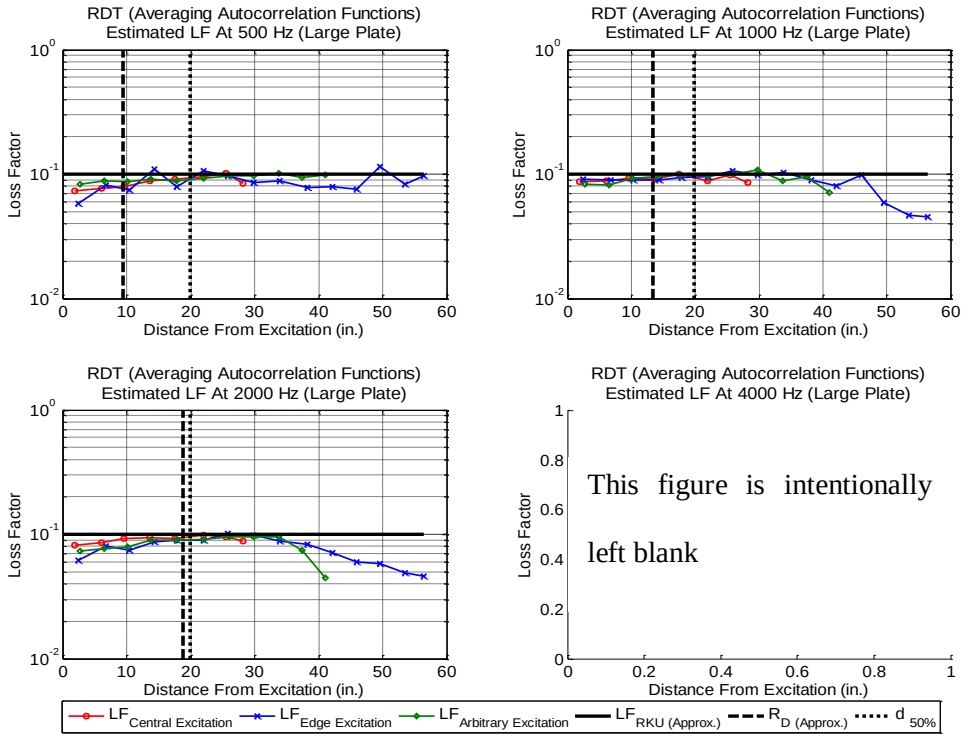


**Figure 4.39: RDT (averaging autocorrelation functions) based estimated loss factor for Large plate (approximate loss factor of 0.10)**

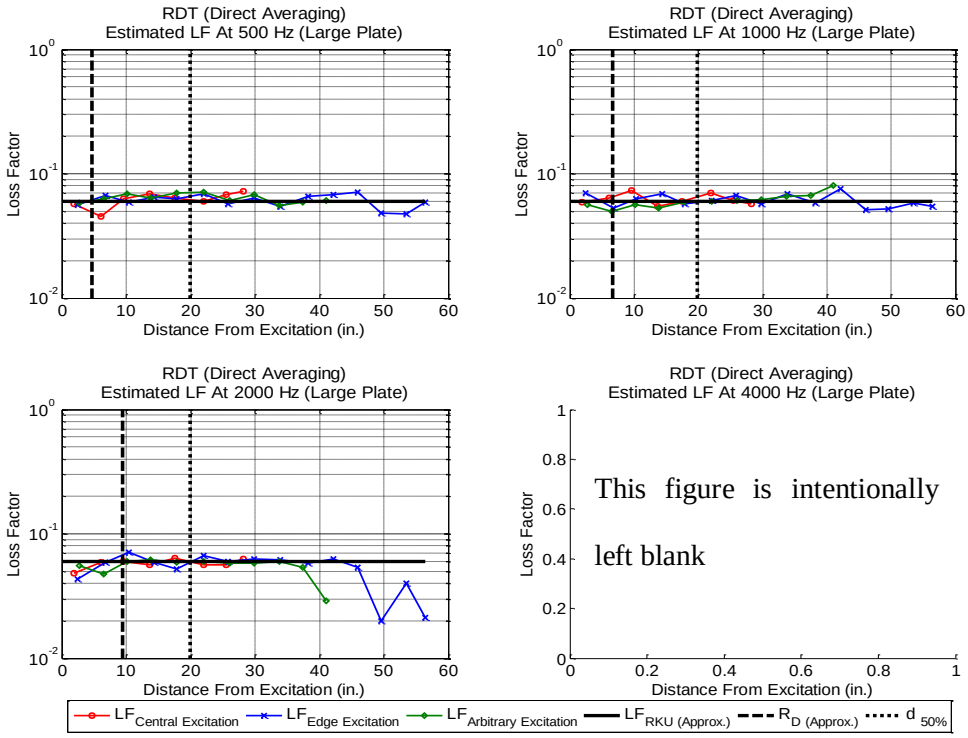


**Figure 4.40: RDT (directly averaging the triggered samples) based estimated loss factor for Large plate (approximate loss factor of 0.06)**

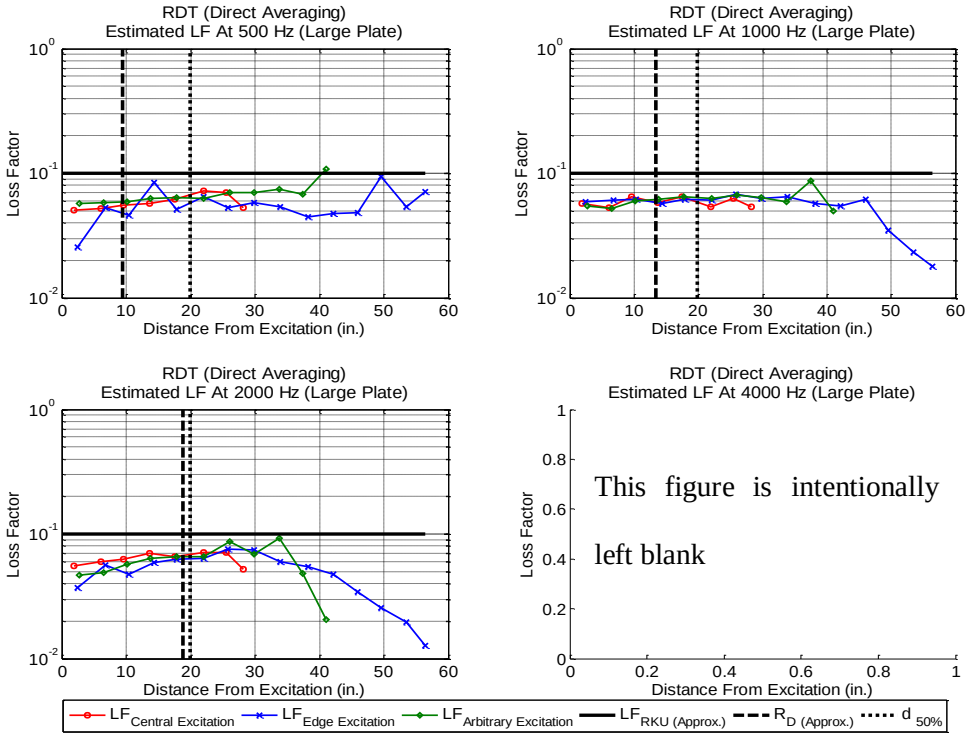


**Figure 4.41: RDT (directly averaging the triggered samples) based estimated loss factor for Large plate (approximate loss factor of 0.10)**

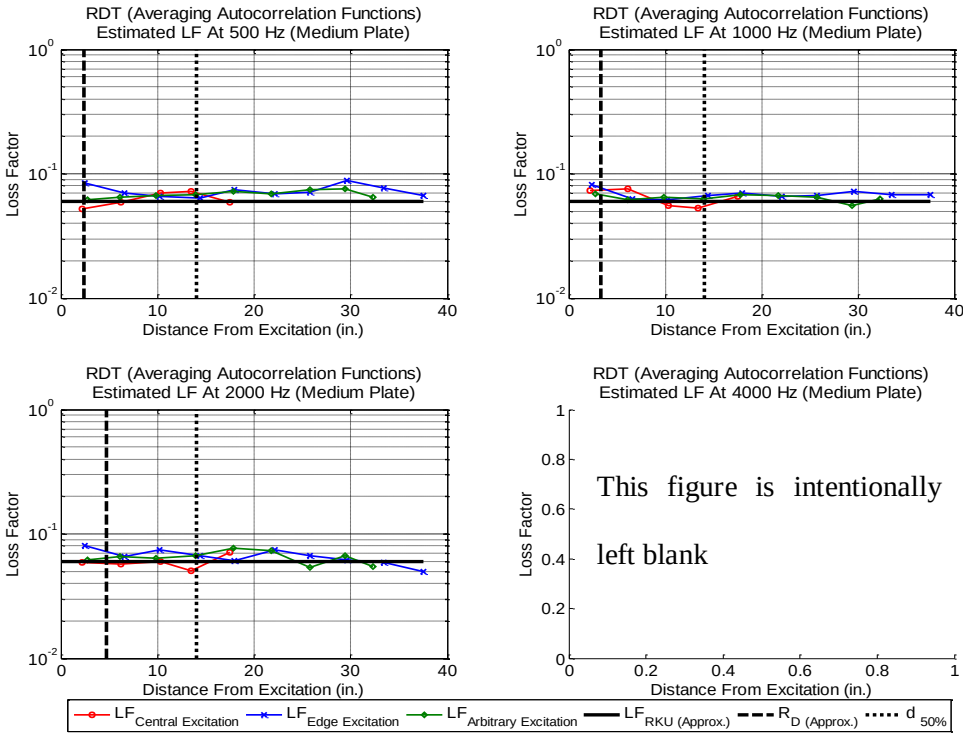


**Figure 4.42: RDT (averaging autocorrelation functions) based estimated loss factor for Medium plate (approximate loss factor of 0.06)**

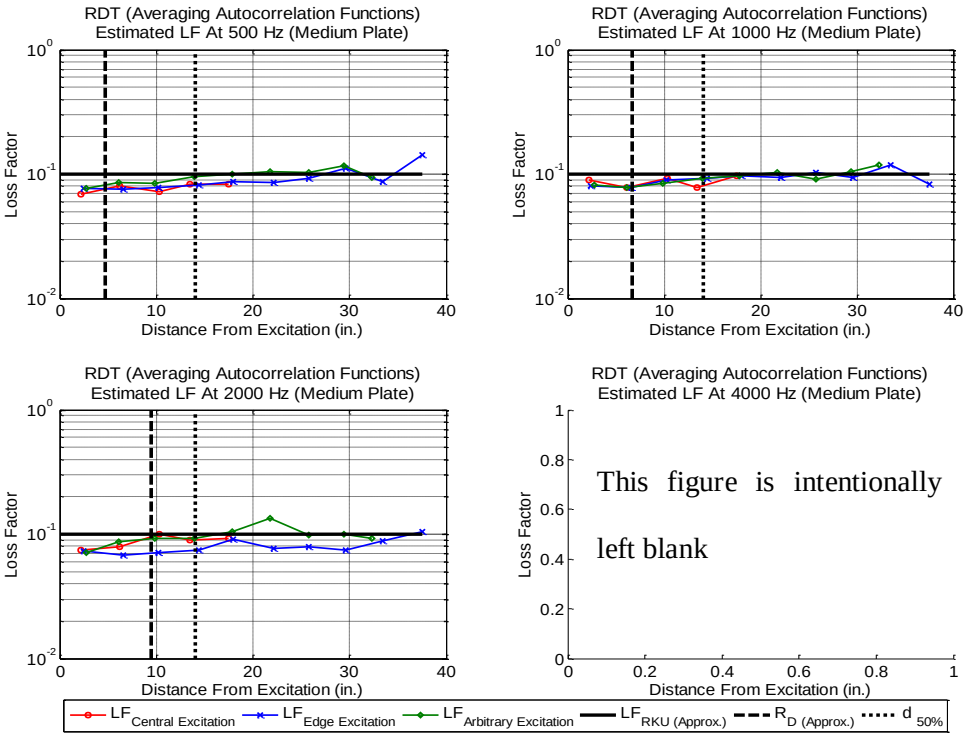


**Figure 4.43: RDT (averaging autocorrelation functions) based estimated loss factor for Medium plate (approximate loss factor of 0.10)**

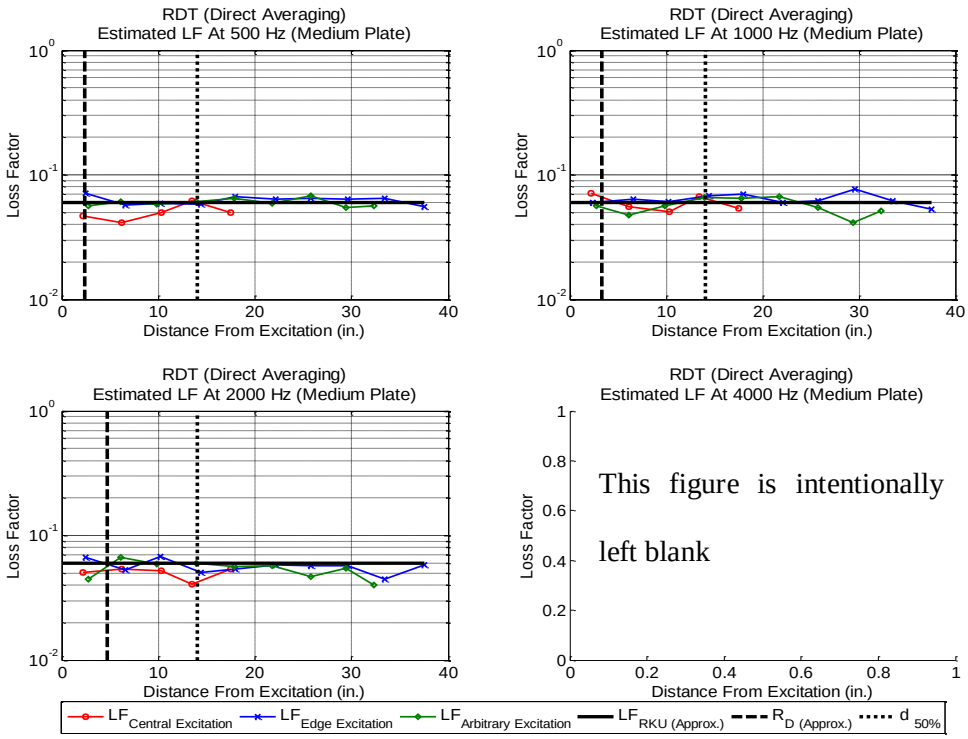


**Figure 4.44: RDT (directly averaging the triggered samples) based estimated loss factor for Medium plate (approximate loss factor of 0.06)**

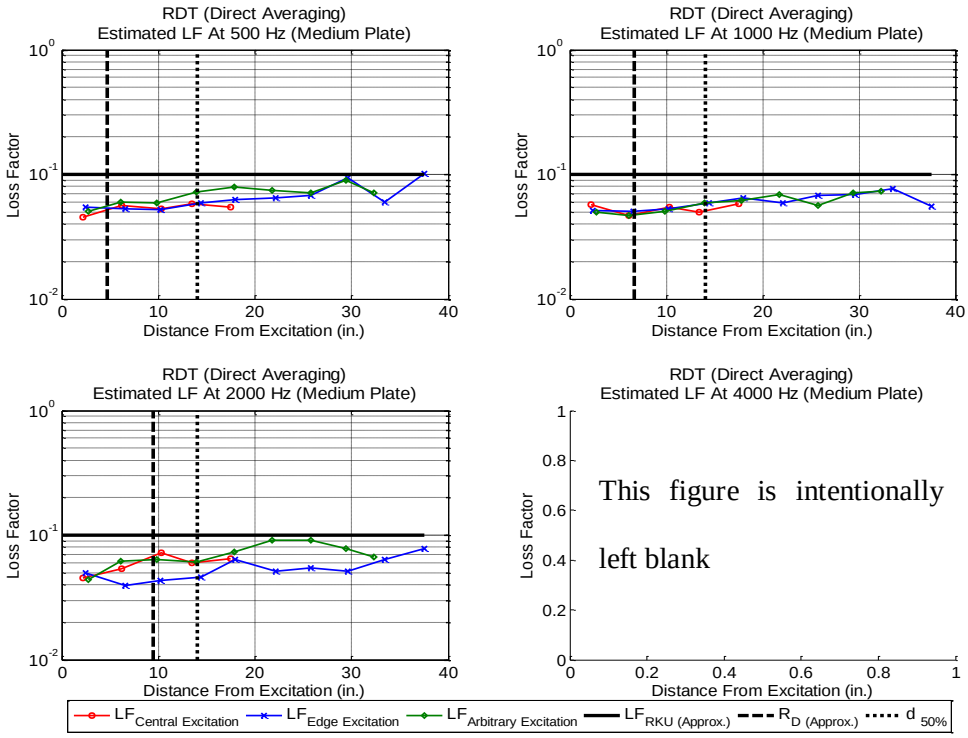


**Figure 4.45: RDT (directly averaging the triggered samples) based estimated loss factor for Medium plate (approximate loss factor of 0.10)**

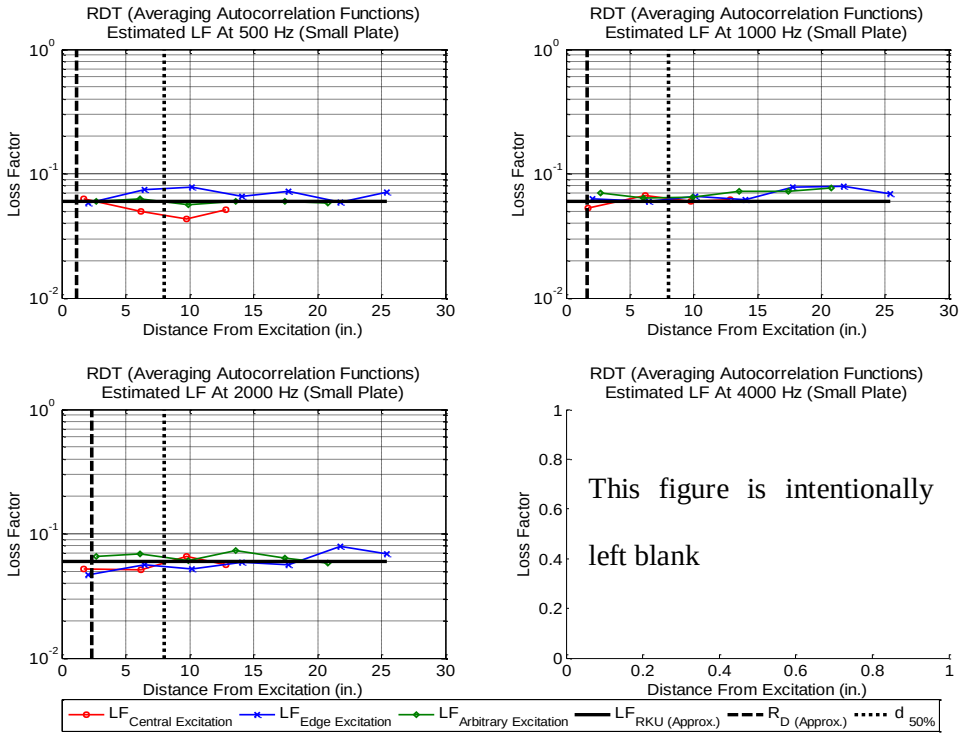


**Figure 4.46: RDT (averaging autocorrelation functions) based estimated loss factor for Small plate (approximate loss factor of 0.06)**

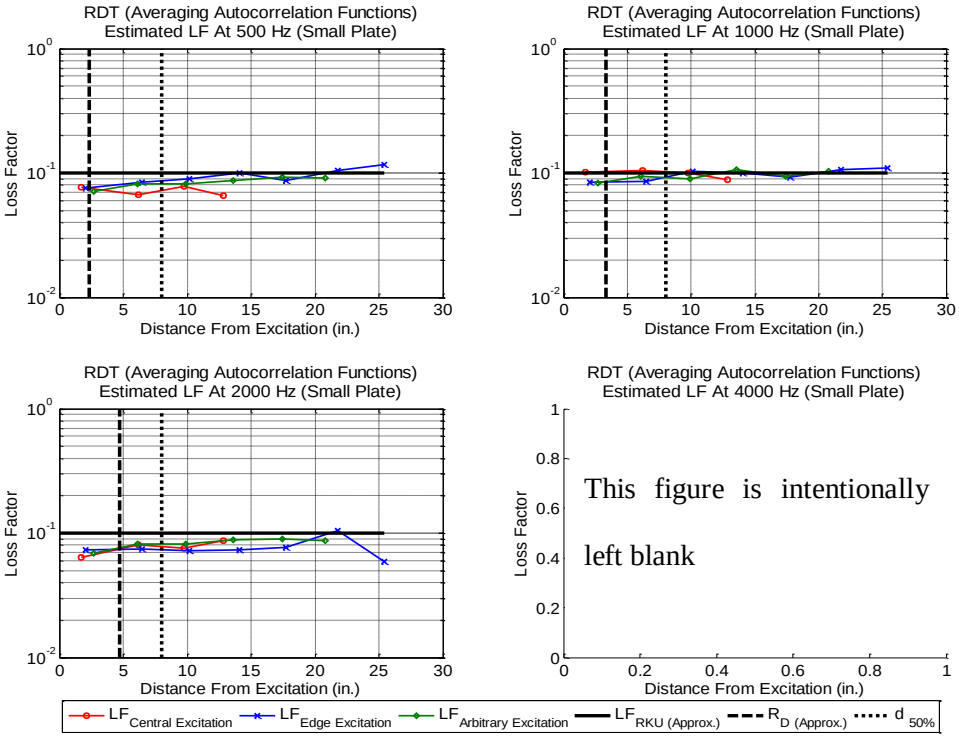


**Figure 4.47: RDT (averaging autocorrelation functions) based estimated loss factor for Small plate (approximate loss factor of 0.10)**

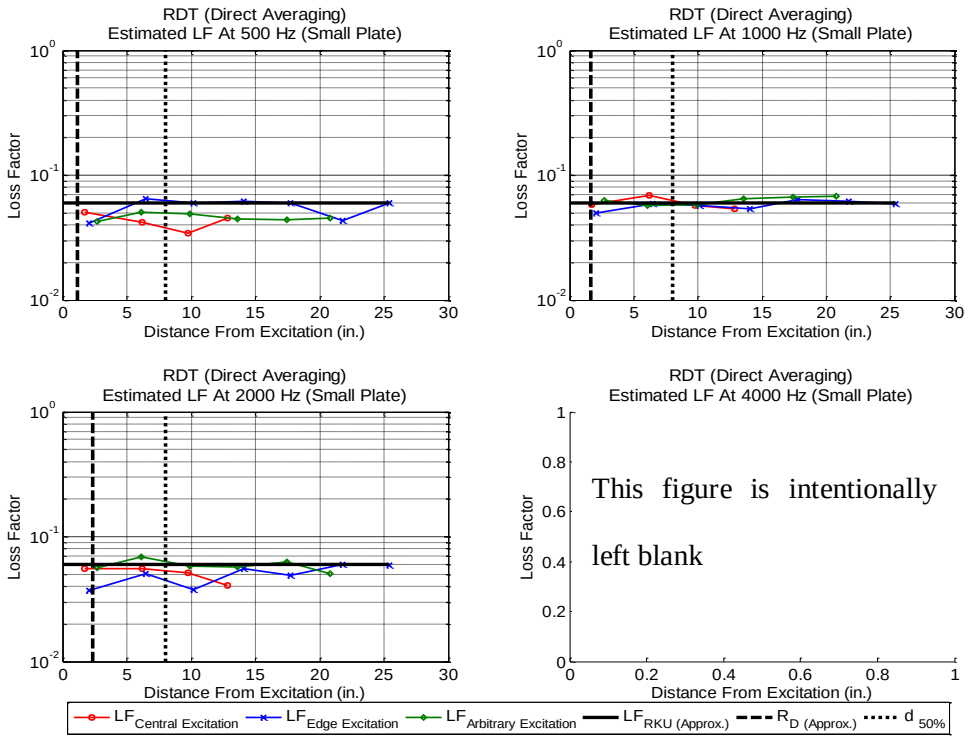


**Figure 4.48: RDT (directly averaging the triggered samples) based estimated loss factor for Small plate (approximate loss factor of 0.06)**

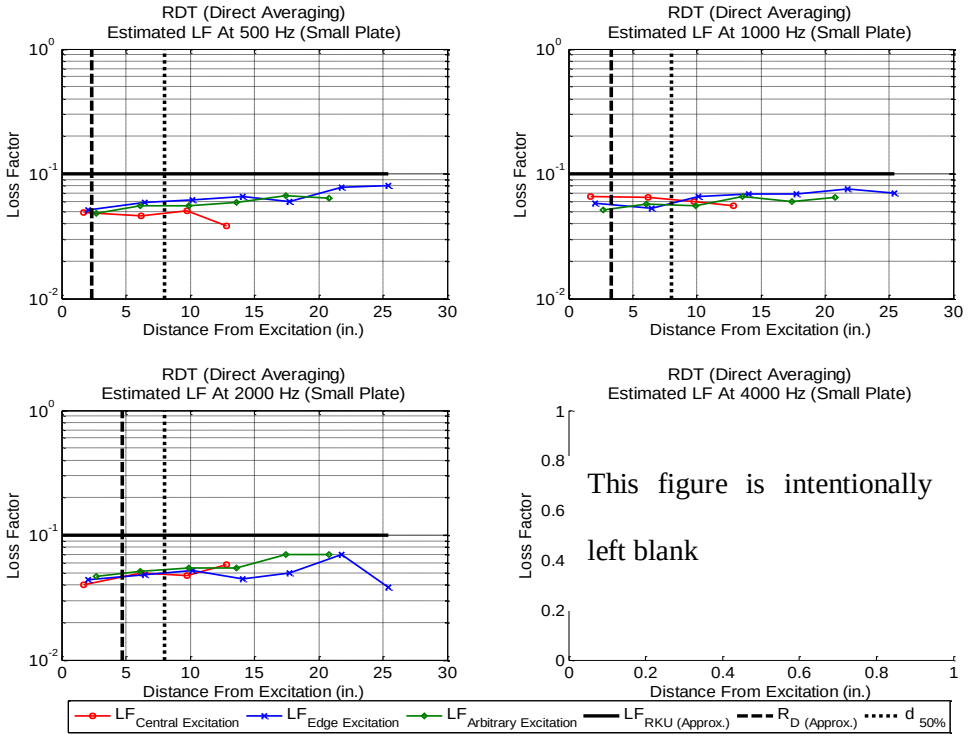


**Figure 4.49: RDT (directly averaging the triggered samples) based estimated loss factor for Small plate (approximate loss factor of 0.10)**

**Table 4.13: RDT based estimated loss factor for panels with approximate loss factor of 0.06**

| | Frequency of Analysis | | | |
|---|---|---|---|---|
| **Measurement Regions** | **500 Hz** | **1000 Hz** | **2000 Hz** | **4000 Hz** |
| **RDT: Large Plate (Approximate Loss Factor = 0.06)** | | | | |
| **Averaging the Autocorrelation Functions** | | | | |
| **Inside the Direct Field** | 0.068 | 0.061 | 0.061 | -- |
| **Inside the Reverberant Field** | 0.068 | 0.064 | 0.068 | -- |
| **Plate Average** | 0.069 | 0.065 | 0.071 | -- |
| **Direct Averaging** | | | | |
| **Inside the Direct Field** | 0.060 | 0.057 | 0.056 | -- |
| **Inside the Reverberant Field** | 0.068 | 0.064 | 0.066 | -- |
| **Plate Average** | 0.064 | 0.061 | 0.059 | -- |
| **RDT: Medium Plate (Approximate Loss Factor = 0.06)** | | | | |
| **Averaging the Autocorrelation Functions** | | | | |
| **Inside the Direct Field** | 0.059 | 0.060 | 0.065 | -- |
| **Inside the Reverberant Field** | 0.070 | 0.061 | 0.065 | -- |
| **Plate Average** | 0.069 | 0.065 | 0.066 | -- |
| **Direct Averaging** | | | | |
| **Inside the Direct Field** | 0.051 | 0.058 | 0.052 | -- |
| **Inside the Reverberant Field** | 0.055 | 0.065 | 0.065 | -- |
| **Plate Average** | 0.059 | 0.060 | 0.056 | -- |
| **RDT: Small Plate (Approximate Loss Factor = 0.06)** | | | | |
| **Averaging the Autocorrelation Functions** | | | | |
| **Inside the Direct Field** | 0.047 | 0.067 | 0.065 | -- |
| **Inside the Reverberant Field** | 0.057 | 0.069 | 0.061 | -- |
| **Plate Average** | 0.060 | 0.068 | 0.064 | -- |
| **Direct Averaging** | | | | |
| **Inside the Direct Field** | 0.037 | 0.054 | 0.050 | -- |
| **Inside the Reverberant Field** | 0.046 | 0.064 | 0.064 | -- |
| **Plate Average** | 0.049 | 0.061 | 0.058 | -- |

Loss factors using RDT can be determined by either averaging the autocorrelation functions of the triggered response or by directly averaging the triggered responses. From the computational studies, it is expected that averaging autocorrelation functions will fairly accurately predict the loss factor of a lightly damped panel and will underestimate the loss factor of a highly damped panel. Extrapolating the outcomes from the computational studies to the experimental analysis, slightly underestimated loss factors were expected for panels with an intermediate damping level. Based on a similar extrapolation for averaging autocorrelation functions, slight overestimation in the predicted loss factors is expected

Using the direct averaging approach on plates, tested experimentally, with intermediate damping level, the range of estimated loss factors is -18% to 7% from the target (0.06) somewhat as expected. The averaging autocorrelation function approach consistently overestimated the panel loss factor by no worse than 18%, also as expected.

It is also observed that the quality of estimated loss factor has no significant correlation with the region(s) of response measurement(s).

**Table 4.14: RDT based estimated loss factor for panels with approximate loss factor of 0.10**

| | Frequency of Analysis | | | |
|---|---|---|---|---|
| **Measurement Regions** | **500 Hz** | **1000 Hz** | **2000 Hz** | **4000 Hz** |
| **RDT: Large Plate (Approximate Loss Factor = 0.10)** | | | | |
| **Averaging the Autocorrelation Functions** | | | | |
| **Inside the Direct Field** | 0.081 | 0.089 | 0.087 | -- |
| **Inside the Reverberant Field** | 0.093 | 0.099 | 0.094 | -- |
| **Plate Average** | 0.091 | 0.095 | 0.090 | -- |
| **Direct Averaging** | | | | |
| **Inside the Direct Field** | 0.057 | 0.057 | 0.060 | -- |
| **Inside the Reverberant Field** | 0.066 | 0.064 | 0.068 | -- |
| **Plate Average** | 0.064 | 0.062 | 0.067 | -- |
| **RDT: Medium Plate (Approximate Loss Factor = 0.10)** | | | | |
| **Averaging the Autocorrelation Functions** | | | | |
| **Inside the Direct Field** | 0.077 | 0.076 | 0.082 | -- |
| **Inside the Reverberant Field** | 0.092 | 0.093 | 0.099 | -- |
| **Plate Average** | 0.090 | 0.091 | 0.097 | -- |
| **Direct Averaging** | | | | |
| **Inside the Direct Field** | 0.059 | 0.053 | 0.074 | -- |
| **Inside the Reverberant Field** | 0.063 | 0.060 | 0.072 | -- |
| **Plate Average** | 0.066 | 0.057 | 0.067 | -- |
| **RDT: Small Plate (Approximate Loss Factor = 0.10)** | | | | |
| **Averaging the Autocorrelation Functions** | | | | |
| **Inside the Direct Field** | 0.069 | 0.087 | 0.072 | -- |
| **Inside the Reverberant Field** | 0.080 | 0.097 | 0.081 | -- |
| **Plate Average** | 0.085 | 0.099 | 0.081 | -- |
| **Direct Averaging** | | | | |
| **Inside the Direct Field** | 0.050 | 0.063 | 0.070 | -- |
| **Inside the Reverberant Field** | 0.053 | 0.059 | 0.053 | -- |
| **Plate Average** | 0.058 | 0.063 | 0.053 | -- |

From the analysis of highly damped plate computational models, it is expected that RDT with the autocorrelation function averaging approach will perform better than the direct averaging approach. The target loss factor of highly damped plate is—tentatively—0.10.

As seen with IRDM, for RDT-based loss factor estimations of highly damped panels, slope fitting challenges associated with the measurement noise floor and out-of-band noise floor exist. For the Large panel, accuracy of the predicted loss factors using the averaging autocorrelation functions approach has an underestimation of 8% to 15%. Using the direct averaging approach has an underestimation of 34% to 39%. For the Medium and Small panel, the loss factor estimate using the direct averaging approach is underestimated by 33% to 45%. Using the averaging autocorrelation function approach the loss factors are underestimated by 5% to 9% for the Medium plate and 9% to 4% for the Small plate.

Using the loss factor estimates from the RKU *beam* model as a "target ", RDT with autocorrelation function averaging slightly underestimated the loss factor. Further, the loss factor estimates from IRDM and RDT were also underestimated and to a greater degree. Therefore, it is concluded that the loss factor of the highly damped panel is apparently between 0.08 and 0.09 instead of RKU estimate (i.e. 0.10). These observations and comparison of all three techniques are discussed in the Section 4.4.

## 4.4 Summary of Experimental Analysis

From the computational analysis of the highly damped panel it is concluded that, in general, IRDM and RDT with direct averaging (or "$RDT_{DA}$") will slightly underestimate the loss factors. RDT with the autocorrelation function averaging approach (or "$RDT_{AA}$") has shown a trend of slight overestimation in the prediction of the high loss factors. For lightly damped panels, IRDM, RDT with direct averaging and PIM based loss factors were within acceptable accuracy ($\pm 20\%$). The autocorrelation function averaging approach of RDT overestimates the loss factor especially for the lightly-damped plates. In comparison to IRDM and RDT, the loss factor estimations using PIM are the least reliable.

Extrapolating the conclusions from the computational analysis of panels, when the loss factor of panels is accurately known, it is proposed that for highly damped panels, the loss factor is somewhere between 0.08 and 0.09 instead of our initial prediction of 0.10. If the value of ***highly damped panel's loss factor is approximated to 0.085*** (vs. 0.10), then the trends observed in the computational analysis remain essentially unchanged. The loss factor estimations using RKU, PIM, IRDM and RDT approaches are summarized in Figure 4.50. The dashed lines in Figure 4.50 indicate a "best estimate" of panel loss factor.

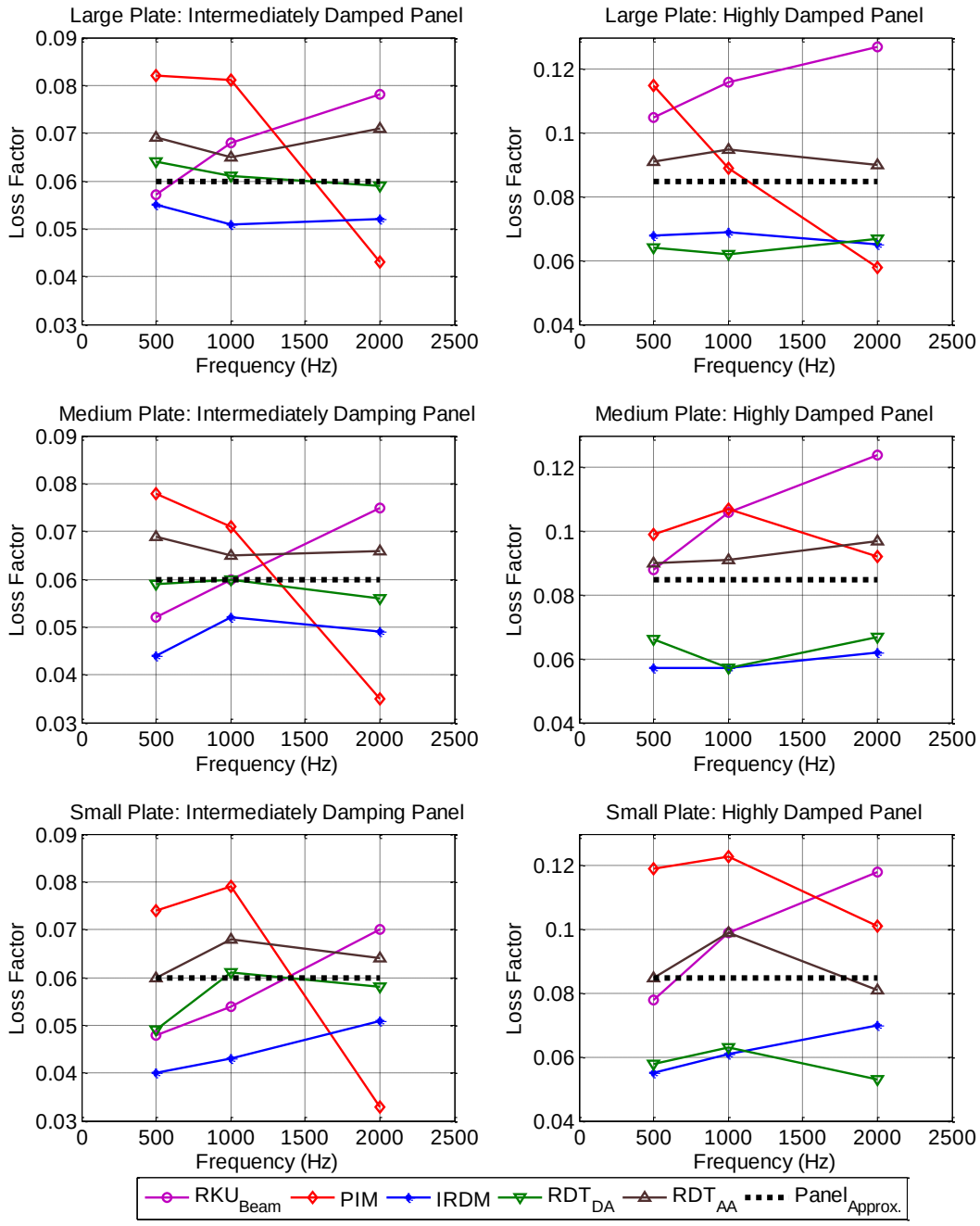


**Figure 4.50: Comparison of experimentally determined loss factors**

# 5 Conclusions & Recommendations

In this chapter conclusions from the computational and experimental analysis of panel loss factor estimations are discussed for a range of damping loss factors from 0.01 to 0.10. For these panels, the selection of excitation and measurement regions are also recommended

## 5.1 Comparison of Loss Factor Estimation Techniques

Even when significantly fewer response locations are considered, it is evident that loss factor estimates from RDT—especially for highly damped panels—are as reliable as IRDM and more reliable than PIM.

RDT with direct averaging, the conventional RDT approach, accurately predicts the loss factor of lightly damped panels and underestimates the loss factor of highly damped panels. RDT with the autocorrelation function averaging approach has a tendency to overestimate the loss factor. For the highly damped panel, this overestimation is somewhat less as compared to that observed for the lightly damped panels. To estimate the loss factors of highly damped panels, based on the computational study, it is recommended to use *both* averaging approaches to establish a "reasonable" bound on the loss factor estimates.

IRDM-based loss factors are underestimated for highly damped panels and are quite accurate for lightly damped panels. For all the cases analyzed, IRDM-based loss factor estimates are comparable to loss factor estimates using RDT with direct averaging.

PIM has shown a strong correlation between the estimated loss factor and the region of response measurement. The measurements from the direct field, in all the analyses, are underestimated. In the case of the lightly damped panel, the size of the direct field is

significantly smaller, as compared to the mean free path, and the loss factor estimates from the reverberant field are similar to loss factors estimated from the responses measured over the entire plate. For the highly damped panels—with a considerably larger direct field—the loss factor estimates from the reverberant field are overestimated.

From the experimental analysis, it is established that PIM-based loss factor estimates are considered to be reliable if: (a) responses from the entire plate are considered, (b) significant outliers are removed, and (c) the size of the direct field is considerably smaller than the panel's mean free path. The denominator term of the PIM-based loss factor estimation (referring to Equation 2.31), that is, the total energy—twice the kinetic energy—should be determined from many evenly-distributed response locations. In cases like these, the use of a laser vibrometer—capable to recording responses from hundreds of locations in one analysis—becomes a practical necessity. As such, if accelerometers are to be used in the loss factor estimation of a damped panel, then IRDM and RDT are recommended.

Panels with three different sizes and two damping levels were analyzed in the computational and the experimental studies. The effect of panel size or mean free path on the quality of loss factor is not observed.

In Table 5.1, the quality of loss factor estimates, from all techniques studied, are summarized. In Table 5.1, the values in bracket correspond to the range of loss factors estimated from all the three plate sizes and damping levels. In the case of computational models the loss factors are known, and thus the estimates are expressed in terms of percent deviation from the target values. Unlike PIM, RDT and IRDM have not displayed a significant dependence between the estimated loss factor and the distance from the response measurement to the excitation.

**Table 5.1: Comparison of loss factor estimation techniques**

| Loss Factors | PIM | IRDM | RDT | |
|---|---|---|---|---|
| | | | **Direct Averaging** | **Averaging Autocorrelation Function** |
| $\eta$ = 0.10 (Computational) | Slightly Underestimates **(-12% to -05%)** | Underestimates **(-28% to -12%)** | Underestimates **(-20% to +03%)** | Slightly Overestimates **(-01% to +15%)** |
| $\eta \approx 0.085$ (Experimental) | Overestimates **(0.089 to 0.123)** | Slightly Underestimates **(0.055 to 0.070)** | Slightly Underestimates **(0.053 to 0.067)** | Slightly Overestimates **(0.081 to 0.099)** |
| $\eta \approx 0.06$ (Experimental) | Overestimates for 500 Hz & 1000 Hz **(0.071 to 0.082)** Underestimates for 2000 Hz **(0.043 to 0.043)** | Slightly Underestimates **(0.040 to 0.055)** | Slightly Underestimates **(0.049 to 0.064)** | Slightly Overestimates **(0.064 to 0.071)** |
| $\eta$ = 0.01 (Computational) | Slightly Underestimates **(-07% to -17%)** | Accurate **(-06% to +08%)** | Accurate **(-13% to +06%)** | Overestimates **(+07% to +27%)** |

Ewing and Dande [32] hypothesized that any process based on input-output measurements would under-predict the loss factor when measurement are made in the near field. This was shown here to be true for PIM, but not for IRDM and RDT.

## 5.2 Excitation Locations

To estimate the loss factors, for these freely-hanging panels, edge (or corner) excitation is not recommended especially for PIM. When estimating loss factors in wide frequency bands, the corner excitation or edge excitation does not seem to significantly affect

IRDM and RDT results. When analyzing panels with known loss factors, as in this case the computational plate models, the loss factors based on arbitrary or central excitation were quite acceptable.

## 5.3 Recommendations for Future Studies

From the experimental and computational analyses it is observed that for highly damped panels, IRDM and RDT have shown systematic trends of over- and under-estimation of loss factors. The reasons for these systematic bias errors, especially for overestimations with the autocorrelation function averaging approach, should be established.

The panels tested were symmetric and made up of isotropic materials. The performance of these loss factor estimation techniques should be also evaluated for panels made up of composite materials. Further, complex structures such as stiffened and/or curved panels should also be tested.

The studies reported here were focused on freely-hanging panels excited mechanically. Analysis of test techniques using acoustical excitation should be conducted.

Finally, the research presented herein could be shared and discussed with industry partners such as Boeing, Spirit AeroSystems, Cessna and others to help them establish testing standards for their aircraft sidewall panels.

# 6 References


[1] Lyon, R. H. and Dejong, R. G., *Theory and Application of Statistical Energy Analysis*, 2nd edition, RH Lyon Corp 1998

[2] Liu, W. B., *Experimental and Analytical Estimation of Damping in Beams and Plates with Damping Treatments***,** PhD Dissertation, The University of Kansas, Aerospace Engineering, 2009

[3] Adhikari, S. and Woodhouse, J., *Identification of Damping: Part1, Viscous Damping*, Journal of Sound and Vibration, 2001, Vol. 243(1), pp. 43–61

[4] Chu, F. H. and Wang, B. P., *Experimental Determination of Damping in Materials and Structures*, American Society of Mechanical Engineers, Applied Mechanics Division, AMD, Vol. 38, pp. 113–122,1980

[5] Bloss, B. C. and Rao, M. D., *Estimation of Frequency–Averaged Loss Factors by the Power Injection and the Impulse Response Decay Methods*, Journal of the Acoustical Society of America, Vol. 117(1), pp. 240–249, 2005

[6] Wu, L., Agren, A. and Sundback, U, *A Study of Initial Decay Rate of Two–Dimensional Vibrating Structures in Relation to Estimates of Loss Factor*, Journal of Sound and Vibration, Vol. 206 (5), pp. 663–684, 1997

[7] Cole, H. A., Jr., *On–The–Line Analysis of Random Vibrations*, AIAA paper No. 68–288, AIAA/ASME 9th Structures, Structural Dynamics and Materials Conference, Palm Springs, CA, 1968

[8] Liu, W. B. and Ewing, M. S., *Experimental and Analytical Estimation of Loss Factors by the Power Input Method*, AIAA Journal, Vol. 45(2), pp. 477–484, 2007

[9] Ewing, M. S., and Dande, H. A., *'Characterizing Plate Damping Loss Factor Estimation Errors',* 53rd Structures, Structural Dynamics and Materials (SDM) Conference, Honolulu, Hawaii, May 2012

[10] Brincker, R., Kirkegaard, P. H., and Rytter, A., *Identification of System Parameters by the Random Decrement Technique,* Proceedings of 16th International Seminar on Modal Analysis, Florence, Italy, 1991

[11] Dande, H. A., *'Panel Damping Loss Factor Estimation Using Random Decrement Technique'*, M.S. Thesis, University of Kansas, December 2010

[12] Ross, D., Ungar E. E., and Kerwin Jr., E. M., *Damping of Plate Flexural Vibrations by Means of Viscoelastic Laminae, in Structural Damping*, ed. By J. E. Ruzicka, ASME, NY, 1959, pp. 49-88

[13] Nashid, A. D., Jones, D. G., and Henderson, J. P., *Vibration Damping*, A Wiley-Interscience Publication, John Wiley & Sons, New York, 1985

[14] Ewing, M. S., Dande, H. and Vatti, K., Validation of Panel Damping Loss Factor Estimation Algorithms Using a Computational Model, Proceedings of 50th AIAA/ASME/ASCE/AHS/ASC Structures, Structural Dynamics and Materials Conference, Palm Springs, CA, 2009

[15] Dande, H. A. and Ewing, M. S., *On the Effect of Mechanical Excitation Position on Panel Loss Factor Estimation With the Power Input Method,* Proceedings of InterNoise 2012, New York, New York, August 2012

[16] Dande, H. and Ewing, M. S., *Panel Damping Loss Factor Estimation Using the Random Decrement Technique*, Proceedings of 51st AIAA/ASME/ASCE/AHS/ASC Structures, Structural Dynamics and Materials Conference, Orlando, FL, 2010

[17] Inman, D. J., *Engineering Vibration,* 3rd edition, Prentice Hall, 2007

[18] Rao, S. S., *Mechanical Vibrations*, 3rd edition, Addison-Wesley Publishing Company, 1995

[19] Bloss, B. C. and Rao, M. D., *Estimation of Frequency–Averaged Loss Factors by the Power Injection and the Impulse Response Decay Methods*, Journal of the Acoustical Society of America, Vol. 117(1), pp. 240–249, 2005

[20] Vandiver, J. K., Dunwoody, A. B., Campbell, R. B. and Cook, M. F., *A Mathematical Basis for the Random Decrement Vibration Signature Analysis Technique*, Journal of Mechanical Design, Vol. 144, pp. 307–313, 1982

[21] Kijewski, T., and Kareem, A., *Reliability of Random Decrement Technique for Estimates of Structural Damping*, 8th ASCE Specialty Conference on Probabilistic Mechanics and Structural Reliability, PMC2000–294, 2000

[22] Hortog J. P. D., *Mechanical Vibrations*, 3rd edition, McGraw-Hill Book Company, Inc., New York and London, 2007

[23] Lai, M. L. and Soom, A., *Prediction of Transient Vibration Enveloped Using Statistical Energy Analysis Techniques*, Journal of Vibration and Acoustics, Vol. 112, pp. 127–137,1990

[24] Lai, M. L., *Modeling of Transient Vibrations With Statistical Energy Analysis Techniques***,** PhD Dissertation, State University of New York at Buffalo, 1988

[25] Manning, J. E., and Lee, K., *Predicting Mechanical Shock Transmission*, The Schock and Vibration Bulletin, 40(4), pp. 65-70, 1968

[26] Mercer, C. A., Rees, P. L., and Fahy, F. J., *Energy Flow Between Two Weekly Coupled Oscillators Subjected to Transient Excitation*, Journal of Sound and Vibration, Vol. 15, No. 3, pp 373-379, 1971

[27] Pinnington , R. J., and Lednik, D., *Transient Statistical Energy Analysis of an Impulsively Excited Two Oscillator System*, Journal of Sound and Vibration, 189(2), pp. 249-264, 1996

[28] Ewing, M. S., and Dande, H. A., *'Damping Loss Factor Estimation for Coupled Plates Using Experimental Transient Statistical Energy Analysis'*, 52nd Structures, Structural Dynamics and Materials (SDM) Conference, Denver, Colorado, April 2011.

[29] Ewing, M. S., Vatti, K., and Vaz, I., *Coupling Loss Factor Factor Estimation for Plates Joined at a Point: Analysis and Experiment*, NoiseCon 2010, Baltimore, Maryland, April 2010

[30] Ewing, M. S., Vatti, K., and Vaz, I., *Coupling Loss Factor Factor Estimation for Plates Joined Along a Point: Analysis and Experiment*, NoiseCon 2010, Baltimore, Maryland, April 2010

[31] Fahy, F., and Walker, J., *Foundations of Engineering Acoustics*, Academic Press, London, 2001

[32] Ewing, M. S., and Dande, H. A., '*Effect of High Damping Levels on Loss Factor Estimation*', 8th International Symposium on Vibration of Continuous Systems, Whistler, BC, Canada, July 2011

[33] Department of Defense, *Military Handbook - Metallic Materials and Elements for Aerospace Vehicle Structures (MIL-HDBK-5H)*, 1998

[34] Rose, T., *An Approach to Properly Account for Structural Damping, Frequency-Dependent Stiffness/Damping, and to Use Complex Matrices in Transient Response*, Presented at the MSC.Software Corporation 2001 Aerospace Conference and Technology Showcase

[35] MD or MSC/NASTRAN Quick Reference Guide, 2011

[36] Fahy, F., and Walker, J., *Fundamentals of Noise and Vibration*, E & FN Spon, New York and London, 1998

[37] Fahy, F., *Sound and Structure Vibration: Radiation, Transmission and Response*, Academic Press, London, 1985

# Appendix A: A Brief Case Study on Time Domain Filtering[1]

If the structure is excited by random white noise, the response will also be random in nature. To extract a response in a narrow frequency band, or for a single mode, band pass filtering needs to be implemented. Computation of a randomdec signature from narrow–band time histories is statistically more efficient [A-1]. By filtering the measured response, noise and the other out–of–band information can be removed and the resulting randomdec signature will be "cleaner" [A-2, A-3 and A-4].

Filtering is the first step to condition the data for analysis; therefore, it should be understood in detail. During the analysis of RDT, it is observed that filtering is one of the most time consuming process, especially when the random response is required to be filtered in multiple frequency bands.

In general, filters can be classified as Infinite–duration Impulse Response (IIR) filter and Finite–duration Impulse Response (FIR) filters. Unlike the IIR filters, the FIR filters are always stable in form. FIR filters can have exactly linear phase and the design methods are generally linear [A-5]. Kaiser window filters (FIR) were chosen over the other FIR filters because of the relatively better control over the filter design parameters and ease in implementation. All the filters used in this study are designed using MATLAB's Filter Design and Analysis Tool (FDA Tool), which is represented in Figure A.1.

[1] Appendix A and C are adapted from KUAE author, Himanshu Dande's, M.S. Thesis[11]

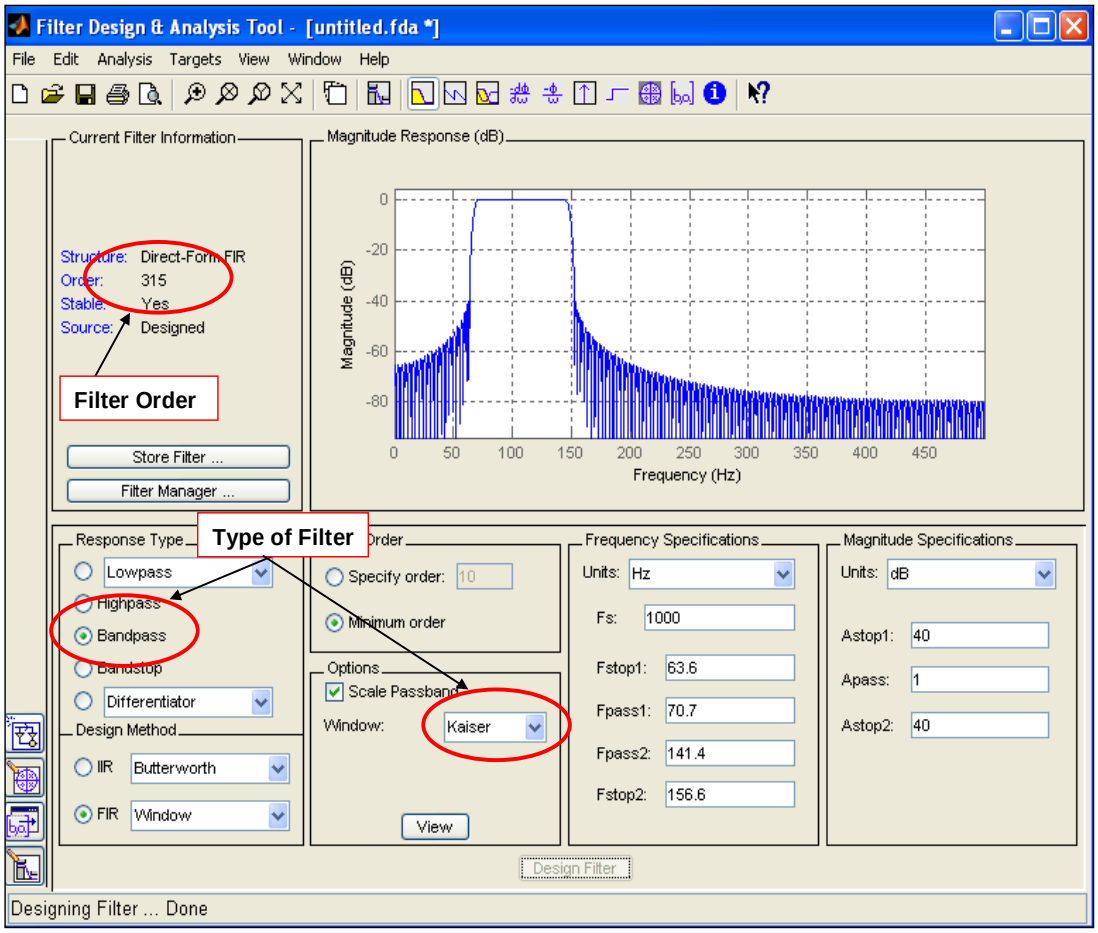


**Figure A.1: FDA Tool design window for The Mathworks MATLAB R2009a**

In the field of structural dynamics and acoustics it is common to analyze a signal in frequency bands with constant percentage bandwidths, for example full and one-third octave bandwidths. In the computational and experimental studies, reported herein, both 1/3$^{rd}$ and full octave bandpass filters are studied. The filter in Figure A.1 is designed for central frequency of 100 Hz for a full octave bandwidth, that is, 70.7 to 141.4 Hz. The parameters associated with this filter design, to be implemented using the MATLAB's FDA Tool, are explained through the following Figures A.2 and A.3.

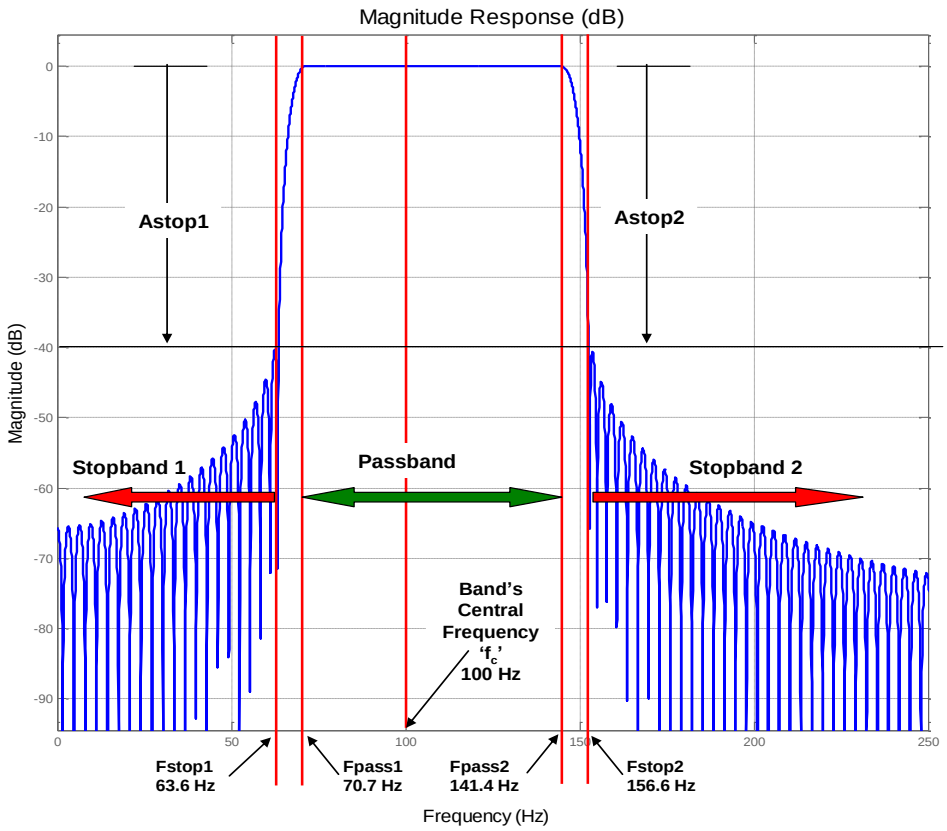


**Figure A.2: Filter design parameters – MATLAB FDA Tool**

For the Figure A.2:

| | |
|---|---|
| *Fstop*1 | is the end of the first stopband (Hz) |
| *Fstop*2 | is the beginning of the second stopband (Hz) |
| *Fpass*1 | is the beginning of the passband (Hz) |
| *Fpass*2 | is the end of the passband (Hz) |
| *Fs* | is the sampling frequency (in Hz) |
| $f_c$ | is the band's central frequency (Hz) |
| *Astop*1 | is the first stopband attenuation (dB) |
| *Astop*2 | is the second stopband attenuation (dB) |
| *Apass* | is the passband attenuation (dB) |

Order is the filter order of the designed filter

For 1/3rd octave bandpass filters "octave factor" or $F_{Octave}$ is $2^{1/6}$. For full octave bandpass filters $F_{Octave}$ is $2^{1/2}$ [A-6].

To define the filter boundaries, the "roll-off" frequencies are calculated in terms of the percentage, or $B_{\%}$ ,of the width of the passband.

$$Fstop1 = (1 - B_{\%}) \cdot f_c / F_{Octave}$$

$$Fpass1 = f_c / F_{Octave}$$

$$Fpass2 = f_c \cdot F_{Octave}$$

$$Fstop2 = (1 + B_{\%}) \cdot f_c \cdot F_{Octave}.$$

The central frequencies, $f_c$, for which the performance of RDT is analyzed, are: 400 Hz, 1000 Hz, 2000 Hz, and 4000 Hz.

The filter design parameters for 1/3rd octave filters and full octave filters are presented in Figure A.3.

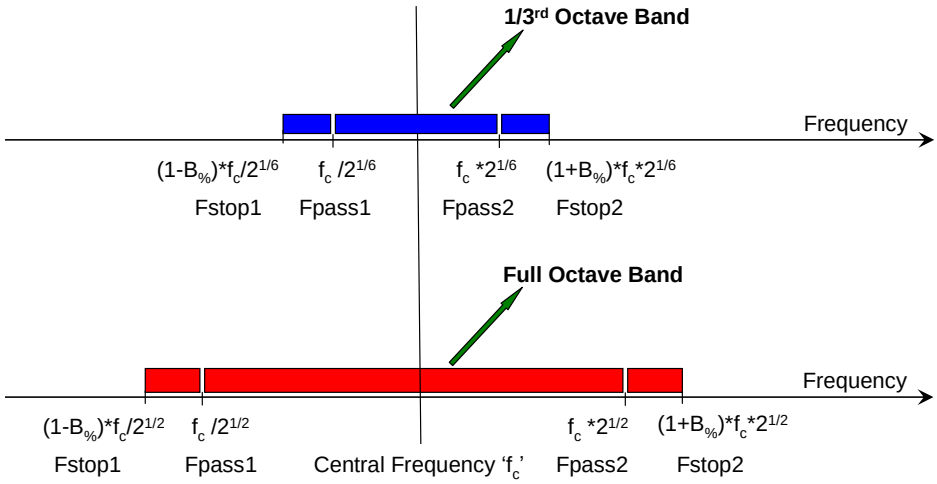


**Figure A.3: Filter design parameters for 1/3rd and full octave bands (Representation only – not to scale)**

"Tight filter bands" correspond to higher stop band attenuations and/or a narrow passband, i.e. higher magnitude of Astop1 and Astop2 and/or smaller $B_{\%}$. As the $F_{Octave}$ for 1/3rd octave is smaller than the $F_{Octave}$ of full octave, the 1/3rd octave bands will be tighter than the full octave filter bands.

To test the effect of filters on decay rate, i.e. loss factor, a simple computational experiment was conducted. In this experiment, the impulse response of a 1DOF system with a natural frequency of 100 Hz and loss factor of 0.01 is "contaminated" with impulse responses of 10Hz, 50Hz and 170Hz. Filters of different attenuations and bandwidth were created and implemented to filter out the unwanted out–of–band frequencies. The following four filters with the same central frequency of 100 Hz and full octave bandwidth were created to study the effect of filters:

1. 10th Order Filter – 6dB stopband attenuation
2. 100th Order Filter – 6dB stopband attenuation
3. 166th Order Filter – 20dB stopband attenuation
4. 315th Order Filter – 40dB stopband attenuation.

All filters cause a "group delay" in the filtered response; however the group delay does not alter the decay characteristics. For a Kaiser Window (FIR filter), the group delay is half of the filter order. Time delay is equal to the product of the group delay and time increment 'dt'. Hence, for a filter with higher order, the associated group delay and time delay will be also higher. In Figure A.4, the filtered response and the time delay associated with different filters are plotted. It can be observed that for this 1DOF computational experiment, the response filtered with 315th order filter has the highest group delay and the response with 10th order filter has the least group delay. This observation is consistent with theory which states that higher filter order causes higher group delay.

The group delay introduced in the filtered response, to be analyzed using RDT, will only delay the detection of the first trigger. Therefore, there is no impact of group delay on the process of loss factor estimation using RDT. When time domain filters are to be used for IRDM, the length of measured response should be long enough to record the complete decay of the impulse response. Failing to follow this may result in inaccurate damping estimation.

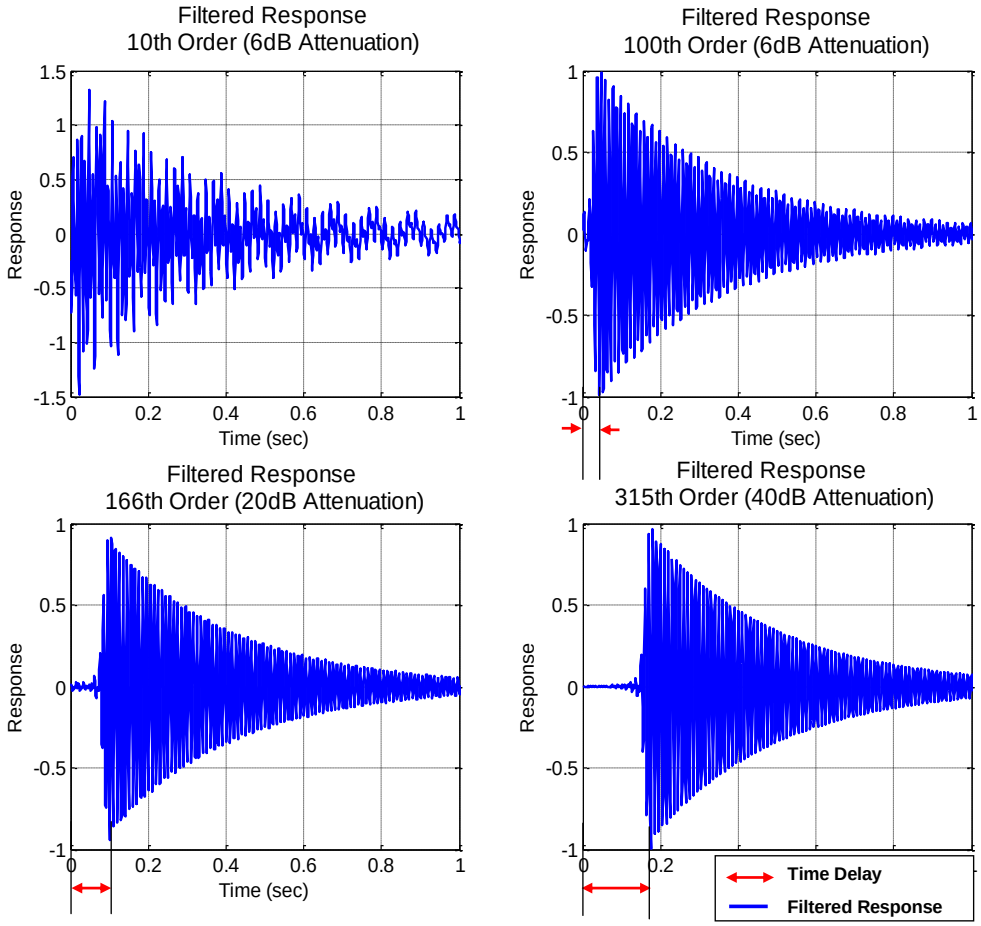


**Figure A.4: Comparison of group delay for different filter order**

## A.1 Quality of the Filtered Response

Filters are evaluated based on their ability to filter out the unwanted out-of-band frequencies. The Fourier transformation of a signal is often used to represent the signal in the frequency domain. In MATLAB, Fast Fourier Transformation (FFT) algorithms are

implemented to analyze the filtered signal in the frequency domain. The peaks in the magnitude of transformed signal (in the frequency domain) correspond to the dominating modes (or frequencies) and for a 1DOF system only one such peak is expected.

The 315$^{th}$ order filter has removed all the out–of–band frequencies as the only peak noted corresponds to the desired 100 Hz mode. In reference to Figure A.5, the 10$^{th}$ order filter failed to eliminate all "out-of-band" frequencies: 10 Hz, 50 Hz and 170 Hz, and this is concluded from the prominent peaks, corresponding to the out-of-band frequencies, in the FFT of the filtered response.

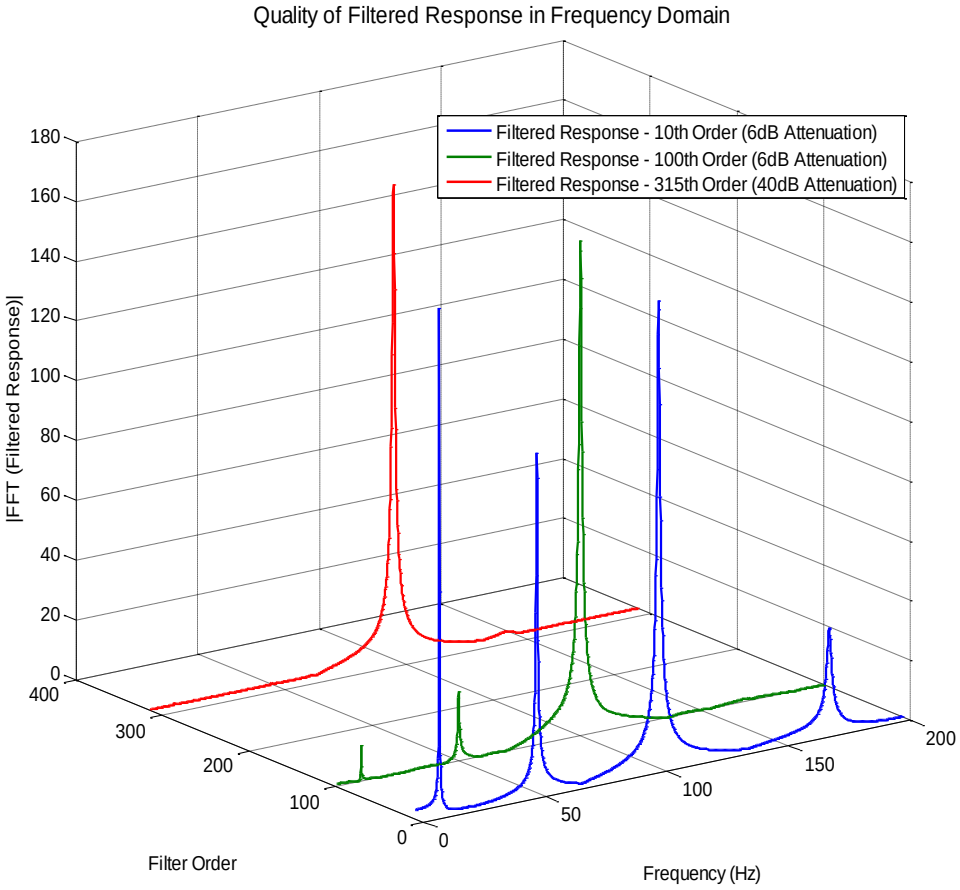


**Figure A.5: Comparison of quality of filtered response**

## A.2 Effect of Filters on dB Decay Curve

As discussed earlier in previous section, the lower order filters fail to clean the contaminated signal. Therefore, the dB decay of the response filtered using the lower order filters will correspond to the decay of long lasting, lower frequency modes, in this case the10 Hz mode. The decay curves of the filtered responses are plotted in Figure A.6. The very initial decay rates of filtered impulse response from all the filters are consistent with the decay rate of the targeted 100 Hz mode with a loss factor of 0.01. From the decay curve of response filtered using the $10^{th}$ order filter (red curve) it is very difficult to identify the region in which the decay rate can be accurately estimated. On the other hand, the filtered response from the $315^{th}$ order filter (magenta curve) has an identifiable region—0 second to 2.5 seconds—in which the decay rate is almost equal to the decay rate of the 100 Hz mode with a loss factor of 0.01.

Clearly, the output from the lower order filters that are contaminated with the out-of-band frequencies makes it difficult to accurately measure the targeted decay rate of simulated 1DOF system. The secondary decay curve of filtered response is of the lower frequency mode, which has a lower decay rate than the decay rate of the 100 Hz mode. Therefore, the loss factor computed from the secondary dB decay curve will underestimate the decay rate of the desired 100 Hz mode.

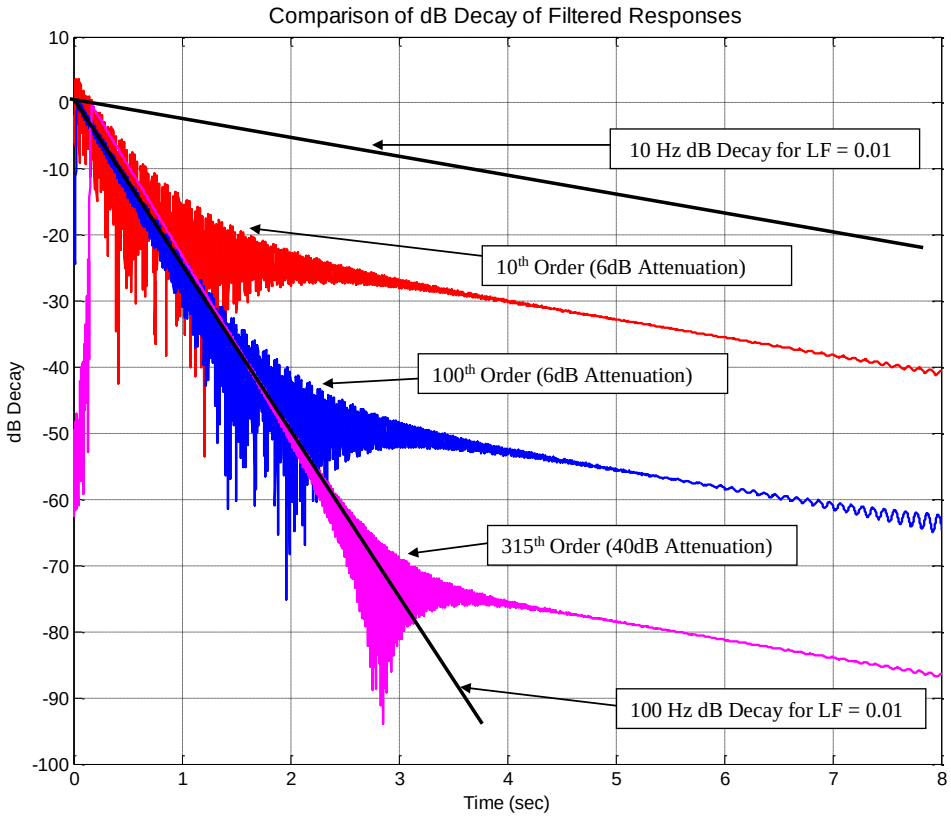


**Figure A.6: Comparison of dB decay for response filtered from different order filters**

## A.3 References

[A-1] Cole, H. A., Jr., *On–The–Line Analysis of Random Vibrations*, AIAA paper No. 68–288, AIAA/ASME 9th Structures, Structural Dynamics and Materials Conference, Palm Springs, CA, 1968

[A-2] Asmussen, J. C., *Modal Analysis Based on The Random Decrement Technique—Application to Civil Engineering Structures*, PhD Dissertation, University of Aalborg, Department of Building Technology and Structural Engineering, 1997

[A-3] Kijewski, T., and Kareem, A., *On the Reliability of a Class of System Identification Techniques: Insights from Bootstrap Theory*, Proceedings of 8th International

Conference on Structural Safety and Reliability, Structural Safety Vol. 24(2–4), pp. 261–280, 2002

[A-4] Kijewski, T., and Kareem, A., *Reliability of Random Decrement Technique for Estimates of Structural Damping*, 8th ASCE Specialty Conference on Probabilistic Mechanics and Structural Reliability, PMC2000–294, 2000

[A-5] MATLAB Product Help, *FIR Filter Design :: Filter Design and Implementation (Signal Processing Toolbox™)*, MATLAB Version 7.8.0.347 (R2009a)

[A-6] Lyon, R. H. and Dejong, R. G., *Theory and Application of Statistical Energy Analysis*, 2nd edition, RH Lyon Corp 1998

# Appendix B: Challenges Associated With Automated Slope Fitting

In a conventional experimental testing, it is typical to manually fit a linear curve—on a decay curve—to determine the decay rates (and loss factor). If a large number decay curves needs to be evaluated, to determine the decay rates, the manual approach could be tedious. In these cases a automated slope fitting algorithm, with requirement of visual inspection, could be implemented. This automated slope fitting algorithm is discussed in Section 2.2.3.1. For highly damped panels, which have relatively lower reverberation time and fewer peaks in decay curve, the automated slope fitting could be biased and need significant supervision.

For lightly damped and highly damped panels, in Figure B.1 and B.2, the impulse response (and it's Hilbert Transformation) is plotted in the top figures and corresponding decay curves are plotted in the bottom figures. By comparing the top Figures of B.1 and B.2, it is evident that for vibrations damp out (or reach the "noise floor") faster for a highly damped panel than the lightly damped panel. It is concluded that the automated slope fitting algorithm works better if higher number of peaks are detected in the decay curve as in the case of a lightly damped panel. If fewer peaks are observed, as with the highly damped case, manual slope fitting could to be implemented.

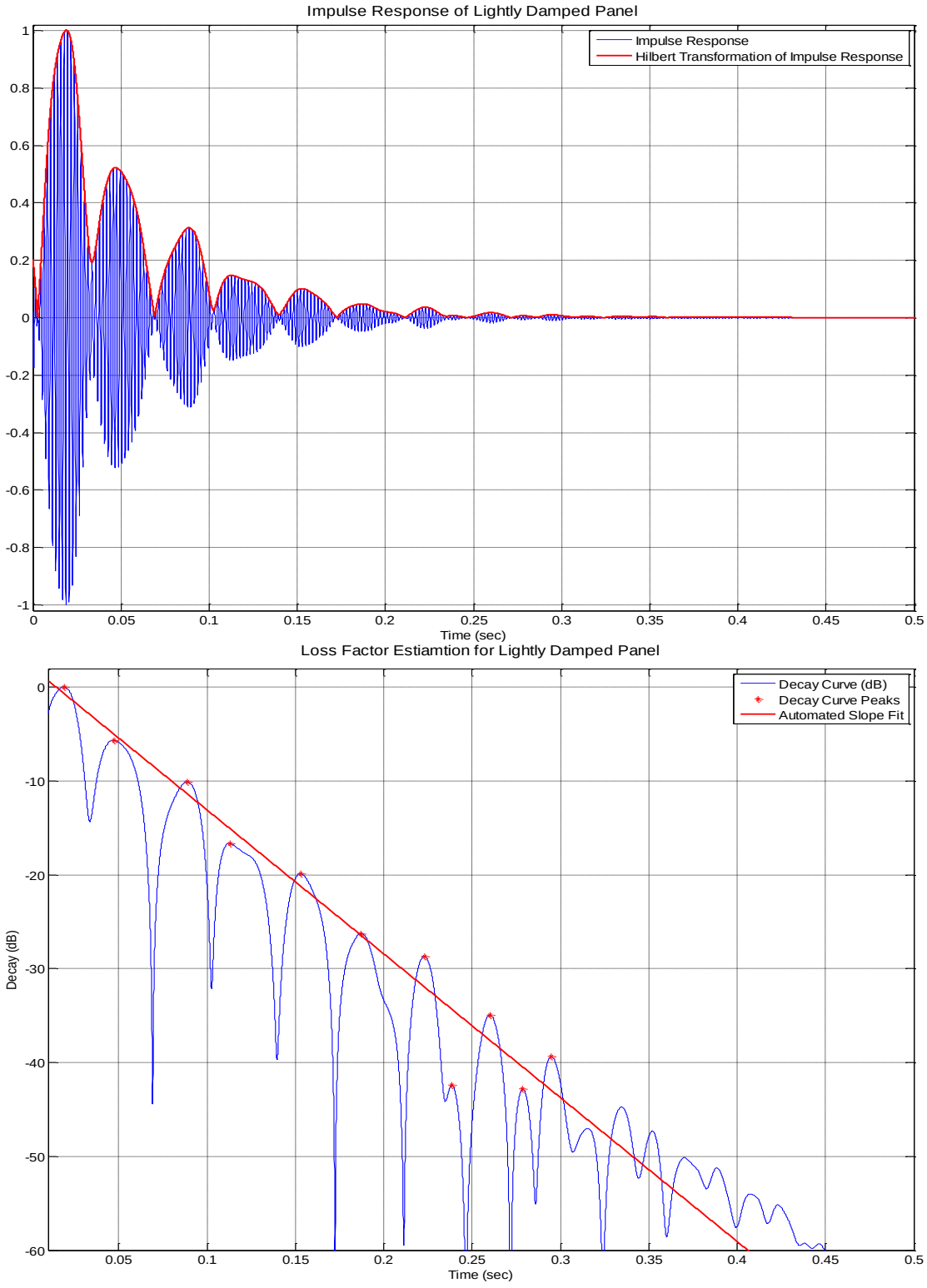


**Figure B.1: Sample of an impulse response (top plot) and decay curve (bottom plot) of lightly damped panel**

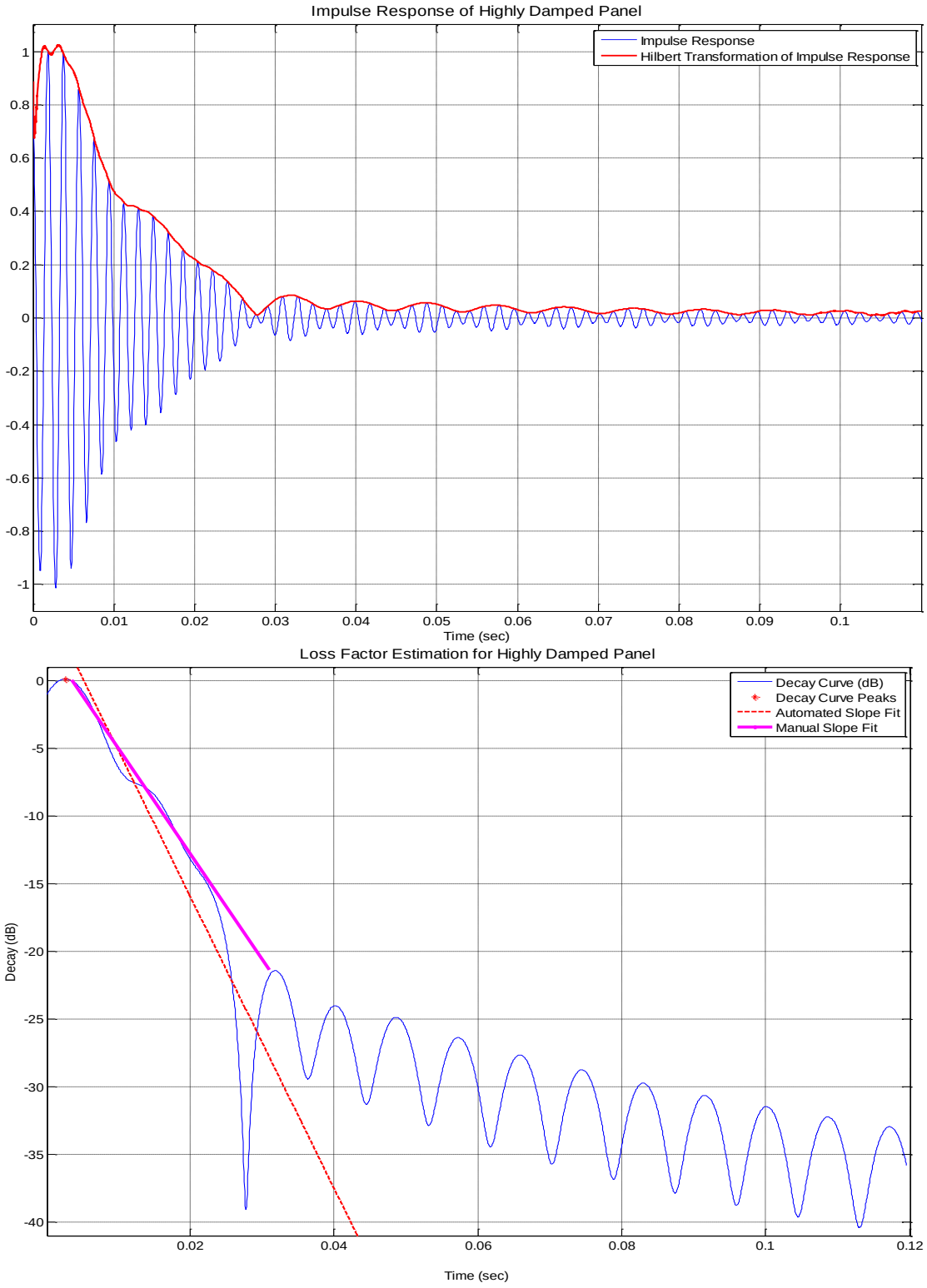


**Figure B.2: Sample of an impulse response (top plot) and decay curve (bottom plot) of a highly damped panel**

# Appendix C: Comparison of RDT-Based Loss Factor Estimations for an 1DOF System—Brief Case Study

The theory of RDT is based on extraction of decaying randomdec signature by averaging samples with the same initial conditions from a narrow–band response measurement. Although, an infinite number of triggered samples are required to retrieve the true free decay (or randomdec signature), only a finite number of triggers can be detected from the finite length of the response measurement. Therefore, a realistic approach would be to average as many triggered responses as possible. To determine the effect of the number of triggers used for loss factor estimation, the following study is performed.

## C.1 Effect of Number of Triggers on dB Decay

The number of triggered samples averaged to compute the free decay controls the quality of dB decay rate, from which the loss factor is to be estimated. In Figures C.1 and C.2, the dB decay curves of normalized randomdec signatures corresponding to different numbers of triggered samples averaged are plotted.

The red line in Figures C.1 and C.2 corresponds to the expected dB decay of a simulated 1DOF system. It is evident that if larger numbers of triggered samples are averaged, a smooth and almost linear dB decay is observed. Alternatively, it can be concluded that the initial dB decay converges to the analytical (or expected) dB decay curve with increase in number of triggered samples that have been averaged. The initial dB decay from averaging the autocorrelation function seems to have a higher slope than expected, and is relatively more linear when compared to the dB decay computed using the direct averaging approach. These observations are consistent for loss factor levels between 1% and 10%.

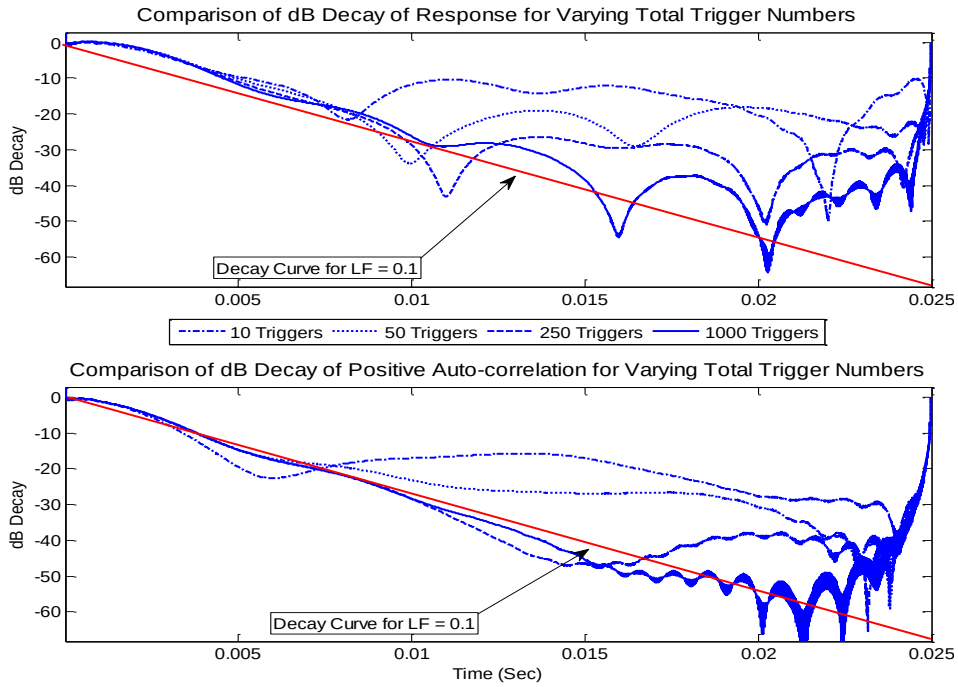


**Figure C.1: Study of the effect of number of triggers on dB decay (for a 1DOF system with simulated LF = 0.1 and $f_n$=1000 Hz).**

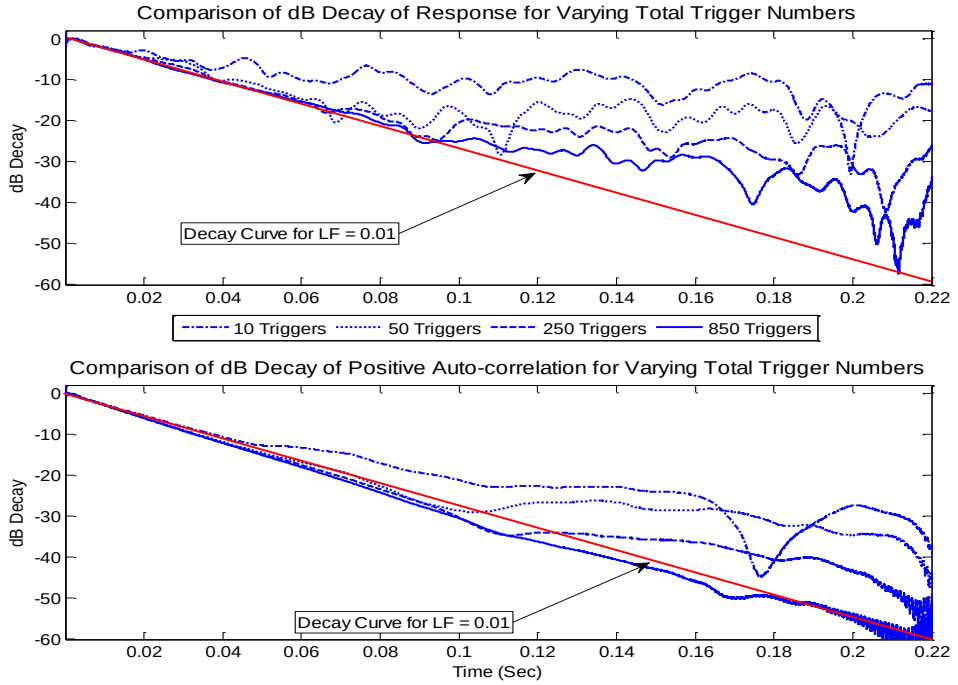


**Figure C.2: Study of the effect of number of triggers on dB decay (for a 1DOF system with simulated LF = 0.01 and $f_n$=1000 Hz)**

## C.2 Direct Averaging or Averaging Autocorrelation Functions

In Chapter 2 and 3, it is established that the decay of autocorrelation function of random response is equivalent to the free decay of response. Thus, the randomdec signature can be measured by averaging either the triggered responses directly or the autocorrelation functions of triggered responses.

The number of samples required to be averaged for accurate estimation of the loss factors are calculated for both averaging schemes (direct averaging and averaging autocorrelation functions). In Figures C.3 and C.4, for a simulated 1DOF system with natural frequency of 1000 Hz and loss factor of 0.1 and 0.01, respectively, the results of this study are reported. The following observations can be drawn from Figures C.3 and C.4:

1. Accuracy of loss factor estimation increases with the number of triggered samples being averaged.
2. Averaging autocorrelation functions converges quickly, i.e. by averaging fewer triggered samples, to a slightly overestimated loss factor.

   From Figure C.3 it can be noted that for a simulated 1DOF system with loss factor of 0.1, the averaging of autocorrelation functions converges to a slightly overestimated loss factor in about 50 triggered samples. A similar trend is observed for the system with a loss factor of 0.01.
3. Directly averaging the triggered responses converges accurately to the simulated loss factor but with a relatively large number of triggered samples.

It is recommended to use the direct averaging approach if sufficiently long time histories are available to extract the required number of samples for averaging. If fewer numbers of triggers are detected, the alternative approach, i.e. averaging the autocorrelation

functions, can be implemented with the knowledge that the estimates will be slightly biased (high).

The averaging autocorrelation functions approach has a potential advantage over the direct averaging approach, particularly in the analysis of lightly damped structure and/or in lower frequency bands. In the experimental and computational studies that are included in later sections of this chapter, loss factor estimates from both approaches will be analyzed.

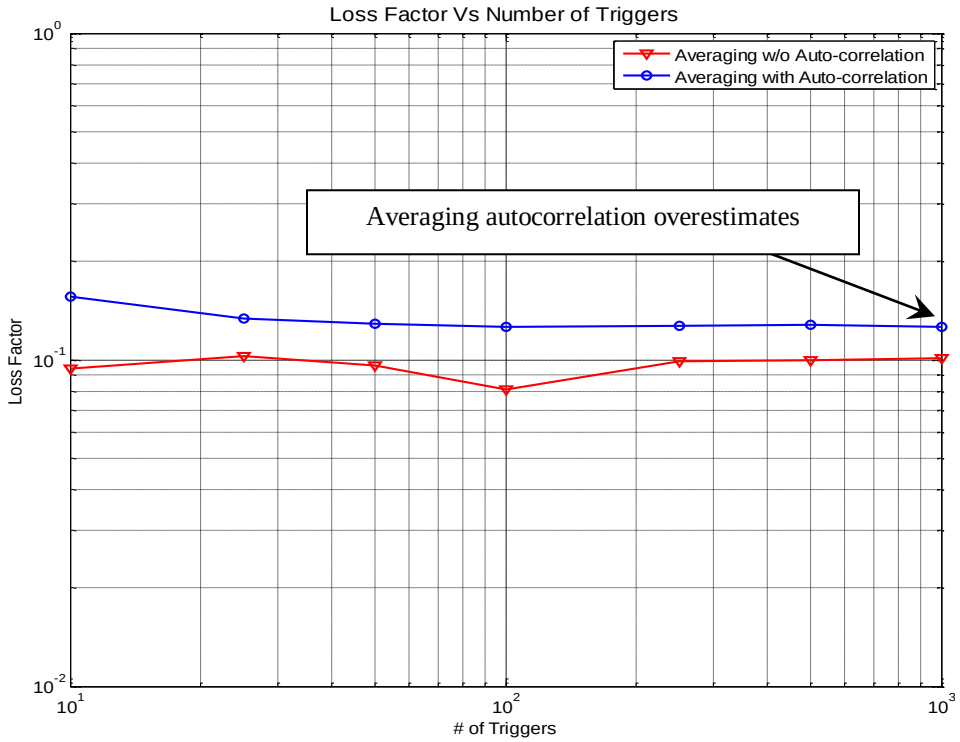


**Figure C.3: Study of effect of number of triggers on loss factor estimation (for a 1DOF system with simulated LF = 0.1)**

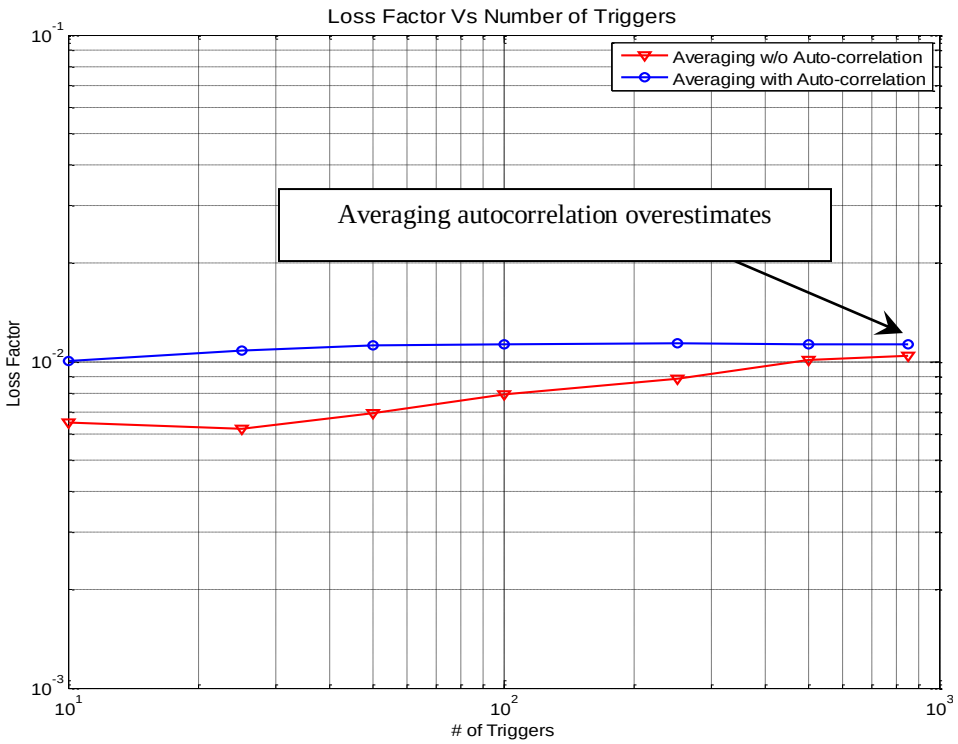


**Figure C.4: Study of effect of number of triggers on loss factor estimation (for a 1DOF system with simulated LF = 0.01)**

# Appendix D: Experimentally Measured Squared Velocity Fields[2]

The analysis of distance based loss factor analysis was driven by the experimentally observed variation in the velocity squared field. For this study, four panels were manufactured for experimental evaluation of effect of size of direct field on loss factor estimation process. Plate dimensions are presented in Table D.1 and excitation locations are presented in Figure D.1. In these tests the plates are labeled as: Highly Damped, Moderately Damped, Lightly Damped and Undamped. In Figures D.2 through D.17 the measured velocity squared field are presented based on the choice of excitation location and frequency.

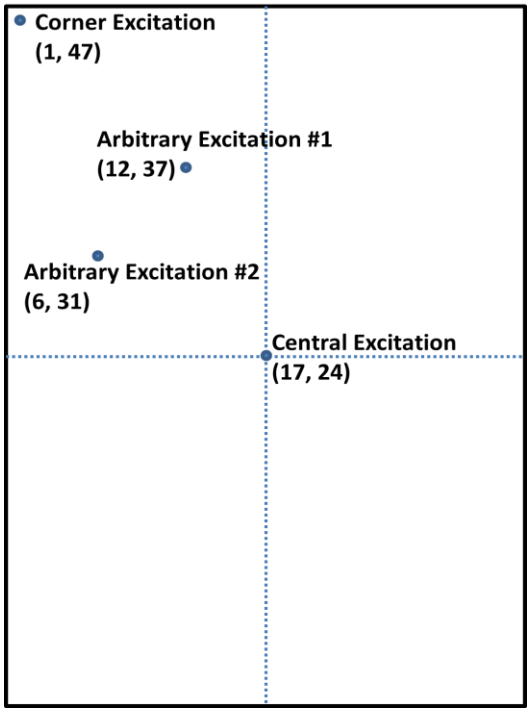


**Figure D.1: Excitation locations for experimental and computational analyses.**

[2] These experiments were conducted at Structural Acoustics Labs, Spirit AeroSystems, Wichita, KS. The velocities were measured using Polytec's scanning laser vibrometer.

**Table D.1: Dimensions of plates used to evaluate experimental loss factor estimation process**

| | **Undamped Plate** | **Lightly Damped Plates** | **Moderately Damped Plates** | **Highly Damped Plate** |
|---|---|---|---|---|
| **Thicknesses** | | | | |
| Base Plate (in.) | 0.08 | 0.125 | 0.08 | 0.04 |
| VEM Layer (in.) | | 0.005 | 0.005 | 0.005 |
| Cover Plate (in.) | | 0.012 | 0.012 | 0.012 |
| Total (in.) | | 0.142 | 0.097 | 0.057 |
| **Estimated loss factor, $\eta$, based on theory presented by Ross *et al.* [12]** | | | | |
| | $\approx 0$ | $\approx 0.06$ | $\approx 0.10$ | $\approx 0.20$ |
| **Panel Size** | | | | |
| Area (in.$^2$)* | 34.125 x 48 | 34.125 x 48 | 34.125 x 48 | 34.125 x 48 |

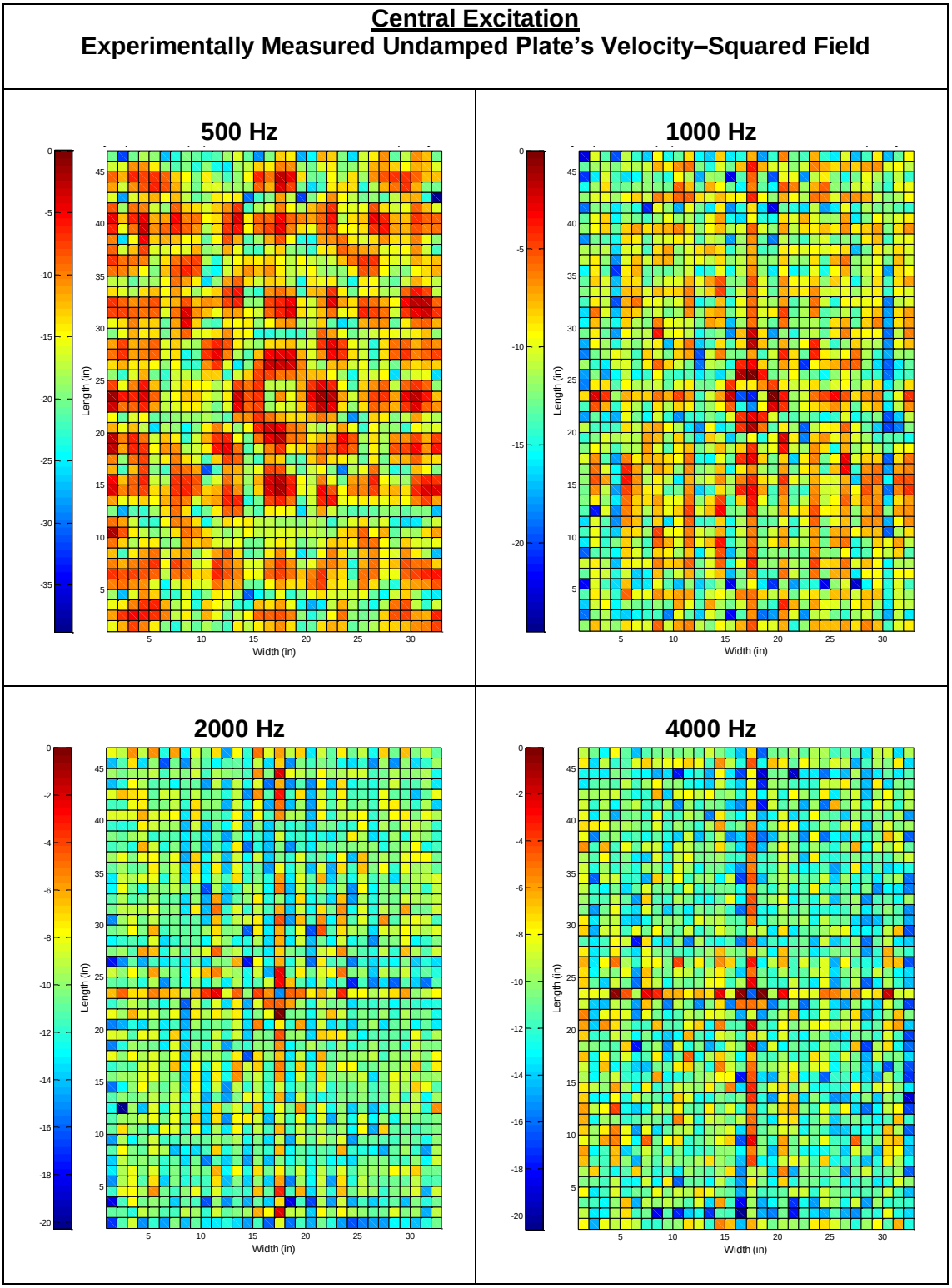


**Figure D.2: Central excitation location: Undamped plate's velocity-squared field**

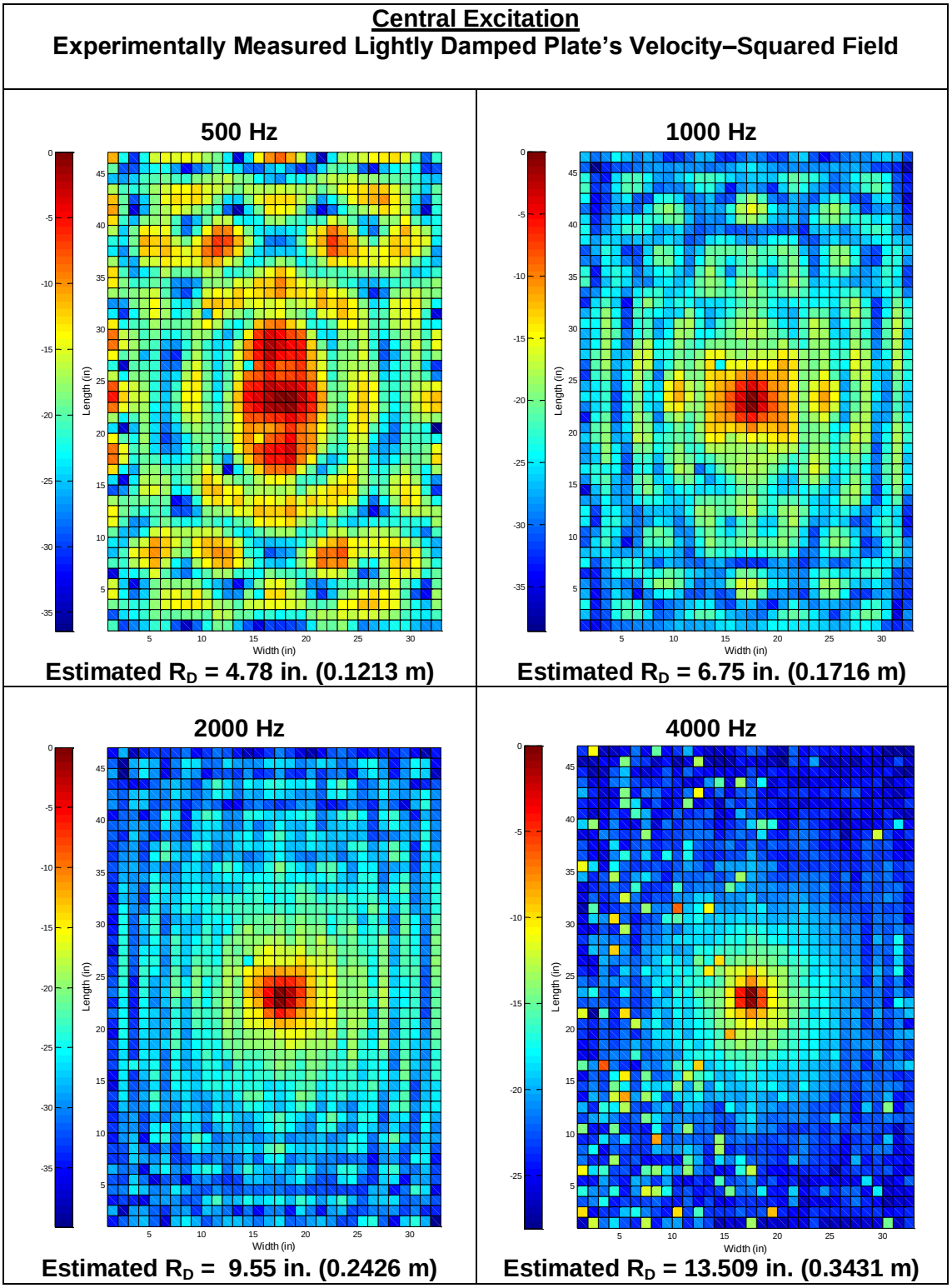


**Figure D.3: Central excitation location: Lightly damped plate's velocity-squared field**

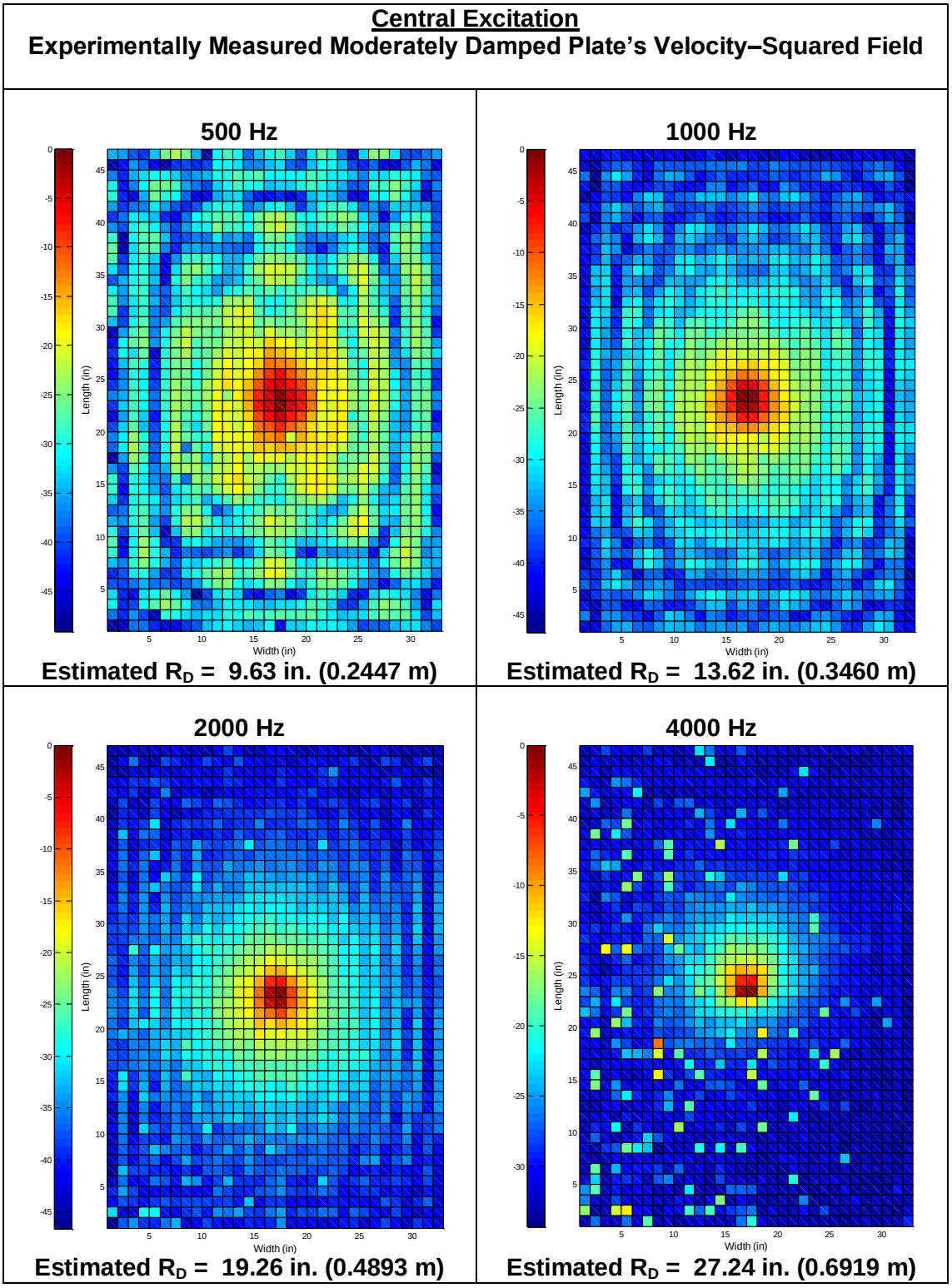


**Figure D.4: Central excitation location: Moderately damped plate's velocity-squared field**

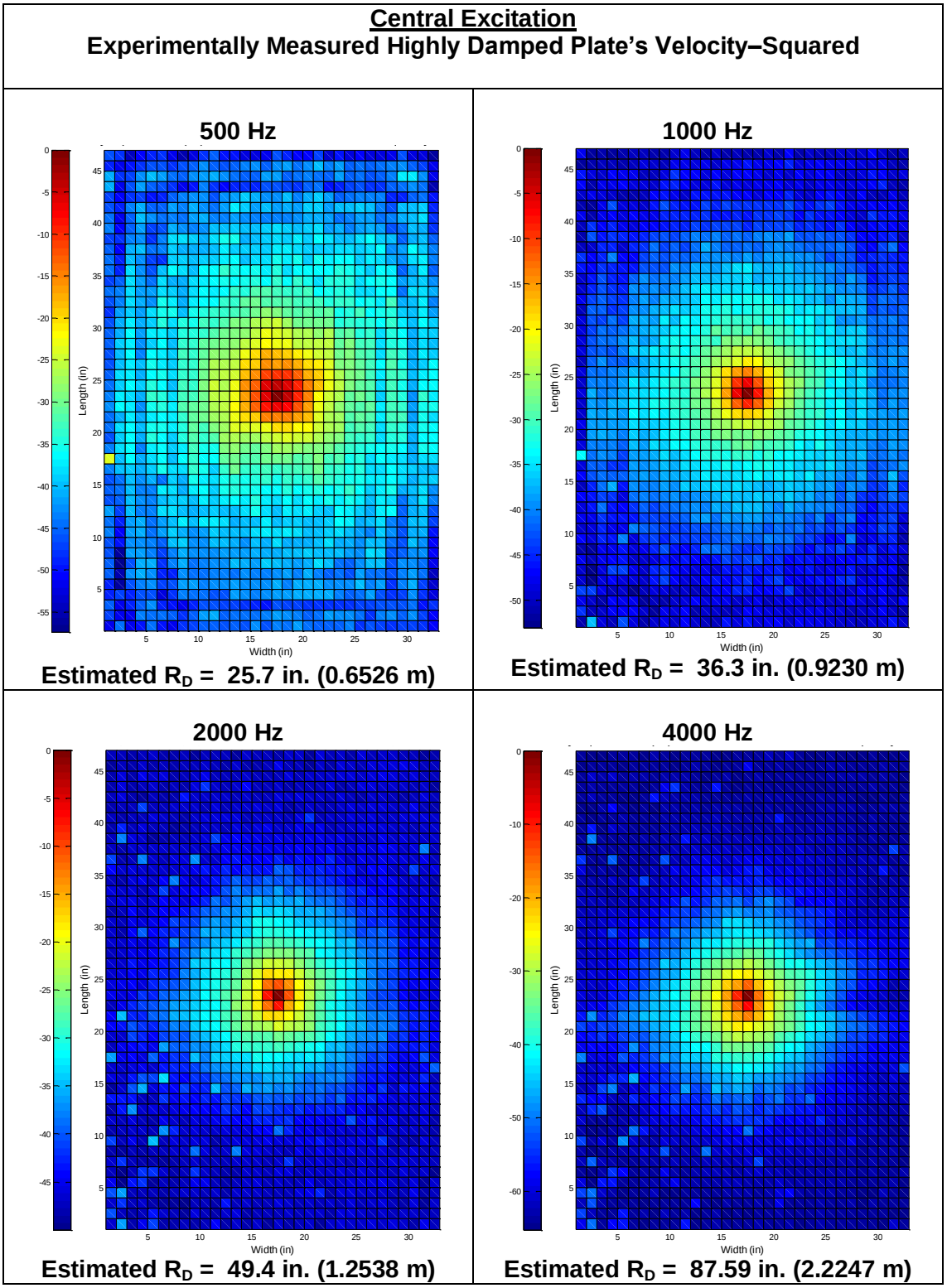


**Figure D.5: Central excitation location: Highly damped plate's velocity-squared field**

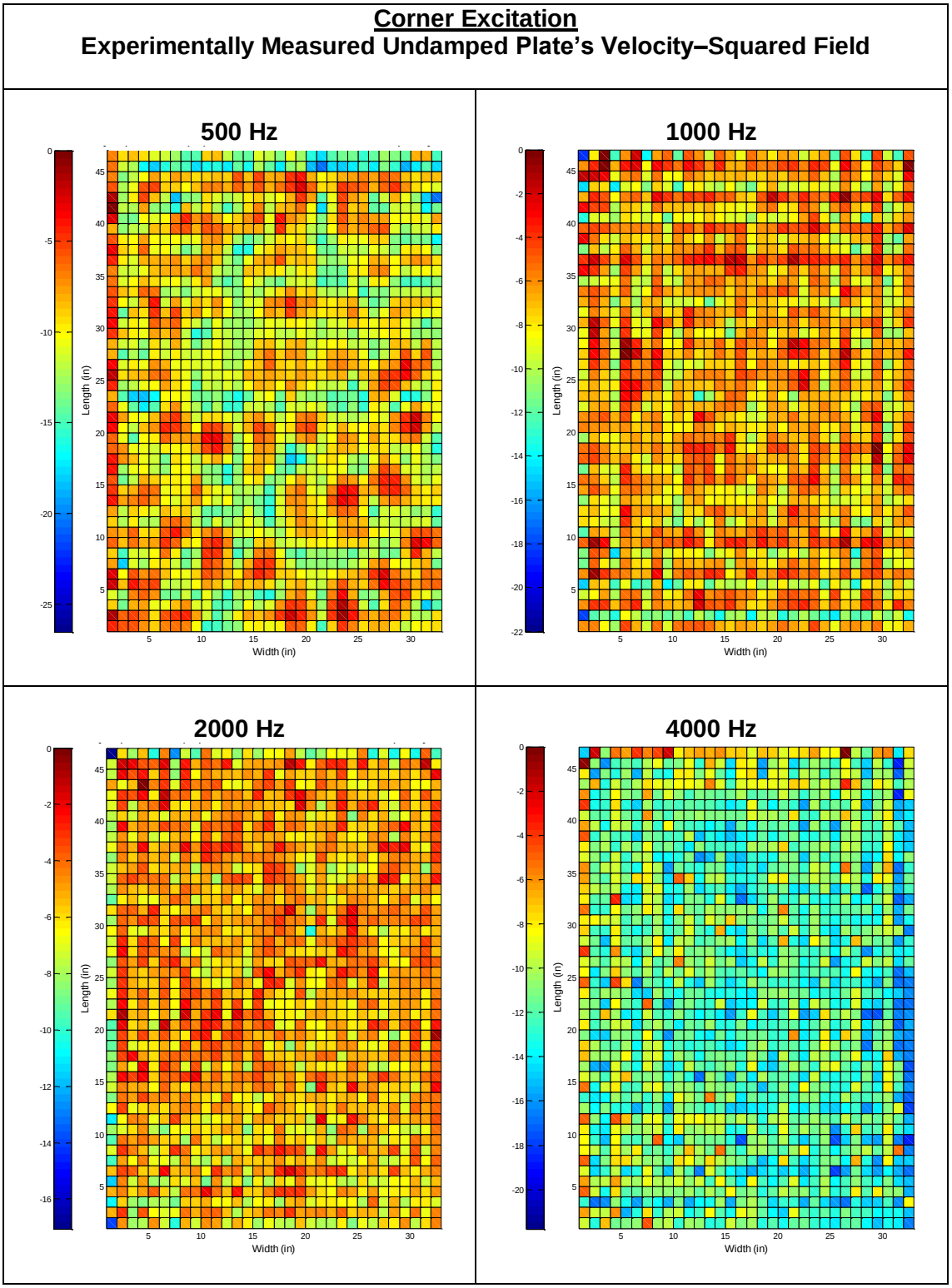


**Figure D.6: Corner excitation location: Undamped plate's velocity-squared field**

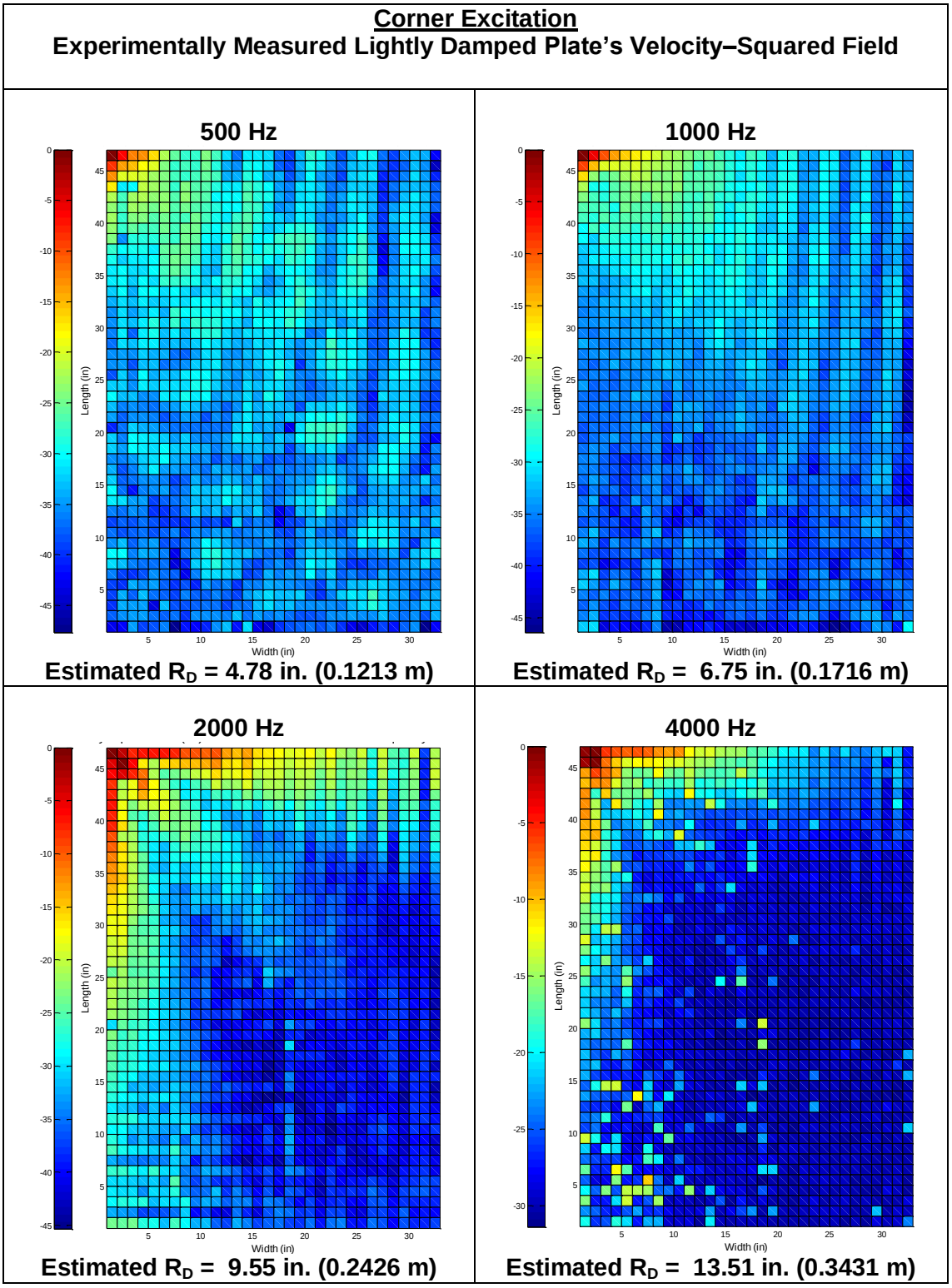


**Figure D.7: Corner excitation location: Lightly damped plate's velocity-squared field**

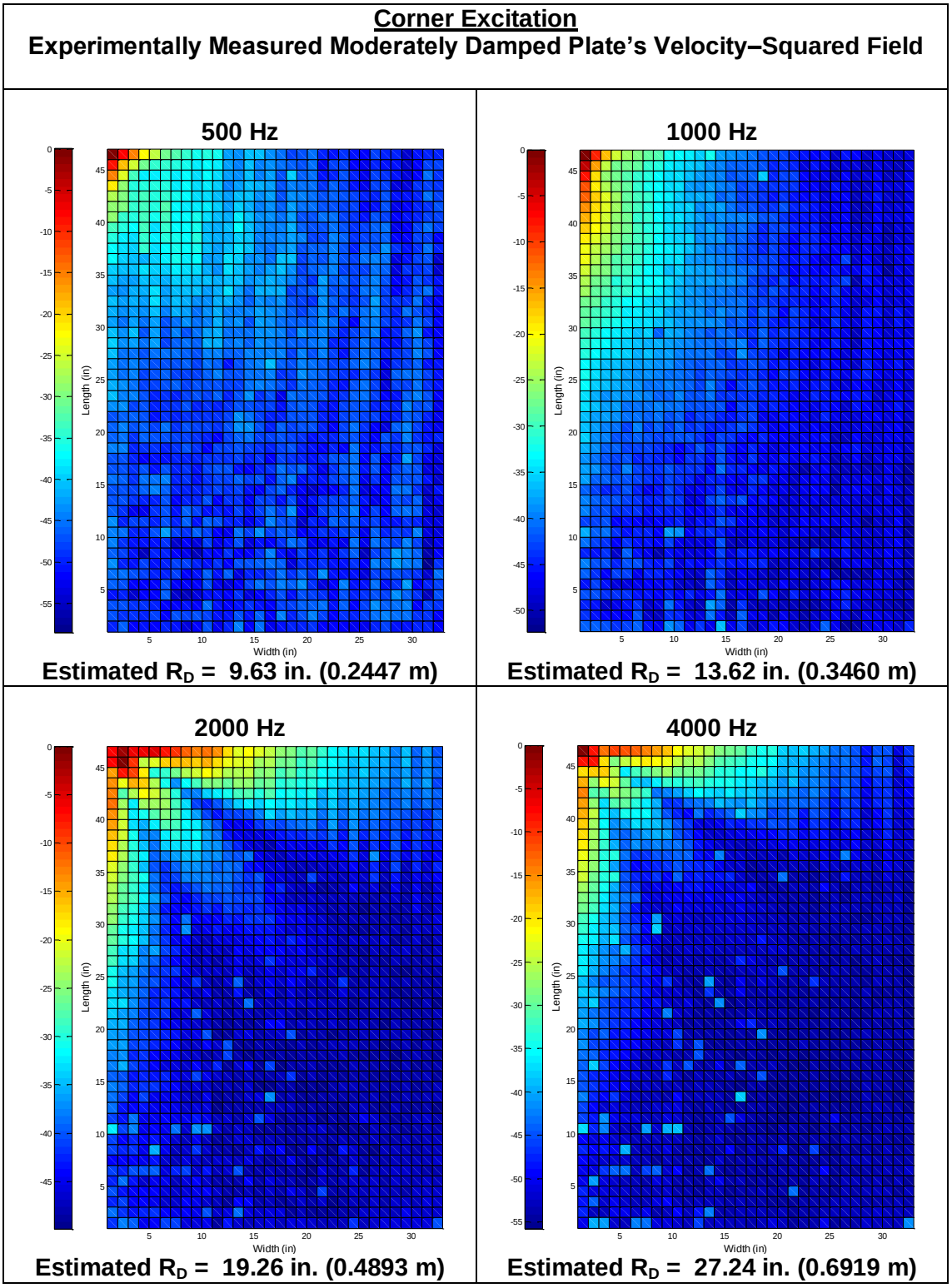


**Figure D.8: Corner excitation location: Moderately damped plate's velocity-squared field**

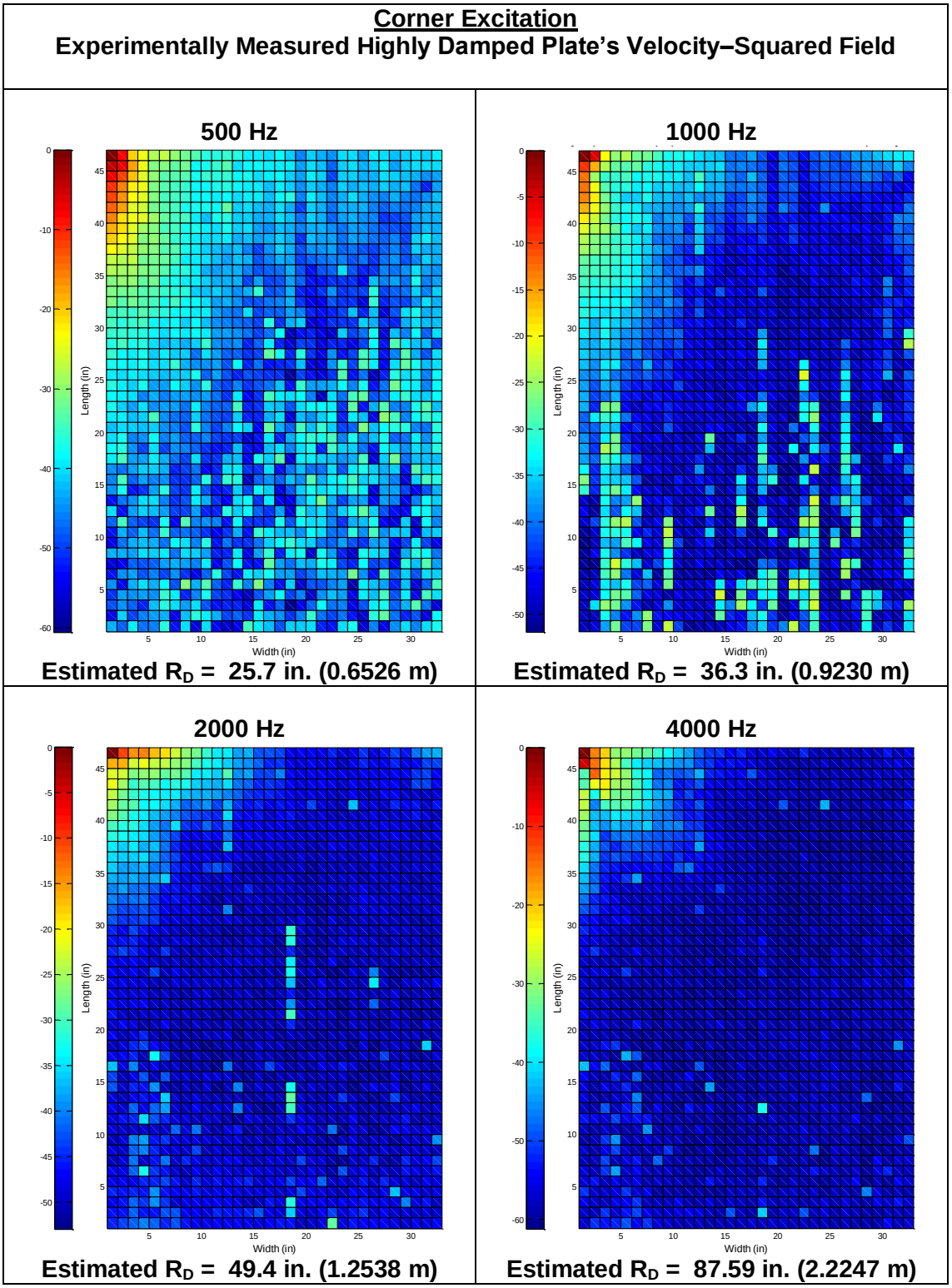


**Figure D.9: Corner excitation location: Highly damped plate's velocity-squared field**

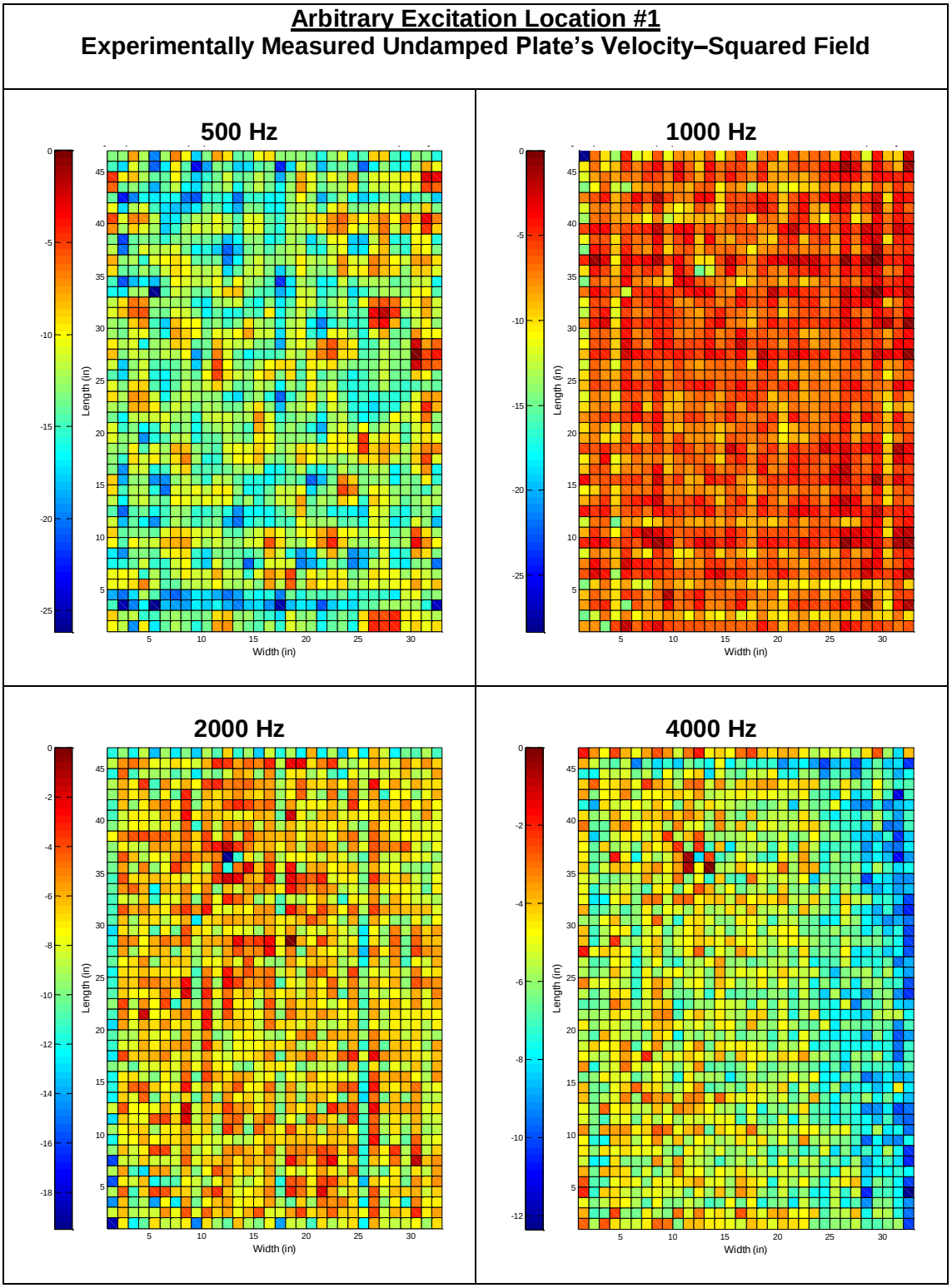


**Figure D.10: Arbitrary excitation location #1: Undamped plate's velocity-squared field**

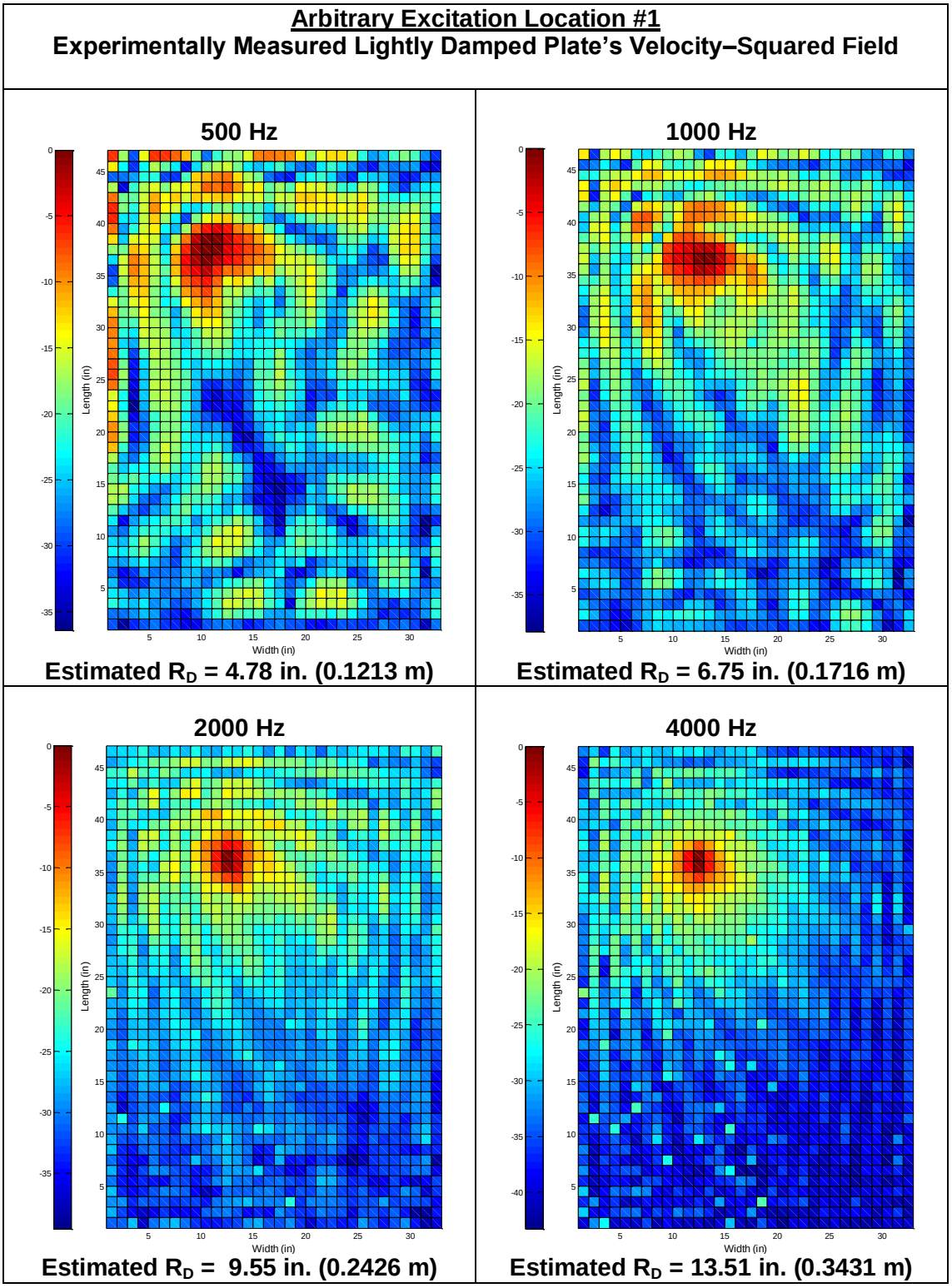


**Figure D.11: Arbitrary excitation location #1: Lightly damped plate's velocity-squared field**

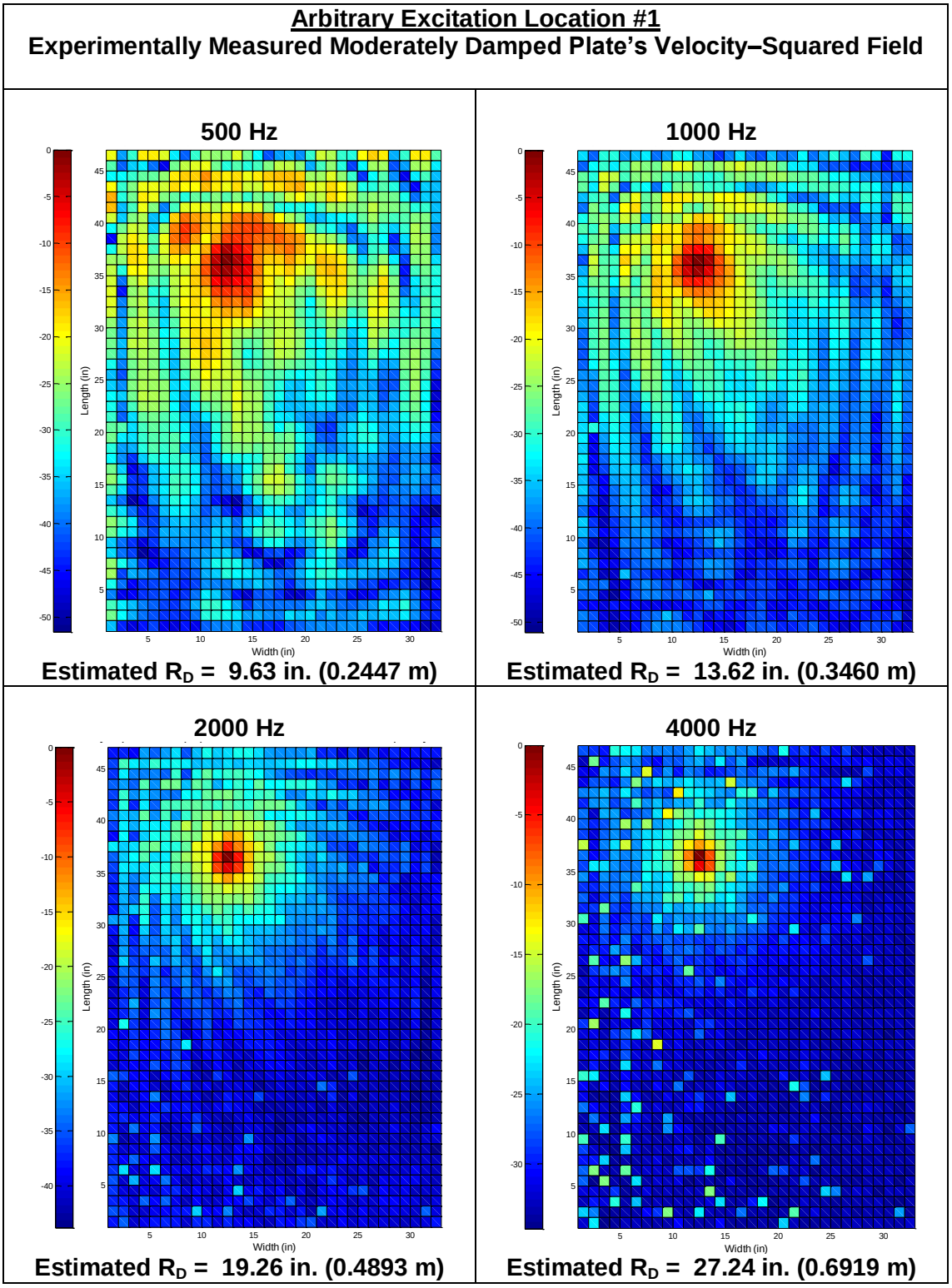


**Figure D.12: Arbitrary excitation location #1: Moderately damped plate's velocity-squared field**

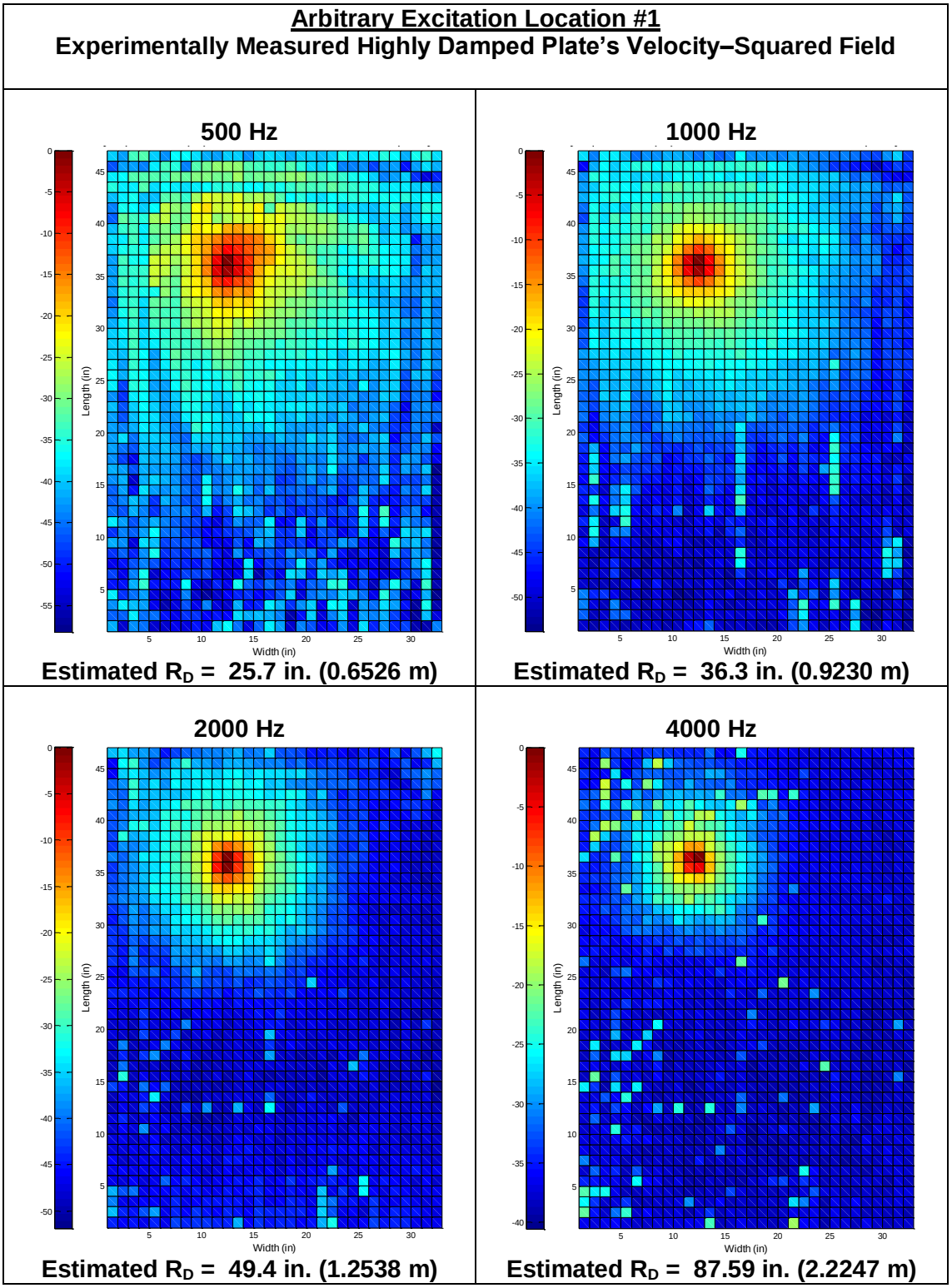


**Figure D.13: Arbitrary excitation location #1: Highly damped plate's velocity-squared field**

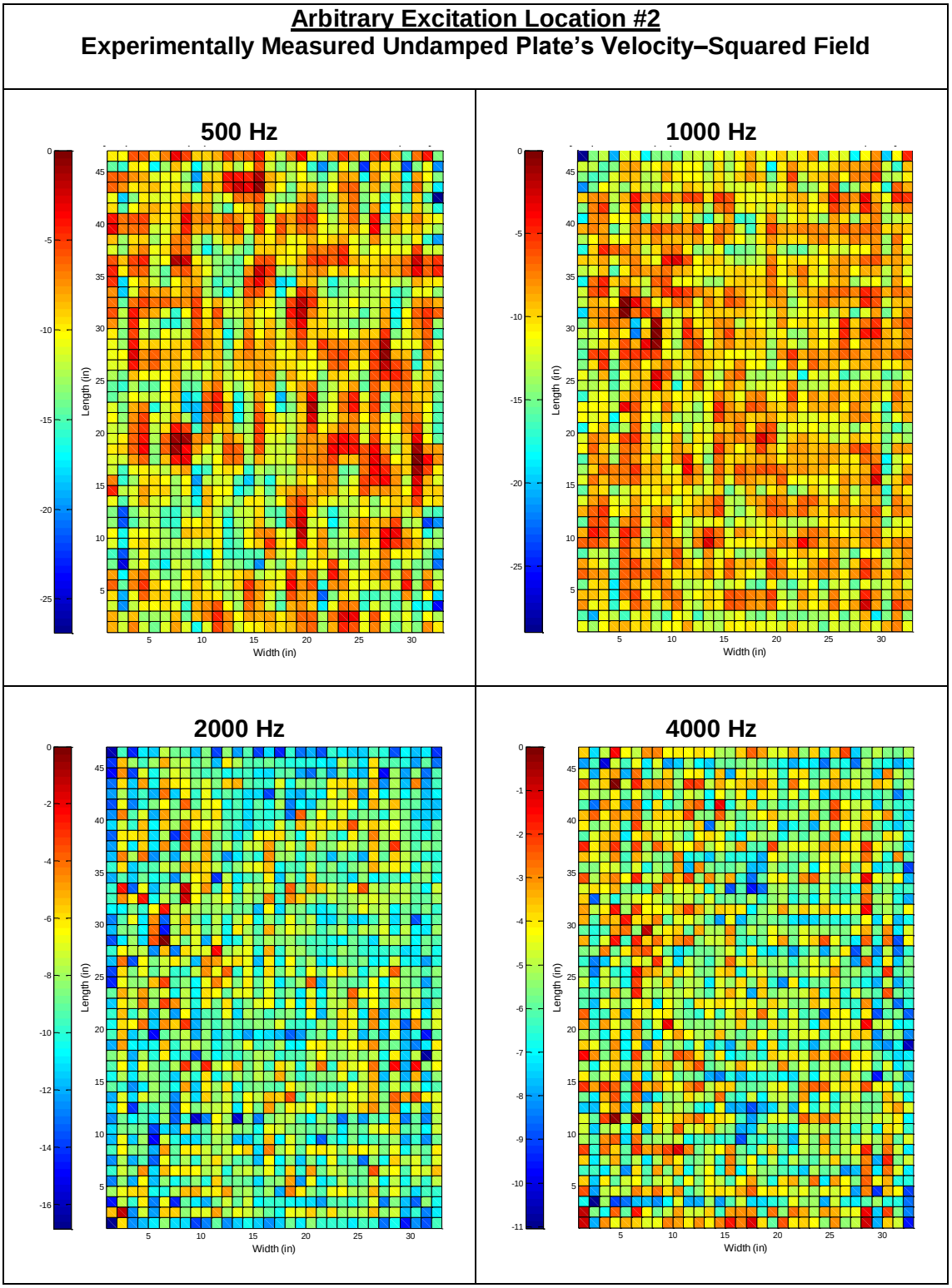


**Figure D.14: Arbitrary excitation location #2: Undamped plate's velocity-squared field**

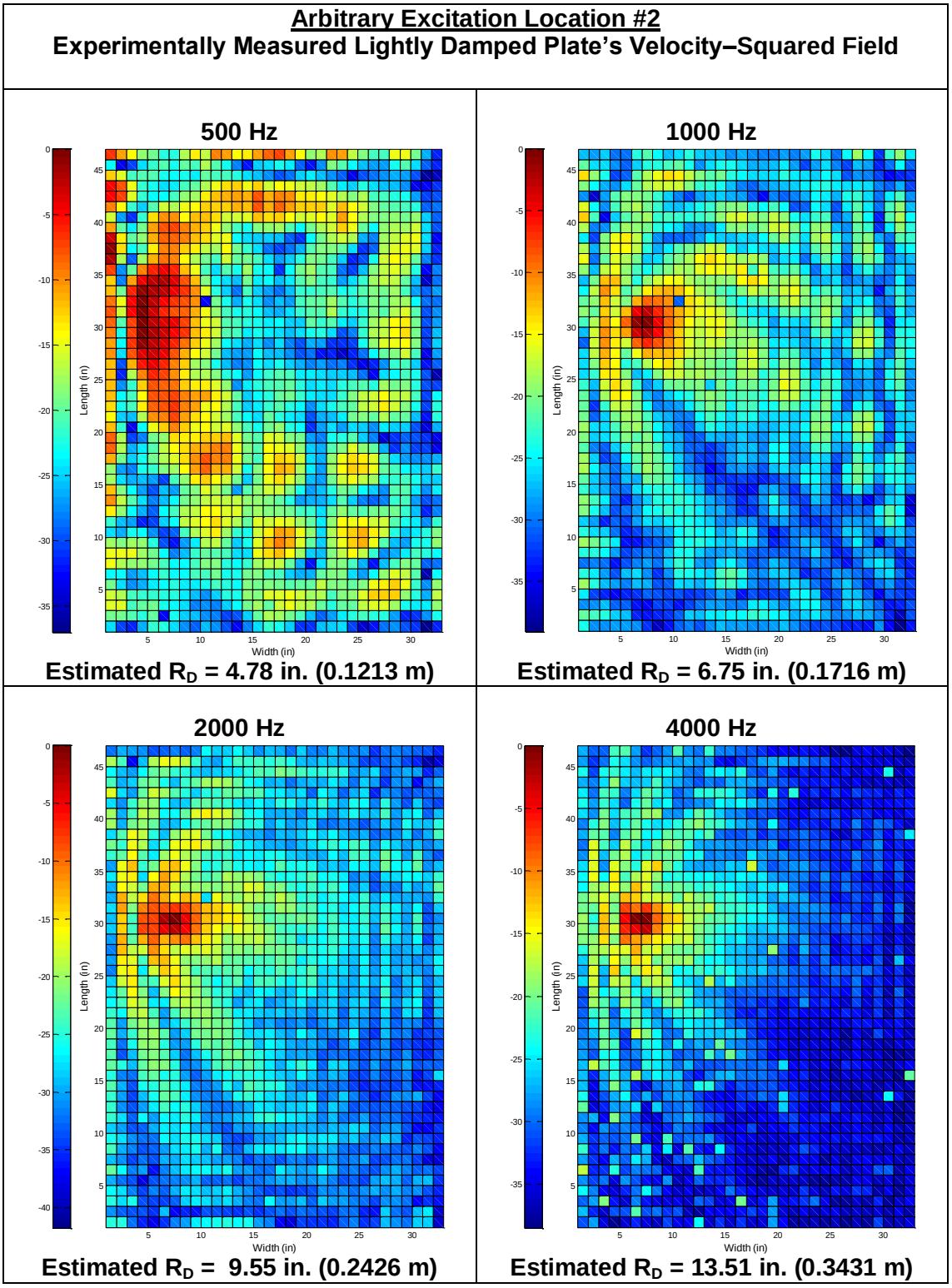


**Figure D.15: Arbitrary excitation location #2: Lightly damped plate's velocity-squared field**

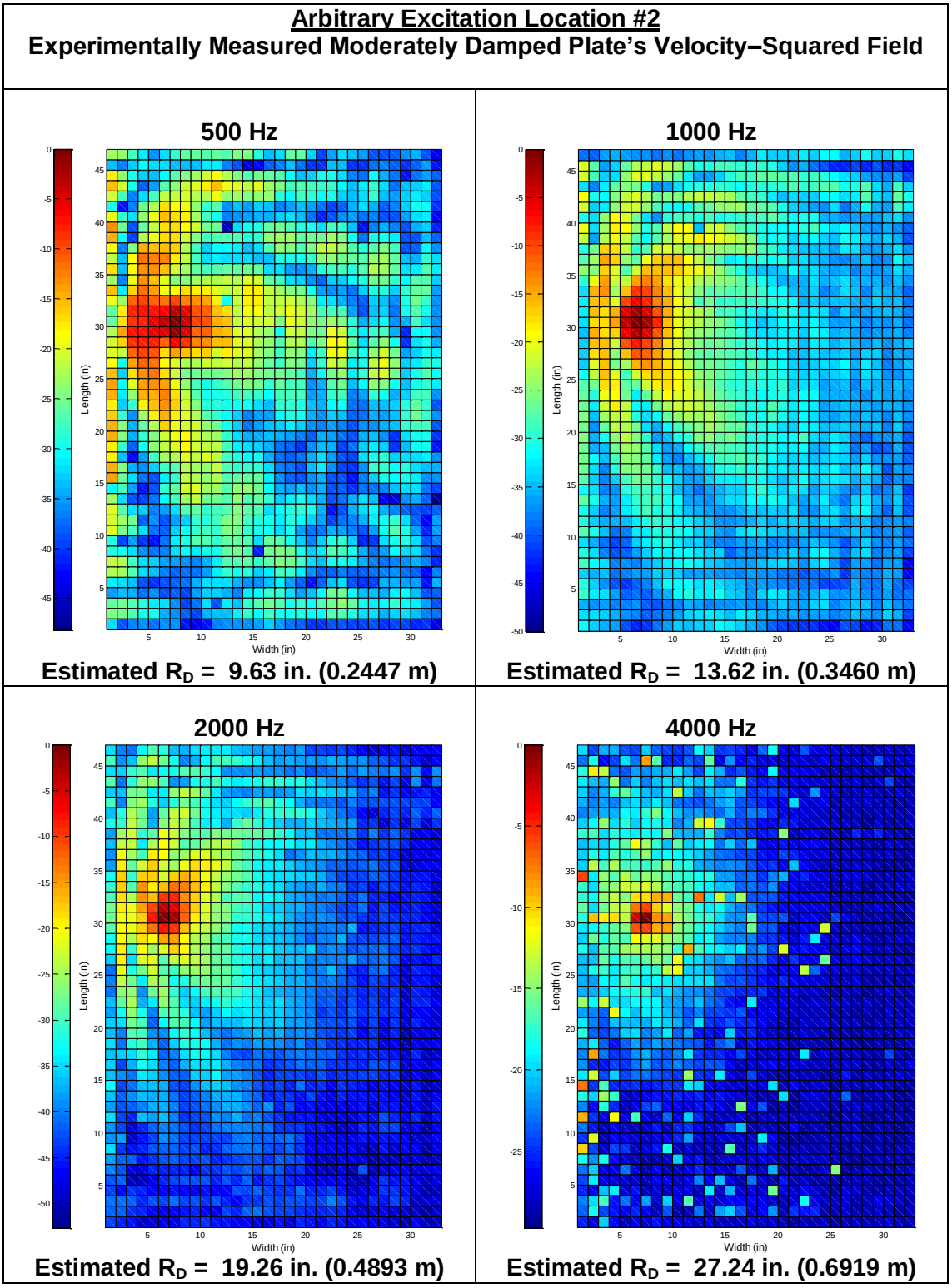


**Figure D.16: Arbitrary excitation location #2: Moderately damped plate's velocity-squared field**

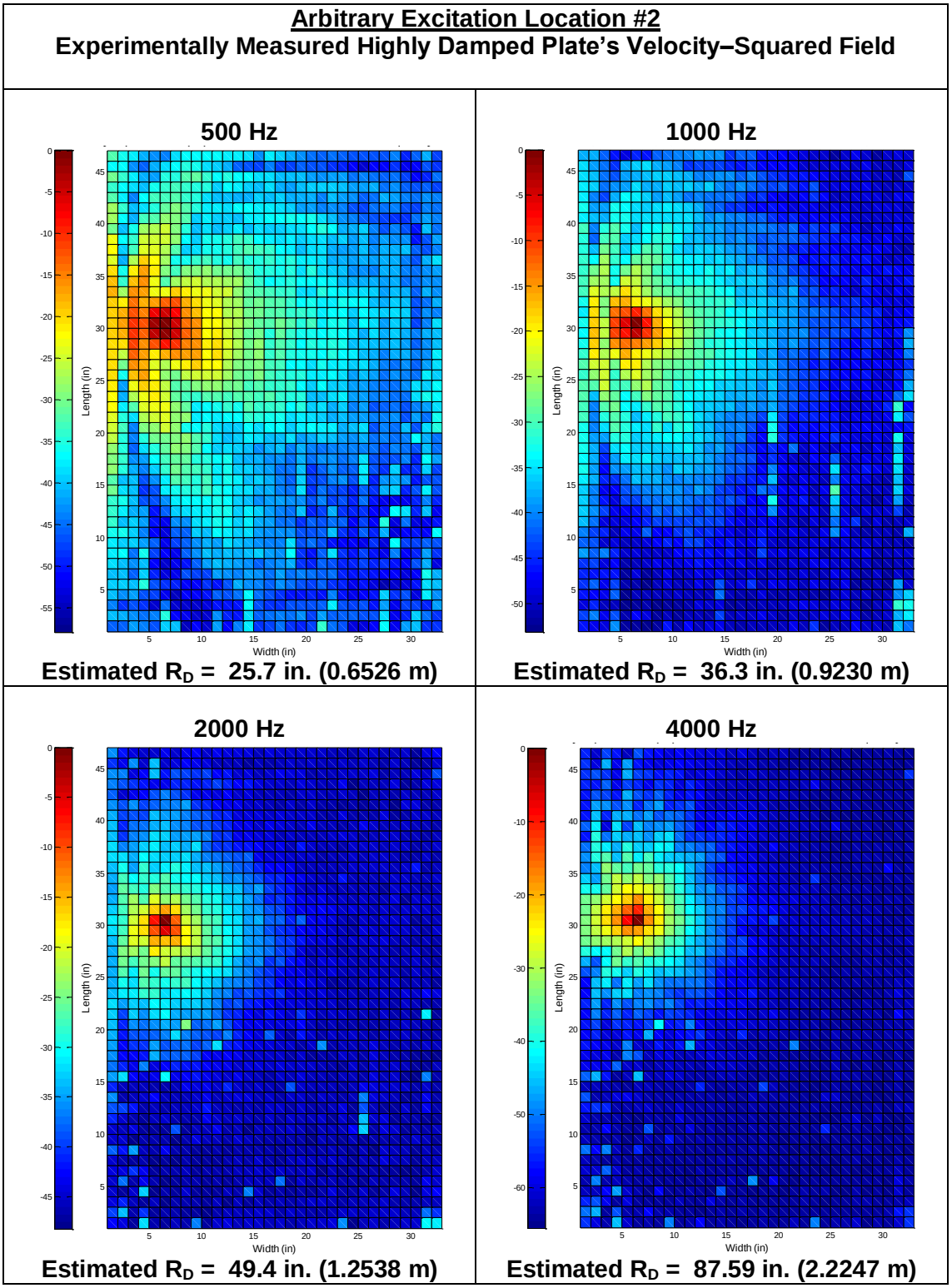


**Figure D.17: Arbitrary excitation location #2: Highly damped plate's velocity-squared field**